A numerical simulation study on the interaction of particles with rough surface and soft structures in suspension systems

A Thesis Presented to
the Faculty of Graduate Studies of Lakehead University.
by Duowei Lu

DEDICATION
To my parents for their unconditional guidance and support

Abstract

Particle interactions in complex colloidal systems are essential in a variety of traditional and emerging industrial processes. This thesis applied the extended Derjaguin-Landau-Verwey-Overbeek (XDLVO) theory to calculate the interactions between particles of different shapes and surface morphologies under different conditions. The past constructed models systematically assessed the critical roles of surface topography on the interfacial interactions of particles of various sizes and shapes. In this research, the surface morphology (via considering asperity size and number, randomness, fractional dimension, and fractional roughness), particle size, particle aspect ratio, particle shape (spherical and ellipsoidal), orientation angle, particle softness, and geometrical structure (solid and hollow) were considered as primary variables in constructing particles. Then, the interaction of assembled particles was simulated according to the rippled particle theory, fractal geometry theory, and three-step model combined with the surface element integral technique. Overall, it was discovered that the shape of particles played a critical role in controlling the interfacial behavior of particles and ellipsoidal particles had more interaction than spherical ones did. The present numerical model also predicted that deformable particles interact more aggressively than rigid particles. Additionally, the simulated results showed that the constructed hollow deformable particles were more easily aggregated compared with the solid ones. As the present work included important parameters of particles found in naturally or industrially produced colloidal systems, such as sludge particles, bacteria, or viruses, the results of this work will provide a guideline for simulating the behavior of such colloidal systems accurately, which can be used in the design of industrial processes or understanding behavior of natural phenomenon.

ACKNOWLEDGEMENTS

Table of contents

Chapter 4: Interfacial interactions of rough spherical surfaces with random topographies 78

Chapter 5: Interfacial interactions of rough ellipsoidal particles with random surface asperities 114

Lists of Tables

Lists of Figures

Chapter 1: Introduction

1.1 Overview

The endless water demand causes huge concerns in the world currently due to population growth, urbanization and higher living standards [1]. Groundwater, surface water and wastewater contained dissolved and suspended particles and contaminants in colloidal forms. The colloidal suspensions may contain organic substances, metal oxides, insoluble toxic compounds, stable emulsions and turbidity-producing substances [2]. To treat such water resources, the ability of particle transportation and stability of the suspension systems played key roles. For example, with coagulation as the most important physical and chemical operation, the particles are removed from water to produce drinking water [1]. In addition to removing turbidity from water, coagulation or flocculation is beneficial for eliminating bacteria and other living cells suspended in the water [3]. Moreover, the purified water is widely used to produce beverages, where the flavor and nutrient retention are controlled by the dispersion stability of beverage suspensions [4, 5].

As the suspended particles varied in source, charge, size, shape and density, the correct application of coagulation and flocculation depend on these factors. Suspended particles in water are negatively charged, and because they have the same type of surface charge, they repel each other when they approach in suspension systems. Therefore, unless proper techniques are used, suspended particles will remain in suspensions and will not separate from water. Therefore, the removal of particles is challenging due to their complex natures, and colloidal and charged properties. To resolve this challenge, the mechanism of controlling interfacial behaviors of particles should be explored. The primary step in identifying the removal or suspension mechanism is to better understand the interfacial interactions of particles in suspension systems. Accurate knowledge of the interaction energy between two surfaces is critical for understanding various colloidal and interfacial phenomena, including particle deposition, heterocoagulation, and transport of colloids and macromolecules in porous media [6-8].

Physical experimentation is acceptable if they can accurately explain physical phenomena and they can be carried out under accepted conditions. However, this cannot always be achieved for studying colloidal systems under desired conditions. For example, the investigation of interaction between

biological cells [9] and colloidal particles [10], experimental works may be time-consuming, difficult and dangerous to carry out. In these cases, it is necessary to construct a mathematical model that expresses a mathematical representation of the relationship between the variables of the system of interest. Many types of models are used to represent a wide variety of physiological systems in very diverse simulation applications. Applying numerical models to predicted results could provide accurate predictions. For examples, areas in wastewater treatment that benefit from modeling and simulation include membrane fouling [11], and membrane surface design [12].Additionally, the dispersion stability of emulsions could be monitored by constructed models [5, 13]. Therefore, the numerical (theoretical) models could make great contributions to helping better understand the mechanisms of interfacial interaction between surfaces of material.

Derjaguin, Landau, Vervey, and Overbeek (DLVO) developed the theory of colloidal stability that currently represents the cornerstone for the understanding of the interactions between colloidal particles and their interfacial behaviors [14]. This theory has been applied tremendously to rationalize the interaction forces between interfaces of particles or substrates and explain the mechanism of particle coagulation, deposition and dispersion. This theory is based on the additional assumption of the dispersion and electric double layer interaction, which include the van der Waals attraction force and electric repulsion force [15]. Nevertheless, the DLVO theory does not consider the short-range interactions that are critical for colloidal particle adhesion. The short-range interactions primarily contain Brownian motion forces and hydrophobic/hydrophilic interactions. The analysis of hydrophobic/hydrophilic interactions provides a molecular thermodynamic framework for identifying the mechanism of interaction that leads to the unique properties of the colloidal surface [16]. Thus, many researchers modified the classic DLVO theory to include non-DLVO factors [17, 18]. In this context, the classical DLVO theory was further developed to the extend-DLVO (XDLVO) theory with considering the non-DLVO forces. However, there are reports that the XDLVO theory would overestimate the interfacial interactions of a mixed system of soft and hard particles, for example, bacteria interacting with a quartz surface [19], which has been related to the surface morphological properties of particles.

Although recognized as a possible source of discrepancies between theoretical and experimental observations since the inception of DLVO theory [20], the effect of surface morphology and chemical

heterogeneity on the interaction energy between colloidal particles and surfaces has only been observed recently and began to attract attention [21, 22]. The rapid improvement of manufacturing technology has led to the fabricating of surfaces with desired roughness and shape at nanoscales [23, 24].

Natural surfaces have generally rough surfaces [21] with various surface topographies (arranged and random roughness). Also, particles in natural or industrial suspensions can have soft or hard structures [25]. Considering the impacts of geometrical structure and softness of particles in understanding the interaction of particles will improve the accuracy of simulations Therefore, a comprehensive simulation work to relate the impact of particle surface properties (including softness and random structures) on the interaction of particles will provide better understanding of particle interaction in environment and industrial settings.

The main goal of this dissertation was to construct the rough particle with various shapes and evaluate the effects of constructing parameters on particle interaction.

1.2 Novelty

The present thesis improved the accuracy of numerical predictions in particle interaction by considering the effects of surface morphologies (uniformly and randomly) for the first time. Additionally, this thesis provided a new model to generate the rough particles with ellipsoidal shapes and to assess interaction energy between particles. Also, a novel numerical model was developed for predicting the deformation of particles and interaction of deformable particles with a rough surface topography.

1.3 Objectives

The overall objectives of this study were to

1. construct a numerical model to simulate uniform asperity shape for representing asperity on rough surface;

2. investigate the effects of asperity ratio, asperity number on particle interactions;

3. investigate the effects of particle size particle aspect ratio, and particle orientation on particle interactions;

4. construct a numerical model to simulate the random asperity size on particle surface;

5. investigate the effects of fractal dimension, fractal roughness, and randomness on the surface of

particles on particle interactions;

6. construct a numerical model to simulate the ellipsoidal particle with randomly rough surface morphology;

7. investigate the effects of ellipsoidal particle shape, aspect ratio, particle orientation on interfacial interaction between ellipsoidal particles;

8. investigate the effects of randomly rough constructed surface on the interaction of ellipsoidal particles;

9. construct a numerical model to simulate soft particles; and

10. investigate the effects of particle size, surface tension, fractal dimension, and fractal roughness on particle deformation and interaction of soft particles.

The following chapters are presented in this thesis in order to address the proposed objectives.

Chapter 1 is the introduction (present chapter) that provides a brief discussion of the thesis.

Chapter 2 provides a brief introduction to the (X)DLVO theory and SEI technique for simulating particle interactions. The literature summarized the numerical methods for constructing different shapes of particles, surface morphologies of rough surfaces and approaches for evaluating interaction energy discussed in past studies.

Chapter 3 introduces a novel numerical method to evaluate the particle interaction with uniform asperities. The effects of asperity ratio, asperity number, particle size and particle orientation on particle interactions were evaluated. The simulated results showed that the total interaction energy between particles decreased with increasing the asperity ratio and number but increasing with particle size.

Chapter 4 demonstrates a method to simulate particle interaction with randomly constructed surface topographies. The effects of randomness, fractal dimension, and fractal roughness on particle interactions were evaluated. The predicted results showed that the total interaction energy increased with elevating the value of fractal dimension but decreased with fractal roughness.

Chapter 5 illustrates a numerical method to simulate the randomly rough ellipsoidal particle interactions. The effects of particle shape, particle size, particle orientation and surface morphology on particle interactions were evaluated. The main results showed that the total interaction energy decreased with increasing the aspect ratio and orientation angle of ellipsoidal particles. Additionally, the interaction energy generated by ellipsoidal particles was stronger than that of spherical particles.

Chapter 6 demonstrated a novel method to simulate the interaction of the rough and soft particles. The

effects of surface tension, particle size, and surface morphology on particle deformation and interactions were evaluated. The main results showed that the increased particle size would strengthen the deformability of deformable solid and hollow particles and their potential interaction. Moreover, the rougher surface would increased the deformability of surface.

Chapter 7 provides conclusions and suggestions for future research.

Chapter 8 provides the supplementary materials of previous chapters.

1.4 The list of publications

Chapter 2 is under review in Chemical Engineering Journal.

Chapter 3 has been published in the Journal of colloids and interface science

Lu, D., & Fatehi, P. (2021). A modeling approach for quantitative assessment of interfacial interaction between two rough particles in colloidal systems. Journal of Colloid and Interface Science, 587, 24-38.

Chapter 4 has been published in Colloids and Surfaces A: Physicochemical and Engineering Aspects

Lu, D., & Fatehi, P. (2022). Interfacial interactions of rough spherical surfaces with random topographies. Colloids and Surfaces A: Physicochemical and Engineering Aspects, 642, 128570.

Chapter 5 has been published in Chemical Engineering Science

Lu, D., & Fatehi, P. (2022). Interaction of rough ellipsoidal particles with random surface asperities in colloidal systems. Chemical Engineering Science, 260, 117869.

Chapter 6 is under review in the journal of Colloid and Interface Science

1.5 References

[1] M. Elimelech, W.A. Phillip, The future of seawater desalination: energy, technology, and the environment, science, 333 (2011) 712-717.

[2] N. Prakash, V. Sockan, P. Jayakaran, Waste water treatment by coagulation and flocculation, International Journal of Engineering Science and Innovative Technology, 3 (2014) 479-484.

[3] F. Renault, B. Sancey, P.-M. Badot, G. Crini, Chitosan for coagulation/flocculation processes–an eco-friendly approach, European Polymer Journal, 45 (2009) 1337-1348.

[4] A. Vilela, F. Cosme, T. Pinto, Emulsions, foams, and suspensions: the microscience of the beverage industry, Beverages, 4 (2018) 25.

[5] S. He, M. Tang, H. Sun, Y. Ye, X. Cao, J. Wang, Potential of water dropwort (Oenanthe javanica DC.) powder as an ingredient in beverage: Functional, thermal, dissolution and dispersion properties after superfine grinding, Powder Technology, 353 (2019) 516-525.

[6] H. Kihira, E. Matijević, An assessment of heterocoagulation theories, Adv. Colloid Interface Sci., 42 (1992) 1-31.

[7] S. Bhattacharjee, A. Sharma, Apolar, polar, and electrostatic interactions of spherical particles in cylindrical

pores, Journal of colloid and interface science, 187 (1997) 83-95.

[8] M. Elimelech, C.R. O'Melia, Effect of particle size on collision efficiency in the deposition of Brownian particles with electrostatic energy barriers, Langmuir, 6 (1990) 1153-1163.

[9] J. Marra, Direct measurement of the interaction between phosphatidylglycerol bilayers in aqueous electrolyte solutions, Biophys. J., 50 (1986) 815-825.

[10] V. Rangari, Polymer nanocomposite materials for structural applications, Advances in Nanocomposites-Synthesis, Characterization and Industrial Applications, (2011) 61-84.

[11] X. Cai, L. Shen, M. Zhang, J. Chen, H. Hong, H. Lin, Membrane fouling in a submerged membrane bioreactor: An unified approach to construct topography and to evaluate interaction energy between two randomly rough surfaces, Bioresour. Technol., 243 (2017) 1121-1132.

[12] D. Lu, P. Fatehi, A modeling approach for quantitative assessment of interfacial interaction between two rough particles in colloidal systems, Journal of Colloid and Interface Science, 587 (2020) 24-38.

[13] P.E. Priepke, L. Wei, A. Nelson, M. Steinberg, Suspension stability of Illinois soybean beverage, J. Food Sci., 45 (1980) 242-245.

[14] G. Trefalt, M. Borkovec, Overview of DLVO theory, (2014).

[15] Z. Adamczyk, P. Weroński, Application of the DLVO theory for particle deposition problems, Adv. Colloid Interface Sci., 83 (1999) 137-226.

[16] S. Utiramerur, M. Paulaitis, Cooperative hydrophobic/hydrophilic interactions in the hydration of dimethyl ether, The Journal of chemical physics, 132 (2010) 04B607.

[17] C.V. Chrysikopoulos, V.I. Syngouna, Attachment of bacteriophages MS2 and ΦX174 onto kaolinite and montmorillonite: Extended-DLVO interactions, Colloids Surf. B. Biointerfaces, 92 (2012) 74-83.

[18] M. Zhang, B.-q. Liao, X. Zhou, Y. He, H. Hong, H. Lin, J. Chen, Effects of hydrophilicity/hydrophobicity of membrane on membrane fouling in a submerged membrane bioreactor, Bioresour. Technol., 175 (2015) 59-67.

[19] S.L. Walker, J.E. Hill, J.A. Redman, M. Elimelech, Influence of growth phase on adhesion kinetics of Escherichia coli D21g, Appl. Environ. Microbiol., 71 (2005) 3093-3099.

[20] S. Bhattacharjee, C.-H. Ko, M. Elimelech, DLVO interaction between rough surfaces, Langmuir, 14 (1998) 3365-3375.

[21] X. Cai, L. Yang, Z. Wang, M. Zhang, L. Shen, H. Hong, H. Lin, G. Yu, Influences of fractal dimension of membrane surface on interfacial interactions related to membrane fouling in a membrane bioreactor, Journal of colloid and interface science, 500 (2017) 79-87.

[22] M. Zhang, H. Hong, H. Lin, G. Yu, F. Wang, B.-Q. Liao, Quantitative assessment of interfacial forces between two rough surfaces and its implications for anti-adhesion membrane fabrication, Separation and Purification Technology, 189 (2017) 238-245.

[23] D. Gamzina, H. Li, L. Himes, R. Barchfeld, B. Popovic, P. Pan, R. Letizia, M. Mineo, J. Feng, C. Paoloni, Nanoscale surface roughness effects on THz vacuum electron device performance, IEEE Transactions on Nanotechnology, 15 (2015) 85-93.

[24] H. Jeon, C.G. Simon Jr, G. Kim, A mini-review: cell response to microscale, nanoscale, and hierarchical patterning of surface structure, Journal of biomedical materials research Part B: applied biomaterials, 102 (2014) 1580-1594.

[25] K. Danov, N. Denkov, D. Petsev, I. Ivanov, R. Borwankar, Coalescence dynamics of deformable Brownian emulsion droplets, Langmuir, 9 (1993) 1731-1740.

Chapter 2: Understanding interfacial interactions in colloidal particle system: a review

2.1 Abstract

Colloidal particles affect the coagulation and stability of colloidal systems that have applications in many fields, such as wastewater treatment, emulsions and suspensions, and surface coating. Also, particle interaction has been studied extensively to simulate several processes including particle deposition, dispersion, and adsorption. In the past, significant efforts have been made to simulate the interaction of particles in different systems for better design of colloidal systems, predict the behavior of colloidal systems under different conditions, and improve processes dealing with colloidal systems. Published reports indicated that interfacial interaction energy could be considered an indicator to monitor the interfacial interaction of suspended particles. The past review work made great efforts in summarizing the approaches for assessing the interaction of particles with smooth surfaces. However, as particles have different surface morphologies, different approaches were considered to simulate such particles in colloidal systems. Therefore, it is necessary to upgrade the recent progress of mathematic interaction models by considering various particle shapes and surface morphologies. In the present work, the numerical models to construct particles and surfaces with different geometrical shapes were summarized. In particular, the present work discusses the recent progress of numerical modeling studies on the construction of rough surfaces and particles, the interaction of rough particles and surfaces, and their advantages and limitations comprehensively. Also, the current challenges of simulating various shapes of asperities, rough non-spherical particle interaction, and potential applications of modeling works were described in this work. The numerical equations for constructing different shapes and various surface roughness were summarized and their applications were discussed. Also, future directions and research gaps are suggested in this work.

Key words: Colloidal particles, rough surface, interfacial interaction, simulation

2.2 Introduction

Colloidal systems have significant impacts on industry and day-to-day life, for example, dairy [1], oil [2], and mineral systems [3]. To control colloidal systems, modeling studies have been carried out to understand the interaction of colloidal particles extensively. In this case, the most influential model of colloidal particle interaction was introduced by Dejaguin, Landau, Verway, and Overbeek which is known as the DLVO theory. This theory explains the interaction of particles based on van der Waals attraction force and electric repulsion force that impact the electric double layer of particles influencing their overall coagulation or dispersion in colloidal systems [4]. This theory has been used as a milestone to describe the interaction of colloidal particles in many applications including wastewater treatment [5, 6], oil recovery [7], drug delivery [8], mineral floatation [9], surface coating [10], bacterial deposition [11], and dye removal [12].

Despite its vast applications, the DLVO theory has a shortcoming: the DLVO theory does not consider the short-range interactions that are critical for colloidal particle adhesion. The short-range interactions primarily contain Brownian motion forces and hydrophobic/hydrophilic interactions, which have been considered non-DLVO factors [13, 14]. The analysis of hydrophobic/hydrophilic interactions provides a molecular thermodynamic framework for identifying the mechanism of interaction that leads to the unique properties of the colloidal surface [15]. Van Oss proposed a new concept to extend the classic DLVO theory, called the XDLVO theory, to include hydrophobic interaction. The XDLVO theory involves the electrical double layer interactions (EL), polar interactions (AB), and the Lifshitz-van der Waals (LW) interactions [16]. Based on the XDLVO theory, the total interfacial energy between colloidal particles could be divided by Lifshitz-Vander Waals (LW), electrostatic double layer (EL), and acid-base (AB) interaction energies [17-20]. These interactions have been depicted in Figure 2.1. As shown, when two particles approach, the electrostatic repulsion energy decreases but the energies of van deer Waals and hydrophobic interaction increase. Therefore, the summation of these forces will result in increased total interaction energy. If DLVO theory is considered, the primary maximum is significant. If XDLVO theory considered, the energy profile would generate a deeper primary minimum. It should be noted that the primary maximum represents the dispersion stability of the colloidal systems while the primary minimum represents the ability of particle attachments and coagulations. Therefore,

to generate a stable suspension or a fast coagulation understanding, and maybe changing, primary minimum and maximum of different systems is crucial. It should be stated that the difference between DLVO and XDLVO is primarily on the altered compositions of attraction energy, where the XDLVO energy profile generates a deeper primary minimum but a smaller energy barrier of the primary maximum.
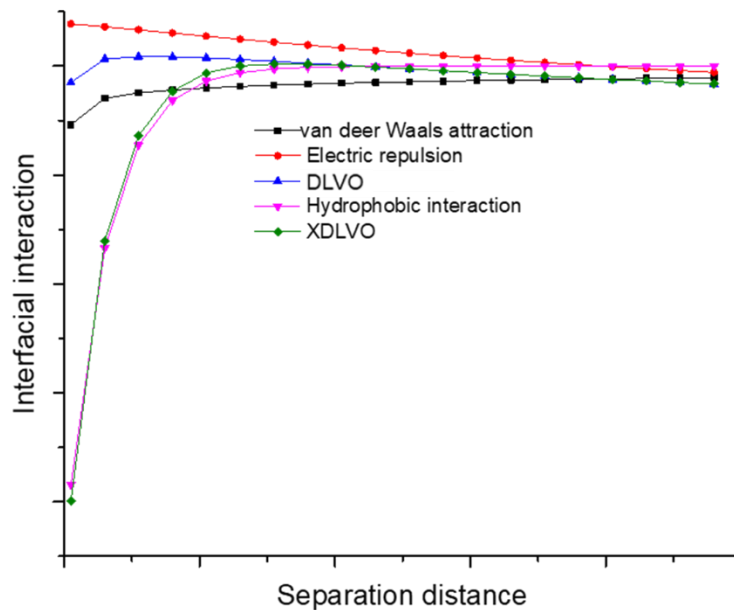
Figure 2.1. The comparison of interaction energy predicted by DLVO and XDLVO theories

Over the past decades, significant progress has been made in understanding the mechanism of colloidal particle interactions for different systems [12, 21-25]. These advancements are attributed to the development of new methods that describe the physicochemical characteristics of altered colloidal systems more accurately so that such colloidal systems can be controlled or designed better. With these significant contributions, the myriad biological, chemical, and physical phenomena controlling the interactions between particles and macro plane surfaces with nano-scale heterogeneity were explored [26]. Also, the colloidal interaction between charged spherical particles and planes has been widely studied [27-29].

Nevertheless, most colloidal particles have rough surface morphologies and irregular geometries. There are reports that the DLVO theory would not be able to fully characterize the interfacial behaviors of such particle systems, for example, bacteria interacting with quartz surface [30], and collectors interacting with minerals in the froth flotation of the mining industry [31]. Therefore, the inclusion of

9

particle geometry and surface properties would be an alternative to improve the accuracy of DLVO in predicting the behavior of such colloidal systems.

Previous literature review studies summarized the progress in theoretical and experimental works for evaluating the interaction between particles. Liang and coworkers reviewed the interaction forces between particle and surface under the framework of DLVO theory and listed the direct measurements of the interaction forces [32]. Taboada-Serrano and coworkers summarized the recent contributions to the understanding of particle aggregation from the molecular approach and DLVO theory [33]. Li and coworkers provided an overview of the importance of interfacial forces in suspended systems and discussed the roles of each force (e.g., electric repulsion force and van deer Waals attraction force) at various stages of colloidal self-assembly [34]. Lu and David reviewed three classes of interacting colloidal particles (crystals, glasses, and gels) and the models to predict their interfacial behaviors [35]. Semenova reviewed some recent advances in the use of diverse protein-polysaccharide interactions in the design of colloidal particles [36]. However, the rapid improvement of manufacturing technology has led to the fabricating of surfaces with desired roughness and patterns at nanoscales. The previous review works mainly summarized the studies on smooth particle interaction without considering the impacts of surface morphologies and the geometrical structure of particles [32-38]. Recent modeling studies demonstrated that the geometrical shape and surface roughness of particles significantly influenced their interactions [39, 40]. However, the previous review studies did not summarize recent advances in the numerical methods to construct rough surface morphologies and the information about the advantages and disadvantages of these modeling works is still lacking. In other words, despite great progress in simulating the interaction of rough surfaces, literature lacks the strategies for evaluating different approaches for predicting the interaction energy of rough particles. Therefore, it is necessary to have a comprehensive review to update the performance of the numerical models for simulation interactions between rough surfaces. This review paper focuses on elaborating on 1) the methodologies used for constructing different three-dimensional particles and altered rough surface morphologies applied for demonstrating interaction of particles and 2) the comparison between different approaches and their applications. This review paper also discussed the challenges and future works in current modeling studies. As the information of constructing various shapes of asperities in current literature is still lacking, the present review could not discuss the numerical methods in this field. Additionally, the

modeling approach of non-spherical particle interaction considering the impacts of surface morphologies was limited, therefore, this literature review work could not summarize the models discussing this topic. Finally, this review work also suggests the potential application of the generated models.

2.3 The methodologies of constructing smooth particles with different geometries

Particle shape has been identified as an essential physical parameter that has a tremendous influence on the interfacial interaction of nanoparticles in colloidal systems, such as particle attachment, dispersion, and deposition. Constructing particles is an important aspect of particle interaction studies. As the circular shape and planer surface is general and simple, Table 2.1 did not include the construction method for these two geometries. Other shapes of particles that are available in the literatures were tabulated in Table 2.1.

Table 2.1 The constructing methods for different shapes of particles

Symbol	Particle shape	Equation	Important parameters	Significant impacts	Particle types	Reference
A1	Ellipsoidal shape	$r = \left[\dfrac{sin^2\theta cos^2\varphi}{a^2} + \dfrac{sin^2\theta sin^2\varphi}{b^2} + \dfrac{cos^2\theta}{c^2} \right]^{-1}$	the semi-axes of the ellipsoid directed along the x, y, and t z-axes	Ellipsoidal particles showed stronger interaction energy than circular shape particle	Protein, cell, virus	[40]
A2	Rod-like particle	$S = 2\pi c^2 + (\dfrac{2\pi ca}{e})sin^{-1}e$	the minor semi-axis, a is the major semi-axis, and e is the ellipticity of a rod-like particle	Rod-like particles produced a higher energy barrier if $a > c$	clay colloids	[41-44]
A3	Cylinder-shape	$D = H + Lcos\varphi + asin\varphi$	the closest distance between particle and collector surface; the distance between particle center and collector surface	The orientation angle of cylinder-shaped particles has significant effects to impact interaction energy	Carbon nanotubes; Cellulose	[45, 46]
A4	Pear-shaped and peanut-shaped	$\varphi = \dfrac{\pi d_{eq}^2}{SA}$	the surface area of the volume-equivalent sphere; the number of superposed ridges	Non-spherical particles produced higher critical flux than spherical particles	Polystyrene foulant particles	[47]

A5	Superellipsoid	$(\left\|\frac{x'}{r_x}\right\|^r + \left\|\frac{y'}{r_y}\right\|^r)^{\frac{n}{r}} + \left\|\frac{z'}{r_z}\right\|^n = 1$	the principal semi-axes of the particle and n and r are parameters that define the particle shape	The resulting potential is a function of the minimum distance between surfaces and the particle's local Gaussian curvature at the minimum distance position.	Polymer colloids	[48]
A6	Cuboidal particle	$\left(\frac{x}{b}\right)^n + \left(\frac{y^n + z^n}{a^n}\right) = 1$	the principal semi-axes of the particle	more robust capillary interactions for increased particle aspect ratios	Airborne particles	[49, 50]
A7	Super quadrics	$f(x,y,z) = \left(\left(\frac{x}{a_1}\right)^{\frac{2}{\varepsilon_2}} + \left(\frac{y}{a_2}\right)^{\frac{2}{\varepsilon_2}}\right)^{\frac{\varepsilon_2}{\varepsilon_1}} + (\frac{z}{a_3})^{\frac{2}{\varepsilon_2}} - 1$	the principal semi-axes of the particle	a drastic improvement in the accuracy of simulations by using super-quadric particles instead of circular elements	Airborne particles Red blood cell	[51, 52]

Generally, the particle shape can be divided into two main parts in colloidal system analysis: spherical and non-spherical. Past modelling work mainly assumed that particles have circular shapes and avoided the analysis of particle shape effects on particle interactions [53-55]. Nevertheless, the interfacial interaction produced by particles is significantly affected by the shapes of particles in colloidal systems. As shown in Table 2.1, one model applied implicit equations to construct ellipsoidal shape particles (A1), which could generate stronger interaction energy than the spherical particles [40]. The main reason for this phenomenon is that, at a constant equivalent size. ellipsoidal shapes have a larger interaction area between particles compared to circular shapes. As the aspect ratio controls the ellipsoidal shape, the ellipsoidal particles could have altered shapes affecting particle interaction differently. The rod-like particle (A2) could be a typical example of ellipsoidal particles if the aspect ratio of the semi-axis of the ellipsoidal particle were extremely large. The rod-like particles would develop different interactions from spherical particles depending on the ratio of their semi-axis [41-44]. The non-spherical particles exist in colloidal systems. One typical type of non-spherical particle is cylinder-shaped particle (A3) that could be simulated. As A3 particles have three areas, the orientation of these particles greatly influences their interaction in colloidal systems [45, 46]. Therefore, assuming cylindrical shape particles found in colloidal systems as spherical particles in simulation studies would generate substantial inaccuracy. The pear and peanut shape particles were found in polystyrene foulant particles (A4) [47], which produced a stronger flux than the regular spherical particles did on the membrane surface. Torres-Diaz and coworkers established an equation with trigonometric function to describe a super ellipsoidal particle (A5), where the particle shape was changed from a regular spherical

shape to a cube with a different ratio of shape parameters [48]. The potential perspectives in Torres-Diaz and coworkers' work would help to model a wide variety of natural and synthetic aspheric and anisotropic colloidal particles in environmental, biological, and advanced material applications. As shown in A6, the cuboidal particles could also be defined numerically by different equations. The aspect ratio of particles changed with the various values of shape parameters, and compared to the spherical particles, the cuboidal particles showed a larger adhesion force between particles [49, 50]. Another model to simulate non-spherical particles is to apply continuous function representations (CFR) to model super quadric (A7). Nevertheless, to date, only symmetric particles have been simulated using this equation, and the CFR still faces considerable challenges to model arbitrary irregular particles [56]. The above models provided mathematical formulations to model different smooth particles in colloidal systems, which could be useful to simulate systems of smooth non-spherical shaped colloids, such as gold particles [57] or TiN particles [58]. Compared with the above construction models, the models to construct ellipsoids could be useful for modeling different shapes of particles by changing the construction parameters only in one equation, such as A5, which will facilitate the comparisons of the interaction of particles with different shapes. However, the natural surface is rarely smooth. The previous numerical models of constructing non-spherical particles mainly assumed the constructed particles had a smooth surface.

2.4 The methodologies of constructing rough surface

The natural particles have rough surface morphologies, which could significantly affect their predicted interaction energy. Surface topography plays a critical role in the lubrication, contact, and wear behavior of materials [59]. Therefore, considering the rough surface in the calculation process of prediction interfacial interaction is important.

Typically, rough surfaces can be generated experimentally and numerically. Although experimental roughness analysis of surfaces is important, there might exist limitations in the experimental design of roughness assessment, for example, the complicated process to modify the roughness or asperity shape of membrane surface [60]. To address this challenge, numerical simulations are conducted extensively in the roughness assessment of surfaces. In this section, we summarized techniques that provide fairly realistic models of simulating rough surfaces.

2.4.1 Generation of a roughly planar surface

Numerical methods for simulating the characteristics of the rough planar surface provide a convenient method to achieve the discrete data of modelling surfaces. The simulation of a rough surface is usually based on controlling two parameters on the surface: the mean of the average height and the mean of the density of asperities. A host of methods were applied to create asperity distribution on the smooth surface to generate rough surfaces [39, 61, 62]. Table 2.2 summarizes the construction approaches for planar surfaces with rough topography.

Table 2.2 The construction methods of the roughly planar surfaces

Symbol	Constructing method	Equation	Important parameters	Significant impacts	Application	Reference
B1	Surfaces with orthogonal arrays of asperities were generated as meshes over an area	$cos\theta_{cylindrical} = -1 + \phi_S(cos\theta_Y + 1)$ $cos\theta_{hemispherical-top} = -1 + \phi_B(cos\theta_Y + 1)$	the ideal contact angle (Young's angle) the solid fraction of cylindrical pillars the ratio of the area of the asperity bases over the total area	Slender pillars are the most stable water-repellent texture; this same topography exhibited super hydrophilicity	Wetting application	[63, 64]
B2	Gaussian rough surfaces	$Z_{p,q} = \sum_{k=0}^{M-1} \sum_{l=0}^{N-1} \sqrt{\widetilde{S_{k,l}}} \exp\left(i2\pi\left[\emptyset_{k,l} + \frac{kp}{M} + \frac{lp}{N}\right]\right)$	the spectral density used for simulation roughness	Surface roughness increased with elevating spectral density	Wetting application Coating application	[65, 66]
B3	Gaussian rough surfaces	$Z = f(x, y)$ $= \frac{1}{L^2} \sum_{m=-\left(\frac{N}{2}\right)}^{\left(\frac{N}{2}-1\right)} \sum_{n=-\left(\frac{N}{2}\right)}^{\left(\frac{N}{2}-1\right)} F(k_{xm}, k_{ym})$ $F(k_{xm}, k_{ym})$ $= 2\pi L \sqrt{W(k_{xm}, k)} \{ \begin{smallmatrix} \frac{N(0,1)+iN(0,1)}{\sqrt{2}} & m,n\neq 0,\frac{N}{2} \\ N(0,1) & m\ or\ n=0,\frac{N}{2} \end{smallmatrix}$ $k_{xm} = \frac{2\pi m}{L}, k_{ym} = \frac{2\pi n}{L}$	the discrete Fourier transformation the number of superposed ridges	Surface roughness increased with elevating number of superposed ridges	Cleaning application	[67, 68]
B4	non-Gaussian rough surface	$S_S k_z = \frac{\sum_{i=-q}^{q} \theta_i^3}{\left(\sum_{i=-q}^{q} \theta_i^3\right)^{3/2}} S_S k_\eta$	the autocorrelation lengths in the two principal directions	Improving the agreement between the spectral characteristics of the generated surfaces	Solid contact application in mechanical design	[69, 70]

				and the prescribed values			

$$Sku_z = \frac{Sku_\eta \sum_{i=-q}^q \theta_i^4 + 6\sum_{i=-q}^{q-1}\sum_{j=i+1}^q \theta_i^2 \theta_j^2}{\left(\sum_{i=-q}^q \theta_i^2\right)^2}$$

$$R_{pq} = \exp\left[\ln(0.2)\sqrt{\left(\frac{p}{\beta_x}\right)^2 + \left(\frac{q}{\beta_y}\right)^2}\right]$$

ID	Name	Equation	Parameters	Surface roughness	Application	Ref
B5	Paraboloidal sine wave	$f(r,\theta) = S\sin\left(\frac{\pi r cos\theta}{2r_a} + \varphi\right)$	the asperity width; the roughness	The surface roughness decreased with increasing asperity width	Cleaning application; Membrane fouling control	[14]
B6	Periodic sinusoidal function	$z = P_x \cos\left(\frac{\pi x}{2w_x}\right) + P_y\cos\left(\frac{\pi y}{2w_y}\right)$	the asperity height; the frequency of asperities along the x-axis and y-axis	The surface roughness increased with elevating asperity height but decreased with increasing	Cleaning application; Membrane fouling control	[71]
B7	Weierstrass-Mandelbrot function	$Z(x) = G^{(D-1)}\sum_{n=n_l}^{\infty}\frac{cos2\pi\gamma^n x}{\gamma^{(2-D)n}}$	the feature-length scale of the surface with a constant value, the fractal dimension,	The surface roughness increased with elevating fractal roughness but decreased with increasing fractal dimension	Solid contact application in mechanical design; Cleaning application; Membrane fouling control	[72-75]
B8	Two variable Weierstrass-Mandelbrot function	$Z = L(\frac{G}{L})^{D_f-2}(\frac{ln\eta}{M})^{\frac{1}{2}}\sum_{m=1}^M\sum_{n=0}^{n_{max}}\eta^{(D_f-3)n}$ $* (\cos\phi_{m,n} - \cos(\frac{2\pi\eta^n(x^2+y^2)^{1/2}}{L}$ $* \cos\left(tan^{-1}(\frac{x}{y}) - \frac{\pi m}{M}\right) + \phi_{m,n}))$	the high-scale parameters independent of frequency (fractal roughness); the fractal dimension,	The surface roughness increased with elevating fractal roughness but decreased with increasing fractal dimension	Cleaning application; Membrane fouling control	[76, 77]

The asperities of hemispheric shapes distributed on a surface were constructed with the method of orthogonal arrays (B1), which simply involved the impacts of surface roughness in the calculation process and increased the accuracy of predictions. But natural products consist of surfaces with depressions and protrusions [63, 64, 78, 79]. The rough surface constructed by the B1 approach and its alternative methods did not consider the depression parts of the asperities. Therefore, the previous studies may not fully describe the surface morphology of naturally rough surfaces. Also, the predicted results may overestimate the actual interfacial interaction energy.

The rough surface could involve Gaussian and non-Gaussian rough surfaces based on the asperity height

distribution [80, 81]. Due to the excellent performance in numerical calculability and the reasonableness of Gaussian distribution in engineering applications, it was considered to represent the asperity height distribution of a nominally rough planer surface. For Gaussian rough surfaces, the fast Fourier transform (FFT) is widely applied, which provides convenience in characterizing the surface morphology. Wu [65], Hu and Tonder [82], and Newland [83] developed the FFT strategy for creating three-dimensional surface topographies (B2). This method provides a useful tool for modelling rough surfaces as long as the spectral density of the rough surface is identified. Nevertheless, Newland's approach may not be accurate in evaluating spectral density because the aforementioned method could not clarify the circular auto-correlation function (ACF) and circular spectral density. To resolve this problem, researchers applied the moving average (MA) time series with the nonlinear conjugate gradient method to generate rough surfaces [70]. However, the main restrictions for applying this method are that 1) this method is time-consuming, which would limit the simulation of a rough surface with complex textures; and 2) the sensitivity of the original value restricts the construction of the rough surface when considering various forms of the autocorrelation functions [69]. With these disadvantages, the Gaussian rough surface is still successfully applied in membrane cleaning applications. For example, Qu and coworkers developed the Gaussian surface simulation with discrete Fourier transform of the asperities height function (B3), which supported the randomness of the high fluctuations of the model surface [67]. With the help of the Johnson translator, the Gaussian input sequence can be transformed into an input sequence (Johnson translator system) with appropriate skewness and kurtosis to generate a non-Gaussian random surface [84]. Wang and coworkers proposed a method combining the Johnson translator system and the FFT [69]. A general example that represents a non-Gaussian rough surface is shown in Table 2.1 (B4). The proposed method considered the influence of truncation lengths and reduced the computation time of correlation lengths by simplifying the ACF. Although numerous mathematical functions could be applied in generating non-Gaussian surfaces, they should cover skewness–kurtosis planes and use as few expressions as possible. To address this challenge, the probability density function (PDF) based on the Johnson translation system was proposed to generate the non-Gaussian surface (B4) [85].

Although the above methods were successfully used for simulating the engineering surface with a high prediction accuracy, these simulation approaches involve complex formulations, which would result in a huge computational load for the quantification of interfacial interactions.

There are reports about the application of the sine function to represent surface roughness [86, 87], which would describe the protruding and depression parts of surfaces. Jacobs and coworkers applied a paraboloid and a sine wave to define a rough surface. In this case, the surface roughness is controlled by the amplitude and frequency of the sine wave [88]. Although this method provides a convenient method for characterizing the rough surface, this strategy is mainly suitable for two-dimensional surfaces, which would limit the construction of the three-dimensional rough surface. In this context, Zhang and coworkers established an equation to represent the pertinent statistical properties of the rough surface for three-dimensional surfaces (B5). This method was used for simulating the rough biomaterial surface and coarse aggregates with a convenient numerical model [89, 90]. In this method, the surface average roughness should be identified independently. If not identified experimentally or numerically, this strategy cannot represent the value of surface roughness. Alternatively, Zhao and coworkers have successfully simulated the rough planar surface with a periodic sinusoidal function. Considering a constant asperity size and use of sinusoidal shapes, Zhao and coworkers reported that the surface roughness increased with increasing the asperity height and asperity density (B6) as shown in Figure 2.2a [71]. The concept of this approach is to apply the sinusoidal function to assign the asperities on the x-axis and y-axis in a three-dimensional coordinate. This method overcomes the limits of the previous method (B5) requiring experiment data to support simulation, where the surface characters (e.g., asperity number and size) would directly generate surface roughness by numerical methods. In this context, Li and coworkers applied this approach to simulate the roughness of the polyvinylidene fluoride membrane [91].

Although the sine function provides simple simulation strategies, it cannot represent the whole nature of the rough surface because the sine function represents uniform asperities. To overcome this difficulty, a fractal geometry theory and Weierstrass-Mandelbrot function was applied to simulate the surface roughness and randomness of a flat surface three-dimensionally. As the simulated asperities had self-affine properties, the profile of a rough surface can be assumed to be continuous at an infinity small length [92] as shown in Figure 2.2b. Thus, the continuous and random asperities on the material surface could be represented by Weierstrass- Mandelbrot (WM) function (B7) [92]. The modified WM function was developed to be a fractal function for three-dimensional isotropic surface construction (B8) because the function involved in this approach correctly characterize the self-affinity surface, which would make

17

a surface with a pattern similar to that of a natural rough surface. For rough surfaces, such as rocks, the fractal dimensions of a three-dimensional (3D) surface could be resolved by the slope of the logography of the power spectrum of the two-dimensional profile [93].

A large number of studies have shown that the fractal features of randomly rough surfaces can be properly described by the fractal geometry theory, where the fractal dimension and fractal roughness have core roles in controlling surface roughness [94-96]. The fractal dimension is the parameter that represents the contour structure complexity on the randomly rough surface. Thus, the larger value of the fractal dimension implies more details in the contour structure of a surface. Fractal roughness is an amplitude coefficient, which affects the size of the contour on the rough surface [97]. Unlike Euclidean geometry, fractal geometry included points, curves, surfaces, and cubes with the integer dimensions of 0,1,2,3, respectively [93]. In addition, the fractal geometry provides new insight into the interface deformation where the fractal dimension can be used as a measure of surface stiffness [76]. Cai and coworkers applied the same theory to simulate the membrane surface and also concluded that the lower value of the fractal dimension represented a smoother membrane surface [5]. Fractal geometry methods are only suitable for the quantification of complex structures which cannot quantify simple structures.

(a)

(b)
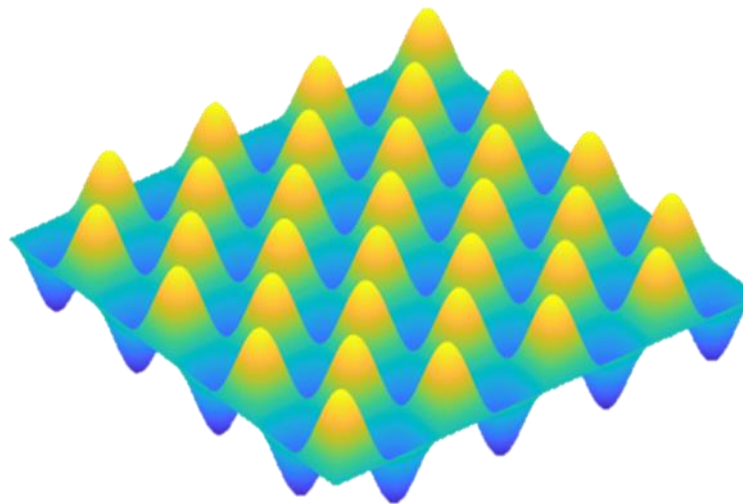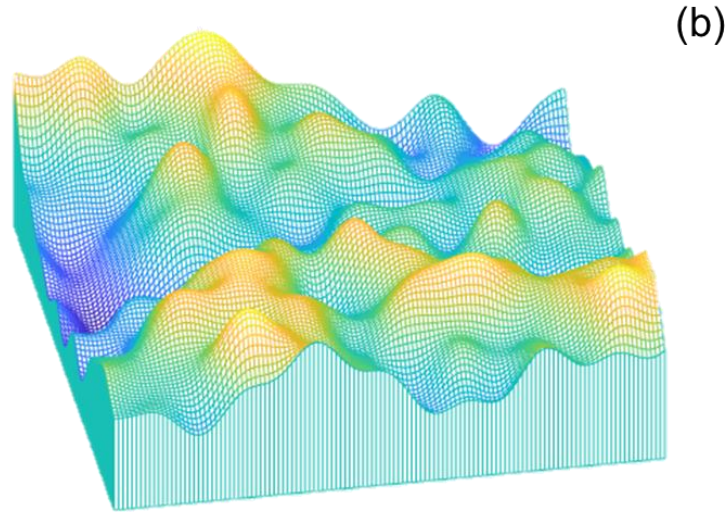
Figure 2.2. The three-dimensional sinusoidal rough planar surfaces generated by MATLAB (a) uniform rough flat surface (B6); (b) randomly rough flat surface (B7)

2.4.2 Generation of a roughly spherical surface

The roughly spherical surface could be created by extending the techniques described in constructing a planer surface. However, these techniques are complex due to the use of complex coordinate transformations. Table 2.3 summarized the contracting approaches of roughly spherical surfaces in literature.

Table 2.3 The constructing methods of the roughly spherical surfaces

Symbol	Constructing method	Equation	Important parameters	Significant impacts	Application	Reference
C1	Surfaces with orthogonal arrays of asperities were generated as meshes over an area	$\theta = 2n\pi(R + \epsilon_s)\,\epsilon_s$	the number density of asperity height of asperity	The surface roughness increased with increasing density and height of asperities	Mineral flotation	[98, 99]
C2	Periodic sinusoidal function	$R = r[1 + \lambda_\theta \cos(n_\theta \theta) + \lambda_\phi \cos(n_\phi \phi)]$	e asperity ratio asperity number	The surface roughness decreased with increasing asperity number and asperity ratio	Membrane fouling control	[39, 100, 101]
C3	A modified two-variable WM	$\Delta r = L(\frac{G}{L})^{D_f-2}(\frac{\ln\eta}{M})^{\frac{1}{2}}\sum_{m=1}^{M}\sum_{n=0}^{n_{max}}\eta^{(D_f-3)n} * (\cos\phi_{m,nmax+1} -$	fractal dimension	The surface roughness	Membrane fouling	[54, 102, 103]

	function	$\cos(\frac{2\pi\eta^n r \sin\theta}{L} * \cos\left(\varphi - \frac{\pi m}{M}\right) + \phi_{m,nmax+1}))$		fractal roughness	decreased with increasing fractal dimension but increased with increasing fractal roughness	control
C4	Gaussian distribution pross	$\Delta r = \frac{1}{L^2}\sum_{m=-(\frac{N}{2})}^{(\frac{N}{2}-1)}\sum_{n=-(\frac{N}{2})}^{(\frac{N}{2}-1)} F(k_{xm},k_{ym})\exp(ik_{xm}x - k_{ym}y)$ $F(k_x,k_y) = 2\pi L\sqrt{w}\begin{cases}\frac{N(0,1)+iN(0,1)}{\sqrt{2}} m,n \neq 0,\frac{N}{2}\\ N(0,1)\ m\ or\ n = 0,\frac{N}{2}\end{cases}$ $k_{xm} = \frac{2\pi m}{L}, k_{yn} = \frac{2\pi n}{L}$	number of superposed ridges applied to simulate rough surface	The surface roughness increased with an increase in the value of the number of superposed ridges	Membrane fouling control Colloids, bacterial, mechanical spheres	[68]

The basic concept of orthogonal arrays of asperities was proposed by Suresh and Walz (C1)[104], which included an element of smooth particle and a rough surface described by numerous and uniform hemispheres. Drelich and Patrick developed this approach with asperity coverage to predict the effects of surface roughness on repulsion energy barriers [99] (Figure 2.3a). Although Drelich and Patrick successfully predicted the asperity surface coverage that had less effect than the asperity radius on controlling interaction energy [99], the generated rough surface by this construction method could not fully reflect the realistic properties of the natural rough surface. In this approach, only the protruding parts of asperities were considered in the numerical simulation. However, the sunken part of asperities generated more surface area and provided significant effects on the particle interaction. Thus, the method proposed by Drelich and Patrick had some limitations in correctly predicting the total interaction energy in the interfacial interface. Alternatively, Bhattacharjee and coworkers applied the rippled sphere model based on its simplicity to provide a suitable equation for rough spherical surface directly (C2) [39]. This approach applied a spherical coordinate (r,θ,ϕ). The terms (n_θ, n_ϕ) and $(\lambda_\theta, \lambda_\phi)$ represented the frequencies and amplitudes of ripples along the θ and ϕ directions in the coordinate. The term r represents a radius of a smooth particle. Therefore, the procedures of C2 could generate a sphere with uniform asperities as shown in Figure 2.3b.

This construction approach has been successfully applied in the assessment of interfacial interaction between the membrane surface and a rough sludge floc [100, 101]. In addition, this method provided an opportunity for exploring a deeper insight into membrane fouling control. Recently, two rough

spherical surface interaction models were developed based on this construction method, which indicated that surface roughness significantly reduced the strength of interfacial interaction [105, 106]. The predicted results suggested that the surface morphology played an important role in affecting interfacial behaviors of the particle in suspension systems. The other studies articulated that the method for surface modelling is to construct a rough surface as a periodic sinusoidal function (C2) [6, 71] or a planar surface with hemisphere pillars (C1)[64]. Once the value of average statistical roughness could be resolved, the interface interaction could be obtained numerically [107, 108]. Although these strategies improved the construction of rough spherical surfaces, the characteristics of the constructed rough surface from these approaches hardly reflected the natural surface morphology of the rough particles. The natural rough surface exhibited randomly rough surface morphologies. Therefore, C1 and C2 had limits in their accuracy of predictions.

Alternatively, it is feasible to generate a rough surface according to the fractal geometry theory, which may represent the fractal characteristics of sludge flocs, for instance [101]. The WM function based on fractal geometry is widely used for generating the randomly rough planer surface [76, 93, 109]. Mei and coworkers developed a two-variable WM function to model the randomly rough spherical surfaces [101] (C3). This constructing method provided a more reasonable approach to simulating natural rough surfaces compared to previous works [100, 101]. The constructed particle was shown in Figure 2.3c, which captured the characteristics of natural rough surface morphologies. Nevertheless, the value of the fractal dimension (D_f) in this approach is usually unknown. The self-similarity of the natural fractal curves is approximate self- affinity [72], and the value of D_f is traditionally evaluated by image analysis [110] and the settling velocity test [111], which are time-consuming and complicated [112]. With the contributions of D_f measurement, the two variable WM function became an advanced and convenient simulation approach to construct three dimensional rough particles. However, this method involves the complex equations and could not characterize the simple structures of asperities.

Past literature studies have demonstrated that a rough surface could be considered a Gaussian surface whose height approximately follows a Gaussian distribution [113-115]. The Gaussian distribution of the dataset means that most data values are clustered in the middle range, with the rest tapering symmetrically towards the extreme [116]. For a given distribution, the parametric skewness indicates

that the distribution deviates from its symmetry, while the parametric kurtosis reflects the tail of the distribution. Due to this feature, Zhao and coworkers applied Gaussian distribution to generate a randomly rough spherical surface (C4) [68]. In this case, C4 is applicable to simulate not only sludge floc surface but also other randomly rough spherical surfaces including bacteria, colloids, and planets. Moreover, C4 applied root mean square surface roughness values as the input parameters instead of fractal parameters (C3), which could be achieved from microscope analysis of the AFM technique.
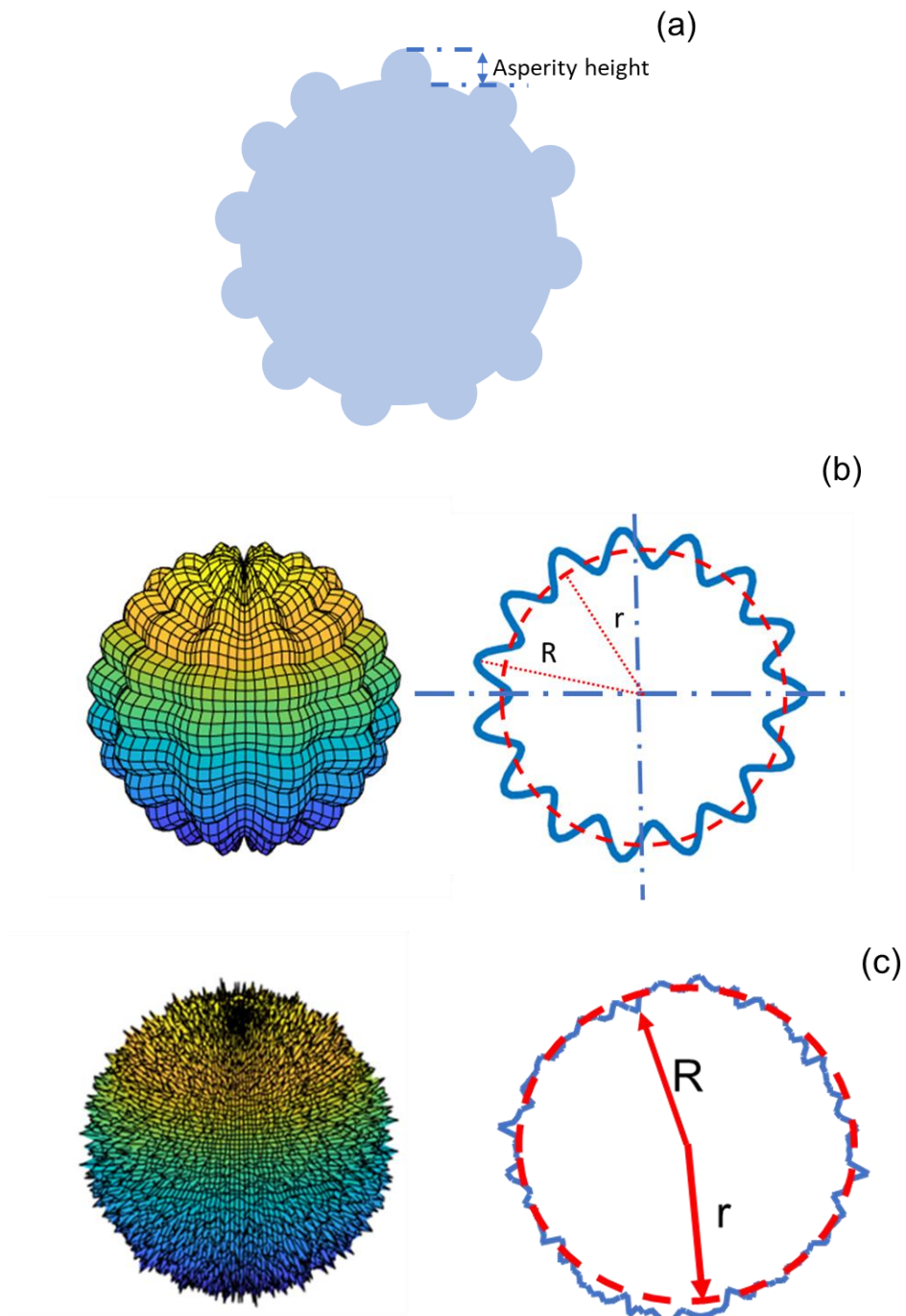
Figure 2.3. Constructed rough spheres (a) the rough sphere is covered with hemispherical asperities [79, 99]; (b) the 3D rippled rough sphere generated by MATLAB [53, 105]; (c) The 3D randomly rough sphere generated by MATLAB [54]

2.5 The quantitative interaction models and applications of interaction scenarios

Approximation in the calculation of the interfacial interaction energy is usually associated with anomalous prediction and calculation errors. The accurate simulation process could be achieved via rigorous mathematical calculations [117]. Therefore, an accurate model to simulate the suitable interaction scenario is necessary to evaluate the interaction energy between target surfaces. The different interaction scenarios and their comparisons are summarized in Table 2.4.

Table 2.4 The comparisons of techniques for simulating interaction energy between surfaces

Symbol	Interaction scenario	Method for generating surface roughness	Simulation technique	Key parameter	Key equation	Applied theory
D1	Smooth particle vs Smooth plate	/	Derjaguin's approximation	The separation distances	$F(h) = 2\pi R_{eff} W(h)$	DLVO potential [118-121]
D2	Smooth particle vs Smooth plate	/	Derjaguin's approximation	The separation distances	$F(h) = 2\pi R_{eff} W(h)$	Lennard-Jones potential [122, 123]
D3	Smooth plate vs Smooth plate	/	Parabolic approximation	The effective radius	$F(h) = -\dfrac{8\pi R_{eff}\Delta\gamma}{3}\left[\dfrac{\varepsilon^2}{d^2} - \dfrac{\varepsilon^8}{4d^8}\right]$	Lennard-Jones potential[124, 125]
D4	Smooth spherical particle vs Smooth spherical particle	/	Lattice Boltzmann model [126, 127]	The dimensionless center-to-center distance between two	$F_A = \dfrac{A}{6a_1}\left\{\dfrac{\dfrac{-4\lambda R_c}{[R_c^2 - (1+\lambda)^2]^2} +}{\dfrac{-4\lambda R_c}{[R_c^2 - (1-\lambda)^2]^2} + \dfrac{-2R_c}{R_c^2 - (1-\lambda)^2}\dfrac{-2R_c}{R_c^2 - (1-}}\right.$	Debye–Hückel approximation

				particles		
D5	Smooth particle vs Rough plate [64, 128]	Cylindrical pillars or hemispherical pillars were considered uniform asperities	SEI	The height of pillars	$U(h) = \iint \Delta G(h)dA$	DLVO potential
D6	Smooth particle vs Rough plate [19, 71, 128-130]	The sinusoidal function was applied to represent uniform roughness	SEI	The height of asperity	$U(h) = \iint \Delta G(h)dA$	DLVO potential
D7	Smooth particle vs Rough plate [131-133]	The sinusoidal function was applied to represent uniform roughness	SEI	The height of asperity	$U(h) = \iint \Delta G(h)dA$	DLVO potential
D8	Smooth particle vs Rough plate [134-136]	Two variable WM function was applied to represent randomly roughness	SEI	The fractal dimension	$U(h) = \iint \Delta G(h)dA$	DLVO potential
D9	Rough particle vs Smooth plate [79, 98]	Uniform hemispherical asperities covered	Derjaguin approximation	The height of asperity	$U(h) = -\frac{AR}{6}\left[\frac{1}{h} + 2\pi n h \ln\left(\frac{h}{h-\varepsilon_s}\right) - 2\pi n\varepsilon_s - \frac{n\varepsilon_s^2\pi}{h}\right]$	DLVO potential
D10	Rough	The	SEI	The	$U(h) = \iint \Delta G(h)dA$	DLVO

	particle vs Smooth plate [39, 100, 137]	sinusoidal function was applied to represent uniform roughness		asperity ratio	potential
D11	Rough particle vs Smooth plate[6]	Two variable WM function was applied to represent randomly roughness	SEI	The fractal dimension	$U(h) = \iint \Delta G(h)dA$	DLVO potential
D12	Rough particle vs Rough plate [108]	The sinusoidal function was applied to represent uniform roughness	SEI	The asperity ratio	$U(h) = \iint \Delta G(h)dA$	DLVO potential
D13	Rough particle vs Rough plate [54, 102]	Two variable WM function was applied to represent randomly roughness	SEI	The fractal dimension	$U(h) = \iint \Delta G(h)dA$	DLVO potential
D14	Rough particle vs Rough particle[53, 105]	The sinusoidal function was applied to represent uniform roughness	SEI	The asperity ratio	$U(h) = \iint \Delta G(h)dA$	DLVO potential
D15	Rough particle vs Rough particle	Two variable WM function was applied to represent randomly	SEI	The fractal dimension	$U(h) = \iint \Delta G(h)dA$	DLVO potential

	roughness					
D16	Smooth ellipsoid vs Smooth flat surface [42]	/	SEI	The orientation angle	$U(D,\varphi) = \int_0^{2\pi} \int_0^{\pi} \hat{n} \cdot \hat{k} \cdot E(h = D - Z) \cdot r^2 \sin\theta \, d\theta \, d\phi$	DLVO potential
D17	Smooth cylinder vs Smooth flat surface [46]	/	SEI	The orientation angle	$U(h) = \iint \Delta G(h) dA$	DLVO potential
D18	Smooth ellipsoid vs Smooth ellipsoid [49]	/	/	The orientation angle	$\dfrac{\Delta E}{\gamma a^2} = -3\pi(2\omega_1 + 2\omega_2)\left(\dfrac{\Delta u}{a}\right)^2 \left(\dfrac{d_{cc}}{a}\right)^{-4}$	Capillary potential
D19	Smooth pearlike particle vs smooth pearlike particle [47]	/	DA	The aspect ratio	$\Delta U_{LW} = 2\pi \Delta G_{LW} \dfrac{y_0^2 a_c}{h}$	XDLVO potential
D20	Smooth cuboidal vs Smooth cuboidal [138]	/	/	The orientation angle	$\Delta G_{da} = \gamma_{aw}(a^2 + (a^2 + 4ah)cos\theta)$	Detachment potential
D21	Smooth super ellipsoids vs Smooth flat surface	/	DA	The orientation angle	$U = \dfrac{2\pi}{\sqrt{\lambda_1 \lambda_2}} Q(h)$	DLVO potential

[48]

The model of smooth spherical particle interaction is commonly applied to simulate the interfacial behaviours of particles. Derjaguin's approximation (DA) provides a simple route for the interaction energy of the corresponding interactive energy per unit area between two infinite parallel flat panels [117]. Previous researchers developed DA by using the relatively simple sphere-plate geometry, which describes an accurate analytical expression for the potential interaction of the sphere and a plate [122, 123, 139] (D1 and D2). The DA method provides the fast calculation of interactions between two colloidal particles in solutions, which is important in industry or lab applications because it is a computational challenge to repeatedly calculate detailed interactions by solving numerically related theories in high-dimensional spaces [140]. Oversteegen and Lekkerkerker articulated that the DA method overestimated the simulation results for sphere-rod interaction, but the DA method provided accurate simulation results in sphere-disk interaction due to the generic intermediate behavior of disks [141]. Parabolic approximation (D3) was also widely applied in simulating smooth surface interaction [124, 125]. The parabolic approximation method offered the advantages of short dynamic response time, small steady-state fluctuation, small error probability, and good comprehensive performance. Nevertheless, a large number of required calculations would be involved in the simulation process. Lattice Boltzmann model (D4) has attracted increasing attention due to its inherent advantages, such as relatively easy handling of complex geometries, high efficiency of parallel computation, and capturing interactions between different phases/components at the mesoscopic level [126, 127, 142]. However, this model has some disadvantages, such as only considering a constant value for surface tension, which limits the analysis at different densities and temperatures [143]. Generally, considering the influence of surface morphology in predicting interfacial interaction energy would increase the accuracy of modeling results.

In the case of a smooth sphere-rough flat surface scenario, Martines and coworkers simulated asperities on the rough surface as cylindrical pillars or hemispherical pillars (D5) [64]. As the D5 did not consider the depression parts of asperities, the simulated predictions may underestimate the actual interaction

energy. To further develop D5, researchers applied the sinusoidal function (D6) to simulate the interaction energy between smooth particles and rough flat surfaces based on the SEI technique [19, 71, 128-130]. With the help of this method, the effect of rough surface properties on interfacial interaction was modelled. Model D7 applied another type of sine function to describe the roughness of a flat surface [131-133]. Lin and coworkers applied D7 to simulate the interactions between sludge particles and membrane surface and reported that a rough membrane generated a weaker interaction for sludge particles than a smooth surface [131]. As we discussed in previous sections, the natural surface has rarely uniform topographies. Previous work suggested that the randomly rough surface morphologies may have a strong anti-adhesion ability [102]. Therefore, the simulation of randomly rough surface morphology attracted attention in the numerical modeling community. The D8 model was constructed to resolve this interaction scenario with randomly rough surface morphology [134-136]. Based on the above approaches, the energy of rough particle-flat surface interaction could be evaluated and the relationship between surface morphology and interaction energy could be explored. Previous works demonstrated that the increased asperities number of the flat surface would significantly drop the interaction energy between rough particles and flat surface [19, 71, 128-130, 144]. The main reason for this phenomenon is that the surface roughness reduced the interaction area between a particle and flat surface. The numerical models (D6-D8) applied the SEI method considering the protrude and sunken parts of asperities in particle surface, which provides an accurate model to evaluate interaction energy and provide deep sight in adsorption or membrane fouling control applications.

In the case of rough particle-smooth flat surface interaction, the past studies simulated the spherical particle covered with hemisphere shape asperities (D9) [79, 98]. Zhu and coworkers simulated a magnesite particle with surface morphology of D9 and studied its interaction with a large bubble, and concluded that with increasing the asperities radius of the particle from 2 nm to 12 nm, the total interaction diminished [79]. Bhattacharjee and coworkers applied rippled particles theory and developed D10 combined with the SEI method to simulate interfacial interactions as shown in Figure 2.4a, which addressed the limitations of D9. Moreover, Bhattacharjee and coworkers included the comprehensive calculation process of the vector units to improve the accuracy of modeling prediction. D10 provides an important tool to analyze the effect of floc roughness in membrane fouling, and an effective membrane fouling control method could be proposed [137]. Past studies developed this

numerical model to consider the realistic properties of the naturally rough surface by applying the fractal geometry theory (Figure 2.4b). In the work explained in (D11), Zhang and coworkers provided the first evaluation of interaction energy between a randomly rough spherical surface and a smooth flat surface [54, 102]. This model is not only suitable for simulating the rough surface of flocs but also for microorganisms and colloids once their surface properties could be translated to numerical values. As the regular rough surface rarely exists in the natural environment, the simulation work from D11 provides more universal application prospects in simulation interfacial interaction compared to D5, which assumed the asperities had uniform shapes [39, 79]. However, the simulated results may underestimate the interfacial interaction energy between the particle and flat surface if the flat surface had a rough surface morphology as the proposed method avoided the sunken part of asperity and its influences. The models involved in this interaction scenario could be applied to monitor the adsorption rate or attachment efficiency in coating applications or surface modifications [145].

Research has progressed in investigating the interaction of two rough surfaces. In this respect, Hong and coworkers applied the sinusoidal function to simulate the rough flat surface (D12) [108], which was applied in simulating the interfacial behavior of sludge flocs in wastewater treatment. However, the randomness of asperities on the particle surface was not involved in the calculation process. To improve the model, the surfaces can be designed to have random morphologies using the WM function, for example [92, 146] (D13). Both of these methods demonstrated that if the surface amplitude increased, the total interaction strength within the separation distance range would decrease significantly. This result is reasonable because the increase in the asperity ratio would increase the surface roughness, which would also increase the separation distance between two opposing rough surfaces (Figure 2.4c)[53, 108]. Cai and coworkers simulated the mechanism of randomly rough membrane fouling control using D13 (Figure 2.4d) [54], which facilitated to identify of fouling behavior and formulation an effective fouling control strategy because the fractal dimension significantly controlled the texture of the randomly rough surface. Therefore, the modification of fractal dimension in membrane surface morphology could be considered the most effective method to control membrane fouling.

Quantifying the interfacial interaction between rough particles is an important step to understanding and control the interface behavior of protein, bacterial, colloids, or floc particles related to coagulation, dispersion, adhesion, membrane fouling, etc, processes. For this purpose, the interaction model of two

rippled particle interactions based on XDLVO theory was developed in previous studies (D14) (Figure 2.4e)[105, 147]. Through extensive efforts [105, 147], this interaction model claimed that the newly proposed method would further improve the accuracy of quantifying the interfacial energy between two rough spherical particles. Lu and Fatehi further developed D14 to construct two randomly rough particles (D15) and provided a model to describe the interaction of roughly spherical particles. The above approaches concluded that the decrease in the asperity size strengthened the interfacial interaction energy (Figure 2.4f), which is attributed to the structured topography of the surface [103]. The numerical models involved two rough particle interactions that could be applied in simulating the stability of suspension systems and the predicted interaction energy could work as an indicator to monitor the interfacial behavior of modeled particles.

Additionally, previous studies proved that the shape of particles had significant effects on particle interaction [148, 149]. Therefore, only considering the regular and circular shapes would not be sufficient to represent all nanoparticles in nature, which may reduce the accuracy of the prediction of the model if the particles owned uncircular shapes. The previous work built the mathematical model of ellipsoidal particle interaction (D16 and D18) and demonstrated the particle interaction energy decreased with increasing the orientation angle [40]. The particles with cylinder shapes were also modeled in the past work [46] (D17) and reported that the DLVO interaction energy decreased with increasing the orientation angle. The pear-like particle interaction under XDLVO theory was evaluated with the DA method (D19) and reported that the pear-like particles exhibited weaker attraction energy than spherical particles [47]. Moreover, the detachment energy of cuboidal particles (D20) was simulated in a previous study and reported that the increased size of cuboidal particles would increase the detachment energy [138]. The interaction energy between super ellipsoids was assessed by the DA method (D21), which reported that the minimum interaction energy could be observed when the super ellipsoids were perpendicular to the flat surface [48]. The interaction energy between super quadrics could be simulated by the method proposed in D21 because the fundamental concepts to construct super quadrics and super ellipsoids are the same, and only the shape parameters are different.

Although the previous studies made great contributions to simulating the interaction between non-spherical particles interaction, the surface morphology effects of non-spherical particles were excluded. According to the above discussion, surface roughness would impact the interfacial interaction between

surfaces. In reality, colloidal particles, especially biocolloids, such as proteins, viruses, and bacteria [40], would have non-spherical shapes. For such particles, the interaction energy becomes dependent on the direction and generates torque. This torque orients the particles in an energy-efficient configuration. Therefore, the development of the particle interaction model should be considered the rough non-spherical particle interaction in the future. Appling some numerical methods to generate a rough layer on the smooth non-spherical particles could be considered a novel strategy to assess the rough non-spherical particle interactions. The naturally occurring colloidal systems are full of particles of various geometric shapes. Considering the surface morphology effects on non-spherical particle interaction, the predicted results could characterize the interaction strength comprehensively.
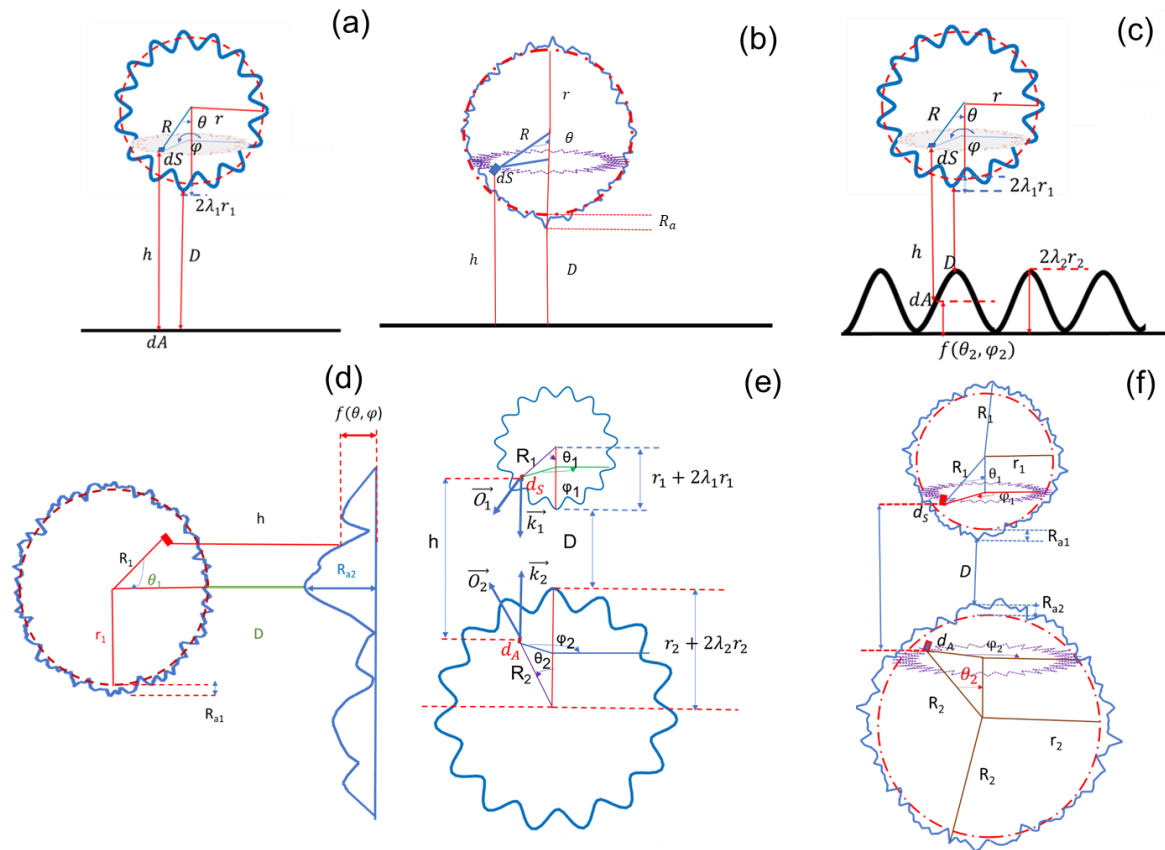
Figure 2.4. *The interaction scenario involved in previous modeling works.* Parameters involved in the interaction of *(a)* rough particles with a smooth plate [137]; (b) randomly rough particles with a smooth plate [6]; (c) rippled rough particles with a rough plate [108];(d) randomly rough particles with a randomly rough plate [54];(e) two rough particles with a uniform topographic [105]; and (f) two rough particles with a randomly topographic [103]

2.6 The future development and challenges

2.6.1 The different geometrical structures of asperities

Asperities could have different shapes in natural environments. For example, an scanning microscopy had showed that the surface topography of particles owned cone-shaped, or column-shaped of asperities [150]. Additionally, previous experimental studies provided evidence for asperities with parabolic, spherical, and cylindrical shapes [151]. However, the past numerical modeling studies only considered the asperities with hemisphere or needle-like structures. To further improve the accuracy of the prediction of modeling, the actual shape of asperities should be modeled in studying the interaction of particles. This is the necessary step to further improve the accuracy of modeling work related the simulating particle interaction.

2.6.2 The effects of surface morphology on particle interaction with irregular shapes

Future modeling studies should correctly simulate the interaction of non-spherical particles considering the actual particle shape and surface morphology. This modeling could provide valuable insights into the interaction and attachment of various particles including carbon nanotubes, nanowires, bacteria, hollow particles, and cylindrical solid particles. The constructed numerical models would be very important for industrial and environmental applications.

There are few theoretical developments in interfacial interaction for rough non-spherical particles, and the available results are only near continuum and free molecule asymptotic solutions [152], which shows that the influence of particle shape and orientation is significant. As most colloidal particles are not always spheres, the simulation models must use more data and better theories to fill this gap in knowledge of rough non-spherical particle interaction.

2.6.3 The potential applications

the presented modeling work has been widely applied in simulating the process of membrane fouling [5, 135], surface coating [153, 154], and particle coagulation [155, 156]. Despite their valuable

information, the modeling that included particle shape and surface morphologies has not been comprehensively used in any particular application, and future studies may expand on such applications. Nanoemulsions are kinetically stable colloidal systems with small droplet sizes. The composition and structure of nanoemulsions can be controlled for encapsulation and efficient delivery of biologically active lipophilic compounds [157]. Nanoemulsions have potential applications in the food industry for the delivery of colorants, nutraceuticals [158], and antimicrobials [159]. The nanoemulsions were reported to have a droplet with rough surfaces [160], such as apremilast nanoemulsions [161]. Despite the advancement in the experimental analysis of such models, the application of numerical modeling studies on nanoemulsions has been limited. The improved accuracy of such numerical analyses would improve the prediction, control, and generation of nanoemulsions used in developing biodegradable coatings and packaging films.

. Grinding in the mineral process is used daily, which affects the surface morphology of particles. Past reports indicate that the surface hydrophobicity of minerals is closely related to surface roughness [162-164]. Although surface chemistry was considered to play a key role in the mineral flotation process, chemical agents such as depressants [165], collectors [166], and activators [167] could be dangerous to the environment, and future efforts must aim to avoid their excessive uses. To better understand the interaction of ground mineral particles and chemical agents (for reducing the use of such chemicals), the simulation analysis on the topic of rough particle interaction would be useful.

 Biocell or biosurface was also widely applied in the medical field, such as biocell trapping [168], biocell delivery [169], and drug delivery [170] and the interaction of such materials with various surfaces is important. However, as some previous reports articulated that the biocell owned rough surface [171], the surface biocell is rarely smooth, previous literature did not apply the numerical model to simulate the biocell interaction and excluded the surface morphology of biocell. Recently, the world is suffering from the covid virus, which also owned rough surface morphology. The covid virus could be considered as a rough particle with randomly rough topographies. The interaction of the covid virus with a surface could be predicted based on DLVO or other theories, but no study has been conducted on it Also, microalgae with their cleaning water potential in wastewater systems has been demonstrated to have rough surface morphology [172]. Therefore, to better evaluate the interaction energy of microalgae with membrane surface, they could be constructed numerically, and their interaction should

be studied.

2.7 Conclusions

Understanding the interaction and behavior of interfaces or colloids in environmental systems is critical for controlling such systems. The particle transportation of the colloidal systems could be comprehensively described by counting Van deer Waals attractive and double layer electric repulsive interaction even with non-DLVO force. Traditional models have been unable to describe the interfacial behaviors of biocolloids with rough surface morphologies [117, 173, 174]. The advancement in rough morphology simulation has paved the way for constructing surfaces with various surface morphologies. In past, non-spherical particles were assumed to have spherical shapes [175]. However, to improve the accuracy of the modeling analysis to understand the behavior of colloidal systems, the numerical analysis should include non-spherical particles. This work summarized numerical models applied for constructing smooth non-spherical particles.

To further improve the accuracy of predictions, the surface morphologies of particles should be involved in the calculation process as particles are rarely smooth in naturally or industrially produced colloidal systems. The recent methodologies of constructing rough flat and spherical surfaces were reviewed in this work. These construction methods were divided into three categories: 1) models that generated regular geometries as protrusions or depressions on a smooth flat surface; 2) models that applied periodic functions; 3) and models that constructed self-similarity randomly rough surfaces. Compared with these methods, the method of constructing randomly rough surfaces could capture more characteristics of surfaces as they could represent particles more accurately.

Accurate knowledge of interfacial energy is critical for understanding many processes in colloidal assembly, such as molecular separation [176], dispersion [177], flocculation [178], filtration [55], and surface coating [66]. Although past theoretical descriptions of these interactions only involved idealized smooth surfaces, the real material surface usually exhibited the characteristics of rough morphologies. The recent developments in interaction models were summarized in this review. With the suitable interaction scenario and surface morphology, the total interfacial interaction between surfaces could be predicted and accurately monitor the interfacial behaviors of particles in such application systems.

A comparison among the numerical models could reveal that approaches constructing randomly rough

flat surfaces and particles were more accurate to characterize the surfaces and particles that are generated naturally or industrially. The most important conclusion drawn from the summarized models is that the surface morphologies played a key role in controlling the interaction energy between surfaces. Generally, the total interaction energy would decrease if the surface became rougher facilitating the coagulation of particles. This finding may facilitate surface modification for designing optimal products such as surface coating.

Current modeling studies still lacked the information on constructing various shapes of asperities on surfaces and rough non-spherical particle interactions. The future modeling studies should focus on resolving these issues. The application fields of such modeling could be extended to the fields of nanoemulsion, grinding minerals, and bio-surfaces.

2.8 Reference

[1] C. Le Floch-Fouéré, L. Lanotte, R. Jeantet, L. Pauchard, The solute mechanical properties impact on the drying of dairy and model colloidal systems, Soft Matter, 15 (2019) 6190-6199.

[2] M. Fathi, M. Vinceković, S. Jurić, M. Viskić, A. Režek Jambrak, F. Donsì, Food-grade colloidal systems for the delivery of essential oils, Food Rev. Int., 37 (2021) 1-45.

[3] R. Das, T. Purakayastha, D. Das, N. Ahmed, R. Kumar, S. Biswas, S. Walia, R. Singh, V. Shukla, M. Yadava, Long-term fertilization and manuring with different organics alter stability of carbon in colloidal organo-mineral fraction in soils of varying clay mineralogy, Sci. Total Environ., 684 (2019) 682-693.

[4] Z. Adamczyk, P. Weroński, Application of the DLVO theory for particle deposition problems, Adv. Colloid Interface Sci., 83 (1999) 137-226.

[5] X. Cai, L. Yang, Z. Wang, M. Zhang, L. Shen, H. Hong, H. Lin, G. Yu, Influences of fractal dimension of membrane surface on interfacial interactions related to membrane fouling in a membrane bioreactor, Journal of colloid and interface science, 500 (2017) 79-87.

[6] M. Zhang, X. Zhou, L. Shen, X. Cai, F. Wang, J. Chen, H. Lin, R. Li, X. Wu, B.-Q. Liao, Quantitative evaluation of the interfacial interactions between a randomly rough sludge floc and membrane surface in a membrane bioreactor based on fractal geometry, Bioresour. Technol., 234 (2017) 198-207.

[7] A. Sanaei, S. Tavassoli, K. Sepehrnoori, Investigation of modified Water chemistry for improved oil recovery: Application of DLVO theory and surface complexation model, Colloids Surf. Physicochem. Eng. Aspects, 574 (2019) 131-145.

[8] N. Pippa, C. Demetzos, E. Danezis, The formalism of fractal aggregation phenomena of colloidal drug delivery systems, J. Liposome Res., 22 (2012) 55-61.

[9] Y. Xing, X. Gui, F. Karakas, Y. Cao, Role of collectors and depressants in mineral flotation: A theoretical analysis based on extended DLVO theory, Minerals, 7 (2017) 223.

[10] A. Sharma, R. Khanna, G. Reiter, A thin film analog of the corneal mucus layer of the tear film: an enigmatic long range non-classical DLVO interaction in the breakup of thin polymer films, Colloids Surf. B. Biointerfaces, 14 (1999) 223-235.

[11] H.H. Rijnaarts, W. Norde, J. Lyklema, A.J. Zehnder, DLVO and steric contributions to bacterial deposition

in media of different ionic strengths, Colloids Surf. B. Biointerfaces, 14 (1999) 179-195.

[12] Y. Guo, F. Kong, P. Fatehi, Generation and use of lignin-g-AMPS in extended DLVO theory for evaluating the flocculation of colloidal particles, ACS omega, 5 (2020) 21032-21041.

[13] C.V. Chrysikopoulos, V.I. Syngouna, Attachment of bacteriophages MS2 and ΦX174 onto kaolinite and montmorillonite: Extended-DLVO interactions, Colloids Surf. B. Biointerfaces, 92 (2012) 74-83.

[14] M. Zhang, B.-q. Liao, X. Zhou, Y. He, H. Hong, H. Lin, J. Chen, Effects of hydrophilicity/hydrophobicity of membrane on membrane fouling in a submerged membrane bioreactor, Bioresour. Technol., 175 (2015) 59-67.

[15] S. Utiramerur, M. Paulaitis, Cooperative hydrophobic/hydrophilic interactions in the hydration of dimethyl ether, The Journal of chemical physics, 132 (2010) 04B607.

[16] C. Van Oss, Polar or Lewis acid-base interactions, Interfacial forces in aqueous media, 1 (1994) 18-46.

[17] C.J. van Oss, Acid—base interfacial interactions in aqueous media, Colloids and Surfaces A: Physicochemical and Engineering Aspects, 78 (1993) 1-49.

[18] C. Liu, D. Song, W. Zhang, Q. He, X. Huangfu, S. Sun, Z. Sun, W. Cheng, J. Ma, Constructing zwitterionic polymer brush layer to enhance gravity-driven membrane performance by governing biofilm formation, Water Res., 168 (2020) 115181.

[19] L. Zhao, X. Qu, M. Zhang, H. Lin, X. Zhou, B.-Q. Liao, R. Mei, H. Hong, Influences of acid–base property of membrane on interfacial interactions related with membrane fouling in a membrane bioreactor based on thermodynamic assessment, Bioresource technology, 214 (2016) 355-362.

[20] C. Van Oss, R. Giese, P.M. Costanzo, DLVO and non-DLVO interactions in hectorite, Clays Clay Miner., 38 (1990) 151-159.

[21] J.-A. Park, S.-B. Kim, DLVO and XDLVO calculations for bacteriophage MS2 adhesion to iron oxide particles, Journal of contaminant hydrology, 181 (2015) 131-140.

[22] D. Quemada, C. Berli, Energy of interaction in colloids and its implications in rheological modeling, Adv. Colloid Interface Sci., 98 (2002) 51-85.

[23] C.Y. Tang, T. Chong, A.G. Fane, Colloidal interactions and fouling of NF and RO membranes: a review, Adv. Colloid Interface Sci., 164 (2011) 126-143.

[24] R. Bhardwaj, X. Fang, P. Somasundaran, D. Attinger, Self-assembly of colloidal particles from evaporating droplets: role of DLVO interactions and proposition of a phase diagram, Langmuir, 26 (2010) 7833-7842.

[25] V. Gupta, M.A. Hampton, J.R. Stokes, A.V. Nguyen, J.D. Miller, Particle interactions in kaolinite suspensions and corresponding aggregate structures, Journal of Colloid and Interface Science, 359 (2011) 95-103.

[26] M. Bendersky, J. Davis, DLVO interaction of colloidal particles with topographically and chemically heterogeneous surfaces, Journal of Colloid and Interface Science, 353 (2011) 87-97.

[27] R.D. Duffadar, J.M. Davis, Interaction of micrometer-scale particles with nanotextured surfaces in shear flow, Journal of colloid and interface science, 308 (2007) 20-29.

[28] R.D. Duffadar, J.M. Davis, Dynamic adhesion behavior of micrometer-scale particles flowing over patchy surfaces with nanoscale electrostatic heterogeneity, Journal of colloid and interface science, 326 (2008) 18-27.

[29] R. Duffadar, S. Kalasin, J.M. Davis, M.M. Santore, The impact of nanoscale chemical features on micron-scale adhesion: Crossover from heterogeneity-dominated to mean-field behavior, Journal of colloid and interface science, 337 (2009) 396-407.

[30] S.L. Walker, J.E. Hill, J.A. Redman, M. Elimelech, Influence of growth phase on adhesion kinetics of Escherichia coli D21g, Appl. Environ. Microbiol., 71 (2005) 3093-3099.

[31] V.L. Morales, B. Gao, T.S. Steenhuis, Grain surface-roughness effects on colloidal retention in the vadose zone, Vadose Zone Journal, 8 (2009) 11-20.

[32] Y. Liang, N. Hilal, P. Langston, V. Starov, Interaction forces between colloidal particles in liquid: Theory and

experiment, Adv. Colloid Interface Sci., 134 (2007) 151-166.

[33] P. Taboada-Serrano, C.-J. Chin, S. Yiacoumi, C. Tsouris, Modeling aggregation of colloidal particles, Current Opinion in Colloid & Interface Science, 10 (2005) 123-132.

[34] Q. Li, U. Jonas, X. Zhao, M. Kappl, The forces at work in colloidal self-assembly: A review on fundamental interactions between colloidal particles, Asia-Pacific Journal of Chemical Engineering, 3 (2008) 255-268.

[35] P.J. Lu, D.A. Weitz, Colloidal particles: crystals, glasses, and gels, Annu. Rev. Condens. Matter Phys, 4 (2013) 217-233.

[36] M. Semenova, Protein–polysaccharide associative interactions in the design of tailor-made colloidal particles, Current Opinion in Colloid & Interface Science, 28 (2017) 15-21.

[37] N.A. Mishchuk, The model of hydrophobic attraction in the framework of classical DLVO forces, Adv. Colloid Interface Sci., 168 (2011) 149-166.

[38] B.W. Ninham, On progress in forces since the DLVO theory, Adv. Colloid Interface Sci., 83 (1999) 1-17.

[39] S. Bhattacharjee, C.-H. Ko, M. Elimelech, DLVO interaction between rough surfaces, Langmuir, 14 (1998) 3365-3375.

[40] S. Bhattacharjee, J.Y. Chen, M. Elimelech, DLVO interaction energy between spheroidal particles and a flat surface, Colloids Surf. Physicochem. Eng. Aspects, 165 (2000) 143-156.

[41] Q. Liu, V. Lazouskaya, Q. He, Y. Jin, Effect of particle shape on colloid retention and release in saturated porous media, J. Environ. Qual., 39 (2010) 500-508.

[42] A. Gomez-Flores, S.A. Bradford, G. Hwang, S. Choi, M. Tong, H. Kim, Shape and orientation of bare silica particles influence their deposition under intermediate ionic strength: A study with QCM–D and DLVO theory, Colloids Surf. Physicochem. Eng. Aspects, 599 (2020) 124921.

[43] M.B. Salerno, M. Flamm, B.E. Logan, D. Velegol, Transport of rodlike colloids through packed beds, Environ. Sci. Technol., 40 (2006) 6336-6340.

[44] K. Li, H. Ma, Rotation and retention dynamics of rod-shaped colloids with surface charge heterogeneity in sphere-in-cell porous media model, Langmuir, 35 (2019) 5471-5483.

[45] L. Wu, B. Gao, Y. Tian, R. Muñoz-Carpena, K.J. Zigler, DLVO interactions of carbon nanotubes with isotropic planar surfaces, Langmuir, 29 (2013) 3976-3988.

[46] A. Gomez-Flores, S.A. Bradford, L. Wu, H. Kim, Interaction energies for hollow and solid cylinders: Role of aspect ratio and particle orientation, Colloids Surf. Physicochem. Eng. Aspects, 580 (2019) 123781.

[47] M.B. Tanis-Kanbur, N.R. Tamilselvam, H.Y. Lai, J.W. Chew, Impact of Particle Shape and Surface Group on Membrane Fouling, Membranes, 12 (2022) 403.

[48] I. Torres-Díaz, M.A. Bevan, General potential for anisotropic colloid–surface interactions, Langmuir, 33 (2017) 4356-4365.

[49] S. Dasgupta, M. Katava, M. Faraj, T. Auth, G. Gompper, Capillary assembly of microscale ellipsoidal, cuboidal, and spherical particles at interfaces, Langmuir, 30 (2014) 11873-11882.

[50] F.N. Ahmad, M. Jaafar, S. Palaniandy, K.A.M. Azizli, Effect of particle shape of silica mineral on the properties of epoxy composites, Composites Sci. Technol., 68 (2008) 346-353.

[51] W. Zhong, A. Yu, X. Liu, Z. Tong, H. Zhang, DEM/CFD-DEM modelling of non-spherical particulate systems: theoretical developments and applications, Powder technology, 302 (2016) 108-152.

[52] G. Delaney, R. Morrison, M. Sinnott, S. Cummins, P. Cleary, DEM modelling of non-spherical particle breakage and flow in an industrial scale cone crusher, Minerals Engineering, 74 (2015) 112-122.

[53] D. Lu, P. Fatehi, A modeling approach for quantitative assessment of interfacial interaction between two rough particles in colloidal systems, Journal of Colloid and Interface Science, 587 (2020) 24-38.

[54] X. Cai, L. Shen, M. Zhang, J. Chen, H. Hong, H. Lin, Membrane fouling in a submerged membrane bioreactor:

An unified approach to construct topography and to evaluate interaction energy between two randomly rough surfaces, Bioresour. Technol., 243 (2017) 1121-1132.

[55] T. Lin, Z. Lu, W. Chen, Interaction mechanisms and predictions on membrane fouling in an ultrafiltration system, using the XDLVO approach, J. Membr. Sci., 461 (2014) 49-58.

[56] J.R. Williams, A.P. Pentland, Superquadrics and modal dynamics for discrete elements in interactive design, Engineering Computations, (1992).

[57] P.S.M. Kumar, D. MubarakAli, R.G. Saratale, G.D. Saratale, A. Pugazhendhi, K. Gopalakrishnan, N. Thajuddin, Synthesis of nano-cuboidal gold particles for effective antimicrobial property against clinical human pathogens, Microb. Pathog., 113 (2017) 68-73.

[58] A. Ghosh, A. Ray, D. Chakrabarti, C. Davis, Cleavage initiation in steel: Competition between large grains and large particles, Materials Science and Engineering: A, 561 (2013) 126-135.

[59] W. Wang, R. Lewis, B. Yang, L. Guo, Q. Liu, M. Zhu, Wear and damage transitions of wheel and rail materials under various contact conditions, Wear, 362 (2016) 146-152.

[60] Y. Wang, G. He, Y. Shao, D. Zhang, X. Ruan, W. Xiao, X. Li, X. Wu, X. Jiang, Enhanced performance of superhydrophobic polypropylene membrane with modified antifouling surface for high salinity water treatment, Separation and Purification Technology, 214 (2019) 11-20.

[61] J. Czarnecki, The effects of surface inhomogeneities on the interactions in colloidal systems and colloid stability, Adv. Colloid Interface Sci., 24 (1985) 283-319.

[62] J. Czarnecki, P. Warszyński, The evaluation of tangential forces due to surface inhomogeneties in the particle deposition process, Colloids and surfaces, 22 (1987) 187-205.

[63] E. Martines, K. Seunarine, H. Morgan, N. Gadegaard, C.D. Wilkinson, M.O. Riehle, Superhydrophobicity and superhydrophilicity of regular nanopatterns, Nano Lett., 5 (2005) 2097-2103.

[64] E. Martines, L. Csaderova, H. Morgan, A. Curtis, M. Riehle, DLVO interaction energy between a sphere and a nano-patterned plate, Colloids Surf. Physicochem. Eng. Aspects, 318 (2008) 45-52.

[65] J.-J. Wu, Simulation of rough surfaces with FFT, Tribology international, 33 (2000) 47-58.

[66] M. Najah, F. Maaboudallah, M. Boucherit, M. Ferguson, L. Fréchette, S. Charlebois, F. Boone, S. Ecoffey, Spectral analysis of the topography parameters for isotropic Gaussian rough surfaces applied to gold coating, Tribology International, 165 (2022) 107339.

[67] X. Qu, X. Cai, M. Zhang, H. Lin, Z. Leihong, B.-Q.J.A.S.S. Liao, A facile method for simulating randomly rough membrane surface associated with interface behaviors, 427 (2018) 915-921.

[68] L. Zhao, X. Qu, H. Lin, G. Yu, B.-Q. Liao, Simulation of foulant bioparticle topography based on Gaussian process and its implications for interface behavior research, Applied Surface Science, 434 (2018) 975-981.

[69] Y. Wang, Y. Liu, G. Zhang, Y. Wang, A Simulation Method for Non-Gaussian Rough Surfaces Using Fast Fourier Transform and Translation Process Theory, Journal of Tribology, 140 (2018).

[70] V. Bakolas, Numerical generation of arbitrarily oriented non-Gaussian three-dimensional rough surfaces, Wear, 254 (2003) 546-554.

[71] L. Zhao, M. Zhang, Y. He, J. Chen, H. Hong, B.-Q. Liao, H. Lin, A new method for modeling rough membrane surface and calculation of interfacial interactions, Bioresour. Technol., 200 (2016) 451-457.

[72] Z. Chen, Y. Liu, P. Zhou, A comparative study of fractal dimension calculation methods for rough surface profiles, Chaos, Solitons & Fractals, 112 (2018) 24-30.

[73] H. Liu, X. Qin, S. Ahmad, Q. Tong, J. Zhao, Molecular dynamics study about the effects of random surface roughness on nanoscale boiling process, International Journal of Heat and Mass Transfer, 145 (2019) 118799.

[74] R.M. Patrikar, Modeling and simulation of surface roughness, Applied Surface Science, 228 (2004) 213-220.

[75] J. Dong, Y. Ju, F. Gao, H. Xie, Estimation of the fractal dimension of Weierstrass–Mandelbrot function based

on cuckoo search methods, Fractals, 25 (2017) 1750065.

[76] Y. Peng, Y. Guo, An adhesion model for elastic-plastic fractal surfaces, Journal of Applied Physics, 102 (2007) 053510.

[77] H. Xiao, Y. Shao, M.J. Brennan, On the contact stiffness and nonlinear vibration of an elastic body with a rough surface in contact with a rigid flat surface, European Journal of Mechanics-A/Solids, 49 (2015) 321-328.

[78] M.C. Herman, K.D. Papadopoulos, A method for modeling the interactions of parallel flat plate systems with surface features, Journal of colloid and interface science, 142 (1991) 331-342.

[79] Z. Zhu, D. Wang, B. Yang, W. Yin, M.S. Ardakani, J. Yao, J.W. Drelich, Effect of nano-sized roughness on the flotation of magnesite particles and particle-bubble interactions, Minerals Engineering, 151 (2020) 106340.

[80] C. Minet, N. Brunetiere, B. Tournerie, D. Fribourg, Analysis and modeling of the topography of mechanical seal faces, Tribology Transactions, 53 (2010) 799-815.

[81] R. Reizer, Simulation of 3D Gaussian surface topography, Wear, 271 (2011) 539-543.

[82] Y. Hu, K. Tonder, Simulation of 3-D random rough surface by 2-D digital filter and Fourier analysis, International journal of machine tools and manufacture, 32 (1992) 83-90.

[83] D.E. Newland, An introduction to random vibrations, spectral & wavelet analysis, Courier Corporation2012.

[84] J.-J. Wu, Simulation of non-Gaussian surfaces with FFT, Tribology International, 37 (2004) 339-346.

[85] W. Li, W. Zhan, P. Huang, A physics-based model of a dynamic tangential contact system of lap joints with non-Gaussian rough surfaces based on a new Iwan solution, AIP Advances, 10 (2020) 035207.

[86] A. Weis, M.R. Bird, M. Nyström, C. Wright, The influence of morphology, hydrophobicity and charge upon the long-term performance of ultrafiltration membranes fouled with spent sulphite liquor, Desalination, 175 (2005) 73-85.

[87] J. Verran, A. Packer, P. Kelly, K.A. Whitehead, The retention of bacteria on hygienic surfaces presenting scratches of microbial dimensions, Lett. Appl. Microbiol., 50 (2010) 258-263.

[88] T.D. Jacobs, K.E. Ryan, P.L. Keating, D.S. Grierson, J.A. Lefever, K.T. Turner, J.A. Harrison, R.W. Carpick, The effect of atomic-scale roughness on the adhesion of nanoscale asperities: a combined simulation and experimental investigation, Tribology Letters, 50 (2013) 81-93.

[89] D. Siegismund, A. Undisz, S. Germerodt, S. Schuster, M. Rettenmayr, Quantification of the interaction between biomaterial surfaces and bacteria by 3-D modeling, Acta Biomater., 10 (2014) 267-275.

[90] L. Hong, X. Gu, F. Lin, Influence of aggregate surface roughness on mechanical properties of interface and concrete, Construction and Building Materials, 65 (2014) 338-349.

[91] R. Li, Y. Lou, Y. Xu, G. Ma, B.-Q. Liao, L. Shen, H. Lin, Effects of surface morphology on alginate adhesion: molecular insights into membrane fouling based on XDLVO and DFT analysis, Chemosphere, 233 (2019) 373-380.

[92] A. Majumdar, C. Tien, Fractal characterization and simulation of rough surfaces, Wear, 136 (1990) 313-327.

[93] W. Yan, K. Komvopoulos, Contact analysis of elastic-plastic fractal surfaces, Journal of applied physics, 84 (1998) 3617-3624.

[94] L. Zhao, L. Yang, H. Lin, M. Zhang, H. Yu, B.-Q. Liao, F. Wang, X. Zhou, R. Li, Modeling three-dimensional surface morphology of biocake layer in a membrane bioreactor based on fractal geometry, Bioresour. Technol., 222 (2016) 478-484.

[95] M. Tanaka, M. Komagata, M. Tsukada, H. Kamiya, Fractal analysis of the influence of surface roughness of toner particles on their flow properties and adhesion behavior, Powder technology, 186 (2008) 1-8.

[96] P. Sahoo, S.R. Chowdhury, A fractal analysis of normal impact between rough surfaces in presence of adhesion, Wear, 261 (2006) 318-327.

[97] S. Feng, G. Yu, X. Cai, M. Eulade, H. Lin, J. Chen, Y. Liu, B.-Q. Liao, Effects of fractal roughness of

membrane surfaces on interfacial interactions associated with membrane fouling in a membrane bioreactor, Bioresour. Technol., 244 (2017) 560-568.

[98] J.W. Drelich, A simplified analysis of the effect of nano-asperities on particle-bubble interactions, Physicochemical Problems of Mineral Processing, 54 (2018).

[99] J.W. Drelich, P.K. Bowen, Hydrophobic nano-asperities in control of energy barrier during particle–surface interactions, Surface Innovations, 3 (2015) 164-171.

[100] X. Cai, M. Zhang, L. Yang, H. Lin, X. Wu, Y. He, L.J.J.o.c. Shen, i. science, Quantification of interfacial interactions between a rough sludge floc and membrane surface in a membrane bioreactor, 490 (2017) 710-718.

[101] R. Mei, R. Li, H. Lin, Z. Shen, M. Zhang, J. Chen, Y.J.B.t. He, A new approach to construct three-dimensional surface morphology of sludge flocs in a membrane bioreactor, 219 (2016) 521-526.

[102] M. Zhang, H. Hong, H. Lin, G. Yu, F. Wang, B.-Q. Liao, Quantitative assessment of interfacial forces between two rough surfaces and its implications for anti-adhesion membrane fabrication, Separation and Purification Technology, 189 (2017) 238-245.

[103] D. Lu, P. Fatehi, Interfacial interactions of rough spherical surfaces with random topographies, Colloids Surf. Physicochem. Eng. Aspects, 642 (2022) 128570.

[104] L. Suresh, J.Y. Walz, Effect of surface roughness on the interaction energy between a colloidal sphere and a flat plate, Journal of Colloid and Interface Science, 183 (1996) 199-213.

[105] G. Yu, X. Cai, L. Shen, J. Chen, H. Hong, H. Lin, R. Li, A novel integrated method for quantification of interfacial interactions between two rough bioparticles, Journal of Colloid and Interface Science, 516 (2018) 295-303.

[106] H. Bargozin, R. Hadadhania, H. Faraji, H.J.J.o.D.S. Yousefzadeh, Technology, Effect of rough nanoparticle orientation on DLVO energy interaction, 36 (2015) 755-764.

[107] E. Martines, L. Csaderova, H. Morgan, A.S.G. Curtis, M.O. Riehle, DLVO interaction energy between a sphere and a nano-patterned plate, Colloids and Surfaces A: Physicochemical and Engineering Aspects, 318 (2008) 45-52.

[108] H. Hong, X. Cai, L. Shen, R. Li, H. Lin, Membrane fouling in a submerged membrane bioreactor: new method and its applications in interfacial interaction quantification, Bioresour. Technol., 241 (2017) 406-414.

[109] P. Liu, H. Zhao, K. Huang, Q. Chen, Research on normal contact stiffness of rough surface considering friction based on fractal theory, Applied Surface Science, 349 (2015) 43-48.

[110] J.J. Ganczarczyk, W.M. Zahid, D.-H. Li, Physical stabilization and embedding of microbial aggregates for light microscopy studies, Water Res., 26 (1992) 1695-1699.

[111] J. Námer, J.J. Ganczarczyk, Settling properties of digested sludge particle aggregates, Water Res., 27 (1993) 1285-1294.

[112] J. Guan, T.D. Waite, R. Amal, Rapid structure characterization of bacterial aggregates, Environ. Sci. Technol., 32 (1998) 3735-3742.

[113] N. Patir, A numerical procedure for random generation of rough surfaces, Wear, 47 (1978) 263-277.

[114] I. Simonsen, Å. Larsen, E. Andreassen, E. Ommundsen, K. Nord-Varhaug, Haze of surface random systems: An approximate analytic approach, Physical Review A, 79 (2009) 063813.

[115] J. Kalda, Description of random Gaussian surfaces by a four-vertex model, Physical Review E, 64 (2001) 020101.

[116] A.K.P. Anninos, The Significance of Limit Cycles in a Neural Model with Poisson and Gauss Connectivity, JApl Theol, 1 (2016) 25-29.

[117] S. Bhattacharjee, M. Elimelech, Surface element integration: a novel technique for evaluation of DLVO interaction between a particle and a flat plate, Journal of colloid and interface science, 193 (1997) 273-285.

[118] R. Hogg, T.W. Healy, D.W. Fuerstenau, Mutual coagulation of colloidal dispersions, Transactions of the Faraday Society, 62 (1966) 1638-1651.

[119] O. Schnitzer, M. Morozov, A generalized Derjaguin approximation for electrical-double-layer interactions at arbitrary separations, The Journal of chemical physics, 142 (2015) 244102.

[120] N. Churaev, The DLVO theory in Russian colloid science, Adv. Colloid Interface Sci., 83 (1999) 19-32.

[121] S. Bayoudh, A. Othmane, L. Mora, H.B. Ouada, Assessing bacterial adhesion using DLVO and XDLVO theories and the jet impingement technique, Colloids Surf. B. Biointerfaces, 73 (2009) 1-9.

[122] J.-J. Wu, Adhesive contact between a cylinder and a half-space, Journal of Physics D: Applied Physics, 42 (2009) 155302.

[123] O. Guzmán, J.J. de Pablo, An effective-colloid pair potential for Lennard-Jones colloid–polymer mixtures, The Journal of chemical physics, 118 (2003) 2392-2397.

[124] J.-J. Wu, The Interactions between Spheres and between a Sphere and a Half-Space, Based on the Lennard–Jones Potential, Journal of adhesion science and technology, 26 (2012) 251-269.

[125] J.-J. Wu, The jump-to-contact distance in atomic force microscopy measurement, The Journal of Adhesion, 86 (2010) 1071-1085.

[126] L. Jiang, M. Rahnama, B. Zhang, X. Zhu, P.-C. Sui, D.-D. Ye, N. Djilali, Predicting the interaction between nanoparticles in shear flow using lattice Boltzmann method and Derjaguin–Landau–Verwey–Overbeek (DLVO) theory, Phys. Fluids, 32 (2020) 043302.

[127] Z. Chai, B. Shi, Simulation of electro-osmotic flow in microchannel with lattice Boltzmann method, Physics Letters A, 364 (2007) 183-188.

[128] E.M. Hoek, S. Bhattacharjee, M. Elimelech, Effect of membrane surface roughness on colloid− membrane DLVO interactions, Langmuir, 19 (2003) 4836-4847.

[129] S. Rajupet, A.A. Riet, Q. Chen, M. Sow, D.J. Lacks, Relative importance of electrostatic and van der Waals forces in particle adhesion to rough conducting surfaces, Physical Review E, 103 (2021) 042906.

[130] L. Zhao, F. Wang, X. Weng, R. Li, X. Zhou, H. Lin, H. Yu, B.-Q. Liao, Novel indicators for thermodynamic prediction of interfacial interactions related with adhesive fouling in a membrane bioreactor, Journal of colloid and interface science, 487 (2017) 320-329.

[131] H. Lin, M. Zhang, R. Mei, J. Chen, H. Hong, A novel approach for quantitative evaluation of the physicochemical interactions between rough membrane surface and sludge foulants in a submerged membrane bioreactor, Bioresour. Technol., 171 (2014) 247-252.

[132] J. Chen, R. Mei, L. Shen, L. Ding, Y. He, H. Lin, H. Hong, Quantitative assessment of interfacial interactions with rough membrane surface and its implications for membrane selection and fabrication in a MBR, Bioresour. Technol., 179 (2015) 367-372.

[133] L. Zhao, L. Shen, Y. He, H. Hong, H. Lin, Influence of membrane surface roughness on interfacial interactions with sludge flocs in a submerged membrane bioreactor, Journal of colloid and interface science, 446 (2015) 84-90.

[134] H. Hong, H. Lin, R. Mei, X. Zhou, B.-Q. Liao, L. Zhao, Membrane fouling in a membrane bioreactor: a novel method for membrane surface morphology construction and its application in interaction energy assessment, J. Membr. Sci., 516 (2016) 135-143.

[135] J. Chen, H. Lin, L. Shen, Y. He, M. Zhang, B.-Q. Liao, Realization of quantifying interfacial interactions between a randomly rough membrane surface and a foulant particle, Bioresour. Technol., 226 (2017) 220-228.

[136] J. Teng, L. Shen, Y. He, B.-Q. Liao, G. Wu, H. Lin, Novel insights into membrane fouling in a membrane bioreactor: elucidating interfacial interactions with real membrane surface, Chemosphere, 210 (2018) 769-778.

[137] X. Cai, M. Zhang, L. Yang, H. Lin, X. Wu, Y. He, L. Shen, Quantification of interfacial interactions between

a rough sludge floc and membrane surface in a membrane bioreactor, Journal of colloid and interface science, 490 (2017) 710-718.

[138] T.G. Anjali, M.G. Basavaraj, Contact angle and detachment energy of shape anisotropic particles at fluid-fluid interfaces, Journal of colloid and interface science, 478 (2016) 63-71.

[139] S. Lin, M.R. Wiesner, Exact analytical expressions for the potential of electrical double layer interactions for a sphere− plate system, Langmuir, 26 (2010) 16638-16641.

[140] S. Zhou, Investigation about validity of the Derjaguin approximation for electrostatic interactions for a sphere-sphere system, Colloid & Polymer Science, 297 (2019) 623-631.

[141] S. Oversteegen, H. Lekkerkerker, On the accuracy of the Derjaguin approximation for depletion potentials, Physica A: Statistical Mechanics and its Applications, 341 (2004) 23-39.

[142] S. Chen, Y. Yan, W. Gong, A simple lattice Boltzmann model for conjugate heat transfer research, International Journal of Heat and Mass Transfer, 107 (2017) 862-870.

[143] F. Qin, A. Mazloomi Moqaddam, Q. Kang, D. Derome, J. Carmeliet, Entropic multiple-relaxation-time multirange pseudopotential lattice Boltzmann model for two-phase flow, Phys. Fluids, 30 (2018) 032104.

[144] X. Huang, S. Bhattacharjee, E.M. Hoek, Is surface roughness a "scapegoat" or a primary factor when defining particle− substrate interactions?, Langmuir, 26 (2010) 2528-2537.

[145] A. Jemat, M.J. Ghazali, M. Razali, Y. Otsuka, Surface modifications and their effects on titanium dental implants, BioMed research international, 2015 (2015).

[146] M. Moosavi, H. Rafsanjani, M. Mehranpour, A. Nazem, A. Shirazi, An investigation of surface roughness measurement in rock joints with a 3D scanning device, ISRM SINOROCK 2013, OnePetro, 2013.

[147] H. Bargozin, R. Hadadhania, H. Faraji, H. Yousefzadeh, Effect of rough nanoparticle orientation on DLVO energy interaction, Journal of Dispersion Science and Technology, 36 (2015) 755-764.

[148] M. Björnmalm, M. Faria, X. Chen, J. Cui, F. Caruso, Dynamic flow impacts cell–particle interactions: sedimentation and particle shape effects, Langmuir, 32 (2016) 10995-11001.

[149] H. Katepalli, V.T. John, A. Tripathi, A. Bose, Microstructure and rheology of particle stabilized emulsions: Effects of particle shape and inter-particle interactions, Journal of colloid and interface science, 485 (2017) 11-17.

[150] J. Chen, T. Moschakis, L.A. Pugnaloni, Surface topography of heat-set whey protein gels by confocal laser scanning microscopy, Food Hydrocolloids, 20 (2006) 468-474.

[151] M. Zanini, C.-P. Hsu, T. Magrini, E. Marini, L. Isa, Fabrication of rough colloids by heteroaggregation, Colloids Surf. Physicochem. Eng. Aspects, 532 (2017) 116-124.

[152] F. Zheng, Thermophoresis of spherical and non-spherical particles: a review of theories and experiments, Adv. Colloid Interface Sci., 97 (2002) 255-278.

[153] S. Amada, H. Yamada, Introduction of fractal dimension to adhesive strength evaluation of plasma-sprayed coatings, Surf. Coat. Technol., 78 (1996) 50-55.

[154] A. Oliva, E. Anguiano, M. Aguilar, Fractal dimension: measure of coating quality, Surface engineering, 15 (1999) 101-104.

[155] Z. Zhang, L. Zhao, Y. Li, M.J.M.P.i.E. Chu, A modified method to calculate critical coagulation concentration based on DLVO theory, 2015 (2015).

[156] B. Derjaguin, On the repulsive forces between charged colloid particles and on the theory of slow coagulation and stability of lyophobe sols, Transactions of the Faraday Society, 35 (1940) 203-215.

[157] J.B. Aswathanarayan, R.R. Vittal, Nanoemulsions and their potential applications in food industry, Frontiers in Sustainable Food Systems, 3 (2019) 95.

[158] G. Li, Z. Zhang, H. Liu, L. Hu, Nanoemulsion-based delivery approaches for nutraceuticals: fabrication, application, characterization, biological fate, potential toxicity and future trends, Food Funct., 12 (2021) 1933-

1953.

[159] E. Marchese, N. D'onofrio, M.L. Balestrieri, D. Castaldo, G. Ferrari, F. Donsì, Bergamot essential oil nanoemulsions: Antimicrobial and cytotoxic activity, Zeitschrift für Naturforschung C, 75 (2020) 279-290.

[160] A. Garg, M.Z. Ahmad, M.A. Barkat, P. Kaushik, J. Ahmad, L.M. Nollet, Imaging Techniques for Characterization of Nanoemulsions, Nanoemulsions in Food Technology, CRC Press2021, pp. 153-168.

[161] M.M. Ahmed, M. Anwer, F. Fatima, A.S. Alali, M.A. Kalam, A. Zafar, S. Alshehri, M.M. Ghoneim, Development of Apremilast Nanoemulsion-Loaded Chitosan Gels: In Vitro Evaluations and Anti-Inflammatory and Wound Healing Studies on a Rat Model, Gels, 8 (2022) 253.

[162] Z. Zhu, Y. Fu, W. Yin, H. Sun, K. Chen, Y. Tang, B. Yang, Role of surface roughness in the magnesite flotation and its mechanism, Particuology, 62 (2022) 63-70.

[163] Y. Chen, W. Xia, G. Xie, Contact angle and induction time of air bubble on flat coal surface of different roughness, Fuel, 222 (2018) 35-41.

[164] X. Wang, Q. Zhang, Role of surface roughness in the wettability, surface energy and flotation kinetics of calcite, Powder technology, 371 (2020) 55-63.

[165] W. Zhou, J. Moreno, R. Torres, H. Valle, S. Song, Flotation of fluorite from ores by using acidized water glass as depressant, Minerals Engineering, 45 (2013) 142-145.

[166] E. Espiritu, G. Da Silva, D. Azizi, F. Larachi, K. Waters, The effect of dissolved mineral species on bastnäsite, monazite and dolomite flotation using benzohydroxamate collector, Colloids Surf. Physicochem. Eng. Aspects, 539 (2018) 319-334.

[167] D. Li, G. Nie, Z. Wang, J. Li, J. Li, Flotation separation of dolomite from fluorapatite using NaF as an activator, Surface and Interface Analysis, 53 (2021) 860-866.

[168] C. Zhou, H. Shen, H. Feng, Z. Yan, B. Ji, X. Yuan, R. Zhang, H. Chang, Enhancing signals of microfluidic impedance cytometry through optimization of microelectrode array, Electrophoresis, (2022).

[169] C.H. Hettiarachchi, Mechanics of biocell landfill settlements, New Jersey Institute of Technology2005.

[170] D. Ramadon, M.T. McCrudden, A.J. Courtenay, R.F. Donnelly, Enhancement strategies for transdermal drug delivery systems: Current trends and applications, Drug Delivery and Translational Research, 12 (2022) 758-791.

[171] E.J. Hall-Findlay, Breast implant complication review: double capsules and late seromas, Plast. Reconstr. Surg., 127 (2011) 56-66.

[172] A. Ozkan, H. Berberoglu, Physico-chemical surface properties of microalgae, Colloids and surfaces B: Biointerfaces, 112 (2013) 287-293.

[173] G. Patey, Interaction of two spherical colloidal particles in electrolyte solution. Application of the hypernetted-chain approximation, J. Chem. Phys.;(United States), 72 (1980).

[174] H. Butt, K. Graf, M. Kappl, „Physics and Chemistry of Interfaces "Wiley-VCH, Weinheim., (2003).

[175] C. Xie, H. Ma, T. Song, Y. Zhao, DEM investigation of SAG mill with spherical grinding media and non-spherical ore based on polyhedron-sphere contact model, Powder Technology, 386 (2021) 154-165.

[176] K. Huang, G. Liu, Y. Lou, Z. Dong, J. Shen, W. Jin, A graphene oxide membrane with highly selective molecular separation of aqueous organic solution, Angewandte Chemie, 126 (2014) 7049-7052.

[177] H. Bargozin, J. Moghaddas, Stability of nanoporous silica aerogel dispersion as wettability alteration agent, Journal of dispersion science and technology, 34 (2013) 1454-1464.

[178] W. Wu, R. Giese, C. Van Oss, Stability versus flocculation of particle suspensions in water—correlation with the extended DLVO approach for aqueous systems, compared with classical DLVO theory, Colloids Surf. B. Biointerfaces, 14 (1999) 47-55.

Chapter 3: A modeling approach for quantitative assessment of interfacial interaction between two rough particles in colloidal systems

3.1 Abstract

Hypothesis and background

The simulation of rough particle surfaces is important to understand and control the interface behavior of particles in colloidal systems. Literature analysis suggested a lack of information for an accurate model simulating the interfacial interaction between two rough particles. It is hypothesized that the total interfacial energy developed between two rough particles would depend on the surface morphologies of particles, and it could be predicted if a mathematical model to represent the interaction of two rough particles were created accurately.

Experiments

In this study, mathematical models were developed to determine the interfacial energy created between two particles according to the XDLVO theory by considering the rippled particle theory and surface element integral (SEI) method. Three different scenarios of particle interactions were assumed in the simulation. The present study provides deep insights into particle interactions by considering the aspect ratio, size, and surface roughness of two particles in colloidal systems.

Findings

The assessment of the interfacial interaction revealed that an increase in the aspect ratio, surface roughness, and relative surface roughness of particles would weaken the total interaction energy generated between particles and promote particle aggregation. Increased interaction energy was predicted for the interaction of particles by increasing the particle size. The asperity ratio was more effective than the asperity number in controlling the interfacial energy between two particles. The results of this study could be used for foreseeing the interaction of rough particles, which has a significant application in particle coagulation or dispersion in colloidal systems.

Keywords: Interfacial energy, particle modeling, colloidal stability, simulation

3.2 Introduction

The interaction forces developed between colloidal particles in suspension systems can determine the stability of the suspensions impacting the shelf life, rheology, and taste of the suspensions [1]. They also affect the rheological behavior of suspensions (e.g., mixing, membrane filtration) and formulations of chemical and pharmaceutical products [2]. Conventional approaches to reconciling differences in the surface energy of particles include the determination of hydrophobic/hydrophilic interactions and chemical and morphological heterogeneity of particles.

Recently, the extended Dejaguin-Landau-Verway-Overbeek (XDLVO) theory was developed to improve the accuracy of the DLVO theory by including the hydrophobic interaction of particles [3-5]. It was observed that the inclusion of hydrophobic interaction contributed to improving the accuracy of the simulation and experimental results for the solutions of proteins, polymeric micelles, particles, and sludge flocs [6-11]. Also, hydrophobic interactions have facilitated the understanding of the interaction of oil droplets in emulsification [12, 13]. The application of the XDLVO theory was previously studied in simulating the interfacial interactions between two smooth flat surfaces [14]. In this theory, Derjaguin's approximation (DA) was practiced simulating the interaction of two smooth spheres in the colloidal systems [15, 16]. However, the DA method is only valid for the interaction of large particles in a close approximation (i.e., the separation distance is much smaller than the size of the objects) [5]. To circumvent this limitation, the surface element integral (SEI) method was introduced to simulate the interaction energy over the entire projected area of two opposing differential planar elements [17]. This method can be theoretically applied for the calculation of interfacial interactions between any two curved surfaces, for example, two rough particles [18].

Generally, particles have different sizes and surface roughness in colloidal systems, which would affect the stability of colloidal systems [19-21]. The particle size and surface roughness have direct effects on the surface functionality of particles, and thus it would be interesting to explore the relationship between particle interaction and particle size or particle roughness to predict the behavior of colloidal systems. However, the previous modeling studies mainly focused on the interaction of one rough particle and a smooth flat plate [22, 23]. Yu and coworkers established a method to evaluate the interaction between two rough particles following the SEI method [24]. However, the previous model simulated two rough particle interactions with only a one-unit vector, which was used in representing the spatial direction

[24]. If a case needed to consider two rough surfaces, the two-unit vectors would predict the interaction of the particles more precisely than the one-unit vector, implying that two spatial directions need to be considered for identifying the interaction of two rough particles [25].

Despite previous attempts to predict the interaction of particles in colloidal systems [19-23], the previous models that considered the XDLVO theory did not include the surface roughness of particles precisely. Also, the studies considering the surface roughness did not consider the alternative patterns in the surface morphology of particles and/or did not follow the XDLVO theory. In this context, the investigation of the interaction between two rough particles has not been fully exploited, and it is necessary to establish models to simulate the interaction of roughly spherical particles with different surface characteristics following the XDLVO theory. The numerical model created in this study is proposed to predict the interfacial interaction energy developed between two rough particles with different surface morphologies more comprehensively than previous models. Therefore, the effects of asperity number, asperity ratio, aspect ratio, particle size, and orientation angle were included in the simulation process based on rippled sphere model because these parameters can fully describe the between different interaction scenarios in the colloidal system. The objectives of the present study are to explore the effects of the surface properties of particles on the total interfacial interaction of the particles based on the XDLVO theory and to evaluate the accuracy of the model created. For the first time, we have reported a comprehensive simulation study for assessing the interaction of rough particles by considering varied parameters for surface roughness, relative roughness, particle size, and relative particle size. In addition, the most effective surface property of particles influencing the interaction of particles in the colloidal systems was identified.

3.3 Theory and Modeling

3.3.1 Developing equations for the interaction of particles following XDLVO theory

The XDLVO theory is a universal method used for describing the thermodynamic interactions between two bodies in an aqueous medium [26]. In this modeling study, we applied the methodology provided by Hog to describe the van der Waals interaction ($\Delta G^{LW}(h)$) [27], and the methodology provided by Hogg and coworkers to express the electric double layer interaction energy [28]. In addition, the calculation method given by Van Osa and Good was applied for determining the hydrophobic

interaction of particles ($\Delta G^{AB}(h)$) [26].

The energy per unit area of these three interactions ($\Delta G^{LW}(h)$, $\Delta G^{AB}(h)$ and $\Delta G^{EL}(h)$) between two infinite planar surfaces can be described following Equations 3.2 to 3.4 [14]:

$$\Delta G^{Total}(h) = \Delta G^{LW}(h) + \Delta G^{AB}(h) + \Delta G^{EL}(h) \tag{3.1}$$

$$\Delta G^{LW}(h) = -\frac{A_H}{12\pi h^2} = \Delta G_{h_0}^{LW}\frac{h_0^2}{h^2} \tag{3.2}$$

$$\Delta G^{AB}(h) = \Delta G_{h_0}^{AB}\exp\left(\frac{h_0-h}{\nu}\right) \tag{3.3}$$

$$\Delta G^{EL}(h) = \varepsilon_0\varepsilon_r\kappa\xi_1\xi_2\left(\frac{\xi_1^2+\xi_2^2}{2\xi_1\xi_2}(1-coth\kappa h) + \frac{1}{sinh\kappa h}\right) \tag{3.4}$$

where particle 1 and particle 2 are labeled with subscript 1 and 2, respectively, and h_0 is the minimum equilibrium cut-off distance assumed to be 0.158 nm [14]. Also, ε, ξ, and κ^{-1} are the permittivity of the medium, zeta potential, and the double-layer thickness, respectively; and ν is the correlation length of molecules in a liquid medium, 0.6 nm [22]. In these equations, ε is expressed as the product of the permittivity of a vacuum ($\varepsilon_0 = 8.854 \times 10^{-12}$ C^2/J·m) and the relative permittivity (i.e., dielectric constant) of the medium ε_r, which is 80 for water at 20°C [29].

Van Osa and Good claimed that interfacial or surface tension analysis would be one of the best methods to analyze the effect of hydrophobic and van der Waals interactions on the total interfacial energy developed between particles [30]. The surface or interface tensions are expressed as the sum of an apolar (Lifshitz–van der Waals) component (γ^{LW}) and a polar component (γ^{AB}) [26]. γ^{AB} can then be separated into an electron-donating component (γ^-) and an electron-accepting component (γ^+) [31]. According to these parameters, the $\Delta G_{h_0}^{LW}$ and $\Delta G_{h_0}^{AB}$ can be calculated following Equations 3.5 and 3.6:

$$\Delta G_{h_0}^{LW} = -2(\sqrt{\gamma_1^{LW}} - \sqrt{\gamma_w^{LW}})(\sqrt{\gamma_2^{LW}} - \sqrt{\gamma_w^{LW}}) \tag{3.5}$$

$$\Delta G_{h_0}^{AB} = 2\left[\sqrt{\gamma_w^+}(\sqrt{\gamma_1^-} + \sqrt{\gamma_2^-} - \sqrt{\gamma_w^-}) + \sqrt{\gamma_w^-}\left(\sqrt{\gamma_1^+} + \sqrt{\gamma_2^+} - \sqrt{\gamma_w^+}\right) - \sqrt{\gamma_1^-\gamma_2^+} - \sqrt{\gamma_1^+\gamma_2^-}\right]$$

(3.6)

where subscripts 1, w, and 2 represent particle 1, water, and particle 2, respectively.

The surface tension of the particles can be obtained by solving a set of three Young's equations (Equation 7) [26]. The values of the surface tension (γ_l^{LW}, γ_l^+, and γ_l^-) and contact angle (α) should be considered for three different liquids (e.g., ultrapure water, glycerol, and diiodomethane) to determine the surface tensions of the solid (γ_1^{LW}, γ_1^+, and γ_1^-). In this modeling study, the above-mentioned parameters are collected from previous literature and summarized in Table A.1.1 [32].

$$\frac{(1+cos\alpha)}{2}\gamma_l^{Tol} = \sqrt{\gamma_l^{LW}}\sqrt{\gamma_1^{LW}} + \sqrt{\gamma_l^-}\sqrt{\gamma_1^+} + \sqrt{\gamma_l^+}\sqrt{\gamma_1^-} \tag{3.7}$$

3.3.2 Developing three-dimensional rough particles

With the contributions of the scanning electron microscope (SEM), the surface morphology of silica particles, polystyrene particles, and methyl methacrylate particles was revealed to have raspberry-like surface morphology with depressions and protrusions [33-35]. In the present work, we applied the ripped rough particle theory to construct the rough particle that can help capture the details of peaks and valleys of the ripples on the particles with similar structures. This construction method was successfully applied in modeling the rough flocs for simulating the interaction between flocs and membranes in the past [20, 22, 24].

To simplify the calculation, the cartesian coordinates (χ, y, z) were replaced by spherical coordinates (R, θ, φ) in this study [24].

$$x = R\sin\theta\cos\varphi \tag{3.8}$$

$$y = R\sin\theta\sin\varphi \tag{3.9}$$

$$z = R\cos\theta \tag{3.10}$$

The surface morphology of particles can represent the surface roughness of colloidal particles. This analytical image can be determined mathematically [36, 37]. The rough surface and radius of rough particles were modeled following Equations 3.11 and 3.12 [25].

$$\Delta r_i = r_i\lambda_\theta\cos(n_\theta\theta_i) + r_i\lambda_\varphi\cos(n_\varphi\varphi_i) \tag{3.11}$$

$$R_i = r_i + \Delta r_i \tag{3.12}$$

Where R_i is the radius of the constructed rough particle; r_i is the radius of the smooth particle that is used as an elementary particle to construct a rough particle; Δr_i is the constructed rough surface; θ_i and φ_i are the coordinate angle value in three-dimensional spherical coordinates. Also, i is the subscript of a particle (i=1,2). The λ_φ and λ_θ are the scaling amplitudes (asperity ratio), and n_θ and n_φ are the asperity numbers of the surface of the particle (Figure A.1.1). To simplify the analysis, these parameters, $(\lambda_\theta, \lambda_\varphi)$ and (n_θ, n_φ), were set to be the same $(\lambda_\theta = \lambda_\varphi, n_\theta = n_\varphi)$ and donated as λ_i and n_i in the following equations. The value of λ_i mainly represents the size of asperity on the particle surface and n_i is assumed to be greater than zero. Figure A.1.2 showed the image of particle constructed following the simulation analysis of Equations 3.11 and 3.12 using MATLAB 2018 (9.4.0.8136540) 64-bit, while Figure A.1.2b and A.1.2c (supplementary materials) shows the same analysis while λ_i and n_i were

varied and made particles with different roughness.

3.3.3 Developing the model to quantify the interfacial interactions between two rough particles

3.3.3.1 Model 1 to simulate interfacial interactions

According to the surface element integral method, the total interaction energy of two particles (U(h)) can be calculated considering the interaction energy per unit area (ΔG(h)) of particles and the projected surface area of the rough particles. This concept can be described by Equations 3.13 and 3.14 [24].

$$U(h) = \iint \Delta G(h) dA \tag{3.13}$$

$$dA = \overrightarrow{o_1 k_1} \overrightarrow{o_2 k_2} dS \tag{3.14}$$

The differential area (*dS*) can be calculated by Eq 3.15 [24, 38]:

$$dS = R_i^2 \sin \theta_i \, d\theta d\varphi \tag{3.15}$$

where *dS* is the differential area of constructed particle 1, *dA* is the projection area of particle 1 on the surface of particle 2, h is the local separation distance between *dS* of particle 1 and the projection area on particle 2, $\overrightarrow{o_1}$ and $\overrightarrow{o_2}$ are unit normal to the opposite surface of asperities, $\overrightarrow{k_1}$ and $\overrightarrow{k_2}$ are unit vectors, which are parallel to the lines connecting to the centers of asperities. The terms ($\overrightarrow{o_1 k_1}$ and $\overrightarrow{o_2 k_2}$) describe the curvature effect of two rough surfaces, and these parameters are the primary components influencing the calculation process in the SEI. In this case, $\overrightarrow{o_1 k_1}$ and $\overrightarrow{o_2 k_2}$ can be expressed by Equations 3.16 and 3.17 [24].

$$\overrightarrow{o_1 k_1} = \frac{R_1 \sin \theta_1 \cos \theta_1 - r_1 \lambda_1 n_1 \sin(n_1 \theta_1) \sin^2 \theta_1}{\sqrt{R_1^2 \sin^2 \theta_1 + r_1^2 \lambda_1^2 n_1^2 \sin^2(n_1 \varphi_1) + r_1^2 \lambda_1^2 n_1^2 \sin^2(n_1 \theta_1) \sin^2 \theta_1}} \tag{3.16}$$

$$\overrightarrow{o_2 k_2} = \frac{R_2 \sin \theta_2 \cos \theta_2 - r_2 \lambda_2 n_2 \sin(n_2 \theta_2) \sin^2 \theta_2}{\sqrt{R_2^2 \sin^2 \theta_2 + r_2^2 \lambda_2^2 n_2^2 \sin^2(n_2 \varphi_2) + r_2^2 \lambda_2^2 n_2^2 \sin^2(n_2 \theta_2) \sin^2 \theta_2}} \tag{3.17}$$

Figure 1 shows the scenario for the interaction of two rough particles of different sizes. In this case, the spatial relationship between two particles can be described using Equation 3.18 [39], which can be used for connecting two-angle coordinates in two particles.

$$\theta_2 = arc \sin \left[\left(\frac{R_1}{R_2} \right) \sin \theta_1 \right] \tag{3.18}$$

The related distance between these two particles' projection areas can be calculated by Equation 3.19 [24]:

$$h = r_1 + 2\lambda_1 r_1 + r_2 + 2\lambda_2 r_2 + D - R_1 cos\theta_1 - R_2 \cos \theta_2 \tag{19}$$

Where r_1 and r_2 refer to radii of smooth particles 1 and 2, R_1 and R_2 refer to radii of modeled rough particles 1 and 2, λ_1 and λ_2 represent the asperity ratios of rough particles 1 and 2.

According to Bhattacharjee and coworkers [25], to simulate the interaction energy of two rough surfaces, the SEI method should be developed to include the curvature effect of both rough surfaces. Thus, according to Equations 3.13-3.19, the interaction energy calculation can be written as shown in equation 3.20:

$$U(h) = \iint \Delta G(h)\overrightarrow{o_1 k_1} \times \overrightarrow{o_2 k_2} \times R_i{}^2 \sin \theta_i \, d\theta d\varphi \tag{3.20}$$

By combining Equations 3.2-3.6 and 3.20, Equations 3.21-3.23 were developed to determine the individual LW, AB, and EL interactions between two rough particles with different radii (When $r_1 = r_2$, the two particles have the same size).

$$U_{LW} = \Delta G_{h_0}^{LW} \int_0^{2\pi} \int_0^{\pi/2} \frac{h_0^2}{h^2} \overrightarrow{o_1 k_1} \overrightarrow{o_2 k_2} R_i{}^2 \sin \theta_i \, d\theta d\varphi \tag{3.21}$$

$$U_{AB} = \Delta G_{h_0}^{AB} \int_0^{2\pi} \int_0^{\pi/2} exp \left(\frac{h_0-h}{\lambda}\right) \overrightarrow{o_1 k_1} \overrightarrow{o_2 k_2} R_i{}^2 \sin \theta_i \, d\theta d\varphi \tag{3.22}$$

$$U_{EL} = \varepsilon_0 \varepsilon_r \kappa \xi_1 \xi_2 \int_0^{2\pi} \int_0^{\pi/2} \left(\frac{\xi_1^2+\xi_2^2}{2\xi_1\xi_2}(1 - coth \, \kappa h) + \frac{1}{sinh \, \kappa h}\right) \overrightarrow{o_1 k_1} \overrightarrow{o_2 k_2} R_i{}^2 \sin \theta_i \, d\theta d\varphi \tag{3.23}$$

MATLAB 2018 (9.4.0.8136540) 64-bit was used for the calculation. The XDLVO energies are expressed in kT units, where k is the Boltzmann constant and T is the absolute temperature taken as 293.15 K.

Figure 3.1 Parameters involved in the interaction of two rough particles with different radii [24].

3.3.3.2 Model 2 to simulate the aspect ratio effect on interfacial interactions

According to Figure A.1.3, at a larger aspect ratio (above 30), particle 1 would regard particle 2 as a rough flat plate. Thus, when the aspect ratio between two particles is above 30, the two-rough particle interaction would be changed to a rough particle-rough plate interaction [39] as shown in Figure A.1.3. This situation may introduce errors because Equation 11 is only suitable for simulating two rough spheres, which considers particle 2 as a sphere, not as a flat plate. The separation distance (h) might be changed if particle 2 is modified to a flat plate. Thus, the Model 1 interaction scenario shown in Figure 1 should be changed from the interaction of two rough particles to one rough particle interacting with a rough flat plate shown in Figure A.1.3. According to Figure A.1.3, the related distance between two different areas of two particles could be changed according to equations 3.24 and 3.25:

$$h = r_1 + D - R_1 \cos\theta_1 + 2\lambda_1 r_1 + 2\lambda_2 r_2 - f(\theta_2, \varphi_2) \tag{3.24}$$

$$f(\theta_2, \varphi_2) = r_2\lambda_2 \cos(n_2\theta_2) + r_2 \lambda_2 \cos(n_2\varphi_2) \tag{3.25}$$

Where $2\lambda_2 r_2$ can be calculated from Equation 11, which represents the maximum value of Δr_2, and the $f(\theta_2, \varphi_2)$ is calculated using Equation 25.

When particle 2 has a significantly larger size compared to particle 1 in Model 2 (aspect ratio higher than 30), Equation 3.24 can be applied instead of Equation 3.19 to calculate h. Thus, the value of h is different in Equations 3.21-3.23. The calculation processes in Model 2 are still the same as those in Model 1, except for using Equation 3.24 in Model 2 instead of equation 3.19 in Model 1. Thus, Model 2 could be applied to simulate the rough particle interaction when the scale of aspect ratio r_2/r_1 ranges from 30 to 50.

3.3.3.3 Model 3 to simulate the aspect ratio effects on the interfacial interaction

If the aspect ratio (r_2/r_1) continues to increase above 50, particle 2 could be seen as an infinite and smooth flat plate by particle 1 [39, 40]. Thus, the interaction will change to a rough particle-smooth flat surface interaction as shown in Figure A.1.4. For the interaction of particle and flat surface, the related distance between two different areas is given in Equation 3.26 [22]:

$$h = r_1 + D - R_1 \cos\theta_1 + 2\lambda_1 r_1 \tag{3.26}$$

where $2\lambda_1 r_1$ can be calculated from Equation 11, which represents the maximum value of Δr_1 [22]. Similar to Model 2, Equation 3.26 is used to replace Equation 3.19, and Equations 3.21-3.23 are still used for modeling the interaction of particles. In this case, Model 3 is constructed to simulate the interaction between two rough particles when the aspect ratio is above 50. We assumed the asperity surface of particle 2 is relatively horizontal to particle 1, which avoids the angle effects depending on the location of the asperity.

3.3.4 Comparison of different models

The ANOVA test with replication was conducted to compare the results of interaction energy generated following Model 1, Model 2, and Model 3 when the aspect ratio changed from 30 to 55. The benefits and weaknesses of the three models were analyzed. The optimal model is selected to test the effects of constructing properties of rough particles on interfacial interaction.

3.3.5 Aspect ratio

In this work, the impact of aspect ratio (r_2/r_1) in the range of 2.5 to 50 on the total interfacial interaction energy between rough particles was considered based on the modeling results.

3.3.6 Particle roughness

Because the asperity number and asperity ratio have been proved to represent the surface roughness [41], two scenarios are found in a colloidal system: two-particle interactions with the same roughness and two-particle interactions with different roughness. It is reasonable to have different particle

interactions because the morphology and thus coagulation affinity of particles are hardly the same. It is necessary to consider the variable surface roughness for studying the interaction of particles. These two scenarios can be described by Equations 3.27 and 3.28:

If the parameters of two particles changed simultaneously, then

$$\begin{cases} R_1 = r_1 + r_1\lambda_1\cos(n_1\theta_1) + r_1\lambda_1\cos(n_1\varphi_1) \\ R_2 = r_1 + r_1\lambda_2\cos(n_2\theta_2) + r_2\lambda_2\cos(n_2\varphi_2) \end{cases} \text{if } n_1 = n_2, \lambda_1 = \lambda_2 \tag{3.27}$$

, and if only the parameters of one particle changed, then

$$\begin{cases} R_1 = r_1 + r_1\lambda_1\cos(n_1\theta_1) + r_1\lambda_1\cos(n_1\varphi_1) \\ R_2 = r_2 + r_2\lambda_2\cos(n_2\theta_2) + r_2\lambda_2\cos(n_2\varphi_2) \end{cases} \text{if } n_1 \neq n_2 \text{ or } \lambda_1 \neq \lambda_2 \tag{3.28}$$

The asperity number, relative asperity number, asperity ratio, and relative asperity ratio effects on the total interfacial energy could be analyzed based on the modeling results.

3.3.7 Particle size

In this modeling study, the weight and density of particles were not taken into account, and only the size of the particles is considered for analysis. Two groups were selected to study particle size effects: 1) the radius of particle 1 was changed from 50 nm to 90 nm, and the radius of particle 2 was 100 nm; 2) the radius of particle 1 was changed from 500 nm to 900 nm, and the radius of particle 2 was 1000 nm. In these cases, the effects of particle size and relative particle size on the total interaction energy of the particles were also analyzed based on the modeling results.

3.3.8 Orientation-averaged effect

The orientation-averaged interaction energy of rough particles at a given distance (h) can be calculated by using the Boltzmann statistics (canonical average) according to equation 3.29 [42-44]:

$$\langle U(h) \rangle_\Pi = \frac{\int U_\Pi(h,\Omega)e^{(-\beta U_\Pi(h,\Omega))}d\Omega}{\int e^{(-\beta U_\Pi(h,\Omega))}d\Omega} \tag{3.29}$$

The orientation-averaged configuration can be expressed according to equation 3.30 [45]:

$$d\Omega = sin\omega_1 sin\omega_2 d\omega_1 d\omega_2 d\psi_1 d\psi_2 \tag{3.30}$$

Where the Π denotes LW, EL, or AB (i.e., three individual interactions in XDLVO theory), the ω_1 and ω_2 represent the orientation angles of two particles in θ direction, ψ_1 and ψ_2 represent the orientation angles of two particles in φ direction and $\beta = (kT)^{-1}$.

3.3.9 Proposed method verification

The correctness of the simulation could be verified in two strategies based on previous studies [22,24,68]. One is by comparing the present simulation with the classical method (DA) under

predefined scenarios. Another one is by analyzing the simulation errors under different numbers of calculation segments. The process of model verification was described in the supplementary material.

3.4 Results and Discussion

3.4.1 Comparison of different models

The comparison of the three models when the aspect ratio was smaller than 30 is not involved in the present study because the relatively large particle can still be considered a sphere when the aspect ratio is smaller than 30 [39]. Therefore, when the aspect ratio is smaller than 30, Model 1 is selected as the most accurate method to calculate the interaction between particles. According to Equations 24 and 26 (Figures A.1.3 and A.1.4), Model 2 and Model 3 were established to simulate rough particle interactions that had significantly different sizes. According to the ANOVA test for three models and the analysis provided in Figure A.1.6, we concluded that when the aspect ratio was greater than 50 (for this situation, no roughness on particle 2 can be observed by particle 1), Model 3 can be used for improving the accuracy of the simulation results. Also, Model 1 can be applied to simulate the particle interactions instead of Model 2 if the aspect ratio is smaller than 50 in the present study. More details about model comparisons were shown in the supplementary material. Based on the above evaluation results, Model 1 and Model 3 were selected to simulate the rough particle interactions in the following analysis. As we discussed in the supplementary material, particle 2 is regarded as a smooth plate in Model 3, and only particle 1 has variable parameters. Thus, Model 3 is mainly used when the relative surface roughness and particle size effect were studied in the next sections.

3.4.2 Aspect ratio effects

Based on the previous discussion, we mainly elaborate on the scale of aspect ratios smaller than 50 using Model 1. In Figure 2, the aspect ratio (r_2/r_1) increased from 2.5 to 50 ($n_1=n_2=20$, $\lambda_1=\lambda_2=0.005$), which dropped the interfacial energy between particles to 0 kT inferring that the smaller particles suffer less repulsion force, and particles might aggregate to a large particle easily. Similar results can be found in Figure A.1.7 based on Model 3. The depth of the primary minimum is critical to evaluating the initial state of systems where the particles could be assumed to be coagulated. The depth of the primary minimum is gradually decreased with increasing the aspect ratio indicating that the effective coagulation rate is reduced in the primary interaction [46]. The results shown in Figures 2 and A.1.7 suggest that the significant difference in the aspect ratio reduces the primary minimum, which caused the low

efficiency of flocculation in a short separation distance.

The height of the primary maximum is an important parameter in determining the charged suspension stability. The primary maximum is the energy obstacle that needs to be overcome to destabilize the system. If the surface charge is low, the energy barrier will be low, and the nanoparticles will slowly aggregate. If the energy barrier is higher than 20 kT at a time, the dispersion system is generally considered to have kinetic stability [47]. When the aspect ratio is around 20 (Figure 2), the primary maximum is smaller than 20 kT indicating that the suspension system becomes unstable and particles tend to aggregate. He and his coworkers had viewed that the particles with different aspect ratios had a different tendency to aggregate [48]. The results suggest that the primary maximum drops with increasing the aspect ratio yield the destabilization of the suspension, which is similar to the prediction reported by He and coworkers [48] even though they did not consider hydrophobic interactions and surface roughness. Generally, a decrease in surface energy would result in particle aggregation. As a larger particle has a relatively larger attraction force than a smaller particle, it can overcome the repulsion force developed between two particles more easily. Consequently, the model predicts that if two particles have a larger difference in the aspect ratio, the two particles tend to aggregate and destabilize the colloidal system more greatly.
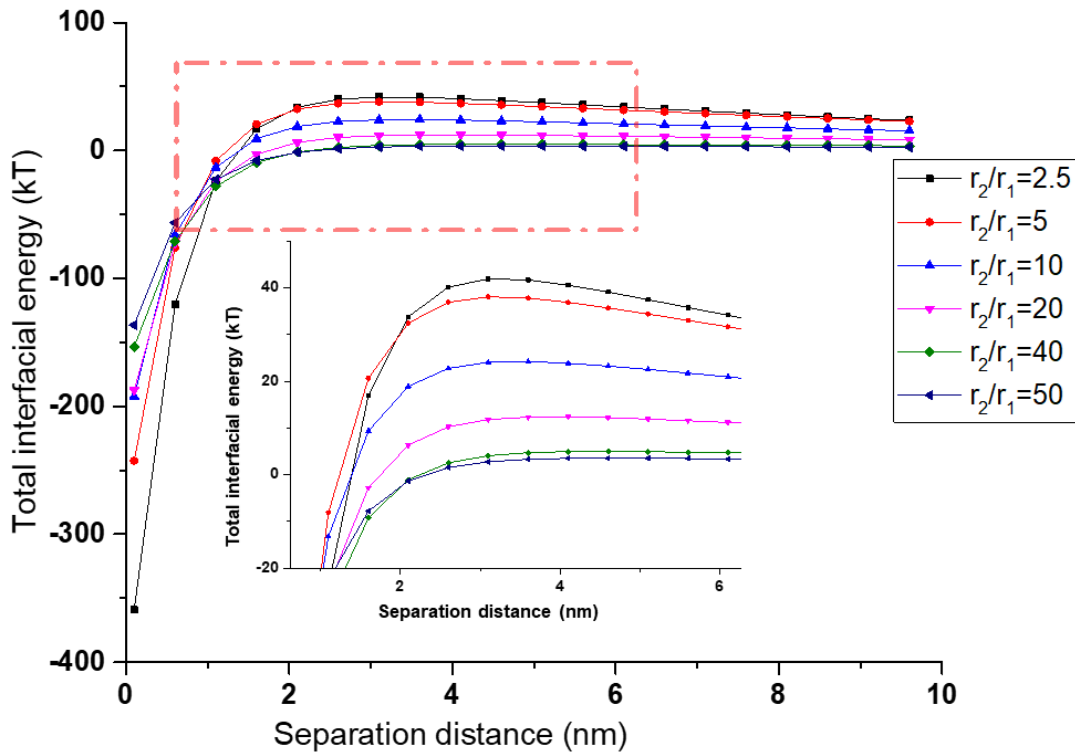
Figure. 3.2 Aspect ratio effect on the total interfacial energy following Model 1 ($n_1=n_2=20$, $\lambda_1=\lambda_2=0.005$)

3.4.3 Asperity number effects

The number of asperities indicated the frequency of modeled ripple or the density of surface roughness. The variations in the total interfacial interaction between two identical rough particles of the same size and asperity ratio ($r_1=r_2=1000$ nm, $\lambda_1=\lambda_2=0.001$) but with different asperity numbers (n) are shown in Figure 3. With increasing the number of asperities from 5 to 20, the energy barrier dropped from 200 kT to 150 kT. Even though the U_{AB}, U_{EL} and U_{LW} were included in this model, the results are similar to the model that only included U_{EL} and U_{LW}, where the energy barrier decreased from 5.5 kT to 3 kT when the particle radius was 25 nm and the asperity ratio was 0.05 [25]. The reduced energy barrier and primary minimum decreased the total interfacial energy, which indicates that the stability of the rough particle is gradually undermined by increasing the asperity number. The primary minimum became close to 0 kT with raising the number of asperities (5 to 20) indicating a reduction in the attraction energy between two particles. This phenomenon is reasonable because the surface roughness decreased the adhesion force between particles [49]. This decrease in attraction energy occurred at the closest approach distance, which led to a shallow primary minimum. The shallow depth of the primary

56

minimum displays the state of the primary aggregation, which includes weak, reversible, and partial aggregation [46, 50]. Therefore, colloidal particles attached based on a shallower primary minimum are more easily separated by the Brownian motion [51]. Interestingly, increasing the surface roughness could directly reduce the primary minimum depth (Figure 3) leading to a low aggregation rate in a short separation distance, which may provide useful information for coating or adsorption applications. Indeed, rough particles can be imaged as smooth particles coated with many small particles. The process of increasing the asperity number is regarded as a coating process. According to the Monte Carlo simulation made by Kamp and coworkers [52], the drop in the absolute value of the primary minimum would be related to the increased surface coverage of small particles on the smooth surface, which could be considered an enhanced asperity number. The surface roughness leads to the drop in attraction forces by reducing the topographic features of particles. One interesting phenomenon could be found when the asperity number increased from 30 to 50 (Figure 3). The total interfacial energy of the particles displayed a slight increase in this variation of asperity number. This is because the electric repulsion energy decayed slower than attraction energy in the short separation distance (less than 5 nm) with increasing n_i. Eom and coworkers had viewed that the surface roughness could eliminate or reduce the primary minimum in the particle interactions [53]. Once the attraction force overtook the repulsion force, the system would generate the primary minimum. In other words, reducing the primary minimum made the electric repulsion force the dominant force in the system. Thus, increasing n_i reduced van der Waals and hydrophobic attraction energy more dominantly than electric repulsion energy. Based on the Equation 3.21-3.23, the U_{LW}, U_{AB}, U_{EL} decreased with increasing n_i, however, the U_{EL} decreased more slowly than the other two energy, and all of these energy components would drop with the distance. That is the reason why the total interaction energy would elevate when the n_i was increased from 30 to 50. Nevertheless, the tendency of surface roughness negatively impacting the interaction energy was not changed.
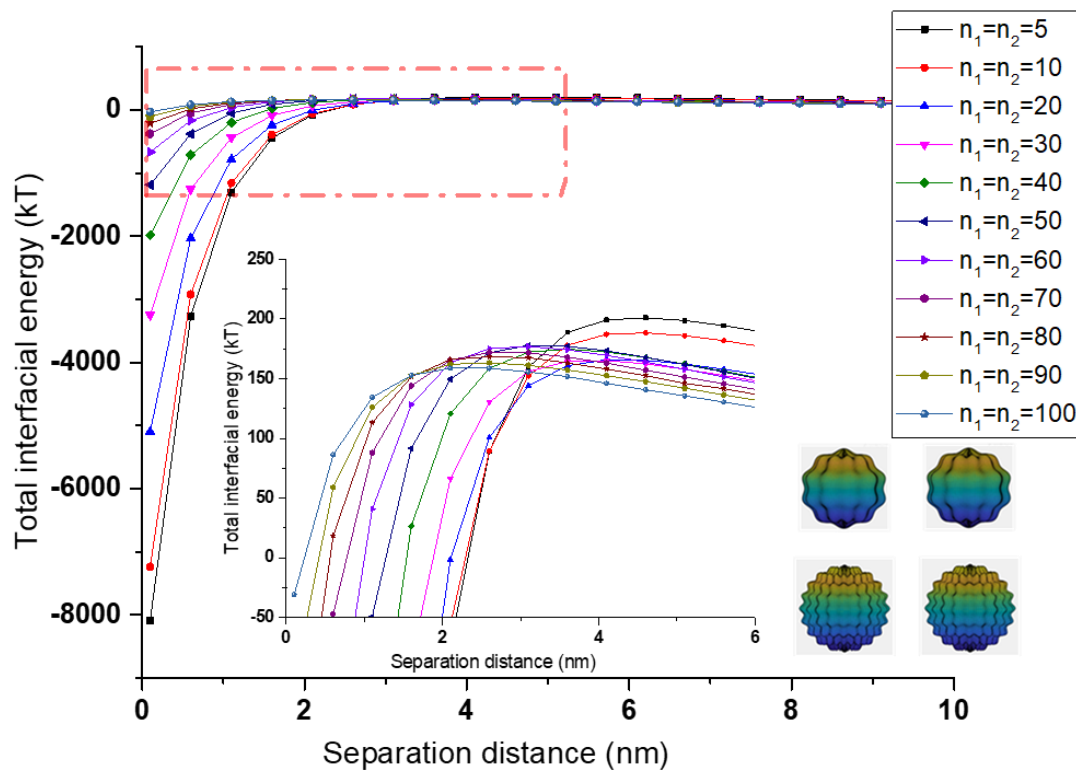
Figure 3.3 Effect of asperity density on the total interfacial energy of two particles ($r_1=r_2=1000$ nm, $\lambda_1=\lambda_2=0.001$) following Model 1.

3.4.4 Relative asperity number effects

As shown in Figure 4, with increasing one particle's asperity number and keeping the asperity number of another particle constant, the total interaction energy dropped ($r_1=r_2=1000$ nm, $\lambda_1=\lambda_2=0.005$). As the surface roughness of particle 2 is not involved in Model 3, Model 3 can only analyze the relative roughness effects on the interfacial interaction. Therefore, similar results can be found even if two particles have a significant difference in aspect ratio as shown in Figure A.1.8. This phenomenon was related to surface hydrophobicity. Increasing the asperity number resulted in asperities arranged more closely based on Equation 11 (Figure A.1.2b and A.1.2c). Das and coworkers claimed that the higher hydrophobicity was displayed by tightly arranged asperities rather than sparse asperities on the particle surface [54]. In another study, De Foggi and coworkers evaluated experimentally the roughness effects of disk-like denture-base acrylic resin on martial hydrophobicity and concluded that the surface roughness could provide greater surface area to enhance surface hydrophobicity [55]. The results of the present study showed that the increase in the hydrophobicity reduced the interaction energy of particles. The effect of relative asperity number between two particles suggested that the relative roughness

negatively impacted the total interaction energy. The low interaction could be explained by the smaller contact area and the larger relative distance between rough particles, which was created because of increasing the asperities of particle 2 in Model 1 or particle 1 in Model 3.
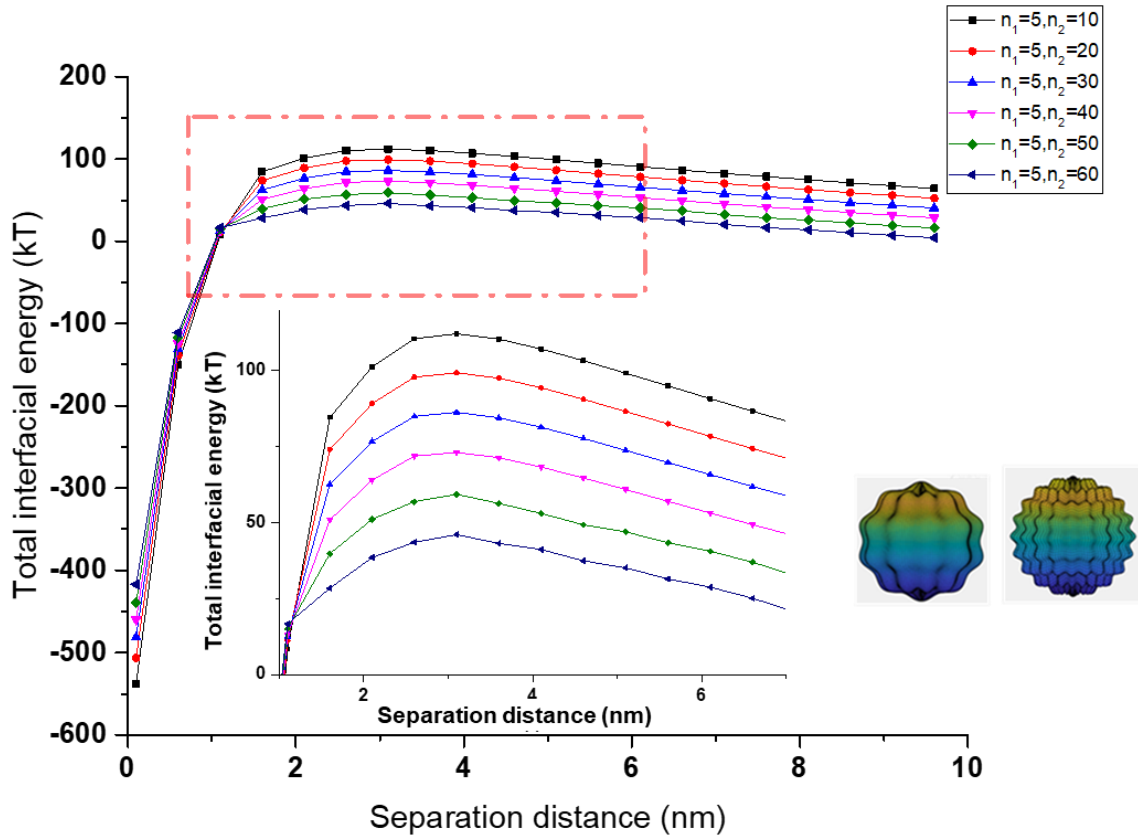
Figure 3.4 The effect of relative asperity density on the total interfacial energy of two particles ($r_1=r_2=1000$ nm, $\lambda_1=\lambda_2=0.005$) following Model 1

3.4.5 Asperity ratio effects

The asperity ratio directly controls the asperity size on the particle surface. This parameter is critical to simulating a rough particle because if the ratio was zero, this particle would be smooth. The contact surface between two rough particles is significantly influenced by the variation in the asperity ratio, which directly impacts the stability of the colloidal system. Figure 5 illustrates the impact of the asperity ratio on the total interaction energy of two approaching particles ($r_1=r_2=1000$ nm, $n_1=n_2=10$). At the asperity ratio of 0.0001, the system displayed strong stability, and Figure 5 showed the most significant primary barrier (216 kT) with no secondary minimum. At the asperity ratio of 0.01, the total energy was close to 0, implying that the stability of the system deteriorated and more colloidal particles tended to agglomerate. This phenomenon indicated that the roughness enhancement altered the interaction of particles and led to system instability [31]. In addition, the energy barrier dropped with increasing the

59

asperity ratio. The particles may aggregate without sufficient electric repulsion force to overcome the attractions among them [56]. In another aspect, surface roughness reduces the contact area of the particles because the asperity height and size were increased with increasing roughness [57, 58]. Moreover, it also increased the separation distance between particles due to the increase in the asperity height, which may enhance the possibility to interlock adjacent particles mechanically.
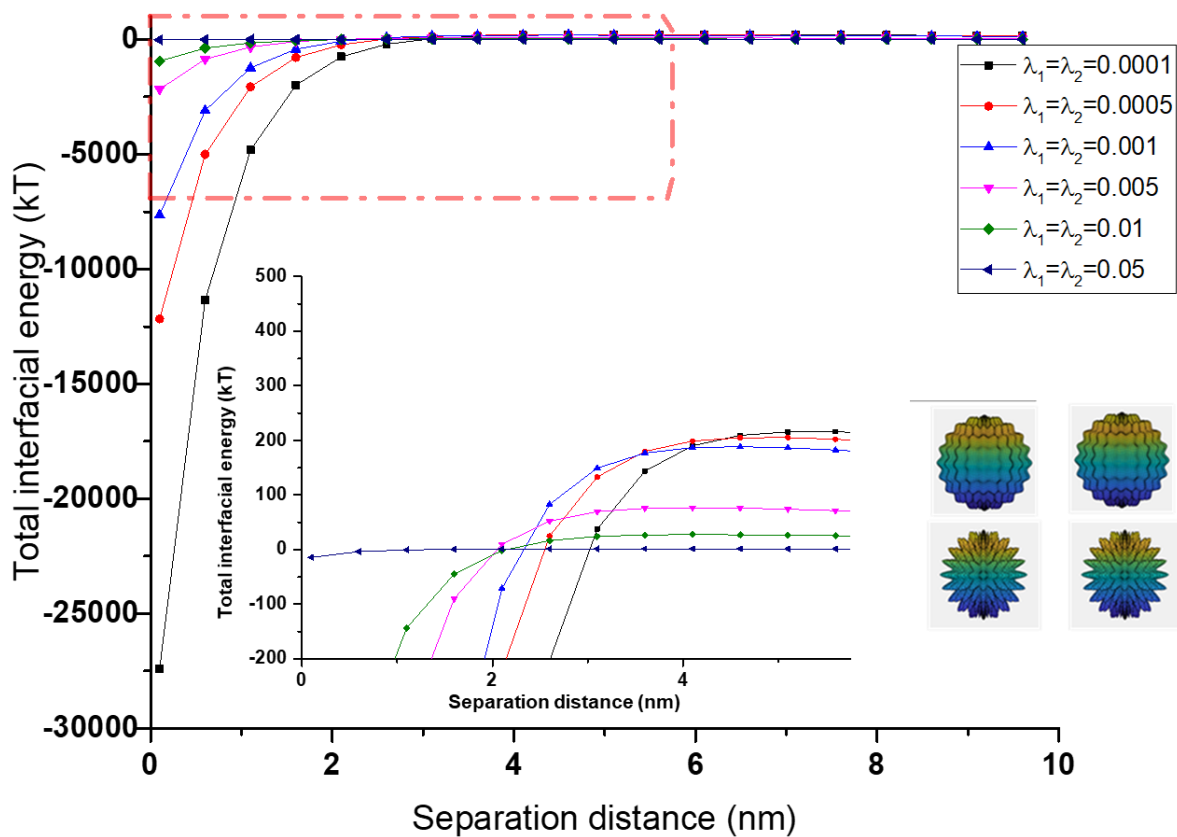
Figure 3.5 Asperity ratio effect on the total interfacial energy between rough particles ($r_1=r_2=1000$ nm, $n_1=n_2=10$) following Model 1

3.4.6 Relative asperity ratio effects

The interfacial energy created between two approaching particles of different asperity ratios ($r_1=r_2=1000$ nm, $n_1=n_2=5$) is shown in Figure 6, which was developed considering Equations 3.22 - 3.24. Even under the conditions considered in Model 3, the variation in the interfacial energy is similar as shown in Figure A.1.9. The total interfacial interaction energy decreased with increasing the asperity ratio of particle 1 without considering the surface roughness of particle 2 in Model 3. The relative asperity ratio directly affected the contact area of the two particles, and it impacted h (i.e., the distance

between particle 1 and any points of particle 2). The asperity ratio of particle 2 significantly influenced the interaction of two particles even if the asperity ratio of particle 1 was constant. As λ_i is a roughness parameter, an increase in λ_i will increase the roughness of the particle surface. A similar phenomenon was discussed by Guven and coworkers investigating the effect of the surface roughness on the particle-bubble colloidal interaction, and the results indicated that increasing the asperity size yielded a decrease in the energy barrier [59]. The bubble was assumed to be smooth ($\lambda_i = 0$) in the literature study, thus the variation occurred on the asperity size of another particle surface could be considered the variation in the asperity ratio. However, the present model considered two particles' surface roughness, where the particle-bubble interaction was only a special case. The variation in the asperity size is the consequence of Equation 11 when λ_i is changed and n_i is maintained constant. When λ_2 changed from 0.002 to 0.01, the total interaction decreased gradually and the primary maximum decreased from 170 kT to 90 kT (Figure 6). The relative difference in the asperity ratio is related to the surface morphology, which would impact the particle attachment because the needle-like asperity (at a high asperity ratio) has more effect in enhancing the particle attachment affinity compared with the rounded tip on the surface [60]. The main reason for increased particle attachment efficiency could be that, compared with the round dip asperity, the sharp asperity would provide a smaller contact area for the opposite particle, which would cause a lower energy barrier for particle interactions. The asperity ratio should have a significant effect on the probability of particle attachment even if it is changed to a nanoscale. Thus, the rougher surface provided a smaller energy barrier that could be overcome more readily by van der Waals attract and hydrophobic interaction forces. These facts also suggest that the surface roughness of particles can influence the properties of colloidal particles because the system stability and particle dispersibility can easily be controlled by surface asperity.
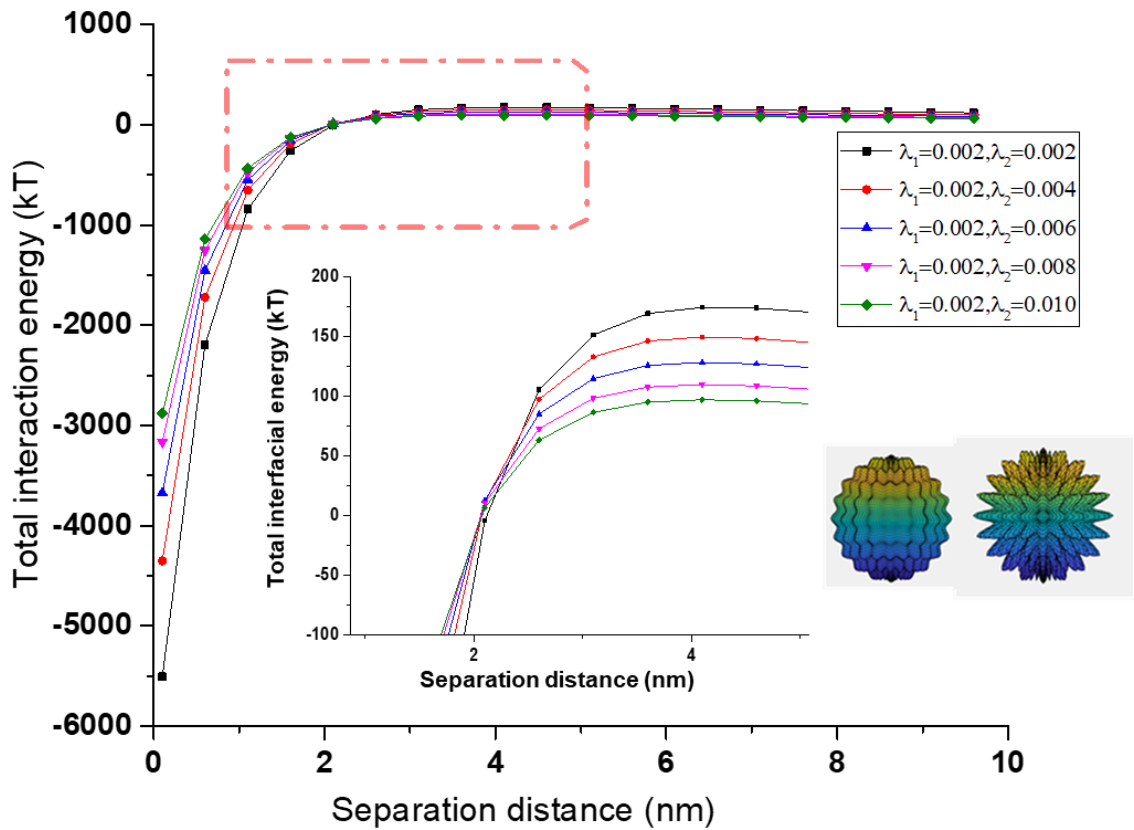
Figure 3.6 Relative asperity ratio effect on the total interfacial energy between rough particles ($r_1=r_2=1000$ nm, $n_1=n_2=5$) following Model 1

3.4.7 The effect of particle size on the interaction of rough particles

In real colloid systems, particles may be available in different sizes. Figure 7 shows the two group of particles ($n_1=n_2=10$, $\lambda_1=\lambda_2=0.001$). In group 1, the radius of particle 1 varied from 50 nm to 90 nm, while particle 2 had a 100 nm radius. In group 2, the radius of particle 1 was changed from 500 nm to 900 nm, and the radius of particle 2 was maintained at 1000 nm (the aspect ratio is constant). As shown in Figure 11, the impact of particle size on the interaction energy of the particles was apparent. The interaction energy between larger particles was greater than that between smaller particles, implying that larger particles were more susceptible to dispersion. Even with Model 3, the results still show a similar tendency in Figure A.1.10. When the radius of particle 1 increased from 50 nm to 200 nm with a constant radius of particle 2 (1000 nm), the interaction energy increased as well. In another work, a higher aggregation rate occurred for smaller particles when investigating the size of nanoparticles (with the sizes of 12, 32, and 65 nm of hematite) on the aggregation and stability [61]. The main reason could

be explained by the elevated surface energy. Reduced particle size will result in a large relative surface energy, which will destabilize the colloidal system [61]. The smaller particles with higher surface energy are more likely to aggregate compared with larger particles because the aggregation will lower the free energy of the system. In this study, when the size of particle 1 increased from 50 nm to 90 nm, the primary maximum slightly increased, which also indicated that the 50 nm particles were aggregated more readily because a smaller energy barrier needed to be overcome for their aggregation. Also, if the size of particles 1 and 2 was increased to 500 and 1000 nm, respectively, the primary maximum significantly increased. Our results also suggested that the larger relative size between particles caused less colloidal stability. Yin and Wang studied the particle size effect on scheelite flotation and concluded that the total interfacial energy and shear force were increased with enlarging the coarse particles, and the coagulation rate decreased with increasing particle size [62].
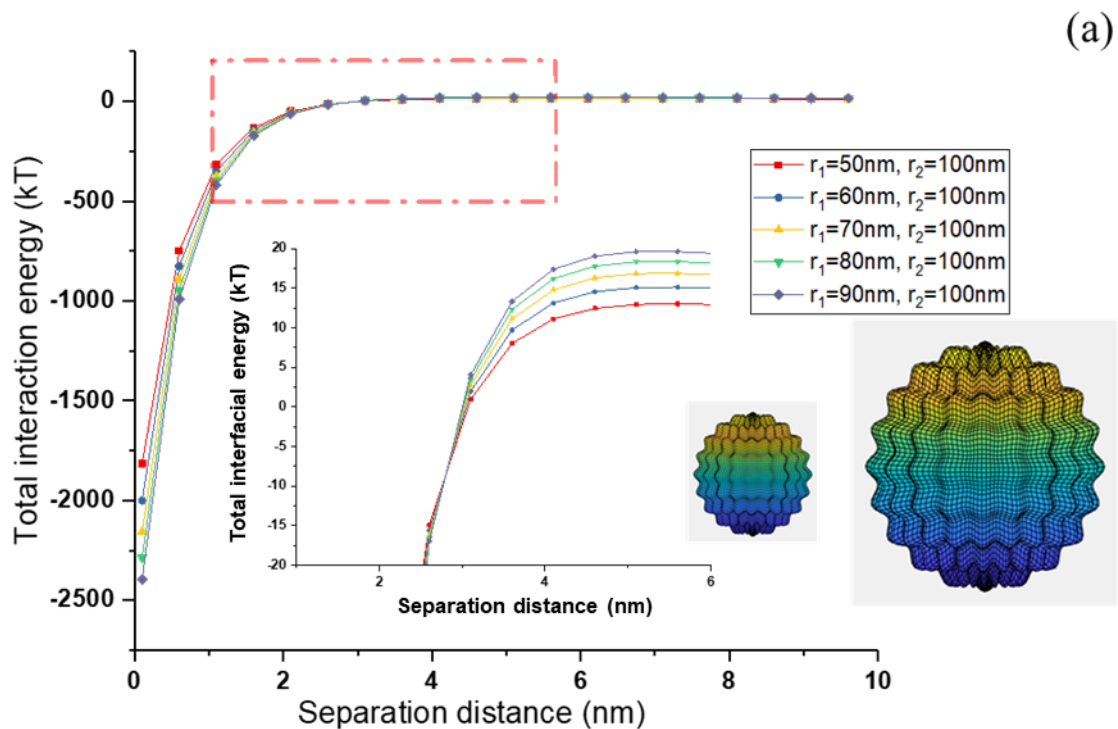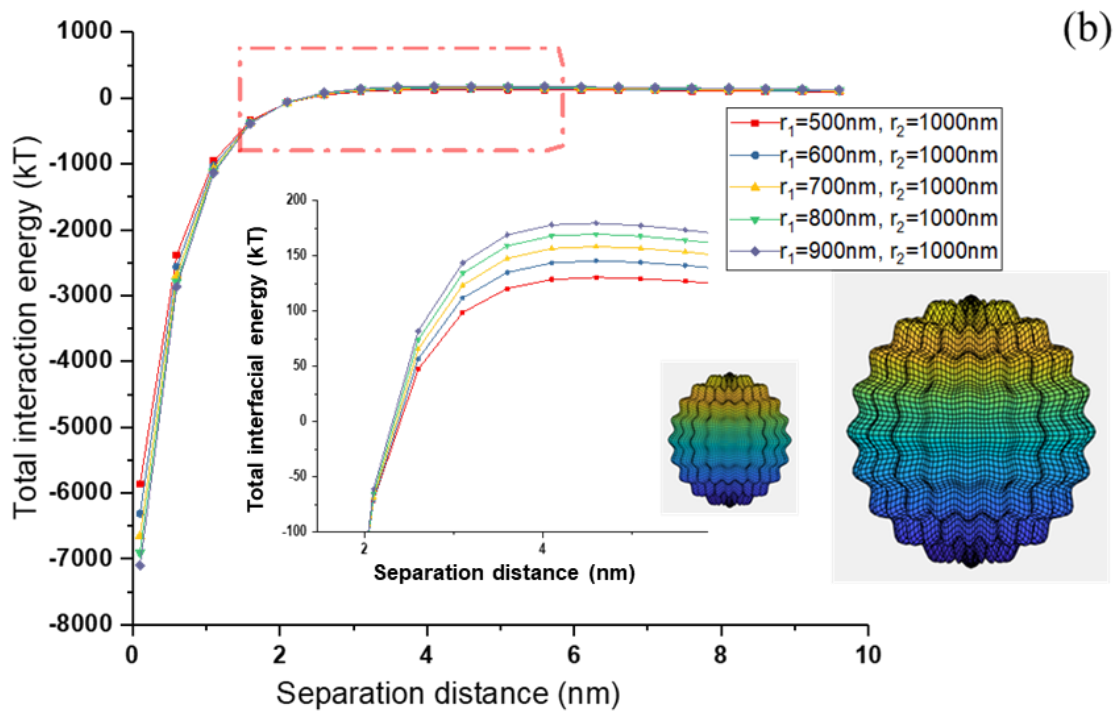
Figure 3.7   Particle size effect on the total interfacial energy between rough particles (n_1=n_2=10, λ_1=λ_2=0.001) following Model 1. (a) r_1 is changed from 50 to 90 nm, r_2 is fixed at 100 nm. (b) r_1 is changed from 500 nm to 900 nm, r_2 is fixed at 1000 nm

3.4.8 Orientation-averaged effects

The orientation-averaged and orientation-absent interfacial energy created between two approaching particles (r_1=r_2=1000 nm, n_1=n_2=10, λ_1=λ_2=0.001) for the same particles are shown in Figure 8, which was developed utilizing equations 3.29 and 3.30. Compared with the interaction energy without considering the orientation, the orientation-averaged interfacial interaction energy dropped at a shorter distance (less than 3 nm) between the particles. Our results indicated that the orientation angle would decrease the total interaction between the particles. The orientation angle influences the effective interaction distance between two rough particles. As the rippled particle possesses protrusions and depressions on its surface, the effective distance between the particles (h) could be changed with different orientation angles because the protrusions of this particle could rotate its place and face the depressions of the opposite particle instead of the protrusions if particles changed orientation angle in θ or φ direction. Li and coworkers applied molecular dynamic simulation to analyze orientation-dependent adhesion force between titanium dioxide nanocrystals and demonstrated that the adhesion

affinity of nanocrystals would decrease when the orientation angle increased from 0° to 90°[63]. Gomez-Flores and coworkers reported that the orientation angle would also affect the DLVO interaction between carbon nanotubes [64]. Our model predicted similar results with a shallower primary minimum for orientation-averaged than orientation-absent particle interactions. Based on the results in section 3.1, when the aspect ratio is above 50, the larger particle will be seen as a smooth plate by particle 2. As the opposite surface of particle 1 is a smooth flat plate that does not seem to possess the protrusions and depressions in Model 3, the orientation effect was not considered for when the aspect ratio is above 50 (Model 3) in the modeling analysis.
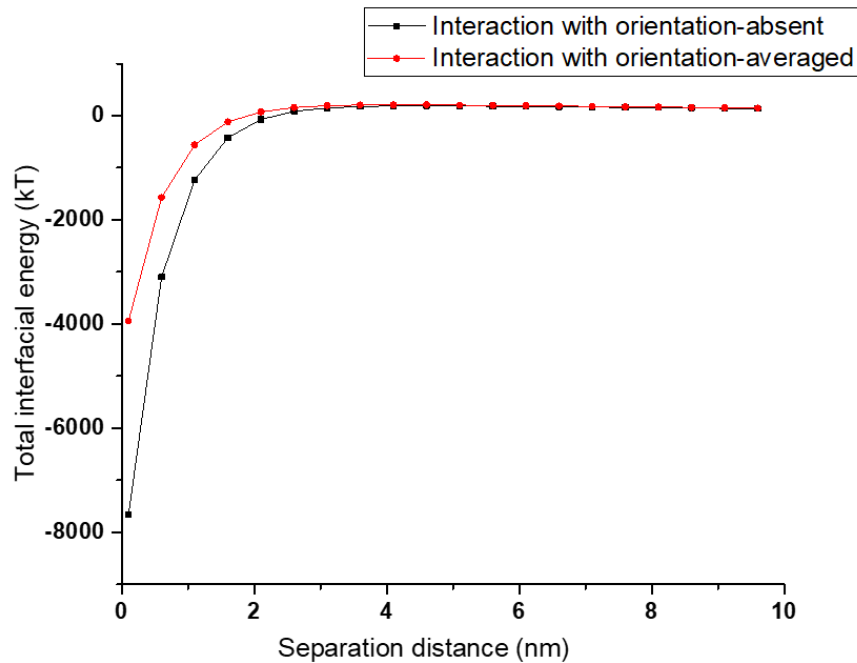
Figure 3.8 The comparison between orientation-averaged and orientation-absent effects on two rough particle interactions following Model 1 ($r_1=r_2=1000$ nm, $\lambda_1=\lambda_2=0.001, n_1=n_2=10$)

3.4.9 The comparison of parameters impacting interfacial energy

As discussed above, the particle size, aspect ratio, asperity ratio, and asperity number affect the interaction of rough particles. The particle size had the most remarkable impact on particle interaction among other parameters (Figure 7). Also, the aspect ratio has the least effect on the total interaction energy. An interesting phenomenon was observed (Figure A.1.11) when changing the asperity ratio and asperity number simultaneously at the particle radius of 1000 nm. When the λ_i was 0.01, the primary maximum was -25 kT at $n_i= 10$. However, when the λ_i was fixed at 0.01, and n_i decreased from 10 to 5, the primary maximum was significantly enhanced (60 kT). Similar behavior was found when λ_i was

0.05 or 0.1, and the total interfacial energy can be improved by decreasing the value of n_i. The main reason is the variation in surface morphology, which is caused by surface roughness. To enhance the stability of the colloidal system, the adjustment in constructing parameters for surface roughness is desirable. The roughness of particles depends on the ripples that are constructed by the asperity ratio and asperity number [65]. The results show that there is a correlation between λ_i and n_i affecting the stability or particle dispersibility in the colloidal system.

In Figure 9, the comparison between the asperity number and the asperity ratio was analyzed with different parameters from the previous analysis. The profile of total interfacial energy under XDLVO theory when the $r_1 = r_2 = 1000$ nm, $n_1 = n_2 = 20$, $\lambda_1 = \lambda_2 = 0.01$ was selected as the control profile. The contrast was built up when the value of n_i and λ_i increased to 1, 5, and 10 times as large as that of the control ones. In this comparison, the effect of n_i at the fixed λ_i had less impact on the interaction energy compared with the effect of λ_i at the fixed n_i in Figure (9b). Suresh and Walz studied the surface roughness effect on the interaction energy between a particle and a smooth flat plate, where they also concluded that the asperity number had smaller effects than the asperity ratio on the interaction energy (only considering van der Waals attraction and electric repulsion) [66]. The present study included hydrophobic interaction between two rough particles, but the same results as Suresh and Walz's results were noticed.

As we discussed earlier, the development of the primary maximum is due to the strength of double-layer interaction. The larger magnitude of the primary maximum represents the more energy that needs to be overcome to agglomerate particles [67]. The different colloidal systems own individual benchmarks of the primary maximum to control the system state. Once the magnitude of the primary maximum in a charged suspension is below 20 kT, the particles will aggregate [47]. Van Oss and coworkers stated that if the primary maximum is less than 1.5 kT, flocculation is allowed to occur in the hectorite suspension system [14]. The prediction under the XDLVO theory had applied successfully in the soil-colloidal system. Calero and coworkers reported that the most favorable aggregation state for iron is that the total interaction energy is less than 100 kT in the agricultural soil system [68].
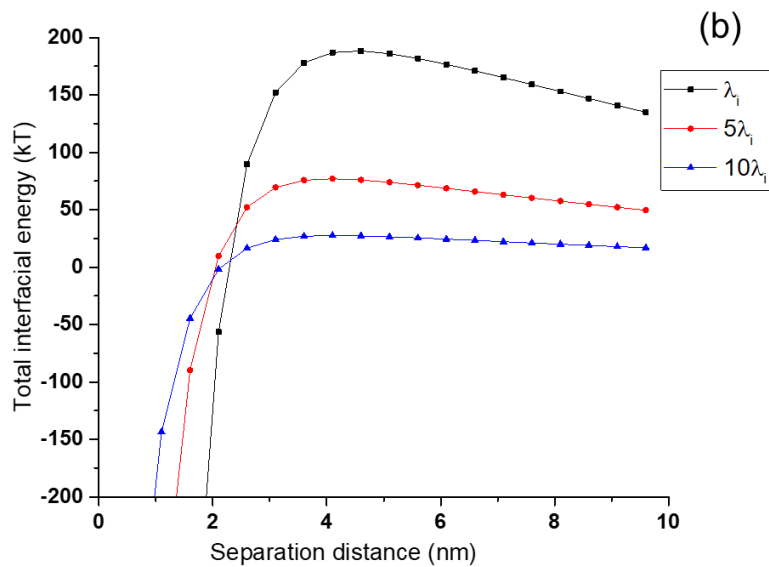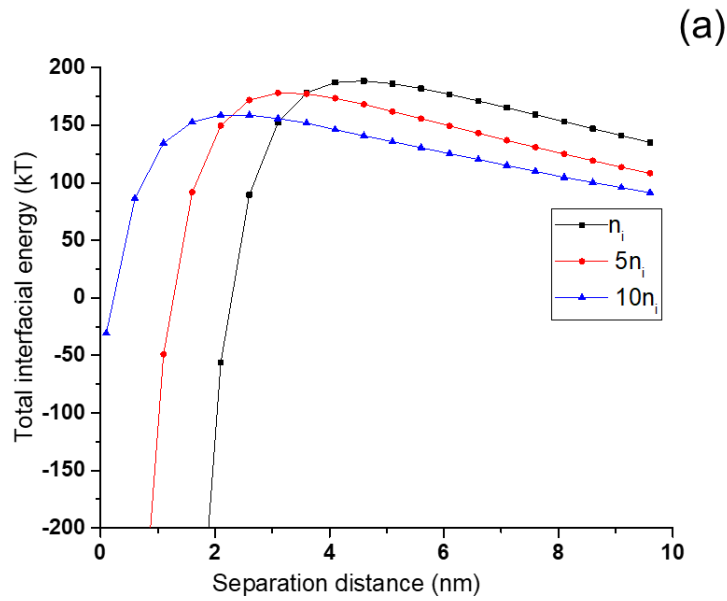
Figure 3.9 (a) The effect of asperity number at a fixed asperity ratio ($r_1=r_2=1000$ nm, $\lambda_1=\lambda_2=0.01$). (b) The effect of the asperity ratio at a fixed asperity number ($r_1=r_2=1000$ nm, $n_1=n_2=20$) following model 1

3.4.10 Comparison of present modeling and experimental outcomes

To investigate the accuracy of the results, the generated results were compared with the experimental and modeling results available in the literature, and the results are shown in Table 3.1.

Table 3.1. The comparison between the present model and the experiment from the literature

Type of analysis, ref	Materials	conditions	variables	Theory	Results	
					Primary minimum	Primary maximum
Experimental, [69]	Silica aerogel particles	Asperity number of 10 and particle radius of 400 nm	Asperity ratio increased from 0.001 to 0.05	DLVO	N/A	Decreased from 23 kT to 0.1 kT
Simulation, present work	-	Asperity number of 10 and particle radius of 400 nm	Asperity ratio increased from 0.001 to 0.05	XDLVO	Decreased from 5100 kT to 59 kT	Decreased from 77 kT to 0.6 kT
Experimental, [69]	Silica aerogel particles	Asperity ratio of 0.005 and particle radius of 400 nm	Asperity number increased from 10 to 20	DLVO	N/A	Decreased from 3 kT to 0.01 kT
Simulation, present work	-	Asperity ratio of 0.005 and particle radius of 400 nm	Asperity number increased from 10 to 20	XDLVO	Decreased from 1260 kT to 420 kT	Decreased from 50 kT to 35 kT
Experimental, [59]	Methylated roughened glass	Asperity number	Asperity height	XDLVO	N/A	Decreased from 105

	particles	N/A and particle radius of 150 µm	increased from 10 to 70 nm			kT to 7 kT
Simulation, present work	-	Asperity number of 10 and particle radius of 150 µm	Asperity ratio increased from 0.01 to 0.07	XDLVO	Decreased from 6000 kT to 4000 kT	Decreased from 98 kT to 5 kT
Experimental, [70]	Fluoresbrite™ carboxyl latex particles	Asperity ratio N/A and particle radius of 10 µm	Asperity number increased from 5 to 20	DLVO	Decreased from 990 kT to 50 kT	N/A
Simulation, present work	-	Asperity ratio of 0.005 and particle radius of 10 µm	Asperity number increased from 5 to 20	XDLVO	Decreased from 9000 kT to 1800 kT	Decreased from 246 kT to 48 kT
Simulation, [71]	Hemi spherical pillars planar interacts with a smooth particle	Asperity number N/A and particle radius of 10 µm	The height of pillars increased from 75 to 150 nm	DLVO	N/A	Decreased from 700 kT to 500 kT
Simulation, present work	-	Asperity number of 10 and particle	Asperity ratio increased from 0.001	XDLVO	Decreased from 21000 kT to 888 kT	Decreased from 640 kT to 168 kT

		radius of 10 µm	to 0.005			
Simulation, [25]	Two rough particles interaction	Asperity ratio of 0.05 and particle radius of 25 nm	Asperity number increased from 10 to 25	DLVO	N/A	Decreased from 5.5 kT to 3 kT
Simulation, present work	-	Asperity ratio of 0.05 and particle radius of 25 nm	Asperity number increased from 10 to 25	XDLVO	Decreased from 12 kT to 6 kT	Decreased from 3 kT to 1.8 kT

In the studies carried out using silica aerogel particles, when the asperity number increased from 10 to 20, the primary maximum dropped from 3 to 0.01 kT [69]. For the same size particles, our modeling results predicted the primary maximum change from 50 to 35 kT. When the asperity ratio of silica particles altered from 0.001 to 0.05, the primary maximum decreased from 23 to 0.1 kT [69]. The present model predicted the primary maximum change from 77 to 0.6 kT. When the asperity number of FluoresbriteTM carboxyl latex particles was altered from 5 to 20 (Table 3.1), the primary minimum decreased from 990 to 50 kT. Under the same conditions, our modeling results predicted the primary minimum change from 9000 to 1800 kT. As the previous experimental work relied on the DLVO theory but the present work was based on the XDLVO theory, the difference between the modeling and experimental results would be related to the inclusion of hydrophobic interaction in the present work, especially for the primary minimum. Hydrophobic interaction had been proved to be a dominant contributor to the system [72]. If the simulation included the energy of hydrophobic interaction, a significant difference between the simulation results (based on the XDLVO theory) and experimental results (based on the DLVO theory) may be observed. In addition, the asperity size in the laboratory experiment could not be controlled accurately. The reason is that it is difficult to increase the asperity number without changing any asperity size in the experiments, which limits the outcomes of the experimental results generally. However, the modeling study, such as the present work, can simulate

these parameters independently and thus the results would predict the significant effect of each parameter independently.

The methylated roughened glass particles were used in investigating the impact of asperity size (a change from 10 nm to 70 nm) in experimental studies (Table 3.1), which predicted a decrease in the primary maximum from 105 to 7 kT [59]. The present modeling investigation showed a similar trend (a change from 98 to 5 kT when the asperity size was changed from 0.01 to 0.07). Both of rough particle simulation analysis included the XDLVO theory, and they predicted similar results as expected. It should be stated that the present modeling investigation considered both asperity radius and height (instead of just asperity height in the previous work) as primary factors in shaping the surface morphology of particles [59].

Alternatively, in one modeling study, hemispherical pillars were applied to generate a rough surface [71], and the study predicted that the primary maximum would decrease from 700 to 500 kT when the height of pillars increased from 75 to 150 nm. Our current work applied a rippled sphere model to simulate the rough particles, and the results predicted that the primary maximum would drop from 640 kT to 180 kT. The difference between the two models would be related to the different approaches considered for constructing the rough surface. Our model simulated the rough surface as a sine wave instead of pillars, which can simplify the process of constructing particles and provides a tractable equation to simulate a rough surface (equation 11) [25]. In another modeling study, Bhattacharjee and coworkers utilized a similar method to that of the present study to construct rough particles, but they considered the DLVO theory for predicting the interaction of particles [25]. They reported that when the asperity number was increased from 10 to 25, the primary maximum decreased from 5.5 to 3 kT [25]. Under the same assumptions, our current studies showed a similar pattern (i.e., a drop from 3 to 1.8 kT). The slight difference between the simulation outcomes is that the interaction scenario in the previous work [25] was particle–plate interaction, and the interaction scenario of the present work was particle-particle interaction. But our model also predicted the primary minimum decreased from 12 kT to 6 kT. As our model considered the hydrophobic interaction in the analysis, our outcomes should be more reliable in predicting the interaction of particles in the real scenario.

Generally, the experimental and modeling results successfully anticipated similar trends for the interaction of particles when the surface morphology of particles was tailored differently. Therefore, the

present simulation analysis displayed an accurate prediction of the rough particle interaction based on the XDLVO theory. However, the comparison between the results available in the literature and current simulation work depicts that there would be a noticeable difference between the results 1) if the XDLVO rather than the DLVO was considered for the same system, 2) if the surface morphology parameters were considered differently, and 3) the construction methods of the rough surface were different.

3.5 Conclusions

We hypothesized that the total interfacial energy developed between two rough particles in colloidal systems would be dependent on the surface morphology of rough particles, and it could be determined following the XDLVO theory if aspects of surface roughness were considered. We constructed rough particles using MATLAB and simulated the interaction of the particles with a novel SEI approach in the XDLVO theory.

Previously, when the XDLVO theory was considered, the reported simulation approaches to surface interactions did not consider variables affecting the surface morphology of the particles [14, 17, 19-23, 36, 69-71]. For example, the method considering hemisphere pillars did not consider various aspects of the asperity shape on the surface of particles [71]. When the impact of surface morphology was considered, the report was primarily focused on the DLVO theory [25]. As the present simulation included the hydrophobic interactions (following the XDLVO theory), it generally predicted the interaction of the particles more comprehensively than previous reports on the experimental and modeling investigations following the DLVO theory [25]. In addition, the present study applied a rippled sphere model to consider more details of surface roughness rather than only considering asperity radius considered in the other theoretical and experimental studies conducted following the XDLVO theory [59].

In the current study, the analysis of the impact of aspect ratio on particle interaction facilitated the selection of the most suitable mathematical model for predicting the interaction of particles. The modeling results showed that the total interfacial energy decreased significantly with the elevation in the asperity number and asperity ratio. The increase in the relative asperity ratio and relative asperity number reduced the total interaction energy, which would be attributed to the improved hydrophobicity and altered surface morphology of particles. The largest changes in the primary maximum and minimum were observed when the particle size was changed because the change in the size led to the altered

interaction area between the two particles. Although the variable relative orientation angle caused the least influence on particle interaction, the simulation results indicated the importance of the movement of protrusions and depressions on a rough surface. In addition, the increased aspect ratio dropped the total interaction energy because of the hampered electric double layer between particles. The most effective parameter of surface morphology in monitoring the interfacial interaction energy was the asperity ratio.

As particles have different morphologies and sizes in colloidal systems, the present model can precisely predict the behavior of colloidal systems, such as metal coating, mineral suspensions, and membrane fouling. To improve the accuracy of the simulation, future studies may include the interaction of ellipsoidal rough particles in the simulation analysis since particles have varied shapes and dimensions in real colloidal systems. As natural-based particles are extensively available in colloidal suspensions, the impact of the surface softness of particles on the interaction of particles may be studied in the future.

3.6 Reference

[1] Y. Liang, N. Hilal, P. Langston, V. Starov, Interaction forces between colloidal particles in liquid: Theory and experiment, Adv. Colloid Interface Sci., 134 (2007) 151-166.

[2] S. Lawton, G. Steele, P. Shering, L. Zhao, I. Laird, X.-W. Ni, Continuous crystallization of pharmaceuticals using a continuous oscillatory baffled crystallizer, Organic Process Research & Development, 13 (2009) 1357-1363.

[3] T. Lin, Z. Lu, W. Chen, Interaction mechanisms and predictions on membrane fouling in an ultrafiltration system, using the XDLVO approach, J. Membr. Sci., 461 (2014) 49-58.

[4] J. Israelachvili, R. Pashley, Measurement of the hydrophobic interaction between two hydrophobic surfaces in aqueous electrolyte solutions, Journal of colloid and interface science, 98 (1984) 500-514.

[5] C. Shen, S. Bradford, Z. Wang, Y. Huang, Y. Zhang, B.J.L. Li, DLVO interaction energies between hollow spherical particles and collector surfaces, 33 (2017) 10455-10467.

[6] M.I. Chaudhari, S.B. Rempe, D. Asthagiri, L. Tan, L. Pratt, Molecular theory and the effects of solute attractive forces on hydrophobic interactions, The Journal of Physical Chemistry B, 120 (2016) 1864-1870.

[7] Y. Shi, T. Lammers, G. Storm, W.E. Hennink, Physico-chemical strategies to enhance stability and drug retention of polymeric micelles for tumor-targeted drug delivery, Macromol. Biosci., 17 (2017) 1600160.

[8] W. Wu, R. Giese, C. Van Oss, Stability versus flocculation of particle suspensions in water—correlation with the extended DLVO approach for aqueous systems, compared with classical DLVO theory, Colloids Surf. B. Biointerfaces, 14 (1999) 47-55.

[9] Y. Chen, M. Tian, X. Li, Y. Wang, A.K. An, J. Fang, T. He, Anti-wetting behavior of negatively charged superhydrophobic PVDF membranes in direct contact membrane distillation of emulsified wastewaters, J. Membr. Sci., 535 (2017) 230-238.

[10] S. Zhang, Q.V. Ly, L.D. Nghiem, J. Wang, J. Li, Y. Hu, Optimization and organic fouling behavior of zwitterion-modified thin-film composite polyamide membrane for water reclamation: A comprehensive study, J. Membr. Sci., 596 (2020) 117748.

[11] A. Sánchez-Iglesias, M. Grzelczak, T. Altantzis, B. Goris, J. Perez-Juste, S. Bals, G. Van Tendeloo, S.H. Donaldson Jr, B.F. Chmelka, J.N. Israelachvili, Hydrophobic interactions modulate self-assembly of nanoparticles, ACS nano, 6 (2012) 11059-11065.

[12] P. Qiu, C. Jensen, N. Charity, R. Towner, C. Mao, Oil phase evaporation-induced self-assembly of hydrophobic nanoparticles into spherical clusters with controlled surface chemistry in an oil-in-water dispersion and comparison of behaviors of individual and clustered iron oxide nanoparticles, J. Am. Chem. Soc., 132 (2010) 17724-17732.

[13] J. Lacava, P. Born, T. Kraus, Nanoparticle clusters with Lennard-Jones geometries, Nano Lett., 12 (2012) 3279-3282.

[14] C. Van Oss, R. Giese, P.M. Costanzo, DLVO and non-DLVO interactions in hectorite, Clays Clay Miner., 38 (1990) 151-159.

[15] S. Bayoudh, A. Othmane, L. Mora, H. Ben Ouada, Assessing bacterial adhesion using DLVO and XDLVO theories and the jet impingement technique, Colloids and Surfaces B: Biointerfaces, 73 (2009) 1-9.

[16] D. Siegismund, A. Undisz, S. Germerodt, S. Schuster, M. Rettenmayr, Quantification of the interaction between biomaterial surfaces and bacteria by 3-D modeling, Acta Biomater., 10 (2014) 267-275.

[17] S. Bhattacharjee, M. Elimelech, M. Borkovec, DLVO interaction between colloidal particles: beyond Derjaguin's approximation, Croatica Chemica Acta, 71 (1998) 883-903.

[18] X. Huang, S. Bhattacharjee, E.M. Hoek, Is Surface Roughness a "Scapegoat" or a Primary Factor When Defining Particle− Substrate Interactions?, Langmuir, 26 (2010) 2528-2537.

[19] G. Wiese, T. Healy, Effect of particle size on colloid stability, Transactions of the Faraday Society, 66 (1970) 490-499.

[20] R. Mei, R. Li, H. Lin, Z. Shen, M. Zhang, J. Chen, Y. He, A new approach to construct three-dimensional surface morphology of sludge flocs in a membrane bioreactor, Bioresour. Technol., 219 (2016) 521-526.

[21] R. Wilson, D. Dini, B.J.P.t. Van Wachem, The influence of surface roughness and adhesion on particle rolling, 312 (2017) 321-333.

[22] X. Cai, M. Zhang, L. Yang, H. Lin, X. Wu, Y. He, L. Shen, Quantification of interfacial interactions between a rough sludge floc and membrane surface in a membrane bioreactor, Journal of colloid and interface science, 490 (2017) 710-718.

[23] C.Q. LaMarche, S. Leadley, P. Liu, K.M. Kellogg, C.M. Hrenya, Method of quantifying surface roughness for accurate adhesive force predictions, Chem. Eng. Sci., 158 (2017) 140-153.

[24] G. Yu, X. Cai, L. Shen, J. Chen, H. Hong, H. Lin, R. Li, A novel integrated method for quantification of interfacial interactions between two rough bioparticles, Journal of Colloid and Interface Science, 516 (2018) 295-303.

[25] S. Bhattacharjee, C.-H. Ko, M. Elimelech, DLVO interaction between rough surfaces, Langmuir, 14 (1998) 3365-3375.

[26] C.J. van Oss, Acid—base interfacial interactions in aqueous media, Colloids and Surfaces A: Physicochemical and Engineering Aspects, 78 (1993) 1-49.

[27] S. Bhattacharjee, A. Sharma, Apolar, polar, and electrostatic interactions of spherical particles in cylindrical pores, Journal of colloid and interface science, 187 (1997) 83-95.

[28] R. Hogg, T.W. Healy, D.W. Fuerstenau, Mutual coagulation of colloidal dispersions, Transactions of the Faraday Society, 62 (1966) 1638-1651.

[29] G. Hwang, C.H. Lee, I.S. Ahn, B.J. Mhin, Analysis of the adhesion of Pseudomonas putida NCIB 9816-4 to a silica gel as a model soil using extended DLVO theory, Journal of Hazardous Materials, 179 (2010) 983-988.

[30] C. van Osa, B. Good, Surface enthalpy and entropy and the physico-chemical nature of hydrophobic and

hydrophilic interactions, Journal of dispersion science and technology, 12 (1991) 273-287.

[31] J. Dann, Forces involved in the adhesive process: I. Critical surface tensions of polymeric solids as determined with polar liquids, J. Colloid Interface Sci., 32 (1970) 302-320.

[32] R.J. Good, C.J. van Oss, The Modern Theory of Contact Angles and the Hydrogen Bond Components of Surface Energies, in: M.E. Schrader, G.I. Loeb (Eds.) Modern Approaches to Wettability: Theory and Applications, Springer US, Boston, MA, 1992, pp. 1-27.

[33] M. Zanini, C. Marschelke, S.E. Anachkov, E. Marini, A. Synytska, L. Isa, Universal emulsion stabilization from the arrested adsorption of rough particles at liquid-liquid interfaces, Nature communications, 8 (2017) 1-9.

[34] M. D'Acunzi, L. Mammen, M. Singh, X. Deng, M. Roth, G.K. Auernhammer, H.-J. Butt, D. Vollmer, Superhydrophobic surfaces by hybrid raspberry-like particles, Faraday Discuss., 146 (2010) 35-48.

[35] S. Shi, L. Zhou, T. Wang, L. Bian, Y. Tang, S.i. Kuroda, Preparation of raspberry-like poly (methyl methacrylate) particles by seeded dispersion polymerization, J. Appl. Polym. Sci., 120 (2011) 501-508.

[36] H. Hong, X. Cai, L. Shen, R. Li, H. Lin, Membrane fouling in a submerged membrane bioreactor: New method and its applications in interfacial interaction quantification, Bioresour. Technol., 241 (2017) 406-414.

[37] A.M. Lenhof, Contributions of surface features to the electrostatic properties of rough colloidal particles, Colloids and Surfaces A: Physicochemical and Engineering Aspects, 87 (1994) 49-59.

[38] S. Bhattacharjee, J.Y. Chen, M. Elimelech, DLVO interaction energy between spheroidal particles and a flat surface, Colloids and Surfaces A: Physicochemical and Engineering Aspects, 165 (2000) 143-156.

[39] H. Bargozin, R. Hadadhania, H. Faraji, H. Yousefzadeh, Effect of rough nanoparticle orientation on DLVO energy interaction, Journal of Dispersion Science and Technology, 36 (2015) 755-764.

[40] H. Bargozin, R. Hadadhania, H. Faraji, M. Yavari, The DLVO energy interaction of nanorough surfaces by spherical coordinates, Journal of Dispersion Science and Technology, 37 (2016) 884-893.

[41] M. Nosonovsky, B. Bhushan, Roughness-induced superhydrophobicity: a way to design non-adhesive surfaces, Journal of Physics: Condensed Matter, 20 (2008) 225009.

[42] A.A. Chialvo, L. Vlcek, Behaviour of rarified steam at very high temperature an orientation-averaged interaction potential approach towards its accurate description, Mol. Phys., 117 (2019) 3922-3940.

[43] Z. Adamczyk, B. Cichocki, M.L. Ekiel-Jeżewska, A. Słowicka, E. Wajnryb, M. Wasilewska, Fibrinogen conformations and charge in electrolyte solutions derived from DLS and dynamic viscosity measurements, Journal of colloid and interface science, 385 (2012) 244-257.

[44] J.H. Bae, T. Reed III, Estimation of Properties of Dilute Polar Gases from a Potential Energy Function, Industrial & Engineering Chemistry Fundamentals, 6 (1967) 67-72.

[45] C. Yigit, J. Heyda, J. Dzubiella, Charged patchy particle models in explicit salt: ion distributions, electrostatic potentials, and effective interactions, The Journal of chemical physics, 143 (2015) 08B606_601.

[46] J. Molina-Bolıvar, F. Galisteo-González, R. Hidalgo-Alvarez, Colloidal aggregation in energy minima of restricted depth, The Journal of chemical physics, 110 (1999) 5412-5420.

[47] R.J. Hunter, Foundations of colloid science, Oxford university press2001.

[48] Y.T. He, J. Wan, T. Tokunaga, Kinetic stability of hematite nanoparticles: the effect of particle sizes, J. Nanopart. Res., 10 (2008) 321-332.

[49] H. Eid, G. Adams, N. McGruer, A. Fortini, S. Buldyrev, D. Srolovitz, A combined molecular dynamics and finite element analysis of contact and adhesion of a rough sphere and a flat surface, Tribology Transactions, 54 (2011) 920-928.

[50] E. Pazmino, J. Trauscht, W.P. Johnson, Release of Colloids from Primary Minimum Contact under Unfavorable Conditions by Perturbations in Ionic Strength and Flow Rate, Environ. Sci. Technol., 48 (2014) 9227-9235.

[51] Z. Wang, Y. Jin, C. Shen, T. Li, Y. Huang, B. Li, Spontaneous detachment of colloids from primary energy minima by Brownian diffusion, PLoS One, 11 (2016) e0147368.

[52] M. Kamp, M. Hermes, C.M. Van Kats, D.J. Kraft, W.K. Kegel, M. Dijkstra, A. Van Blaaderen, Selective depletion interactions in mixtures of rough and smooth silica spheres, Langmuir, 32 (2016) 1233-1240.

[53] N. Eom, D.F. Parsons, V.S. Craig, Roughness in surface force measurements: Extension of DLVO theory to describe the forces between hafnia surfaces, The Journal of Physical Chemistry B, 121 (2017) 6442-6453.

[54] S.N. Das, J.H. Choi, J.P. Kar, J.M. Myoung, Tunable and reversible surface wettability transition of vertically aligned ZnO nanorod arrays, Applied Surface Science, 255 (2009) 7319-7322.

[55] C.C. De Foggi, A.L. Machado, C.A. Zamperini, D. Fernandes, A.F. Wady, C.E. Vergani, Effect of surface roughness on the hydrophobicity of a denture-base acrylic resin and C andida albicans colonization, J. Investig. Clin. Dent., 7 (2016) 141-148.

[56] C. Shen, S. Bradford, Z. Wang, Y. Huang, Y. Zhang, B. Li, DLVO interaction energies between hollow spherical particles and collector surfaces, Langmuir, 33 (2017) 10455-10467.

[57] B. Ilhan, C. Annink, D. Nguyen, F. Mugele, I. Sîretanu, M.H. Duits, A method for reversible control over nano-roughness of colloidal particles, Colloids and surfaces A: Physicochemical and engineering aspects, 560 (2019) 50-58.

[58] E. Tomanik, M. El Mansori, R. Souza, F. Profito, Effect of waviness and roughness on cylinder liner friction, Tribology International, 120 (2018) 547-555.

[59] O. Guven, M.S. Celik, J.W. Drelich, Flotation of methylated roughened glass particles and analysis of particle–bubble energy barrier, Miner. Eng., 79 (2015) 125-132.

[60] M.S. Hassan, R. Lau, Inhalation performance of pollen-shape carrier in dry powder formulation: effect of size and surface morphology, International journal of pharmaceutics, 413 (2011) 93-102.

[61] T. He, J. Wan, T. Tokunaga, Kinetic stability of hematite nanoparticles: The effect of particle sizes, J. Nanopart. Res., 10 (2008) 321-332.

[62] W.-z. Yin, J.-z. Wang, Effects of particle size and particle interactions on scheelite flotation, Transactions of Nonferrous Metals Society of China, 24 (2014) 3682-3687.

[63] D. Li, H. Wang, D. Xiao, M. Song, B. Legg, J. Chun, Investigating the magnitude and source of orientation-dependent interactions between TiO 2 crystal surfaces, Nanoscale, 9 (2017) 10173-10177.

[64] A. Gomez-Flores, S.A. Bradford, L. Wu, H. Kim, Interaction energies for hollow and solid cylinders: Role of aspect ratio and particle orientation, Colloids Surf. Physicochem. Eng. Aspects, 580 (2019) 123781.

[65] J. Raula, F. Thielmann, M. Naderi, V.P. Lehto, E.I. Kauppinen, Investigations on particle surface characteristics vs. dispersion behaviour of L-leucine coated carrier-free inhalable powders, International Journal of Pharmaceutics, 385 (2010) 79-85.

[66] L. Suresh, J.Y. Walz, Effect of surface roughness on the interaction energy between a colloidal sphere and a flat plate, J. Colloid Interface Sci., 183 (1996) 199-213.

[67] G. Trefalt, M. Borkovec, Overview of DLVO theory, Laboratory of Colloid and Surface Chemistry, University of Geneva, Switzerland, (2014) 1-10.

[68] J. Calero, A. Ontiveros-Ortega, V. Aranda, I. Plaza, Humic acid adsorption and its role in colloidal-scale aggregation determined with the zeta potential, surface free energy and the extended-DLVO theory, European Journal of Soil Science, 68 (2017) 491-503.

[69] H. Bargozin, J. Moghaddas, Stability of nanoporous silica aerogel dispersion as wettability alteration agent, Journal of dispersion science and technology, 34 (2013) 1454-1464.

[70] J. Argent, S. Torkzaban, S. Hubbard, H. Le, T. Amirianshoja, M. Haghighi, Visualization of micro-particle retention on a heterogeneous surface using micro-models: influence of nanoscale surface roughness, Transport in

Porous Media, 109 (2015) 239-253.

[71] E. Martines, L. Csaderova, H. Morgan, A. Curtis, M. Riehle, DLVO interaction energy between a sphere and a nano-patterned plate, Colloids Surf. Physicochem. Eng. Aspects, 318 (2008) 45-52.

[72] C.N. Pace, H. Fu, K.L. Fryar, J. Landua, S.R. Trevino, B.A. Shirley, M.M. Hendricks, S. Iimura, K. Gajiwala, J.M. Scholtz, Contribution of hydrophobic interactions to protein stability, J. Mol. Biol., 408 (2011) 514-528.

Chapter 4: Interfacial interactions of rough spherical surfaces with random topographies

4.1 Abstract

A mathematical model was created based on surface element integral (SEI) and XDLVO theory for assessing the interfacial interaction between rough spherical surfaces with random topographies, which were generated following a modified two-variable Weierstrass-Mandelbrot (WM) function. The surface construction and interfacial interaction simulation approaches involved in this study could increase the accuracy of predictions in particle interface behaviors compared to previous works. The involved equations in this study constructed a randomly rough spherical surface which played an important role in increasing the accuracy of simulating particle interfacial interaction because the surface morphology characters of a natural surface could be generated accurately by the present model. This modeling study presented discussions on the interaction of rough surfaces having different asperity heights, asperity positions, random landscapes, and roughness in colloidal systems. We observed that the asperity number and ratio were primary parameters for influencing the interfacial interaction between spherical surfaces. The arrangement and randomness in the position of asperities on the surface had a negligible effect on the interfacial interaction. The elevated asperity height, as a result of increased fractal roughness or relative fractal roughness on spherical surfaces, could hamper the interfacial energy between surfaces. However, increasing the fractal dimension and relative fractal dimension generated smoother surfaces and thus elevated the interfacial energy developed between surfaces. The most impactful parameter of surface morphologies in altering interfacial energy was fractal dimension as it could control the asperity height and asperity number simultaneously. The largest primary maximum was predicted (216 kT) when the fractal dimension was 2.43, which represented the strongest stability of particles in a suspension.

Keywords: Interfacial interaction, rough surface, colloid, simulation, random topography

4.2 Introduction

Colloidal systems play key roles in our daily life, as they are ingredients of some important formulations, such as medicines and food [1]. Most colloids are thermodynamically unstable, in which their particles

tend to aggregate. The redispersion process of particles in an aggregated system is generally controlled by altering the stability of the particles, which would significantly affect the properties of the particles. The balance among electric double layer repulsive force, van der Waals attractive force, and non-Derjaguin-Landau-Verwey-Overbeek (DLVO) force (hydrophobic interaction force) controls the stability of particles in the colloidal system, which is comprehensively described by the extended DLVO (XDLVO) theory [2, 3]. This concept is widely used for assessing the interfacial interaction in different interaction models including smooth planer-planer interaction [4], smooth particle-rough planer interaction [5], and rough particle-rough planer interaction [6].

The surface of particles in colloidal suspensions is rarely smooth, which presents considerable challenges in predicting particle interactions. To resolve this problem, the surface element integration (SEI) technique could be applied to assess the interfacial energy of two rough surfaces by validating the interfacial interaction of a spherical area if the surface roughness could be created correctly by mathematical equations [7-10]. Over the past few decades, extensive progress has been made in simulating rough surfaces. The common method for generating rough surfaces is by considering the asperity shape on the surface as the periodic sinusoidal function or hemisphere pillars [5, 11]. Although pioneering studies made great efforts in simulating interfacial energy and deepened our understanding of rough surface modeling studies, the past modeling studies could not accurately characterize the surface profiles of natural materials as they constructed rough surfaces with uniform roughness distributions [7-10, 12]. Thus, the information on the prediction of particle interaction for two rough particles with a random topography is insufficient.

The interfacial interactions of rough spherical surfaces with random morphologies are important for predicting the susceptibility of aggregation or dispersion in a colloidal suspension system. Many researchers investigated the randomness in the surface morphology for different applications. Some reported that the non-uniform surface would enhance the adhesion of polymers to a surface, which would be influenced by the randomness of the surface topography [13-15]. However, the previous studies could not distinguish between surface roughness and randomness because they considered surface heterogeneity as the randomness of the surface [13-15]. For this reason, the results of randomness in surface morphology on the adhesion of particles were inconclusive. It is necessary to explore how the roughness and randomness in the surface topography of particles affect their interaction

in colloidal systems, which would remarkably influence their practical uses in industry.

For naturally made rough surfaces, the small-scale roughness owns repeatability of geometry [16, 17]. Additionally, the profile of the heterogeneous surface follows the power law [18]. Therefore, the process of constructing a rough surface could be satisfied by employing a modified two-variable Weierstrass-Mandelbrot (WM) function, which originated from the theory of fractal geometry [19]. The WM function had been applied for simulating the self-affine randomly rough surface which could fully describe the characteristics of natural surface morphology [18, 20-22]. As the fractal dimension (D_f) and fractal roughness (G) from the WM function are core parameters in controlling the surface roughness [23-25], this function can be used as a popular working tool to describe two and three dimensional rough surfaces with random surface morphologies [26-28]. Once the rough surfaces with random surfaces are constructed following the fractal geometry, the XDLVO theory and SEI method can be combined to investigate the rough surface interactions.

In the present study, a numerical model was created based on the theory of fractal geometry, which intended to estimate the interfacial energy of rough particles owned by random surface topographies. It was previously stated that randomness would represent the random spatial distribution of the asperities on the particle surface [29], which is an important factor in surface morphology. The influence of asperity height, number, and position on the surface of spherical particles on particle interaction was discussed, which could serve as the foundation for the investigation of the interaction of particles with random surface morphologies. This work aims to explore how the randomness and roughness positioned on the particle surface will alter the interaction energy of particles following the SEI method and XDLVO theory. For the first time, two rough spherical particles with arranged and random asperity positions were designed and their interactions were assessed in colloidal systems. This study reported how the interfacial energy of two rough spherical particles with various surface morphologies would change when asperity number, asperity ratio, asperity position, surface randomness, surface roughness, and relative randomness and roughness of surfaces were varied. Moreover, the most powerful parameter of surface morphologies manipulating the interfacial energy between rough particles with random surface morphology was identified.

4.3 Research Methods

4.3.1 Constructing particles with the arranged surface morphology

In this section, we studied the effect of the position of asperities on particle interaction. We considered two types of construction methods for asperity-arranged particles. The first type was used for analyzing the effect of vertical positions of asperities on the particle interaction if the locations of asperities with different heights are switched longitudinally on the particle surface. Such simulated particles with longitudinally arranged asperities could represent hybrid Ag-ZnO nano-structured microparticles [30]. The second type is used for analyzing the effect of the horizontal position of asperities on particle interaction if the locations of asperities with different heights are switched latitudinally in poles and equator. Such simulated particles could represent the Janus particles composed of polystyrene surface and rough gold surface [31].

The first construction method was developed from the rippled particle theory discussed by Bhattacharjee and coworkers [32], who applied this theory to generate particles with uniform roughness distributions (i.e., the height of asperities was kept the same on the particle). In our current study, we aim to construct a rough particle with longitudinally arranged asperities (i.e., the height of asperities was different longitudinally) and analyze the effect of longitudinally switching positions of asperities on particle interaction, which was shown in Equation 4.1:

$$R_{\text{longitudinal}} = r_1 + r_1\lambda_o \cos(n_o\theta_1) + r_1\lambda_o \cos(n_o\varphi_1) + r_1\lambda_\eta \cos(n_\eta\theta_1) + r_1\lambda_\eta \cos(n_\eta\varphi_1) \qquad (4.1)$$

Where r represents the radius of element particle (smooth), θ and φ represent the angle coordinates in 3D spherical coordinate, λ and n represent the asperity ratio and asperity number, respectively, and the subscripts o and η represent the column with small asperities and large asperities, respectively and subscript 1 represents the constructed particle 1.

The constructed rough particle was shown in Figures 1(a) and 1(b), where column A and column B represent the column that owns small asperities before and after switching with the column that has large asperities.

The second method is based on the piecewise function to analyze the effects of latitudinally switching positions of asperities on the particle interaction (Equation 4.2):

$$R_{\text{latitudinal}} = \begin{cases} r_1 + r_1\lambda_\alpha \cos(n_{\alpha 1}\theta_1) + r_1\lambda_\alpha \cos(n_\alpha \varphi_1) & 0 \le \theta_1 \le \pi/4 \\ r_1 + r_1\lambda_\beta \cos(n_\beta \theta_1) + r_1\lambda_\beta \cos(n_\beta \varphi_1) & \pi/4 < \theta_1 < 3\pi/4 \\ r_1 + r_1\lambda_\alpha \cos(n_\alpha \theta_1) + r_1\lambda_\alpha \cos(n_\alpha \varphi_1) & 3\pi/4 \le \theta_1 \le \pi \end{cases} \tag{4.2}$$

where the subscript of α and β represent the polar and equator areas, respectively. The constructed rough particles were shown in Figures 1(c) and 1(d).
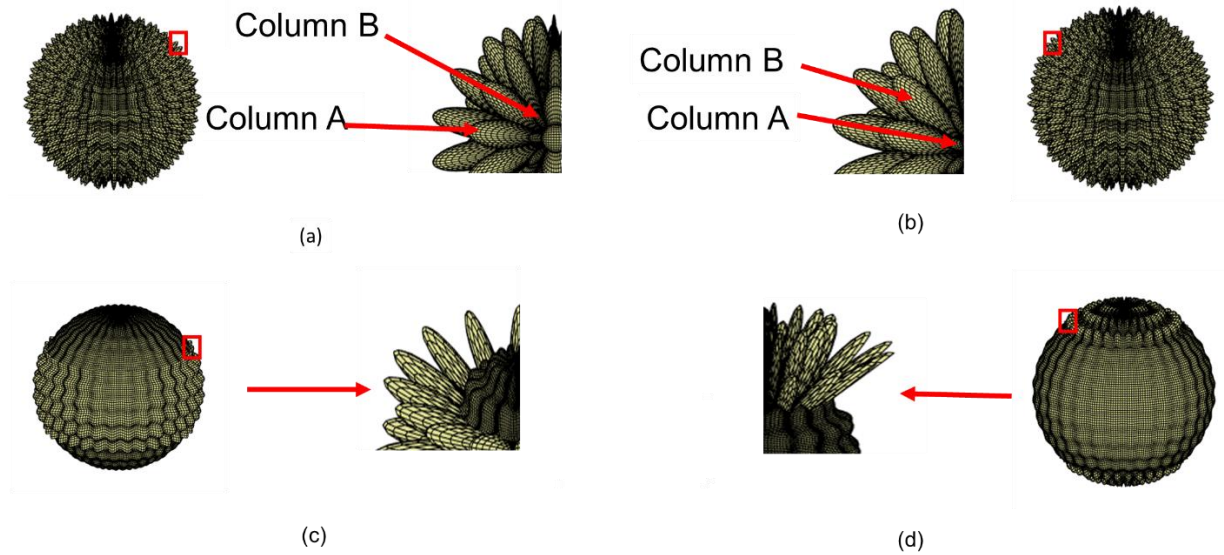
Figure 4.1 The structure of rough spherical surfaces with arranged asperities: (a) Longitudinally arranged rough particle with larger asperities in column A, (b) Longitudinally arranged rough particle with larger asperities in column B (the difference between "Column A" and "Column B" is the difference in the position of the large height of asperities and small height of asperities. Both Figures 1(a) and (b) were generated using the same model (Equation 1). The only difference is the value of asperity ratio λ based on Equation 1), (c) Latitudinally arranged rough particle with rougher equator, (d) Latitudinally arranged rough particle with rougher poles

4.3.2 Interaction of rough particles with arranged surface asperities

In the simulation process, one particle was constructed with uniform asperity on the surface as the control particle (Equation 4.3). Another particle was constructed with the above methods (Equation 4.1 or 4.2) to investigate the impact of the relative position of asperities on particle interfacial energy (according to Figures A.2.1 and A.2.2).

The rough particle, as a control sample, was modeled following Equation 4.3 [33].

$$R_{control} = r_{\text{control}} + r_{\text{control}}\lambda_{\text{control}} \cos(n_{\text{control}}\theta_{\text{control}}) + r_{\text{control}}\lambda_{\text{control}} \cos(n_{\text{control}}\varphi_{\text{control}})$$

Where the subscript control represents the control spherical rough surface.

The spatial relationship of the two particles could be expressed as shown in Equation 4 [34].

$$\theta_{control} = arc \sin \left[\left(\frac{R_1}{R_{control}} \right) \sin \theta_1 \right] \tag{4.4}$$

The separation distance between the rough particle with longitudinally arranged asperities and the control particle can be given by Equation 4.5:

$$h = r_1 + 2r_1\lambda_o + 2r_1\lambda_\eta + r_{control} + 2r_{control}\lambda_{control} + D - R_{longitudinal} \cos(\theta_1) -$$

$$R_{control} \cos(\theta_{control}) \tag{4.5}$$

Where r_1 and $r_{control}$ refer to radii of element particle 1 and element of control particle, $R_{longitudinal}$

and $R_{control}$ refer to radii of modeled longitudinally arranged rough particles and control particles.

The separation distance between the rough particle with latitudinally arranged asperities and the control particle can be determined by Equation 4.6:

$$h =$$

$$\begin{cases} r_1 + 2r_1\lambda_\alpha + r_{control} + 2r_{control}\lambda_{control} + D - R_{\text{latitudinal}} \cos(\theta_1) - R_{control} \cos(\theta_{control}) & 0 \le \theta_1 \le \pi/4 \\ r_1 + 2r_1\lambda_\beta + r_{control} + 2r_{control}\lambda_{control} + D - R_{\text{latitudinal}} \cos(\theta_1) - R_{control} \cos(\theta_{control}) & \pi/4 < \theta_1 < 3\pi/4 \\ r_1 + 2r_1\lambda_\alpha + r_{control} + 2r_{control}\lambda_{control} + D - R_{\text{latitudinal}} \cos(\theta_1) - R_{control} \cos(\theta_{control}) & 3\pi/4 \le \theta_1 \le \pi \end{cases}$$

$$\tag{4.6}$$

Where $R_{\text{latitudinal}}$ refer to radii of a rough particle with latitudinally arranged asperities.

The simulation process between two types of asperity-arranged particles was carried out by MATLAB 2020a (9.8.0.1323502).

4.3.3 Developing three-dimensional rough particles with random topographies

In the past, a scanning electron microscope (SEM) study reported that the surface morphologies of poly(methyl methacrylate), poly(vinylidene fluoride-trifluoroethylene), and titanium dioxide nanoparticles were determined to have random arrangements of protrusions and depressions [35-37]. In the present study, the fractal geometry theory was applied to construct rough particles with random surface morphologies to represent these nanoparticles, which could express the features of valleys and peaks of the surface topography of particles. This simulation technique had been applied to create rough particles for predicting adhesion forces developed between a flat surface and a rough particle in the past [38].

In this work, the transformation process of cartesian coordinates to spherical coordinates follows the methodology expressed in the pioneering work and is shown in the supplementary material (Equations A.2.1-A.2.3) [32]. According to the fractal geometry theory, the surface morphology of particles could be affected by the roughness and randomness of spherical particles, which could be defined mathematically [39]. In this study, a mathematical model applied to a modified WM function, which was developed from fractal geometry, was employed for constructing rough particles with random topographies [6, 19, 40, 41].

In the current work, the rough surface with the random surface morphology was modeled following Equations 4.7 and 4.8, respectively [32].

$$\Delta r_i = L(\frac{\tau_i}{L})^{D_{f_i}-2}(\frac{ln\psi}{M})^{\frac{1}{2}}\sum_{m=1}^{M}\sum_{n=0}^{n_{max}}\eta^{(D_{f_i}-3)n} \times (\cos\phi_{m,nmax+1_i} - \cos(\frac{2\pi\psi^n r\sin\theta}{L} *$$

$$\cos\left(\varphi - \frac{\pi m}{M}\right) + \phi_{m,nmax+1})) \tag{4.7}$$

$$R_i = r_i + \Delta r_i \tag{4.8}$$

where R_i and r_i represent the radii of modeled rough and smooth particles, respectively; D_{fi} represents the fractal dimension; τ_i represents the fractal roughness; L represents the sample length; ψ represents the parameter that expresses the frequency density in the profile; $\phi_{m,nmax+1}$ is a random phase; M represents the number of overlapped ridges contributing to constructing a random surface; n_{max} is the highest frequency where $n_{max} = int((log\,L/v_s)/log\,\eta$ [19], v_s represents the cutoff frequency, and $int(...)$ represents the largest integer value of the number in parentheses. In the present model, D_f represents the contour structure complexity on the rough surface. Thus, the larger value of D_f implies more contour structures. Also, τ is an amplitude coefficient that affects the size of the contour on the rough surface [42]. The numerical definitions of D_f and τ were shown in supplementary material (Equations A.2.4-A.2.6). Generally, fractal geometry includes points, curves, areas, and cubes with the integer values of 0, 1, 2, and 3 [43, 44]. Moreover, i represents the subscript of modeled particle (i=1,2). Following Equations 4.7 and 4.8, different rough particles with random topographies could be constructed as shown in Figure A.2.3.

4.3.4 Interaction of rough particles with random surface structures

Based on the XDLVO theory, the total interfacial energy of rough spherical surfaces (Equation 4.9) includes acid-base (AB), Lifshitz-Vander Waals (LW), and electrostatic double layer (EL) interaction energies [2, 5].

The energies per unit area ($\Delta G^{LW}(h)$, $\Delta G^{AB}(h)$ and $\Delta G^{EL}(h)$) of rough surfaces was calculated by Equations 4.10 to 4.12 [2].

$$\Delta G^{Total}(h) = \Delta G^{LW}(h) + \Delta G^{AB}(h) + \Delta G^{EL}(h) \tag{4.9}$$

$$\Delta G^{AB}(h) = \Delta G_{h_0}^{AB} \exp\left(\frac{h_0 - h}{\lambda}\right) \tag{4.10}$$

$$\Delta G^{LW}(h) = -\frac{A_H}{12\pi h^2} = \Delta G_{h_0}^{LW} \frac{h_0^2}{h^2} \tag{4.11}$$

$$\Delta G^{EL}(h) = \varepsilon_0 \varepsilon_r \kappa \xi_1 \xi_2 \left(\frac{\xi_1^2 + \xi_2^2}{2\xi_1\xi_2}(1 - \coth\kappa h) + \frac{1}{\sinh\kappa h}\right) \tag{4.12}$$

where subscript 1 and 2 represent spherical surfaces 1 and 2, respectively, λ is set to be 0.6 nm, which represents the correlation length of molecules in a liquid medium [19]. Also, κ, ζ, and ε are the reciprocal Debye screening length, zeta potential, and the permittivity of the medium, respectively; h_0 is the minimum equilibrium cut-off distance, which is set as 0.158 nm [2]. In Equation 12, ε usually represents the product of the permittivity of a vacuum ($\varepsilon_0 = 8.854 \times 10^{-12}$ C^2/J·m) and the ε_r presents the dielectric constant of the medium, which is 80 for water at 20°C [45].

In addition, surface or interface tensions are represented via the sum of an apolar (Lifshitz–van der Waals) component (γ^{LW}) and a polar (acid-base) component (γ^{AB}) [46]. γ^{AB} could be divided into an electron-accepting part (γ^+) and an electron-donating part (γ^-) [47]. Based on these parameters, the ΔG^{LW} and ΔG^{AB} can be calculated following Equations 4.13 and 4.14:

$$\Delta G_{h_0}^{LW} = -2\left(\sqrt{\gamma_1^{LW}} - \sqrt{\gamma_w^{LW}}\right)\left(\sqrt{\gamma_2^{LW}} - \sqrt{\gamma_w^{LW}}\right) \tag{4.13}$$

$$\Delta G_{h_0}^{AB} = 2\left[\sqrt{\gamma_w^+}\left(\sqrt{\gamma_1^-} + \sqrt{\gamma_2^-} - \sqrt{\gamma_w^-}\right) + \sqrt{\gamma_w^-}\left(\sqrt{\gamma_1^+} + \sqrt{\gamma_2^+} - \sqrt{\gamma_w^+}\right) - \sqrt{\gamma_1^- \gamma_2^+} - \sqrt{\gamma_1^+ \gamma_2^-}\right]$$

$$\tag{4.14}$$

where subscript w, 1, and 2 represented water, particle 1, and particle 2.

In this study, the Young Equation (Equation S7) was applied to determine the solid surface tension, and the input parameters were collected from the pioneering study, which is shown in the support material (Table A.2.1) [42].

Based on the surface element integral (SEI) technique, the energy of two rough spherical surfaces ($\Delta G^{Total}(h)$) could be resolved following Equations 4.9-4.12. The total interfacial interaction (U(h)) can be described by Equations 4.15-4.17 [32, 48]. Such calculations were carried out using MATLAB 2020a (9.8.0.1323502). The total interfacial energy is expressed in kT units, where T is the absolute temperature (293.15 K) and k is the Boltzmann constant.

$$U(h) = \iint \Delta G(h) dA \tag{4.15}$$

$$dA = \overrightarrow{o_1 k_1} \overrightarrow{o_2 k_2} dS \tag{4.16}$$

The differential area (dS) of Equation 16 can be calculated following Equation 4.17 [32].

$$dS = R_i^2 \sin \theta_i \, d\theta d\varphi \tag{4.17}$$

where dA expressed the projection area of spherical surface 1 located on another surface, and dS expressed the differential area of rough spherical surface 1, h represented the separation distance between two particles. As the present modeling study considered two spherical surfaces with rough surface morphologies, the unit vector of both rough surfaces should be involved in the simulation process [32]. Therefore, the terms in Equation 16 ($\overrightarrow{o_1 k_1}$ and $\overrightarrow{o_2 k_2}$) were used to represent the curvature effect (unit vector) between rough surfaces as shown in Equations 4.18 and 4.19 [49].

$$\overrightarrow{o_1 k_1} = \frac{R_1 \cos \theta_1 + \Gamma_1 \sin \theta_1 \sum_{m=1}^{M} \sum_{n=0}^{nmax} \Gamma_3 \cos\left(\varphi - \frac{\pi m}{M}\right) \cos \theta_1}{\sqrt{R_1^2 + \Gamma_1^2 \sum_{m=1}^{M} \sum_{n=0}^{nmax} \Gamma_3^2 \sin^2\left(\varphi - \frac{\pi m}{M}\right) + \Gamma_1^2 \sum_{m=1}^{M} \sum_{n=0}^{nmax} \Gamma_3^2 \cos^2\left(\varphi - \frac{\pi m}{M}\right) \cos^2 \theta_1}} \tag{4.18}$$

$$\overrightarrow{o_2 k_2} = \frac{R_2 \cos \theta_2 + \Gamma_2 \sin \theta_2 \sum_{m=1}^{M} \sum_{n=0}^{nmax} \Gamma_4 \cos\left(\varphi - \frac{\pi m}{M}\right) \cos \theta_2}{\sqrt{R_2^2 + \Gamma_2^2 \sum_{m=1}^{M} \sum_{n=0}^{nmax} \Gamma_4^2 \sin^2\left(\varphi - \frac{\pi m}{M}\right) + \Gamma_2^2 \sum_{m=1}^{M} \sum_{n=0}^{nmax} \Gamma_4^2 \cos^2\left(\varphi - \frac{\pi m}{M}\right) \cos^2 \theta_2}} \tag{4.19}$$

Where $\Gamma_1, \Gamma_2, \Gamma_3$ and Γ_4 are coefficients and can be expressed by Equations 4.20-4.23:

$$\Gamma_1 = L\left(\frac{\tau_1}{L}\right)^{D_{f1}-2}\left(\frac{ln\psi}{M}\right)^{\frac{1}{2}} \tag{4.20}$$

$$\Gamma_2 = L\left(\frac{\tau_2}{L}\right)^{D_{f2}-2}\left(\frac{ln\psi}{M}\right)^{\frac{1}{2}} \tag{21}$$

$$\Gamma_3 = \psi^{(D_{f1}-3)n} \sin\left(\frac{2\pi\psi^n r_1 \sin \theta_1}{L} \times \cos(\varphi - \frac{\pi m}{M}) + \phi_{m,n}\right) \times \frac{2\pi\psi^n r_1}{L} \tag{22}$$

$$\Gamma_4 = \psi^{(D_{f2}-3)n} \sin\left(\frac{2\pi\psi^n r_2 \sin \theta_2}{L} \times \cos(\varphi - \frac{\pi m}{M}) + \phi_{m,n}\right) \times \frac{2\pi\psi^n r_2}{L} \tag{23}$$

Where the values of L and ψ were collected from the literature and set as 5000 nm and 1.5, respectively [50]. Hong and coworkers stated that the value of M should be above 3 to make the simulated surface closer to reality [51]. Thus, M was set to 8 in this study following the value stated in a previous study [49]. Also, ν_s is the cutoff frequency and the n_{max} was calculated as 5, which was adopted from the work of Zhang and coworkers [11]. The numerical equations for calculating unit vectors were shown in support material (Equations A.2.8-A.2.10).

The series of $\phi_{m,n}$ was created from the random number generator with a scale of $[0, 2\pi]$ to avoid coincidences of different frequencies of any point on a rough surface, and this series was generated by

Equation 4.24:

$$[\phi_{M\times(n_{max}+1)}] = \begin{bmatrix} 2.2681 & 3.4148 & 5.1977 & 5.3991 & 3.9171 & 3.2029 \\ 3.7282 & 0.3488 & 3.0793 & 5.0153 & 5.0239 & 1.1093 \\ 4.0971 & 0.0225 & 0.9963 & 5.6497 & 1.8793 & 4.6751 \\ 4.4089 & 0.3153 & 1.5343 & 3.4391 & 4.3598 & 4.1709 \\ 1.2114 & 5.3985 & 4.3828 & 4.6273 & 3.9585 & 1.3544 \\ 5.1218 & 5.3310 & 0.5640 & 4.7376 & 5.1990 & 3.5070 \\ 4.9327 & 5.4101 & 0.3967 & 5.9858 & 2.4364 & 0.1511 \\ 2.8786 & 1.3616 & 0.3829 & 0.2327 & 4.0411 & 3.7663 \end{bmatrix} \tag{4.24}$$

Figure 2 shows the interaction scenario of two randomly rough particles. The spatial relationship of rough particles was expressed as shown in Equation 4.25 [34].

$$\theta_2 = arc \sin\left[\left(\frac{R_1}{R_2}\right) \sin \theta_1\right] \tag{4.25}$$

The separation distance between the projection areas of these rough particles was given by Equation 26:

$$h = D + R_{a1} + R_{a2} - R_1 * \cos \theta_1 - R_2 * \cos \theta_2 + r_1 + r_2 \tag{4.26}$$

Where r_1 and r_2 represent the radii of element two particles (smooth), R_1 and R_2 represent the radii of modeled two rough particles with random surface topography, R_{a1} and R_{a2} refer to the root-mean-square roughness of interaction area in particles 1 and 2, which could be calculated by following Equation 4.27 [42]:

$$R_{ai} = \sqrt{\frac{\sum_{i=1}^{N} \Delta r_i^2}{N}} \quad (i = 1, 2) \tag{4.27}$$

Thus, based on Equations 15-25, the interfacial interaction can be given following Equation 28:

$$U(h) = \iint \Delta G(h) \overrightarrow{o_1 k_1} * \overrightarrow{o_2 k_2} * R_i^2 \sin \theta_i \, d\theta d\varphi \tag{4.28}$$

By combining Equations 4.10-4.12, and 4.26-4.28, Equations 4.29-4.31 were developed for measuring the interaction energies of LW, AB, and EL.

$$U_{LW} = \Delta G_{h_0}^{LW} \int_0^{2\pi} \int_0^{\pi/2} \frac{h_0^2}{h^2} \overrightarrow{o_1 k_1} \overrightarrow{o_2 k_2} R_i^2 \sin \theta_i \, d\theta d\varphi \tag{4.29}$$

$$U_{AB} = \Delta G_{h_0}^{AB} \int_0^{2\pi} \int_0^{\pi/2} exp\left(\frac{h_0 - h}{\lambda}\right) \overrightarrow{o_1 k_1} \overrightarrow{o_2 k_2} R_i^2 \sin \theta_i \, d\theta d\varphi \tag{4.30}$$

$$U_{EL} = \varepsilon_0 \varepsilon_r \kappa \xi_1 \xi_2 \int_0^{2\pi} \int_0^{\pi/2} \left(\frac{\xi_1^2 + \xi_2^2}{2\xi_1\xi_2}(1 - coth \, \kappa h) + \frac{1}{sinh \, \kappa h}\right) \overrightarrow{o_1 k_1} \overrightarrow{o_2 k_2} R_i^2 \sin \theta_i \, d\theta d\varphi \tag{4.31}$$
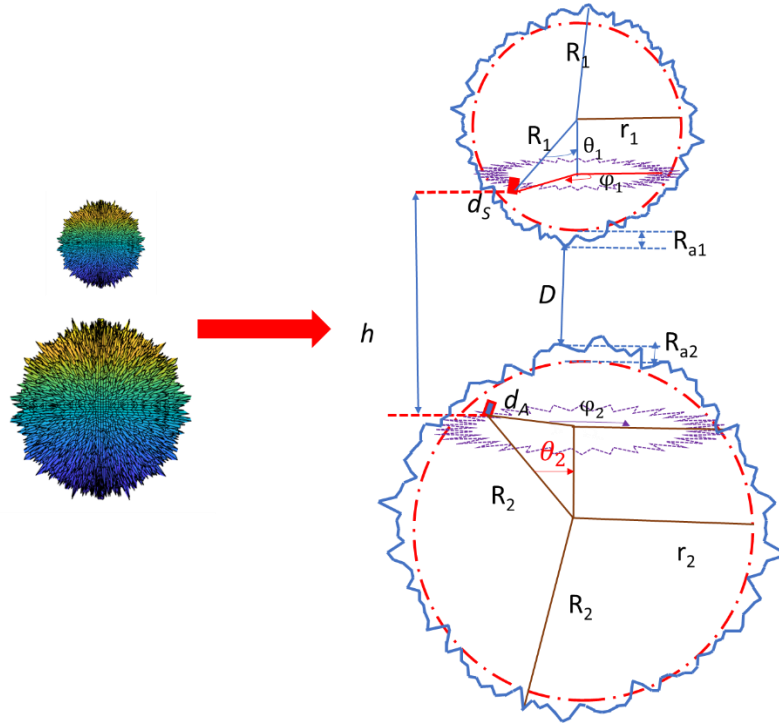
Figure 4.2 Parameters involved in the interaction between two rough spherical surfaces with random surface morphologies

4.3.5 Development of altered scenarios for analyzing the interaction of particles with random surface morphologies

The randomness of surface topography is used for describing how the localization of roughness can affect surface morphology. In this modeling study, the $\phi_{m,nmax+1}$ directly describes the disorganized arrangement of asperities of a surface without changing the average surface roughness (Equation 4.7). To simplify the subscript, the $\phi_{m,nmax+1}$ of particles 1 and 2 are donated as ϕ_1 and ϕ_2, respectively. To study the influence of surface randomness and to eliminate the interference of the effects of surface roughness on particle interactions, the parameters controlling surface roughness of particle surface were fixed ($\tau_1 = \tau_2 = 0.1$ nm, $D_{f1} = D_{f2} = 2.23$), and only the value of $\phi_{2\xi}$ was changed, where ξ represented the surface with different values of randomness. In this case, ten random phases were generated for constructing ten rough surfaces with different randomly distributed asperities following Equation 4.7. Then, the interactions between particle 1, as the control particle, and particle 2 with ten different random topographies were analyzed ten times using ANOVA as shown in Table A.2.2. Among ten trials, four particles with different surface randomness (particle 2 ($\phi_{2\xi}$)) were calculated using Equations A.2.11-

A.2.15 as examples.

4.3.6 Fractal dimension impacts

The fractal dimension had been proved as an important parameter to control the surface roughness and topology of rough surfaces [50]. Previous studies reported that the scale of 2-3 for the fractal dimension was used for representing a three-dimensional rough surface [43, 44], which could be calculated experimentally considering the hydrodynamic and radius of the gyration of particles [52]. In the current study, the value of the fractal dimension was selected to be between 2.03 and 2.93. The other parameters of constructing rough particles were fixed ($\tau_1 = \tau_2 = 0.1$ nm and $r_1 = r_2 = 1000$ nm) when assessing the interaction of particles. To investigate the impact of the relative fractal dimension on the particle interactions, the constructing parameters of particle 1 were fixed ($\tau_1 = 0.1$ nm, $r_1 = 1000$ nm, $D_{f1} = 2.93$) to exhibit the low degree of surface roughness, and the D_{f2} of particle 2 was ranged between 2.03 and 2.93.

4.3.7 Fractal roughness impacts

The fractal roughness characterizes the asperity height of the rough surface. This important parameter is independent of the frequency used in the modified two-variable WM function for constructing rough surfaces with random topographies [11]. In the current work, the fractal roughness between 0.5 nm and 10 nm was considered [11], which can be determined experimentally using an atomic force microscope, for example. In this set of analyses, $D_{f1} = D_{f2} = 2.23$ and $r_1 = r_2 = 1000$ nm were selected for constructing the surface roughness of particles because the simulation process should ensure the asperities existed on the particle surface in case the larger D_f value eliminates the surface roughness. To investigate the impact of relative fractal roughness on the particle interactions, the constructing parameters of particle 1 were fixed ($\tau_1 = 0.1$ nm, $r_1 = 1000$ nm, $D_{f1} = 2.23$), and the τ_2 of particle 2 was varied from 0.5 nm to 10 nm ($r_2 = 1000$ nm, $D_{f2} = 2.23$).

4.5 Results and Discussion

4.5.1 The interaction of particles with arranged asperities

Based on the methodology described in section 4.3.1 and following Equation 4.1, the surface of particles had asperities with the longitudinal arrangement, in which the surface of particles had one set of asperity with a small ratio and another set of asperity with a larger ratio. The impacts of asperity number on the

interfacial energy of spherical surfaces that had longitudinally arranged asperities were evaluated, and the predictions of total interfacial energies are shown in Figure 3(a). It can be seen that the total interfacial energy between the particles dropped by elevating the number of asperities. The effect of the asperity ratio on interfacial interaction between particles that had longitudinally arranged asperities was shown in Figure 3(b). It showed that the increased asperity ratio negatively impacted particle interaction because the increased size of asperities reduced the interaction area between rough particles.

Based on Equation 2, the position of asperities was arranged latitudinally, and the surface of constructed particles had asperities with a large ratio at the polar area and asperities with a small ratio at the equator area. With the combination of rippled particle theory and piecewise continuous functions, the impacts of asperity number and ratio on the interaction of particles with latitudinally arranged asperity were simulated, and the predicted results were shown in Figures Figure 3(c) and (d). It is found that the total interfacial interaction of particles that had latitudinally arranged asperities decreased with increasing the asperity number, while the ratio of asperities on the surface of two particles was kept constant. Moreover, when the asperity number was constant in the equator and polar areas on both particles, the energy of interfacial interaction generated between the particles decreased by increasing the asperity ratio latitudinally, which could be explained by the decreased interaction area of particles due to the enlarged size of asperities on particles.

The effects of asperity number and ratio without changing the position of asperities located on the particle interaction were discussed above. Now, the impact of the position of asperities on the particle surface on the interfacial energy is studied to resolve how the position of arranged-asperity particles influences the interaction of particles. In this experiment, one particle was constructed with the uniform asperity on the surface, as the control particle, and the other particle was constructed following Equation 4.1 or 4.2. As shown in Figure 4 (a), if the position of the column with the large asperity is switched longitudinally with the adjacent one with a smaller asperity (switched from column A to column B), the asperity position insignificantly affected the total interfacial energy between the rough particle and control particle (ANOVA: $p > 0.05$). A similar phenomenon was observed (ANOVA: $p > 0.05$) for the larger asperities changing their positions with smaller asperities from the polar area to the equator area as shown in Figure 4(b). In these interaction scenarios, only the asperity position was changed. Therefore, it can be claimed that changing the asperity position had a negligible effect on the particle

interaction if the asperity number and ratio were maintained constant.

The main reason for this behavior might be that the interaction energy of the rough surface depends primarily on the asperity number and ratio, rather than on the assignment of spatial positions of the asperities on the surface [29]. To prove this hypothesis, we reconstructed the particle with arranged asperity following Equation S16. In this case, the constructed range of angle factor, θ, was $\frac{\pi}{3}$ in Equation S16 instead of the previously used value of $\frac{\pi}{4}$ in Equation 4.2. With this change, the area of large asperities would not be equal to the area of small asperities impacting the interaction area of particles. If the large asperities switched their positions with small asperities from the equator to poles, the surface roughness would be changed and vice versa. The surface morphologies of the particles constructed following Equations 4.2 and A.2.16 are shown in Figure A.2.4, where the particle in Figure A.2.4(a) has a larger area of small asperities than the particle shown in Figure A.2.4(b) does. The total interaction increased substantially when the positions of large asperities switched from the polar area (λ_α=0.005) to equator area (λ_β=0.005) (Figure A.2.5 following Equation A.2.16). The reason is that the total area of two poles in the particle constructed by Equation A.2.16 is larger than the area of the equator of the particle. The reconstructed particle followed Equation A.2.16 and had three parts with the same area: two parts with large asperities (poles) and one part with small asperities (equator). If the large asperities changed their position from the poles to the equator, the reconstructed particle would have two areas with small asperities (poles) and one area with large asperities (equator). This position change would decrease the surface roughness of the particle because the area with large asperities was reduced, which would lead to an increase in the interfacial interaction as demonstrated in Figure A.2.5.

(c)

(d)
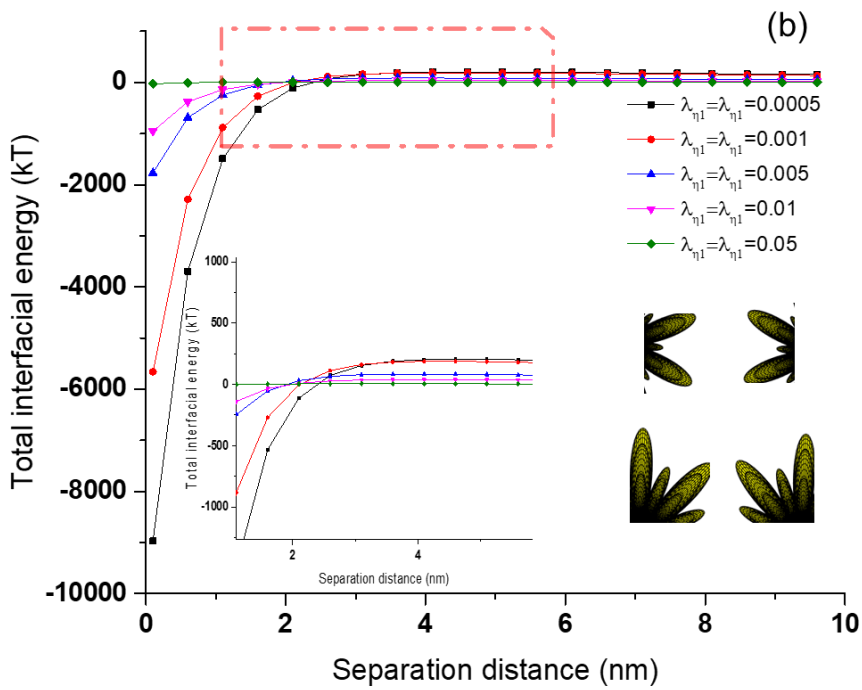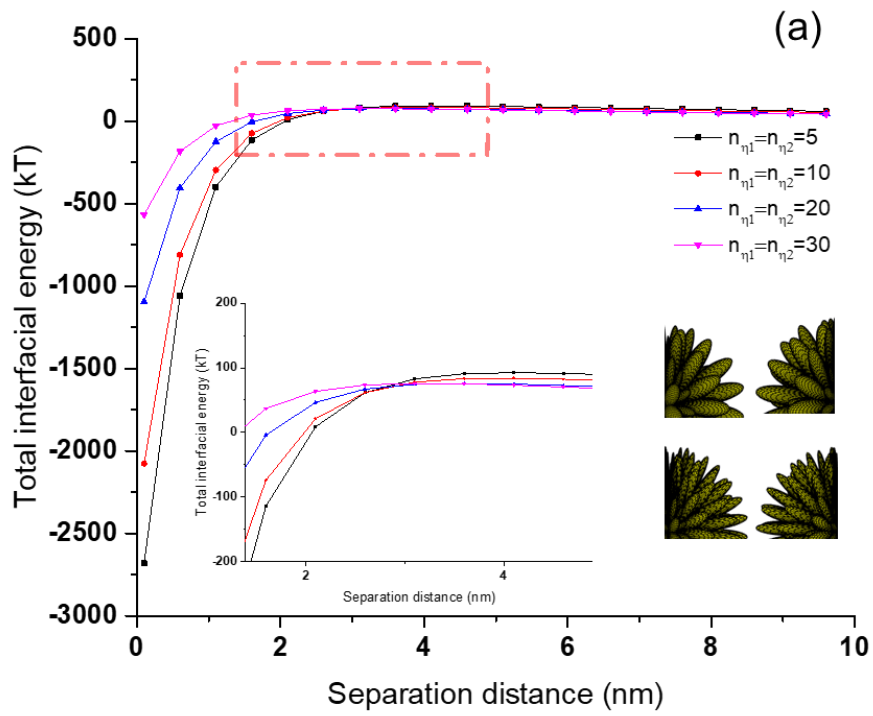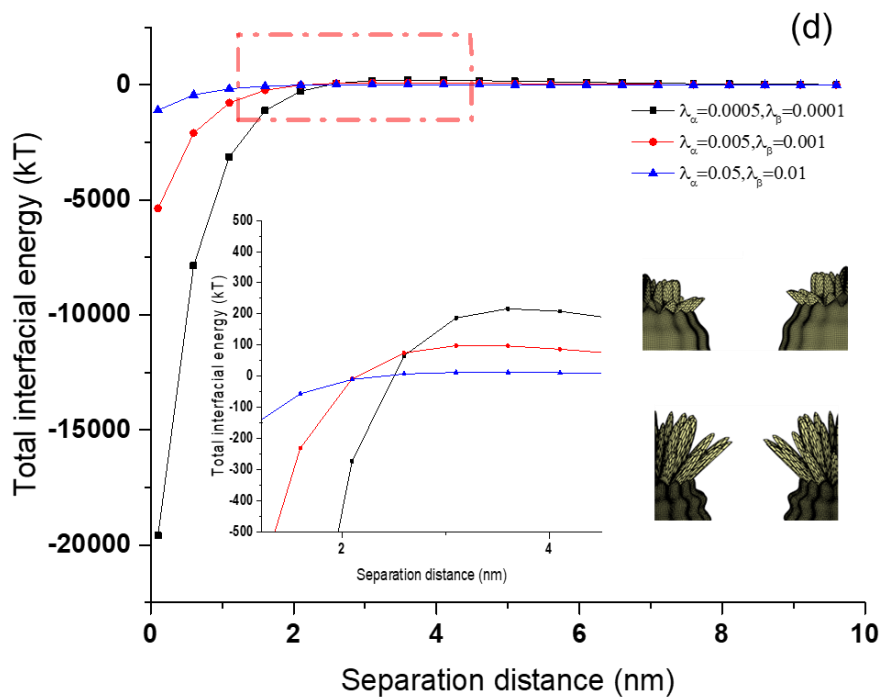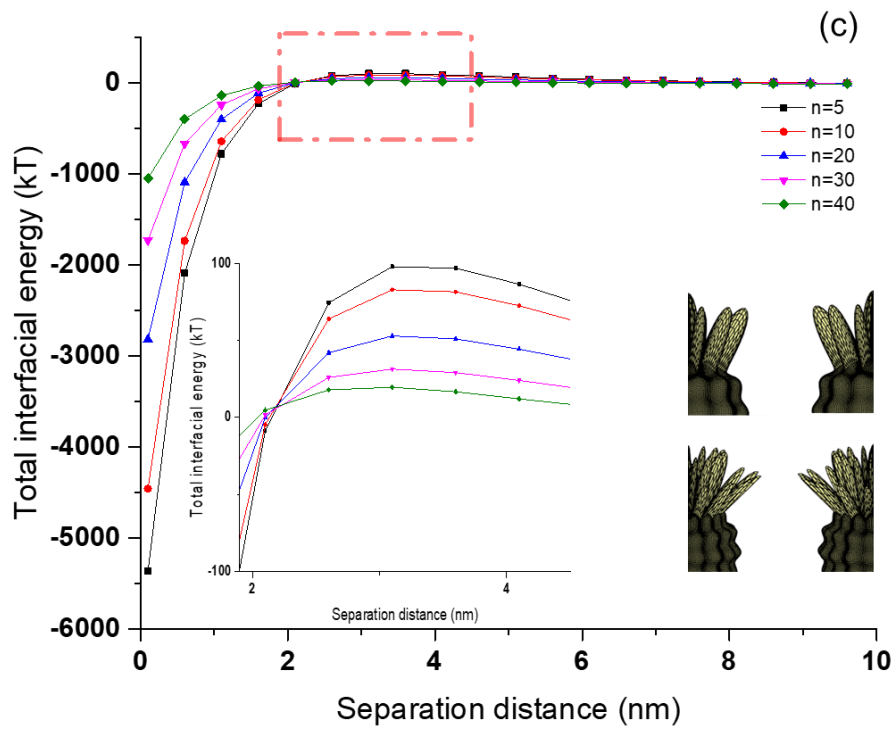
Figure 4.3 The influences of surface roughness on the interfacial energy of the spherical surfaces with arranged asperities. (a) the effects of asperity number with longitudinally arranged asperities when r_1=r_2=1000 nm, $n_{o1} = n_{o2} = 5$, $\lambda_o = 0.001$, $\lambda_\eta = 0.005$, (b) the effects of asperity ratio with longitudinally arranged asperities when r_1=r_2=1000 nm, $n_{o1} = n_{o2} = 5$, $n_{\eta1} = n_{\eta2} = 10$, $\lambda_{o1} = \lambda_{o2} = 0.0001$,(c) the effects of asperity number with latitudinally arranged asperities when r_1=r_2=1000 nm, $\lambda_\alpha = 0.005$, $\lambda_\beta = 0.001$,(d) the effects of asperity ratio when r_1=r_2=1000 nm, n=5
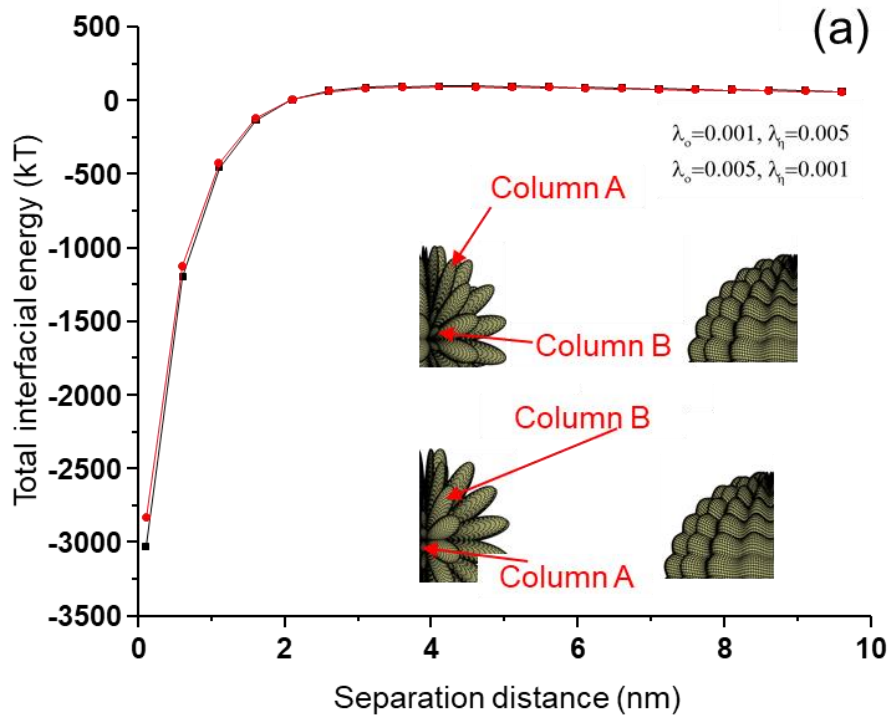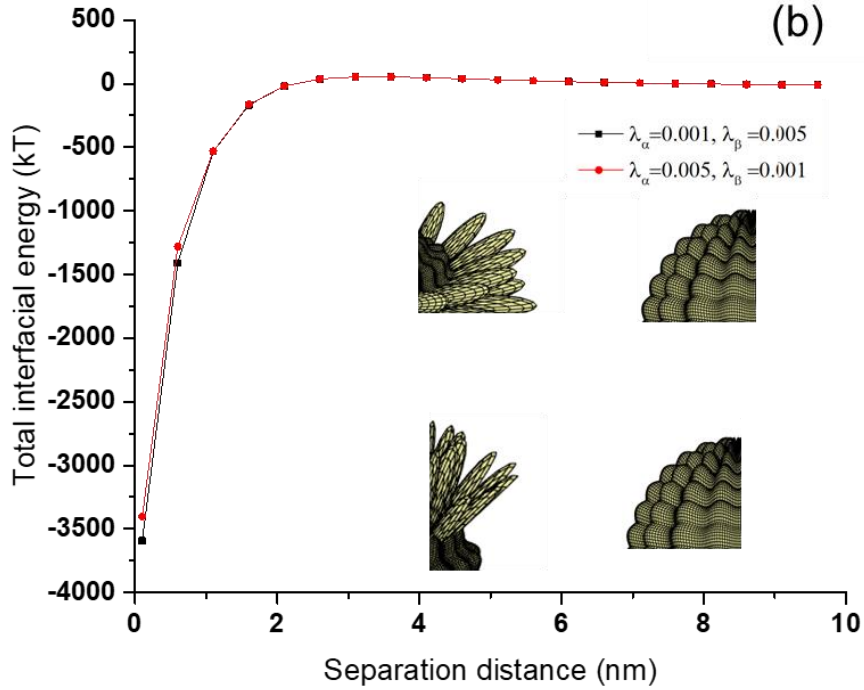
Figure 4.4 The energy of interfacial interaction between rough spherical surfaces (a) with longitudinally different asperity height ($r_1 = r_{control} = 1000\ nm, n_1 = n_{control} = 5, \lambda_{control} = 0.005$), (b) with different asperity heights in the equator and poles ($r_1 = r_{control} = 1000\ nm, n_1 = n_{control} = 5, \lambda_{control} = 0.005$).

4.5.2 Randomness effects

As stated in the previous section, the impact of the arranged-asperity position on the surface of particles was not significant. As randomness is a parameter to characterize the surface morphology and always exists in any real colloidal particle, the influence of randomness on the location of asperities on the rough spherical surface on the interaction of particles was investigated (Figure 5). The only difference in the model of rough particle 2 with randomly oriented asperities compared with particle 1 with a random surface morphology is the compositions of ϕ_1 and ϕ_{2a-d} shown in Equations A.2.11-A.2.15, as this parameter makes the asperities assigned randomly on the surfaces, where the subscript 2a-2d of ϕ shown in Figure 5 represents the different random surface morphologies of particle 2. It can be seen that the effect of randomness on the surface morphology on the total interfacial energy of particles is insignificant. According to previous studies, roughness and randomness can control surface morphology

[53, 54]. The surface roughness represents the surface heterogeneity and the randomness describes the random arrangement of asperities on a spherical surface [55]. Within the content of the randomness investigation, the separation distance and the contact area between two rough particles have not changed by changing randomness, as randomness only randomly changed the locations of asperities, and the overall roughness of particles was maintained constant. The reason for such results is attributed to the calculation process of the separation distance between particles in Equation 4.26 since it considers the root mean square roughness (Ra) of two rough particles. Table A.2.2 lists the results for 10 repetitions for generating rough particle 2 with different randomly located asperities (control particle 1 with constant ϕ_1 and 10 $\phi_{2\xi}$ for 10 times of particle 2). The results demonstrated that no significant difference existed among these groups ($p > 0.05$), which proved that the random distribution of asperities indeed had an insignificant effect on the interaction of particles if the overall surface roughness is not changed.

As observed in the previous section, when the asperity changed their positions in longitudinal or latitudinal direction or randomly, but the surface roughness was maintained constant, no significant difference existed in the total interaction energy among different pairs of rough particles.
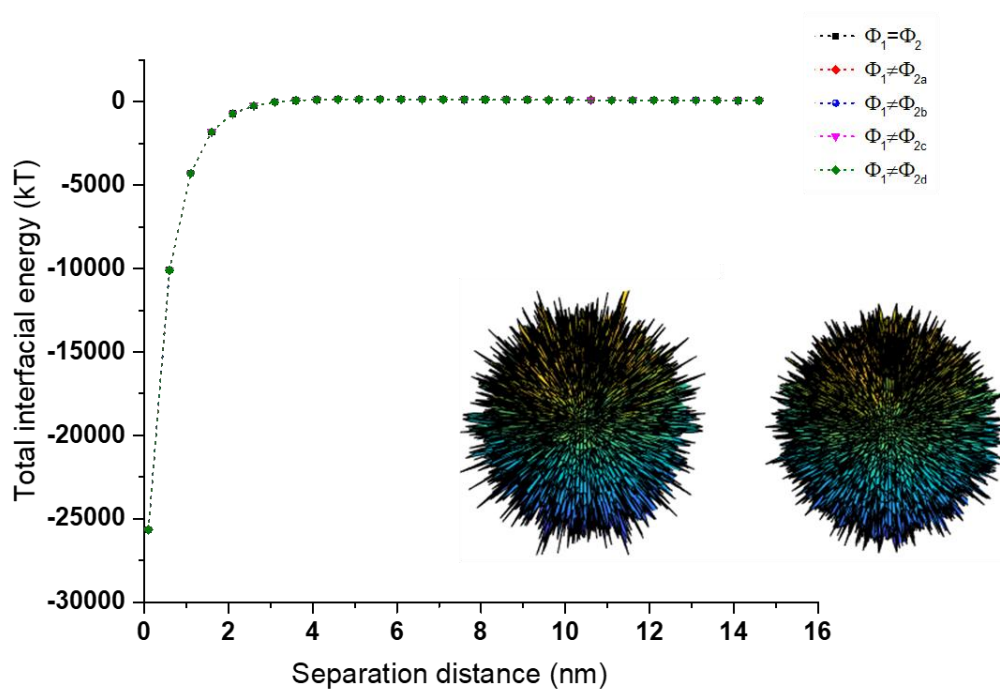
Figure 4.5 The effect of surface randomness on total interfacial energy when $\tau_1 = \tau_2 = 0.1$ nm,

$r_1 = r_2 = 1000$ nm, and $D_{f1} = D_{f2} = 2.23$

4.5.3 Fractal dimension effects (D_{fi})

Surface roughness is a critical parameter to control surface morphology. The primary parameter to control surface roughness in the present study is the fractal dimension. A previous study applied fractal geometry to generate a randomly rough flat surface and concluded that the fractal dimension would control the surface roughness and topography because the number and height of fine asperities will significantly be changed with the value of the fractal dimension [50]. In the present study, the randomly rough spherical surface was constructed with the developed fractal geometry as shown in Figure A.2.3. The influence of fractal dimension on the interaction of particles with random surface structures is shown in Figure 6. With increasing the fractal dimension value from 2.03 to 2.93, the total interfacial energy of rough particles increased. This tendency is expected as the surface roughness is diminished with the fractal dimension [56]. As indicated in a previous study, the surface roughness is decreased by elevating the fractal dimension value [11]. The depth of the primary minimum and the magnitude of the primary maximum increase with fractal dimension value as shown in Figure 6. Shen and coworkers reported that the nanoscale asperities not only reduced the energy barrier of the primary minimum but also promoted the separation of initially attached two white carboxyl-modified polystyrene latex particles at the primary minimum interaction [57]. Therefore, our results suggested that the colloidal particle detachment is proportional to the value of the fractal dimension because the attachment ability would be worsened with a rougher spherical surface, which could be controlled by the fractal dimension. Torkzaban and Bradford also reported that the surface roughness reduced the depth of the primary minimum when analyzing the interfacial energy of quartz sand and carboxylate-modified latex particles [58]. However, Totkzaban and Bradford considered short-range repulsion interactions as the non-DLVO force in their simulation process and applied grid surface integration simulation. In our simulation, the surface roughness can be heightened by fractal dimension, which decreases the contact area and increases the separation distance between two particles [59]. In addition, the decrease in the interaction energy with lessened fractal dimension may be related to surface hydrophobicity. It was reported that rougher surfaces could produce more hydrophobic surfaces [60, 61]. De Foggi and coworkers, who

analyzed the impact of surface roughness of denture-base acrylic resin with the disk shape structure on the material hydrophobicity experimentally, reported that the illustrated surface roughness enhanced surface hydrophobicity [62]. The drop in the energy barrier demonstrated in Figure 6 is the outcome of hydrophobicity improvement via increasing surface roughness (i.e., decreasing the fractal dimension) as predicted by Equation 28. Moreover, the dropped energy barrier may explore the mechanisms of antifouling in the membrane design. Liu and coworkers articulated that the antifouling process could be evaluated by the XDLVO theory and that the large magnitude of the primary maximum indicated a strong antifouling ability [63]. The findings of this work support our simulation results, in that with increasing the value of a fractal dimension, the primary maximum increased (Figure 6), implying the stronger repulsion force between particles.

Interestingly, the variation in the total interfacial energy becomes insignificant when the fractal dimension changed from 2.53 to 2.93 (Figure 6). According to Figure A.2.3, the rough particle becomes smooth with increasing the fractal dimension to $D_{fi} = 2.4$ and $D_{fi} = 2.5$. Cai and coworkers reported that the surface roughness lessened exponentially by increasing the value of the fractal dimension [50]. The predicted interaction energy in this study could only be changed with the fractal dimension ranging between 2.03 and 2.43 because the surface would become smoother if the fractal dimension was larger than 2.4 (Figure A.2.3). Thus, there existed a critical value of fractal dimension (i.e., 2.43) for eliminating the surface topography when studying the interaction of two rough particles following the fractal geometry theory.
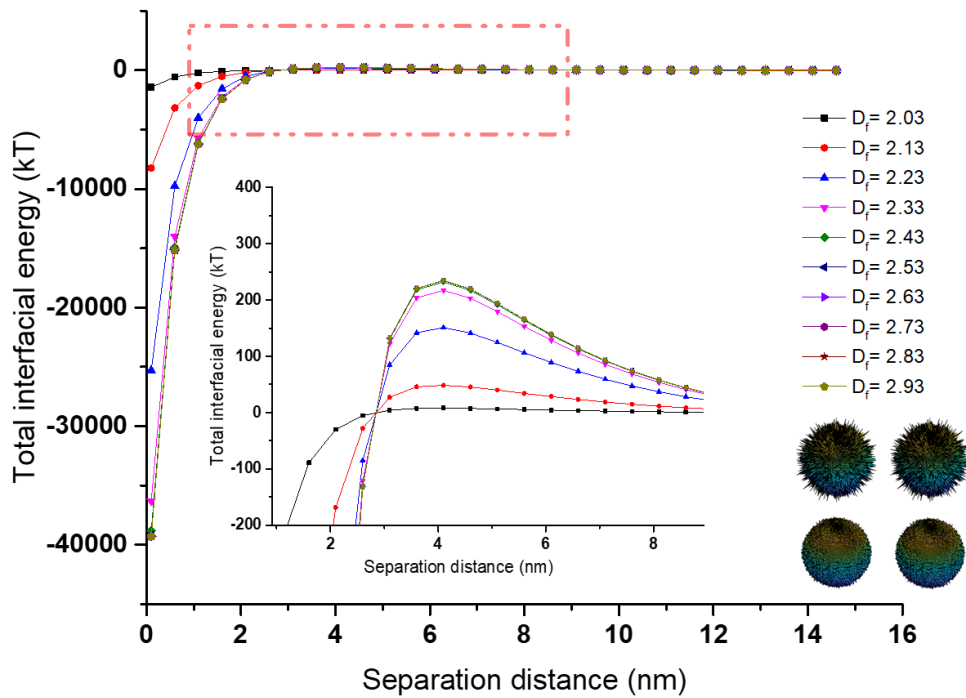
Figure 4.6 The effect of fractal dimension on the total interfacial energy when $\tau_1 = \tau_2 = 0.1$ nm and $r_1 = r_2 = 1000$ nm

4.5.4 Relative fractal dimension effects (D_{f2})

Figure 7 displays the effect of the relative fractal dimension on the total interfacial energy for particles with random surface morphologies. The fractal dimension of particle 1 is set at $D_{f1} = 2.93$ (> critical value of 2.43) to construct a relatively smooth particle, while the fractal dimension of particle 2 (D_{f2}) is changed from 2.03 to 2.93. Figure 7 shows that the absolute value of the interaction increased gradually with a greater value of D_{f2}. This result shows that the stability of the system with rough particles was improved by elevating the relative fractal dimension. The increase in D_{f2} reduces the average roughness of particle 2 exponentially. Therefore, it is expected that the reduction in the relative roughness of particle 2 shortens the separation distance between two rough particles, thus increasing the magnitude of the interaction.

The fractal dimension controls the topography of rough particles, implying that the value of D_{f2} represents the relative surface roughness of two particles, which provides a significant impact on the asperity size of particle 2 [19]. Additionally, when D_{f2} is above 2.43 in the present modeling study, the effect of the relative fractal dimension is negligible because the size of the asperities has no significant influence (smooth surface). When D_{f2} is smaller than 2.43, the increased value of D_{f2} lowered the

asperity size of the surface, which empowered the total interfacial interaction of rough particles. The phenomenon can be explained by the increased asperity height that reduced the area of particle interaction affecting the interfacial energy negatively [64]. Although a larger relative fractal dimension constructs more asperities, the average roughness of particles decreases because the texture of the surface becomes denser and finer with increasing the value of the relative fractal dimension [65, 66]. This discovery may provide more directions for the colloid release and retention on natural rough surfaces, for example, contaminant dissemination [67] because the predicted value of primary minimum and maximum could be valuable indicators for altering the state of particles in the system. Therefore, the simulated results suggested that modifying the texture of rough surfaces with random surface morphologies played a critical role in influencing the stability of the suspension system.
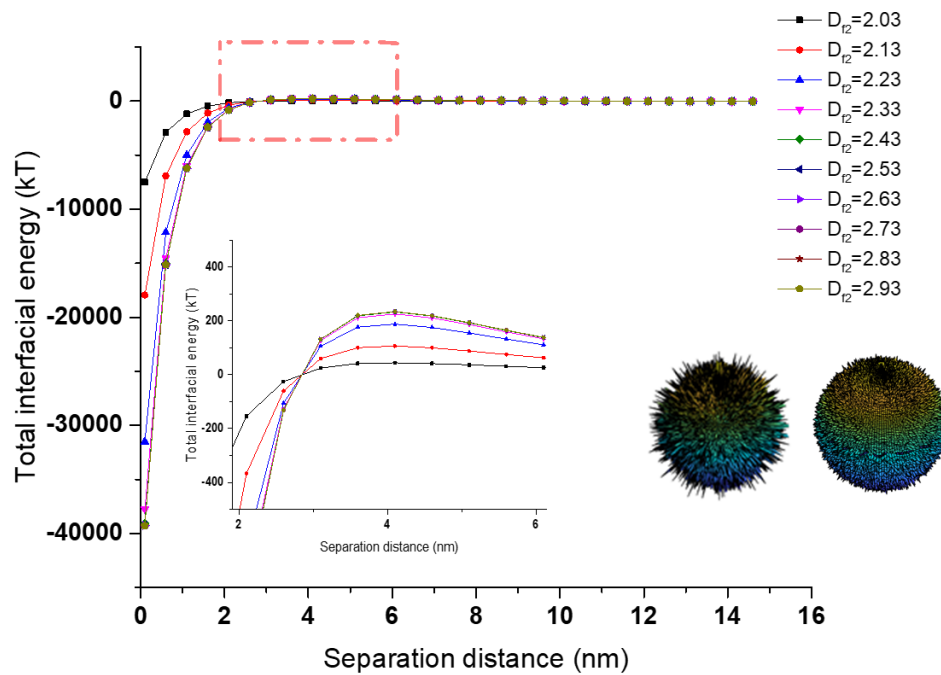
Figure 4.7 The effect of relative fractal dimension on total interfacial energy when $\tau_1 = \tau_2 = 0.1$ nm, $r_1 = 1000$ nm, and $D_{f1} = 2.93$

4.5.5 Fractal roughness effects (τ_i)

Different from the fractal dimension, fractal roughness only characterizes the magnitude of surface roughness [42]. In other words, the asperity height on the rough surface with randomly oriented asperities is controlled by the value of fractal roughness in this analysis. The influence of fractal

roughness on the interfacial interaction generated between particles is reported in Figure 8. The interfacial interaction lessened by elevating the value of fractal roughness from 0.5 nm to 10 nm. The total interfacial energy was closed to 0 kT when the value of fractal roughness is 10 nm, which indicates that the system dispersion stability has deteriorated. This phenomenon explains that the increased value of fractal roughness elevated the value of surface roughness of particles negatively affected the interfacial interaction between particles. For a given value of a fractal dimension, the larger values of τ_1 and τ_2 result in a rougher surface based on Equation 7 because the amplitude of the surface wavelength is increased by τ_1 and τ_2 [68]. Therefore, the larger peak of asperities would be generated on the particle surface by increasing the fractal roughness value, which in turn would drop the overall interface energy because the larger value of the asperity height would tend to enlarge the separation distance and diminish the interaction area between the particles [69, 70]. Thus, the dispersion stability of the colloidal system would decrease with increasing the fractal roughness, which would suggest that the particles might aggregate without sufficient electric repulsion force if the rough particles had large fractal roughness. Moreover, the increased surface roughness would increase the surface area of particles, which may facilitate particle attachment. Wu and coworkers prepared a thin-film composite (TFC) membrane from polyvinylidene fluoride (PVDF) substrate and reported that the rougher surface provides a lower detach rate of Na_2SO4 and $MgSO4$ from the membrane [71]. Although the interaction scenario of this work was based on the simulation of a particle-flat surface [68], our particle-particle model predicted similar results, where the increased roughness reduced the repulsion energy barrier that assisted the particle attachment [72]. Guo and coworkers also investigated the influence of surface roughness on calcium–magnesium–alumina–silicate corrosion and reported that the surface roughness provided a remarkable impact on the wettability of the material surface [73]. The conclusion made by Guo and coworkers suggested that surface roughness would increase the water contact angle because the rough surface morphology would increase the hydrophobicity of the surface. The predicted results from our model presented a similar conclusion to previous literature [73]. Therefore, the present model may provide some insights into the wettability of the material surface. As the fractal roughness controlled the average roughness of rough particles with random surface morphologies, our results indicated that the value of fractal roughness may provide a prediction of material wettability.
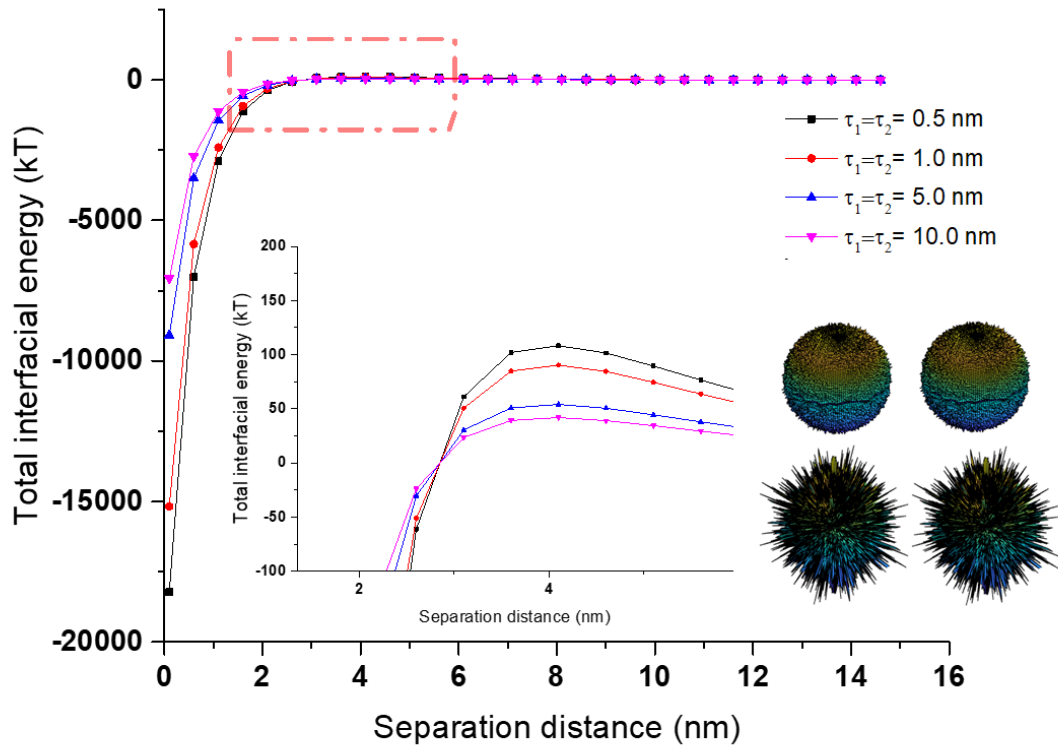
Figure 4.8 The effects of fractal roughness on total interfacial energy when $D_{f1}=D_{f2}=2.23$ and $r_1=r_2=1000$ nm

4.5.6 Relative fractal roughness effects (τ_2)

Figure 9 shows the total interfacial interaction of rough particles with different fractal roughness. It showed that the total interaction became poor when the relative fractal roughness of the particle surface increased. The increased relative fractal roughness (τ_2) diminished the dispersion stability between particles, which might facilitate the aggregation of particles. This result is in harmony with the fact that the relatively rougher surfaces represent the larger asperity height and minimize the interaction energy [74]. The previous literature mainly discussed that the fractal dimension was critical in interfacial interaction between particles [75, 76]. Nevertheless, our predicted results showed that the relative fractal roughness has a noteworthy impact on particle interactions. Consequently, our results obtained from Equations 7,17, and 28 indicated that the relative fractal roughness is an impactful factor in the adhesion of particles to surfaces because this parameter represents the average asperity height of rough particles affecting the particle interaction remarkably [77], which may facilitate the coagulation of colloidal particles, for example, the coagulation of sulfonated azo-dyes in acidic solutions [78].
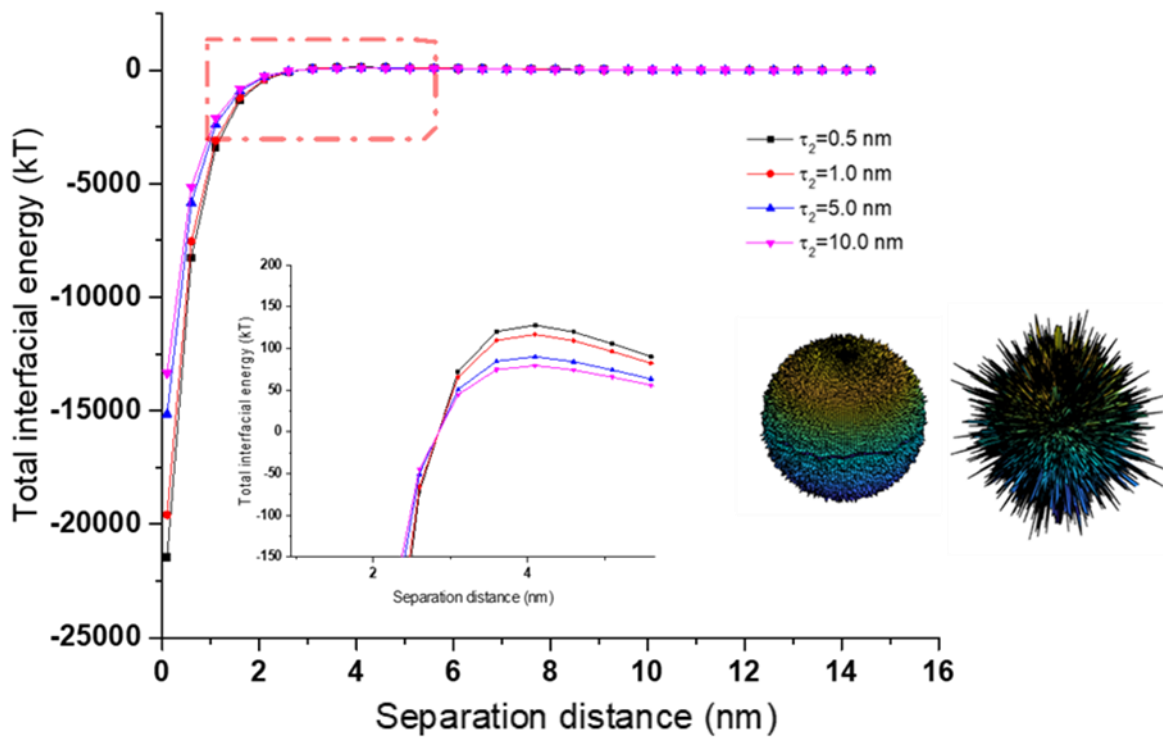
Figure 4.9 The effect of relative fractal roughness on interfacial energy when $r_1 = r_2 = 1000$ nm, $D_{f1} = D_{f2} = 2.23$ and $\tau_1 = 0.1$ nm

4.5.7 The most effective parameter in controlling particle interaction

The constructed parameters of rough particles with randomly decorated asperities have significant effects on controlling particle interaction. The randomness of the surface asperities displayed the least effect in controlling interfacial interaction energy. It should be noted that changing the asperity size to increase the separation distance or reduce the interaction area (Figures 6-9) has more effects on interfacial interaction energy between particles than only altering the positions of asperities on the surface (Figure 5). Therefore, surface roughness is more critical than the spatial distribution of asperities in particle interactions. The fractal dimension displayed the most significant effect on the particle interaction where the largest value of the primary maximum was predicted to be 216 kT (Figure 6). However, the significant variation in the interaction energy could only be obtained in the fractal dimension ranging between 2.03 and 2.43 because the particle surface became smooth once the value of the fractal dimension was larger than 2.43. The dispersion stability of different colloidal systems is

103

managed by their primary maximum (i.**e.,** repulsion energy). The magnitude of the primary maximum would not be elevated significantly when the value of the fractal dimension was beyond 2.43. Therefore, the strongest dispersion stability between particles could be obtained when the fractal dimension was 2.43 in the present work. Nevertheless, if a system owned a small primary maximum, the dispersion stability between particles would be hampered easily and particles might tend to aggregate or coagulate. When the primary maximum was smaller than 1.5 kT in a hectorite suspension system, flocculation tends to happen [2]. If the value of the primary maximum dropped < 20 kT, the aggregation would dominate [79]. Based on the predicted value of the primary maximum, modifying the fractal dimension via applying different coating material or blast pressure, for example [80, 81], could be selected as the most effective method for the surface modification of particles to control the system dispersion stability (e.g., cellulose nanocrystals [82]).

4.5.8 Comparison of present modeling and previously available results

The simulation results of this work were compared with previously available results and summarized in Table 4.1.

Table 4.1 Information on present and past models in creating rough surfaces

Applied constructing theory, ref	Equations for constructing rough surface	Variables	Results
Fractional area coverage, [83]	$\varsigma = 2n\pi(R + \epsilon_s)\epsilon_s$	ς increased from 0.01 to 0.1	The maximum total interaction decreased from 105 to 81 kT/μm
Modified two-variable WM function (present model)	$\Delta r_i = L(\frac{G_i}{L})^{D_{f_i}-2}(\frac{ln\eta}{M})^{\frac{1}{2}} \sum\limits_{m=1}^{M} \sum\limits_{n=0}^{n_{max}} \eta^{(D_{f_i}-3)n}$ $\times (\cos\phi_{m,nmax+1_i}$ $- \cos(\frac{2\pi\eta^n r \sin\theta}{L}$ $* \cos\left(\varphi - \frac{\pi m}{M}\right)$ $+ \phi_{m,nmax+1}))$	D_f decreased from 2.23 to 2.03	The maximum total interaction decreased from 150 to 8 kT/μm

Rippled rough particle theory, [33]	$R_{rough} = r_{element} + r_i \lambda_i \cos(n_i \theta_i) + r_i \lambda_i \cos(n_i \varphi_i)$	n_i increased from 5 to 20	The maximum total interaction decreased from 200 to 150 kT
Modified two-variable WM function (present model)	$\Delta r_i = L(\frac{G_i}{L})^{D_{f_i}-2} (\frac{ln\eta}{M})^{\frac{1}{2}} \sum_{m=1}^{M} \sum_{n=0}^{n_{max}} \eta^{(D_{f_i}-3)n}$ $\times (\cos \phi_{m,nmax+1_i}$ $- \cos(\frac{2\pi\eta^n r \sin\theta}{L}$ $* \cos\left(\varphi - \frac{\pi m}{M}\right)$ $+ \phi_{m,nmax+1}))$	D_{fi} decreased from 2.43 to 2.03	The maximum total interaction decreased from 231 to 8 kT
Modified Derjaguin approaches, [74]	$h = D + a - \sqrt{a^2 - r^2 \pm \sqrt{a_i^2 - r_i^2}}$	The average height (or radius) of a hemispherical asperity increased from 9 to 45 nm	The maximum total interaction decreased from 15.8 to 8.7 kT
Modified two-variable WM function (present model)	$\Delta r_i = L(\frac{G_i}{L})^{D_{f_i}-2} (\frac{ln\eta}{M})^{\frac{1}{2}} \sum_{m=1}^{M} \sum_{n=0}^{n_{max}} \eta^{(D_{f_i}-3)n}$ $\times (\cos \phi_{m,nmax+1_i}$ $- \cos(\frac{2\pi\eta^n r \sin\theta}{L}$ $* \cos\left(\varphi - \frac{\pi m}{M}\right)$ $+ \phi_{m,nmax+1}))$	τ_i increased from 9 to 45 nm	The maximum total interaction decreased from 8.0 to 4.1 kT
Fractional area coverage, [84]	$\varsigma = 2n\pi(R + \epsilon_s)\epsilon_s$	ϵ_s increased from 10 to 40 nm	The maximum total interaction decreased from 105 to 10 kT/μm

Modified two-variable WM function (present model)	$$\Delta r_i = L(\frac{G_i}{L})^{D_{f_i}-2}(\frac{\ln\eta}{M})^{\frac{1}{2}}\sum_{m=1}^{M}\sum_{n=0}^{n_{max}}\eta^{(D_{f_i}-3)n}$$ $$\times(\cos\phi_{m,nmax+1_i}$$ $$-\cos(\frac{2\pi\eta^n r\sin\theta}{L}$$ $$*\cos\left(\varphi-\frac{\pi m}{M}\right)$$ $$+\phi_{m,nmax+1}))$$	τ_i increased from 10 to 40 nm	The maximum total interaction decreased from 152 to 82 kT/μm

In the studies carried out using the fractional area coverage to represent the asperity number, when the asperity coverage, ς, increased from 0.01 to 0.1, the maximum total interaction energy dropped from 105 to 81 kT/μm [83]. With the same size of rough particles, the present study reported the maximum total interaction energy decreasing from 150 to 8 kT/μm when the fractal dimention D_{fi} changed from 2.23 to 2.03, which elevated the total surface roughness. In addition, when the asperity number on the particles with arranged surface morphologies, n, increased from 5 to 20, the maximum total interaction decreased from 200 to 150 kT [33]. Similarly, for the same particle size, when the surface roughness increased by changing D_{fi} from 2.43 to 2.03, the maximum total interaction energy decreased from 231 to 8 kT in the present study. The different predictions in the total interaction energy could be explained by the different methods of constructing rough surfaces. In other words, the impact of constructing parameters for the particle surface morphologies in this model and the previous one [33] is dissimilar. In the current study, when the value of D_{fi} increased, the asperity height would decrease but more fine asperities would be generated on the rough surface [16, 50]. The value of D_{fi} controlled the asperity size and asperity number simultaneously, which would provide information about the complexity of rough surface [85].

The modified Derjaguin approaches were also applied to simulate rough surface interaction when a hemispherical asperity height (or radius) increased from 9 to 45 nm, and the maximum interaction decreased from 15.8 to 8.7 kT [74]. Compared to the literature [74], the present model randomly distributed the asperities on a rough surface, which could accurately simulate the self-affine features of a naturally rough surface [86] and predicted that the maximum interaction decreased from 8.0 to 4.1 kT when the τ_i increased from 9 to 45 nm for particles of the same size.

In the study considering the fractional area coverage, when the height of asperities, ϵ_s, was elevated

from 10 to 40 nm, and the maximum total interaction energy dropped from 105 to 10 kT/μm [84]. With the same assumptions, the present study shows a drop from 152 to 82 kT/μm. The present model generated the rough surface as random waveform (Equation 7) instead of uniform hemispherical asperities or hemispheres [49, 52], which can describe the roughness of the naturally produced surface (e.g., coal surface) [87]. Thus, the outcomes of our work could be more reliable than the models used previously [74, 84] in assessing the interfacial energy of particles in the real scenario, as the asperities are usually randomly assigned on the surface of naturally produced particles.

In addition, the results indicated that the approach to constructing the rough surface is key to simulating particle interactions. Generally, the primary step to accurately evaluate the interaction energy of spherical surfaces is to characterize the surface morphology correctly. Our model applied the modified two-variable WM function to construct a rough surface, which could characterize the natural surface more accurately than the previous models [33, 74, 84]. Therefore, the present model and particle construction method elevated the accuracy of prediction for the interaction of rough surfaces with randomly located asperities based on the proposed modified two-variable WM function.

The present modeling study provides a novel method to evaluate the interaction energy between two particles with randomly rough surface morphology. By applying this strategy, the effect of roughness existing on the surface of natural products on the interaction of particles can be addressed. Moreover, the modeling approach undertaken in the present work can provide a guideline on the possibility to design of particles with favorable morphologies that have strong interfacial interaction, for example, the fractal dimension could be modified by different coating material or blast pressure [80, 81]. The present model could be also potentially used to investigate various phenomena, such as coagulation, dispersion, turbulence, deposition, and flocculation that occur among natural products.

4.6 Conclusion

The present study applied a modified two-variable WM function based on the fractal geometry to construct a randomly rough spherical surface, which accurately characterized the surface morphology of a naturally rough surface and explored the impact of factors affecting the construction of rough particles with randomly located asperities on spherical surface interaction considering the XDLVO theory. As the previous studies did not consider the impact of the location of asperities on the rough

surface of the particles, they neglected the impact of the actual topographic characteristic products on particle interaction. In this case, the proposed approach of this study could increase the accuracy of prediction in the interaction of particles with randomly constructed rough surface morphologies.

Two types of asperity-arranged spherical surfaces were constructed to investigate the impact of asperity position on the interfacial interaction of spherical surfaces. The predictions showed that changing the position of asperities in longitude and latitude directions has more limited impacts than the number and ratio of asperities of the particle surface on particle interactions, which indicated that changing the number and ratio of asperities are the primary factor in influencing the particle attachment compared with arranging the location of asperities. Also, the randomness in the position of asperities on the spherical surfaces with random surface morphologies had a marginal impact on the interfacial energy of particles, when the roughness of the surface was unchanged.

Furthermore, the increase in the fractal dimension (D_{fi}) and relative fractal dimension (D_{f2}) strengthened the interfacial interaction energy, which is related to the creation of fine topography on the surface of particles. However, the total interfacial interaction lessened significantly with the growth in the fractal roughness. The increase in the fractal roughness (τ_i) and relative fractal roughness (τ_2) affected the interaction energy significantly, which was attributed to an improvement in the average roughness of the particle surface by increasing the asperity height on the particle surface. The largest primary maximum could be obtained when the D_{fi} reached the critical value of 2.43, where the strongest stability of the colloidal system would be obtained. According to the predicted value of the primary maximum in colloidal particle interaction evolved from XDLVO theory, modifying the fractal dimension of spherical surfaces by a coating process could be considered the most effective method of material surface morphology modification to control the system stability.

The present model generated randomly arranged asperities on the particle surface, which could reflect the natural topography of spherical surfaces more precisely. To enhance the accuracy of our modeling study, future works may consider the analysis of interfacial interaction between rough spherical surfaces with ellipsoidal shapes as they are available in nature.

4.7 Reference

[1] J. Matusiak, E. Grządka, Stability of colloidal systems-a review of the stability measurements methods, Annales Universitatis Mariae Curie-Sklodowska, sectio AA–Chemia, 72 (2017) 33.

[2] C. Van Oss, R. Giese, P.M. Costanzo, DLVO and non-DLVO interactions in hectorite, Clays Clay Miner., 38 (1990) 151-159.

[3] J.F. Carstens, J. Bachmann, I. Neuweiler, A new approach to determine the relative importance of DLVO and non-DLVO colloid retention mechanisms in porous media, Colloids Surf. Physicochem. Eng. Aspects, 560 (2019) 330-335.

[4] E.M. Hoek, G.K. Agarwal, Extended DLVO interactions between spherical particles and rough surfaces, Journal of Colloid and Interface science, 298 (2006) 50-58.

[5] L. Zhao, M. Zhang, Y. He, J. Chen, H. Hong, B.-Q. Liao, H. Lin, A new method for modeling rough membrane surface and calculation of interfacial interactions, Bioresour. Technol., 200 (2016) 451-457.

[6] H. Hong, X. Cai, L. Shen, R. Li, H. Lin, Membrane fouling in a submerged membrane bioreactor: new method and its applications in interfacial interaction quantification, Bioresour. Technol., 241 (2017) 406-414.

[7] D. Dantchev, G. Valchev, Surface integration approach: A new technique for evaluating geometry dependent forces between objects of various geometry and a plate, Journal of colloid and interface science, 372 (2012) 148-163.

[8] J. Chen, H. Lin, L. Shen, Y. He, M. Zhang, B.-Q. Liao, Realization of quantifying interfacial interactions between a randomly rough membrane surface and a foulant particle, Bioresour. Technol., 226 (2017) 220-228.

[9] E. Martines, L. Csaderova, H. Morgan, A. Curtis, M. Riehle, DLVO interaction energy between a sphere and a nano-patterned plate, Colloids Surf. Physicochem. Eng. Aspects, 318 (2008) 45-52.

[10] S. Bhattacharjee, J.Y. Chen, M. Elimelech, DLVO interaction energy between spheroidal particles and a flat surface, Colloids Surf. Physicochem. Eng. Aspects, 165 (2000) 143-156.

[11] M. Zhang, X. Zhou, L. Shen, X. Cai, F. Wang, J. Chen, H. Lin, R. Li, X. Wu, B.-Q. Liao, Quantitative evaluation of the interfacial interactions between a randomly rough sludge floc and membrane surface in a membrane bioreactor based on fractal geometry, Bioresour. Technol., 234 (2017) 198-207.

[12] Z. Zhu, D. Wang, B. Yang, W. Yin, M.S. Ardakani, J. Yao, J.W. Drelich, Effect of nano-sized roughness on the flotation of magnesite particles and particle-bubble interactions, Minerals Engineering, 151 (2020) 106340.

[13] R.R. Netz, D. Andelman, Neutral and charged polymers at interfaces, Phys. Rep., 380 (2003) 1-95.

[14] A. Polotsky, F. Schmid, A. Degenhard, Polymer adsorption onto random planar surfaces: Interplay of polymer and surface correlations, The Journal of chemical physics, 121 (2004) 4853-4864.

[15] A.P. Angelopoulos, Enthalpy-driven adsorption of chain molecules onto chemically heterogeneous surfaces, Journal of colloid and interface science, 243 (2001) 292-299.

[16] Y. Peng, Y. Guo, An adhesion model for elastic-plastic fractal surfaces, Journal of Applied Physics, 102 (2007) 053510.

[17] M.Y. Marusina, A.P. Mochalina, E.P. Frolova, V.I. Satikov, A.A. Barchuk, V.I. Kuznetcov, V.S. Gaidukov, S.A. Tarakanov, MRI image processing based on fractal analysis, Asian Pacific journal of cancer prevention: APJCP, 18 (2017) 51.

[18] Y. Chen, C. Zhang, M. Shi, G. Peterson, Role of surface roughness characterized by fractal geometry on laminar flow in microchannels, Physical Review E, 80 (2009) 026301.

[19] X. Cai, M. Zhang, L. Yang, H. Lin, X. Wu, Y. He, L. Shen, Quantification of interfacial interactions between a rough sludge floc and membrane surface in a membrane bioreactor, Journal of colloid and interface science, 490 (2017) 710-718.

[20] A. Majumdar, B. Bhushan, Role of fractal geometry in roughness characterization and contact mechanics of surfaces, (1990).

[21] Y. Jin, J. Zheng, X. Liu, J. Pan, S. Liu, Control mechanisms of self-affine, rough cleat networks on flow dynamics in coal reservoir, Energy, 189 (2019) 116146.

[22] J. Zheng, Y. Jin, X. Liu, C. Wang, X. Liu, Validity of triple-effect model for fluid flow in mismatched, self-affine fractures, Advances in Water Resources, 140 (2020) 103585.

[23] L. Zhao, L. Yang, H. Lin, M. Zhang, H. Yu, B.-Q. Liao, F. Wang, X. Zhou, R. Li, Modeling three-dimensional surface morphology of biocake layer in a membrane bioreactor based on fractal geometry, Bioresour. Technol., 222 (2016) 478-484.

[24] M. Tanaka, M. Komagata, M. Tsukada, H. Kamiya, Fractal analysis of the influence of surface roughness of toner particles on their flow properties and adhesion behavior, Powder technology, 186 (2008) 1-8.

[25] P. Sahoo, S.R. Chowdhury, A fractal analysis of normal impact between rough surfaces in presence of adhesion, Wear, 261 (2006) 318-327.

[26] Y. Chen, C. Zhang, M. Shi, G.P. Peterson, Slip boundary for fluid flow at rough solid surfaces, Applied Physics Letters, 100 (2012) 074102.

[27] M. Papanikolaou, M. Frank, D. Drikakis, Nanoflow over a fractal surface, Phys. Fluids, 28 (2016) 082001.

[28] M. Papanikolaou, M. Frank, D. Drikakis, Effects of surface roughness on shear viscosity, Physical Review E, 95 (2017) 033108.

[29] A. Chervanyov, G. Heinrich, What really enhances the adsorption of polymers onto chemically nonuniform surfaces: Surface randomness or its heterogeneity?, The Journal of chemical physics, 125 (2006) 084703.

[30] P. Bazant, J. Klofac, L. Munster, I. Kuritka, Antibacterial powders for medical application prepared by microwave hydrothermal assisted synthesis, Nanoscience and Nanotechnology, 6 (2016) 88-91.

[31] S. Yang, F. Guo, B. Kiraly, X. Mao, M. Lu, K.W. Leong, T.J. Huang, Microfluidic synthesis of multifunctional Janus particles for biomedical applications, Lab on a Chip, 12 (2012) 2097-2102.

[32] S. Bhattacharjee, C.-H. Ko, M. Elimelech, DLVO interaction between rough surfaces, Langmuir, 14 (1998) 3365-3375.

[33] D. Lu, P. Fatehi, A modeling approach for quantitative assessment of interfacial interaction between two rough particles in colloidal systems, Journal of Colloid and Interface Science, 587 (2020) 24-38.

[34] H. Bargozin, R. Hadadhania, H. Faraji, H. Yousefzadeh, Effect of rough nanoparticle orientation on DLVO energy interaction, Journal of Dispersion Science and Technology, 36 (2015) 755-764.

[35] B. Peng, A. Imhof, Surface morphology control of cross-linked polymer particles via dispersion polymerization, Soft Matter, 11 (2015) 3589-3598.

[36] M. Benz, K.J. Rosenberg, E.J. Kramer, J.N. Israelachvili, The deformation and adhesion of randomly rough and patterned surfaces, The Journal of Physical Chemistry B, 110 (2006) 11884-11893.

[37] A. Movafeghi, A. Khataee, M. Abedi, R. Tarrahi, M. Dadpour, F. Vafaei, Effects of TiO2 nanoparticles on the aquatic plant Spirodela polyrrhiza: evaluation of growth parameters, pigment contents and antioxidant enzyme activities, Journal of Environmental Sciences, 64 (2018) 130-138.

[38] S. You, M.P. Wan, Mathematical models for the van der Waals force and capillary force between a rough particle and surface, Langmuir, 29 (2013) 9104-9117.

[39] J.A. Commito, B.R. Rusignuolo, Structural complexity in mussel beds: the fractal geometry of surface topography, J. Exp. Mar. Biol. Ecol., 255 (2000) 133-152.

[40] A. LENHOFF, Contributions of surface features to the electrostatic properties of rough colloidal particles, Colloids and surfaces. A, Physicochemical and engineering aspects, 87 (1994) 49-59.

[41] X. Qu, X. Cai, M. Zhang, H. Lin, Z. Leihong, B.-Q. Liao, A facile method for simulating randomly rough membrane surface associated with interface behaviors, Applied Surface Science, 427 (2018) 915-921.

[42] S. Feng, G. Yu, X. Cai, M. Eulade, H. Lin, J. Chen, Y. Liu, B.-Q. Liao, Effects of fractal roughness of membrane surfaces on interfacial interactions associated with membrane fouling in a membrane bioreactor, Bioresour. Technol., 244 (2017) 560-568.

[43] W. Yan, K. Komvopoulos, Contact analysis of elastic-plastic fractal surfaces, Journal of applied physics, 84 (1998) 3617-3624.

[44] R. Pitchumani, B. Ramakrishnan, A fractal geometry model for evaluating permeabilities of porous preforms used in liquid composite molding, International Journal of Heat and Mass Transfer, 42 (1999) 2219-2232.

[45] G. Hwang, C.H. Lee, I.S. Ahn, B.J. Mhin, Analysis of the adhesion of Pseudomonas putida NCIB 9816-4 to a silica gel as a model soil using extended DLVO theory, Journal of Hazardous Materials, 179 (2010) 983-988.

[46] C. Van Oss, Acid—base interfacial interactions in aqueous media, Colloids Surf. Physicochem. Eng. Aspects, 78 (1993) 1-49.

[47] J. Dann, Forces involved in the adhesive process: I. Critical surface tensions of polymeric solids as determined with polar liquids, Journal of Colloid and Interface Science, 32 (1970) 302-320.

[48] S. Bhattacharjee, M. Elimelech, M. Borkovec, DLVO Interaction between Colloidal Particles: Beyond Derjaguin's Approximation, Croat. Chem. Acta, 71 (1998) 883-903.

[49] M. Zhang, H. Hong, H. Lin, G. Yu, F. Wang, B.-Q. Liao, Quantitative assessment of interfacial forces between two rough surfaces and its implications for anti-adhesion membrane fabrication, Separation and Purification Technology, 189 (2017) 238-245.

[50] X. Cai, L. Yang, Z. Wang, M. Zhang, L. Shen, H. Hong, H. Lin, G. Yu, Influences of fractal dimension of membrane surface on interfacial interactions related to membrane fouling in a membrane bioreactor, Journal of colloid and interface science, 500 (2017) 79-87.

[51] H. Hong, H. Lin, R. Mei, X. Zhou, B.-Q. Liao, L. Zhao, Membrane fouling in a membrane bioreactor: a novel method for membrane surface morphology construction and its application in interaction energy assessment, J. Membr. Sci., 516 (2016) 135-143.

[52] R. Mei, R. Li, H. Lin, Z. Shen, M. Zhang, J. Chen, Y. He, A new approach to construct three-dimensional surface morphology of sludge flocs in a membrane bioreactor, Bioresour. Technol., 219 (2016) 521-526.

[53] J. Zheng, A. He, J. Li, J. Xu, C.C. Han, Studies on the controlled morphology and wettability of polystyrene surfaces by electrospinning or electrospraying, Polymer, 47 (2006) 7095-7102.

[54] Y. Kurokawa, O. Aonuma, T. Tayagaki, I. Takahashi, N. Usami, Effects of surface morphology randomness on optical properties of Si-based photonic nanostructures, Japanese Journal of Applied Physics, 56 (2017) 08MA02.

[55] M. Zribi, N. Baghdadi, C. Guérin, Analysis of surface roughness heterogeneity and scattering behavior for radar measurements, IEEE transactions on geoscience and remote sensing, 44 (2006) 2438-2444.

[56] E. Thormann, Surface forces between rough and topographically structured interfaces, Current Opinion in Colloid & Interface Science, 27 (2017) 18-24.

[57] C. Shen, L.-P. Wang, B. Li, Y. Huang, Y. Jin, Role of surface roughness in chemical detachment of colloids deposited at primary energy minima, Vadose Zone Journal, 11 (2012).

[58] S. Torkzaban, S.A. Bradford, Critical role of surface roughness on colloid retention and release in porous media, Water Research, 88 (2016) 274-284.

[59] R. Elleuch, K. Elleuch, H. Ben Abdelounis, H. Zahouani, Surface roughness effect on friction behaviour of elastomeric material, Materials Science and Engineering: A, 465 (2007) 8-12.

[60] B.W. Chieng, N.A. Ibrahim, N. Ahmad Daud, Z.A. Talib, Chapter 8 - Functionalization of Graphene Oxide via Gamma-Ray Irradiation for Hydrophobic Materials, in: S.A. Rashid, R.N.I. Raja Othman, M.Z. Hussein (Eds.) Synthesis, Technology and Applications of Carbon Nanomaterials, Elsevier2019, pp. 177-203.

[61] C.-T. Hsieh, J.-M. Chen, R.-R. Kuo, T.-S. Lin, C.-F. Wu, Influence of surface roughness on water-and oil-repellent surfaces coated with nanoparticles, Applied Surface Science, 240 (2005) 318-326.

[62] C.C. de Foggi, A.L. Machado, C.A. Zamperini, D. Fernandes, A.F. Wady, C.E. Vergani, Effect of surface

roughness on the hydrophobicity of a denture-base acrylic resin and Candida albicans colonization, Journal of Investigative and Clinical Dentistry, 7 (2016) 141-148.

[63] Y. Liu, L. Shen, Z. Huang, J. Liu, Y. Xu, R. Li, M. Zhang, H. Hong, H. Lin, A novel in-situ micro-aeration functional membrane with excellent decoloration efficiency and antifouling performance, J. Membr. Sci., 641 (2022) 119925.

[64] Y. Xing, X. Gui, F. Karakas, Y. Cao, Role of collectors and depressants in mineral flotation: A theoretical analysis based on extended DLVO theory, Minerals, 7 (2017) 223.

[65] J. Das, B. Linke, Evaluation and systematic selection of significant multi-scale surface roughness parameters (SRPs) as process monitoring index, Journal of Materials Processing Technology, 244 (2017) 157-165.

[66] Q. Wang, Z. Liang, X. Wang, W. Zhao, Y. Wu, T. Zhou, Fractal analysis of surface topography in ground monocrystal sapphire, Applied Surface Science, 327 (2015) 182-189.

[67] N. Sefrioui, A. Ahmadi, A. Omari, H. Bertin, Numerical simulation of retention and release of colloids in porous media at the pore scale, Colloids Surf. Physicochem. Eng. Aspects, 427 (2013) 33-40.

[68] H. Wang, W. Zhang, S. Zeng, C. Shen, C. Jin, Y. Huang, Interactions between nanoparticles and fractal surfaces, Water research, 151 (2019) 296-309.

[69] L. Si, X. Wang, G. Xie, N. Sun, Nano-adhesion and friction of multi-asperity contact: a molecular dynamics simulation study, Surface and Interface Analysis, 47 (2015) 919-925.

[70] L. Si, X. Wang, Nano-adhesion influenced by atomic-scale asperities: A molecular dynamics simulation study, Applied surface science, 317 (2014) 710-717.

[71] J. Wu, M. Xia, Z. Li, L. Shen, R. Li, M. Zhang, Y. Jiao, Y. Xu, H. Lin, Facile preparation of polyvinylidene fluoride substrate supported thin film composite polyamide nanofiltration: Effect of substrate pore size, J. Membr. Sci., 638 (2021) 119699.

[72] Z. Huang, Q. Zeng, Y. Liu, Y. Xu, R. Li, H. Hong, L. Shen, H. Lin, Facile synthesis of 2D TiO2@ MXene composite membrane with enhanced separation and antifouling performance, J. Membr. Sci., 640 (2021) 119854.

[73] L. Guo, G. Li, G. Zhilin, Effects of surface roughness on CMAS corrosion behavior for thermal barrier coating applications, Journal of Advanced Ceramics, 10 (2021) 472-481.

[74] E.M. Hoek, S. Bhattacharjee, M. Elimelech, Effect of membrane surface roughness on colloid− membrane DLVO interactions, Langmuir, 19 (2003) 4836-4847.

[75] L. Zhao, X. Qu, H. Lin, G. Yu, B.-Q. Liao, Simulation of foulant bioparticle topography based on Gaussian process and its implications for interface behavior research, Applied Surface Science, 434 (2018) 975-981.

[76] J. Liu, W.Y. Shih, M. Sarikaya, I.A. Aksay, Fractal colloidal aggregates with finite interparticle interactions: Energy dependence of the fractal dimension, Physical Review A, 41 (1990) 3206.

[77] L. Suresh, J.Y. Walz, Effect of surface roughness on the interaction energy between a colloidal sphere and a flat plate, Journal of Colloid and Interface Science, 183 (1996) 199-213.

[78] A. Szyguła, E. Guibal, M. Ruiz, A.M. Sastre, The removal of sulphonated azo-dyes by coagulation with chitosan, Colloids Surf. Physicochem. Eng. Aspects, 330 (2008) 219-226.

[79] R.J. Hunter, Foundations of colloid science, Oxford university press2001.

[80] A. Oliva, E. Anguiano, M. Aguilar, Fractal dimension: measure of coating quality, Surface engineering, 15 (1999) 101-104.

[81] S. Amada, H. Yamada, Introduction of fractal dimension to adhesive strength evaluation of plasma-sprayed coatings, Surf. Coat. Technol., 78 (1996) 50-55.

[82] T.-D. Ngo, C. Danumah, B. Ahvazi, Production of cellulose nanocrystals at InnoTech Alberta, Nanocellulose and sustainability, CRC Press2018, pp. 269-287.

[83] J.W. Drelich, A simplified analysis of the effect of nano-asperities on particle-bubble interactions,

Physicochemical Problems of Mineral Processing, 54 (2018).

[84] O. Guven, M.S. Celik, J.W. Drelich, Flotation of methylated roughened glass particles and analysis of particle–bubble energy barrier, Minerals Engineering, 79 (2015) 125-132.

[85] D. Risović, S.M. Poljaček, K. Furić, M. Gojo, Inferring fractal dimension of rough/porous surfaces—A comparison of SEM image analysis and electrochemical impedance spectroscopy methods, Applied Surface Science, 255 (2008) 3063-3070.

[86] A. Majumdar, C. Tien, Fractal characterization and simulation of rough surfaces, Wear, 136 (1990) 313-327.

[87] W. Friesen, R. Mikula, Fractal dimensions of coal particles, Journal of Colloid and Interface Science, 120 (1987) 263-271.

Chapter 5: Interfacial interactions of rough ellipsoidal particles with random surface asperities

5.1 Abstract

Currently, information on the fundamental interaction of ellipsoidal particles with rough topography is limited. In this work, a mathematical model was developed based on the extended Derjaguin-Landau-Verwey-Overbeek (XDLVO) theory and surface element integral (SEI) to simulate the total interaction energy created between ellipsoidal particles with rough surfaces, which were constructed by the modified two-variable Weierstrass-Mandelbrot (WM) function. The simulated results revealed that an increase in the fractal roughness and relative fractal roughness of particle surface would increase the surface roughness of particles and weaken the total interaction energy between ellipsoidal particles. Compared with spherical shape particles, the ellipsoidal particles provided greater interaction energy because an ellipsoidal shape would generate a greater interaction area than a spherical shape between particles. Amplifying the aspect ratio diminished the interaction energy between particles but enlarging particles would strengthen the interaction energy. In addition, the orientation angle of ellipsoidal particles would affect their interaction.

Keywords: Interaction energy, randomly rough ellipsoidal particles, surface roughness, simulation, XDLVO

5.2 Introduction

Generally, nano- or macro-colloidal particles, e.g., bacteria, soil particles, and viruses have random shapes in nature [1]. Generally, the interaction of these substances controls the interaction energy between the substances in colloidal systems. For this reason, previous studies focused on understanding the interaction mechanisms of colloidal particles [2-4]. Spherical particles have received much attention in the past because they are suitable for simulating nanoparticles [5]. However, those studies may not accurately predict the interaction of particles with ellipsoidal shapes [3, 4]. The shape of particles was

114

proved to play an important role in controlling interaction energy [6]. Colloids with ellipsoidal shapes have broad applications in medical and manufacturing fields. Müller and coworkers reported that ellipsoidal particles are favorable for drug delivery in blood flow because the ellipsoidal particles displayed slower rotation dynamics in the blood [7]. The ellipsoidal particles may also provide benefits to manufacturing processes. For example, the α-Fe$_2$O$_3$ ellipsoids displayed high stable cyclic performance and high specific capacity in lithium-ion battery applications [8]. Therefore, it is important to understand how various shapes of ellipsoids interact in colloidal systems as ellipsoidal particles have different geometrical properties.

Recently, the numerical approach provided prospects for exploring the mechanism of colloidal particle interaction. The most common method for predicting particle-particle interaction is the Derjaguin approximation (DA) based on the classical Derjaguin-Landau-Verwey-Overbeek (DLVO) or extend DLVO (XDLVO) theory [9, 10]. The predicted interaction energy between colloidal particles can serve as an indicator for evaluating the dispersion stability of the colloidal systems and provide a theoretical understanding of various colloidal phenomena including particle coagulation [11] deposition [12], and transportation [13]. Significant progress has been made in simulating the interaction energy for simple geometrical shapes, such as cylinders, flat planner surfaces, and spherical spheres [14, 15]. Although great efforts have been made to demonstrate that the particle shape has significant impact on particle retention in suspensions [16], and deposition [5] on surfaces, the previous work only considered the particle-flat interaction scenario. However, the interaction mechanism of ellipsoidal particles in a suspension system has not been studied in detail. Therefore, the main objective of this work was to establish a numerical model to simulate ellipsoidal particle interactions based on the XDLVO theory and to explore the fundamentals associated with the impact of the shape of the particles on their interaction behavior.

Moreover, the surface properties of particles impact their interaction significantly. For example, the asperities on the surface of natural products would significantly change the properties of the surface, e.g., hydrophobicity [17, 18]. The surface roughness could also impact the heat transport across the solid-solid interface, for example, VO$_2$ microbeam on Si substrate (VO$_2$/Si) [19]. In addition, ellipsoidal particle with a rough surface could be found in nature, such as ZnO [20], and trilayer hematite/silica/poly(divinylbenzene) hybrid particles [21].

However, the previous investigations mainly focused on the interaction energy of smooth surfaces [22, 23]. For naturally made rough surfaces, the small-scale roughness owns the repeatability of geometry, and the profile of the rough surface mostly follows the power law [24-26]. In this context, the surface roughness of spherical particles with uniform shapes of asperities was reported to impact their interactions significantly [27-29]. Therefore, it is crucial to consider the surface roughness in the simulation of ellipsoidal particles. However, no modeling study has explored rough ellipsoid interactions yet. To achieve a rough surface with defined morphologies, a modified two-variable Weierstrass-Mandelbrot (WM) function involving the transformation of fractal geometry theory can be considered, which will generate a rough surface with randomly located asperities [30]. Previous studies have shown that the fractal features of a rough surface with randomly located asperities can be properly predicted by the fractal geometry theory, where the fractal dimension (D_f) and fractal roughness (o) have core roles in tailoring surface roughness [31-33]. Additionally, the past numerical work related to the rough surface did not consider the ellipsoidal shape effects on particle interactions [30, 34, 35], and the work related to the ellipsoidal particles did not involve the impacts of surface morphology on particle interfacial behaviors [5, 22]. Our previous work only considered the spherical particle interaction which ignored the shape factors of natural particles (Lu and Fatehi, 2022). This problem may underestimate the real interaction energy of particles in colloidal systems as they may have ellipsoidal shapes. Additionally, to the best of our knowledge, there has been no specific work related to the simulation of rough ellipsoidal particle interactions. Therefore, the novelty of the present work was the investigation of the impacts of rough surface morphology on particle interaction for ellipsoidal particles, which could further improve the accuracy of the predictions of the interaction of rough ellipsoidal particles in colloidal systems.

This study aims to construct a model to simulate the interaction of rough ellipsoidal particles with randomly located asperities and analyze the effects of particle size, particle shape, and roughness on the interaction energy developed between rough ellipsoids. The SEI strategy and a modified two-variable WM function were applied to quantify the total interaction energy and construct the rough surface of ellipsoids, respectively. For the first time, the mechanisms of rough ellipsoidal particle interaction were explored based on the XDLVO theory, which was the primary novelty of this work.

5.3 Research methods

5.3.1 Developing equations for the interaction of particles following XDLVO theory

The XDLVO theory correlates the total interaction energy between colloidal particles (Equation 5.1) with Lifshitz-Vander Waals (LW), Lewis acid-base (AB), and electrostatic double layer (EL) interaction energies [36]. The specific energy (i.e., energy per unit area) of interactions ($\Delta G^{LW}(h)$, $\Delta G^{AB}(h)$ and $\Delta G^{EL}(h)$) between two rough surfaces could be expressed as (Equations 5.2 to 5.4) [37]. The past studies demonstrated that the Born repulsion in the total interaction energy profile decayed steeply in a very short range (about 0.136 nm from the origin) [38, 39]. However, the minimum interaction distance in the present model is 0.158 nm to prevent overlapping, therefore, the Born repulsion was not included in our simulation process.

$$\Delta G^{Total}(h) = \Delta G^{LW}(h) + \Delta G^{AB}(h) + \Delta G^{EL}(h) \tag{5.1}$$

$$\Delta G^{LW}(h) = -\frac{A_H}{12\pi h^2} = \Delta G_{h_0}^{LW} \frac{h_0^2}{h^2} \tag{5.2}$$

$$\Delta G^{AB}(h) = \Delta G_{h_0}^{AB} \exp\left(\frac{h_0 - h}{\lambda}\right) \tag{5.3}$$

$$\Delta G^{EL}(h) = \varepsilon_0 \varepsilon_r \kappa \xi_1 \xi_2 \left(\frac{\xi_1^2 + \xi_2^2}{2\xi_1 \xi_2}(1 - coth\kappa h) + \frac{1}{sinh\kappa h}\right) \tag{5.4}$$

where ellipsoid 1 and ellipsoid 2 were labeled with subscripts 1 and 2, respectively, h_0 described the minimum equilibrium cut-off distance, which is assumed to be 0.158 nm in this study [37]. Based on a previous study, it is assumed that two surfaces can approach each other with a minimum separation distance (0.158 nm)[40], which is the shortest distance to prevent overlapping. Therefore, the present work assumed that it always had a minimum separation distance (0.158 nm) between two peaks of asperities of approached particles even with the various asperity heights (no overlap). In addition, κ^{-1}, ε, and ζ are the double-layer thickness, the permittivity of the medium, and zeta potential, respectively; λ represents the correlation length of molecules in a liquid medium, which is selected as 0.6 nm [27]. In these equations, ε is usually expressed as the product of the permittivity of a vacuum (ε_0= 8.854 × 10^{-12} C^2/J·m) and the dielectric constant of the medium ε_r, which is 80 for water at 20°C [41].

The surface tensions are expressed as the sum of an apolar (Lifshitz–van der Waals) component (γ^{LW}) and a polar (acid-base) component (γ^{AB}) [36]. Also, γ^{AB} can be separated into an electron-donating component (γ^-) and an electron-accepting component (γ^+) [42]. According to these parameters, the ΔG^{LW} and ΔG^{AB} can be calculated following Equations 5.5 and 5.6:

$$\Delta G_{h_0}^{LW} = -2(\sqrt{\gamma_1^{LW}} - \sqrt{\gamma_w^{LW}})(\sqrt{\gamma_2^{LW}} - \sqrt{\gamma_w^{LW}}) \tag{5.5}$$

$$\Delta G_{h_0}^{AB} = 2\left[\sqrt{\gamma_w^+}(\sqrt{\gamma_1^-} + \sqrt{\gamma_2^-} - \sqrt{\gamma_w^-}) + \sqrt{\gamma_w^-}\left(\sqrt{\gamma_1^+} + \sqrt{\gamma_2^+} - \sqrt{\gamma_w^+}\right) - \sqrt{\gamma_1^- \gamma_2^+} - \sqrt{\gamma_1^+ \gamma_2^-}\right] \tag{5.6}$$

where subscript 1, w, and 2 represent ellipsoid 1, water, and ellipsoid 2, respectively.

The surface properties of particles can be obtained by solving a set of three Young equations (Equation 5.7) [36]. The values of the surface tensions for liquid (γ_l^{LW}, γ_l^+, and γ_l^-) and contact angles (θ) should be measured for at least three different liquids (e.g., water, glycerol and, diiodomethane) to determine the surface tensions of the solid (γ_1^{LW}, γ_1^+, and γ_1^-).

$$\frac{(1+cos\theta)}{2}\gamma_l^{Tol} = \sqrt{\gamma_l^{LW}}\sqrt{\gamma_1^{LW}} + \sqrt{\gamma_l^{-1}}\sqrt{\gamma_1^+} + \sqrt{\gamma_l^+}\sqrt{\gamma_1^{-1}} \tag{5.7}$$

The present model focused on investigating the stability of ellipsoidal particles in a water-based system. This may represent colloidal particles, including clay minerals with ellipsoidal shapes, in water [43]. Therefore, the constant solution (water) and solid phase (assumed particle) were considered in the calculation process. The above-mentioned parameters were collected from previous reports and summarized in Table 8.3.1 in the supplementary material [39, 44]. The values of contact angle and zeta potential were selected from a previous modeling study [45], which were used for calculating the surface tension of modeled particles. The details were shown in Table 8.3.2.

5.3.2 Developing three-dimensional rough ellipsoidal particles

The simulation process applied two coordinate systems. One is a body-fixed coordinate used to solve the internal geometric characteristics of ellipsoidal particles. Another is a space-fixed coordinate system for solving the orientation of ellipsoidal particle 1 relative to the fixed ellipsoidal particle 2. The equation of an ellipsoid at a Cartesian coordinate system is expressed according to equation 5.8:

$$\frac{x^2}{a^2} + \frac{y^2}{b^2} + \frac{z^2}{c^2} = 1 \tag{5.8}$$

Where a, b, and c are the semi-axes of the ellipsoid along the x, y, and z axes, respectively.

To simplify the calculation, the cartesian coordinates (χ, y, z) were replaced by spherical coordinates (r, θ, φ), and the relationship between an ellipsoidal coordinate and a Cartesian coordinate can be expressed as follows (Equation 5.9):

$$r^2 = \left[\frac{sin^2\theta cos^2\varphi}{a^2} + \frac{sin^2\theta sin^2\varphi}{b^2} + \frac{cos^2\theta}{c^2}\right]^{-1} \tag{5.9}$$

The surface morphology can represent the surface roughness of the colloidal particles. To stimulate the surface roughness, one object with a rough surface should be built. In this case, a mathematical model

applied to a modified two-variable Weierstrass-Mandelbrot (WM) function is often used for constructing the rough surface of particles [46-48]. The rough surface and radius of rough ellipsoids can be modeled following Equations 5.10 and 5.11 [14].

$$\Delta r = L \left(\frac{o}{L}\right)^{D_f-2} \left(\frac{ln\eta}{M}\right)^{\frac{1}{2}} \sum_{m=1}^{M} \sum_{n=0}^{n_{max}} \eta^{(D_f-3)n} \times (\cos\phi_{m,nmax+1} - \cos(\frac{2\pi\eta^n r \sin\theta}{L} \times \cos\left(\varphi - \frac{\pi m}{M}\right)$$
$$+\phi_{m,nmax+1})) \tag{5.10}$$

$$R^2 = \left[\frac{sin^2\theta cos^2\varphi}{(a+\Delta r)^2} + \frac{sin^2\theta sin^2\varphi}{(b+\Delta r)^2} + \frac{cos^2\theta}{(c+\Delta r)^2}\right]^{-1} \tag{5.11}$$

Where R and r are the radii of a modeled rough particle and an elementary particle (i.e., smooth surface particle), respectively; L is the sample length; η is the parameter that represents the frequency density in the profile; M is the number of superposed ridges that contributes to constructing random surface; $\phi_{m,nmax+1}$ is used for describing a random phase; n_{max} represents the highest frequency where $n_{max} = int((log\ L/Vs)/log\ \eta$ [49], and Vs is the cutoff frequency. In the present modeling work, D_f represents the texture of constructed rough surface, which controlled the contour structure complexity of surface [24], o is an amplitude coefficient that affects the asperity height of generated surface, which could also control the average roughness of the particle surface [50]. The numerical definition of D_f and o were shown in supplementary material (Equations A.3.1-A.3.3).

Table 8.3.3 lists the parameters involved in this modeling study to construct a particle with random surface morphology. The values of L, o, and η were collected from the literature [51]. Hong and coworkers stated that the value of M should be above 3 to make the simulated surface closer to reality [52]. Thus, M was set as 8 in this modeling study following the value stated in a previous study [45] and the n_{max} was calculated to be 5 in the current study.

The series of $\phi_{m,n}$ was generated via a random number generator within the scale of $[0, 2\pi]$ to avoid the coincidences of different frequencies at any point on the rough surface according to Equation 5.12:

$$[\phi_{M\times(n_{max}+1)}] = \begin{bmatrix} 2.2681 & 3.4148 & 5.1977 & 5.3991 & 3.9171 & 3.2029 \\ 3.7282 & 0.3488 & 3.0793 & 5.0153 & 5.0239 & 1.1093 \\ 4.0971 & 0.0225 & 0.9963 & 5.6497 & 1.8793 & 4.6751 \\ 4.4089 & 0.3153 & 1.5343 & 3.4391 & 4.3598 & 4.1709 \\ 1.2114 & 5.3985 & 4.3828 & 4.6273 & 3.9585 & 1.3544 \\ 5.1218 & 5.3310 & 0.5640 & 4.7376 & 5.1990 & 3.5070 \\ 4.9327 & 5.4101 & 0.3967 & 5.9858 & 2.4364 & 0.1511 \\ 2.8786 & 1.3616 & 0.3829 & 0.2327 & 4.0411 & 3.7663 \end{bmatrix} \tag{5.12}$$

5.3.3 Developing a model to quantify the interaction energy between two rough ellipsoids

Generally, the DLVO theory is used along with Surface Element Integration (SEI) to consider not only the shape but also the orientation angle of the particles relative to the surface [35]. The SEI method is suitable for studying the effects of shape, orientation, and aspect ratio on the interaction of particles with surfaces [22]. According to the SEI method, the total interaction energy of two particles ($U(h)$) can be calculated by considering the interaction energy per unit area ($\Delta G(h)$) of particles and projected surface area of the rough particles according to Equations 5.13 and 5.14 [14, 53].

$$U(h) = \int_0^{2\pi} \int_0^{\frac{\pi}{2}} \Delta G(h) dA \tag{5.13}$$

$$dA = \vec{n}\vec{k}dS \tag{5.14}$$

The differential area (dS) can be determined according to Equation 5.15 [14].

$$dS = R_i^2 \sin\theta_i \, d\theta d\varphi \tag{5.15}$$

The tangent vectors of the θ and φ curves at any point of the interaction area are expressed as $\frac{d\vec{R}}{d\theta}$ and $\frac{d\vec{R}}{d\varphi}$, respectively. Therefore, the unit normal at point P can be expressed as follows [14]:

$$\vec{n} = \frac{\frac{d\vec{R}}{d\theta} \times \frac{d\vec{R}}{d\varphi}}{\left|\frac{d\vec{R}}{d\theta} \times \frac{d\vec{R}}{d\varphi}\right|} \tag{5.16}$$

Where the $\frac{d\vec{R}}{d\theta}$ and $\frac{d\vec{R}}{d\varphi}$ can be calculated according to Equations 5.17 and 5.18:

$$\frac{d\vec{R}}{d\theta} = \vec{i} \times \frac{\partial(R\sin\theta\cos\varphi)}{\partial\theta} + \vec{j} \times \frac{\partial(R\sin\theta\cos\varphi)}{\partial\theta} + \vec{k} \times \frac{\partial(R\cos\theta)}{\partial\theta} \tag{5.17}$$

$$\frac{d\vec{R}}{d\varphi} = \vec{i} \times \frac{\partial(R\sin\theta\cos\varphi)}{\partial\varphi} + \vec{j} \times \frac{\partial(R\sin\theta\cos\varphi)}{\partial\varphi} + \vec{k} \times \frac{\partial(R\cos\theta)}{\partial\varphi} \tag{5.18}$$

More details of calculations of vectors were available in the supplementary material.

It should be noted that the unit normal is usually defined within a body-fixed coordinate system of the ellipsoidal particle. However, if the simulation process needs to consider the orientation impacts on the particle interactions, a space-fixed coordinate system should be established to generate the new unit normal. Therefore, the orientation of the ellipsoid particles can be solved by considering the rotation of the fixed coordinates relative to the fixed space coordinate system (X, Y, Z), which associates with two sets of coordinates [22]:

$$X = l_{11}x + l_{12}y + l_{13}z \tag{5.19}$$

$$Y = l_{21}x + l_{22}y + l_{23}z \tag{5.20}$$

$$Z = l_{31}x + l_{32}y + l_{33}z \tag{5.21}$$

Where l_{ij} $(i, j = 1,2,3)$ represents the directional cosine of the X, Y, and Z axes relative to the x, y, and z axes, respectively. The expressions of directional cosines were collected from previous work [54].

As with any unit normal can be expressed in body-fixed coordinate as:

$$\vec{n} = \overrightarrow{n_1 i} + \overrightarrow{n_2 j} + \overrightarrow{n_3 k} \tag{5.22}$$

Then, the unit normal should be transformed to the expression of the space fixed coordinates according to Equation 5.23 [22]:

$$\vec{n} = (\overrightarrow{n_1}l_{11} + \overrightarrow{n_2}l_{21} + \overrightarrow{n_3}l_{31})\bar{\vec{i}} + (\overrightarrow{n_1}l_{12} + \overrightarrow{n_2}l_{22} + \overrightarrow{n_3}l_{32})\bar{\vec{j}} + (\overrightarrow{n_1}l_{13} + \overrightarrow{n_2}l_{23} + \overrightarrow{n_3}l_{33})\bar{\vec{k}} \tag{5.23}$$

Therefore, based on Equations 5.14, 5.15, and 5.23, Equation 5.13 could be transformed as

$$U(h) = \int_0^{2\pi} \int_0^{2/\pi} \Delta G(h)\vec{n}\vec{k}R_i^2 \sin\theta_i \, d\theta d\varphi \tag{5.24}$$

Figure 5.1 shows the scenario for the interaction of two rough particles of different sizes. In this particular case, the spatial relationship between two particles can be described as shown in Equation 5.25, which was also used to connect two angle coordinates in two particles[55].

$$\theta_2 = arc\sin\left[\left(\frac{R_1}{R_2}\right)\sin\theta_1\right] \tag{5.25}$$

The separation between rough ellipsoidal particles with randomly oriented asperities can be given by Equation 5.26:

$$h = D + R_{a1} + R_{a2} - R_1 \times \cos\theta_1 - R_2 \times \cos\theta_2 + c_1 + c_2 \tag{5.26}$$

Where c_1 and c_2 refer to the semi-axis of ellipsoids 1 and 2 along with Z-direction [22], R_1 and R_2 refer to equivalent radii of modelled rough ellipsoids 1 and 2, R_{a1} and R_{a2} represent the root-mean-square roughness in the interaction area of ellipsoids 1 and 2. Based on the recorded data, the R_{ai} in Equation 5.26 could be calculated following Equation 5.27:

$$R_{ai} = \sqrt{\frac{\sum_{i=1}^{N}\Delta r_i^2}{N}} \qquad (i = 1,2) \tag{5.27}$$

The series of asperity height data (Δr_i) in the process of the generation of random particle surface was recorded by MATLAB 2020a (9.8.0.1323502).
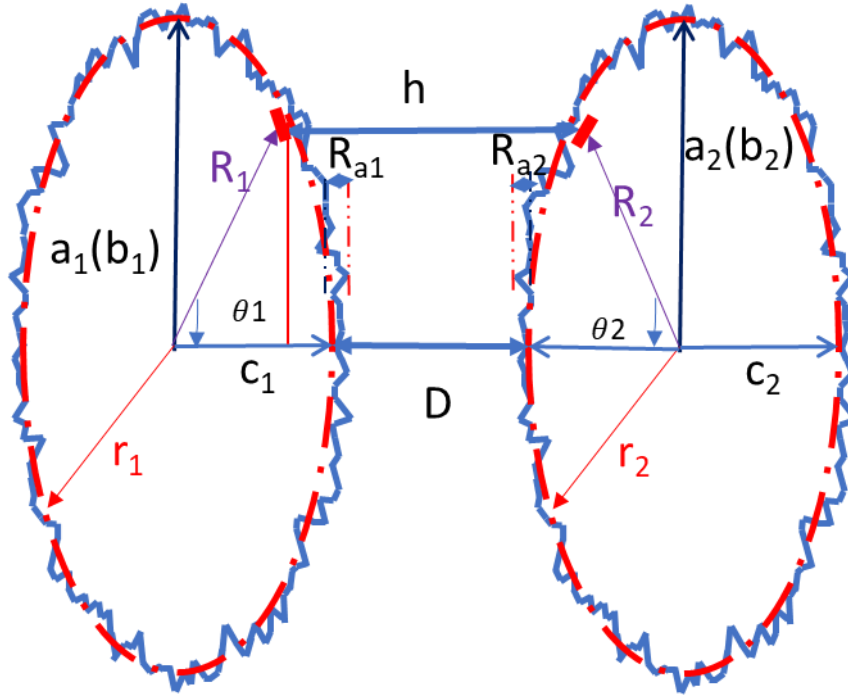
Figure 5.1. Parameters involved in the interaction of two rough ellipsoids

5.3.4 Fractal dimension impact

The fractal dimension can directly control the topology of the rough surface, which may impact the roughness of the target surface [56]. Therefore, the mechanism behind the influence of surface morphology on particle interaction could be explored by investigating the impact of the fractal dimension on interaction energy between ellipsoidal particles (Equation 5.10) [50, 57]. Following Equation 5.10, the scale of the fractal dimension should be between 2 and 3 to correctly simulate the rough spherical surface [49, 58]. The initial value of the fractal dimension of the ellipsoidal particle was set as 2.03 in the present study, and the testing range was 2.03-2.93 ($o_1= o_2= 0.1$ nm and $a = b = 1000$ nm, $c = 500$ nm). Moreover, to study the effect of relative fractal dimension on the particle interactions, the parameter of particle 1 was fixed ($o_1= 0.1$ nm, $r_1=1000$ nm, $D_{f1}= 2.83$) to exhibit the low degree of rough surface, and only the fractal dimension of particle 2 was changed from 2.03 to 2.63. Following Equations 5.24 and 5.26, the effects of fractal dimension on the total interaction energy were predicted.

5.3.5 Fractal roughness impact

Using Equation 5.10, the fractal roughness (o_i) represents the amplitude coefficient, which can impact the magnitude of the contour of asperities on the surface [50]. The fractal values of o_i changed from 0.1 nm to 10 nm, which was collected from the literature [51]. In this set of experiment, the other parameters were maintained constant ($o_1=o_2= 0.1$ nm and $a = b =1000$ nm, $c =500$ nm). To study the impact of

the relative fractal roughness on particle interactions, the parameter of particle 1 was fixed (o_1= 0.1nm, $a_1 = b_1$ =1000 nm, D_{f1}= 2.03), and only the value of fractal roughness on particle 2 was changed from 0.5 nm to 10 nm (r_2=1000nm, D_{f2}= 2.03). Following Equations 5.24 and 5.26, the effects of fractal roughness on the total interaction energy were predicted.

5.3.6 Shape impact

In this set of analyses, the effect of particle shape on the interaction energy between particles could be simulated following Equation 5.11. The parameters of particle 1 were kept constant ($a_1 = b_1$ =1000 nm, c_1 =500 nm), while the shape of particle 2 was changed from a sphere ($a_2 = b_2 = c_2 = 1000$ nm) to an ellipsoidal pancake with the various value of c_2 from 50 nm to 1000 nm (a_2 =1000 nm, b_2 =1000 nm) to investigate how the shape of a spherical particle changed from a spherical particle to an ellipsoidal pancake-like particle would impact its interaction with another particle. According to a previous study, a rougher surface morphology could be constructed with a lower value of D_{fi} [56]. Therefore, $D_{fi} = 2.03$ was selected as the constant value to construct the roughest surface morphology in this study when investigating the effects of shape, aspect ratio, particle size and orientation of particles on the particle interaction. It should be noted that D_{fi} and o_i were independent parameters to construct the surface roughness according to Equation 5.10. To create the same roughness conditions in this investigation, these two parameters were kept constant to obtain the same asperity density, asperity height, and surface texture even though the colloidal particle aspect ratio and orientation changed.

5.3.7 Aspect ratio impact

The impact of aspect ratio (a/c) of ellipsoid on the total interaction energy between rough ellipsoids was investigated based on Equation 5.11, while other parameters were considered constant ($D_{fi} = 2.03, o_i = 0.1\ nm$). To simplify the simulation process, we assumed that a = b in the ellipsoid particle and a/c ranged from 0.05 to 20 according to the previous literature [59]. Prolate-prolate and oblate-oblate ellipsoidal particle interaction scenarios were considered based on the different shapes of rough ellipsoidal particles (Figure A.3.1). Similarly, to create the same surface roughness conditions, the D_{fi} and o_i were necessary to keep constant in this section.

5.3.8 Particle size impact

In this set of analyses, the value of a (or b) ranged from 10 to 1000 nm and the aspect ratio of a/c was maintained constant at 2 to construct the typical ellipsoidal shape particle, and other parameters were

considered constant ($D_{fi} = 2.03, o_i = 0.1\ nm$) in Equation 5.11. The relative particle size effect on particle interaction was also investigated in this study. The size of particle 1 was changed from $a_1 = b_1 = 10$ nm, and $c_1 = 5$ nm to $a_1 = b_1 = 500$ nm, and $c_1 = 250$ nm, while the size of particle 2 was kept constant ($a_2 = b_2 = 1000$ nm, $c_2 = 500$ nm).

5.3.9 Orientation impact

The relative orientation angle (0 and $\frac{\pi}{2}$) was investigated in the present modeling study according to equations 5.34 and 5.35, where particle 2 was kept constant and particle 1 was rotated with 0 or $\frac{\pi}{2}$ of orientation angle.

When the fractal parameters were $D_{fi} = 2.03, o_i = 0.1\ nm$, the orientation-averaged interaction energy of rough particles ($\langle U(h)\rangle_{\Pi}$) at a given distance ($h$) could be calculated by using the Boltzmann statistics according to Equation 5.28 [60-62]:

$$\langle U(h)\rangle_{\Pi} = \frac{\int U_{\Pi}(h,\Omega) e^{(-\beta U_{\Pi}(h,\Omega))} d\Omega}{\int e^{(-\beta U_{\Pi}(h,\Omega))} d\Omega} \tag{5.28}$$

Where Π denotes LW, EL, or AB (i.e., three aforementioned interactions in the XDLVO theory), U_{Π} represents the interaction between rough ellipsoidal particles, located by the separation distance h and the space orientation Ω and $\beta = (kT)^{-1}$.

The orientation-averaged configuration could be expressed according to Equation 5.29 [63]:

$$d\Omega = sin\omega_1 sin\omega_2 d\omega_1 d\omega_2 d\psi_1 d\psi_2 \tag{5.29}$$

Where the ω_1 and ω_2 are the orientation angles of two particles in the θ direction, ψ_1 and ψ_2 were the orientation angles of rough particles in φ direction.

5.3.10 Interaction energy comparison between rough and smooth particles

In this set of investigations, two groups of rough ellipsoidal particles were constructed to own the roughest surface morphology where $D_{fi} = 2.03$ and $o_i = 10\ nm$ ($a = b = 1000$nm, $c = 500$ nm). The ellipsoidal particles owned smooth surfaces were also constructed where $D_{fi} = 2.93$ ($a_1 = b_1 = 1000$nm, $c_1 = 500$ nm) because the surface roughness would decrease with increasing the value of D_{fi} [56].

5.4 Results and discussion

5.4.1 Fractal dimension effect

Previously, the DA method was used for simulating the interaction of two smooth ellipsoidal particles [64]. However, the previous work did not consider the effect of surface roughness on the interaction, which may not predict the interaction of particles found in nature very well. Therefore, particles with rough surfaces and roundly located asperities were generated following Equation 5.10 in the present study to explore the effect of surface roughness on the interaction of ellipsoidal particles. The fractal dimension (D_f) controls the asperity size and asperity number simultaneously and expresses the complexity of the surface morphology of solid particles [50]. The results and discussion were shown in the supplementary material. It could conclude that the total interaction energy increased with increasing the fractal dimension of modeled particles.

5.4.2 Fractal roughness effects

Fractal roughness (o) is an amplitude coefficient that can affect the size of the asperity profile [49]. The effect of fractal roughness on the particle interaction was available in the supplementary material. The main conclusion is that the total interaction energy decreased with increasing the value of fractal roughness.

5.4.3 Shape effects

Previous models investigated the spherical particle-particle interaction and spherical particle-flat surface interactions [3, 65]. In our modeling study, the shape of particles could be controlled by the value of c in Equation 5.11. The investigation of the shape effect on the particle interaction via controlling the value of c could be regarded as a strategy to fill the previous research gap for results on the interaction of ellipsoidal particles. The predicted interaction energies between particle 1 and particle 2 with various shapes were shown in Figure 5.2. In this figure, parameter c_2 was changed from c_2 of 1000 nm to 50 nm, which makes the variation from a spherical shape to an ellipsoidal pancake-like shape. It could be seen that the interaction energy between two particles was reduced by decreasing the value of c_2. Therefore, the simulation and predictions of various ellipsoidal shape effects on particle interaction could be considered as a bridge to connect the previous spherical particle-particle model and particle-flat surface model. As shown in Figure 5.2, with an increase in c_2, the total interaction energy

125

was elevated indicating that the particle with an ellipsoidal shape has more interaction strength than spherical shape particles do. Salerno and coworkers reported that the rod-shaped smooth colloids had a stronger retention ability on a surface compared with spherical ones [66]. Similar predictions were found in our model considering the different shapes of rough ellipsoids (from a spherical shape to an ellipsoidal pancake shape by reducing c_2). Therefore, the results confirmed that the rough ellipsoids provided better adhesion affinity compared to spherical particles.
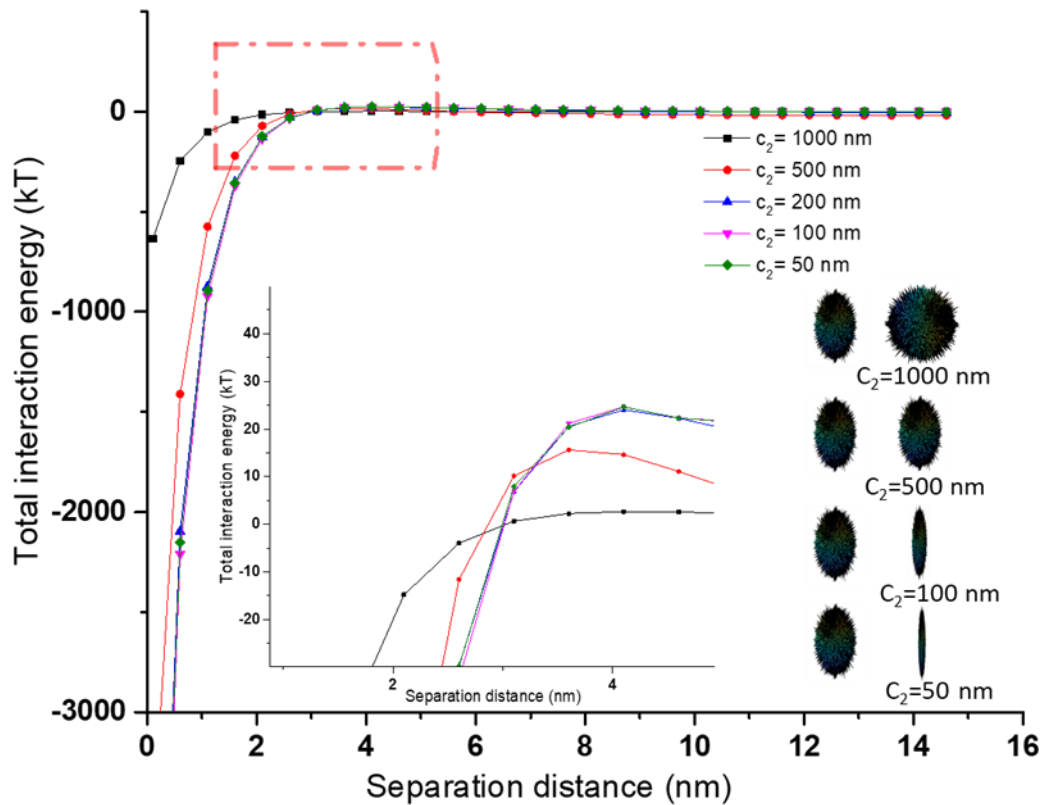
Figure 5.2 The interaction energy of particles when c2 was changed from 1000 to 50 nm. ($D_{f1} = D_{f2} = 2.03, o_1 = o_2 = 0.1$ nm, $a_1 = b_1 = 1000$ nm, $c_1 = 500$ nm, $a_2 = b_2 = 1000$ nm)

5.4.4 Aspect ratio effect

The effect of aspect ratio ($\frac{c}{a}$) of rough ellipsoid on their interaction is shown in Figure 5.3. The simulation results depicted (Figure 5.3a) that increasing the aspect ratio from 1 to 10 decreased the interaction energy developed between oblate particles ($a = b < c$). In the prolate particle ($a = b > c$) (Figure 5.3b), when the aspect ratio ($\frac{c}{a}$) increased from 0.1 to 1, and the interaction energy dropped. These simulation results follow the expectation because the aspect ratio significantly controls the

126

interacting area between ellipsoidal particles [27, 55]. The term dS in Equation 5.15 represents the differential area between two rough ellipsoidal particles and is controlled by R. According to Equation 5.11, the variation in a or c can significantly change R. Therefore, the aspect ratio plays an essential part in the interaction energy. Gomez-Flores and coworkers also reported that with elevating the aspect ratio, the interaction of a cylinder and flat surface decreased, which was determined following the DLVO theory [67]. Our results considering XDLVO theory complemented these findings on the interaction of rough ellipsoidal particles and illustrated that controlling the aspect ratio of ellipsoidal particles could be a tool to improve the colloidal particle interaction with the application, for example, in the adsorption of proteins on nanoparticles [68]. As seen in Figure 5.3, the increased aspect ratio would decrease the repulsive energy, destabilizing the particles as they could overcome the repulsive potential energy barrier development between them more effectively, which might have applications in drug delivery, for instance [69].

In addition, the simulation results exhibited an interesting phenomenon in that the prolate particle interaction generated much stronger interaction energy than the oblate particle interaction did. This phenomenon is reasonable because prolate-prolate interaction would provide a larger interaction area than oblate-oblate interaction. Therefore, the prolate-prolate interaction scenario would provide a stronger repulsive potential energy barrier for stabilizing the suspension colloidal system because more repulsive energy could be generated to prevent particle aggregation. It should be noted that when $\frac{c}{a} = 1$, the particle becomes a sphere, and its interaction would be developed between prolate and oblate particle. Liu and coworkers simulated the interaction of rod-like particles and spherical particles based on the DLVO theory and concluded that the highest repulsive energy barrier could be obtained by the prolate rod-like particle [70]. The predicted phenomenon could be verified by previous experimental works. Seymour and coworkers investigated carboxylate-modified fluorescent polystyrene particle deposition rate on a silica sensor and reported that the spherical shape particle obtained a larger deposition rate than rod-like particle did [71]. Gomez-Flores and coworkers used a different fabrication method to prepare a spherical particle and bullet-like silica particle and compared the deposition rate of these two particles on a flat surface and reported that the deposition rate of a spherical particle was higher than the bullet-like particle [5]. In our current study, by considering XDLVO theory and particle-particle interaction instead of particle-flat surface interaction, similar results were predicted. Our

predictions suggested that if the energy barrier decreased, the nanoparticles would slowly aggregate due to the reduced repulsive energy for separating particles. The previous experimental observations [5, 71] strongly supported the present modeling results that the prolate ellipsoidal particles in our model experienced higher repulsion energies in the suspension system, which greatly counterbalanced the attractive energies and decreased the particle deposition. Consequently, the model predicts that if two ellipsoidal particles have different interaction scenarios (e.g., prolate or oblate shape), the colloidal system tends to have different stability.
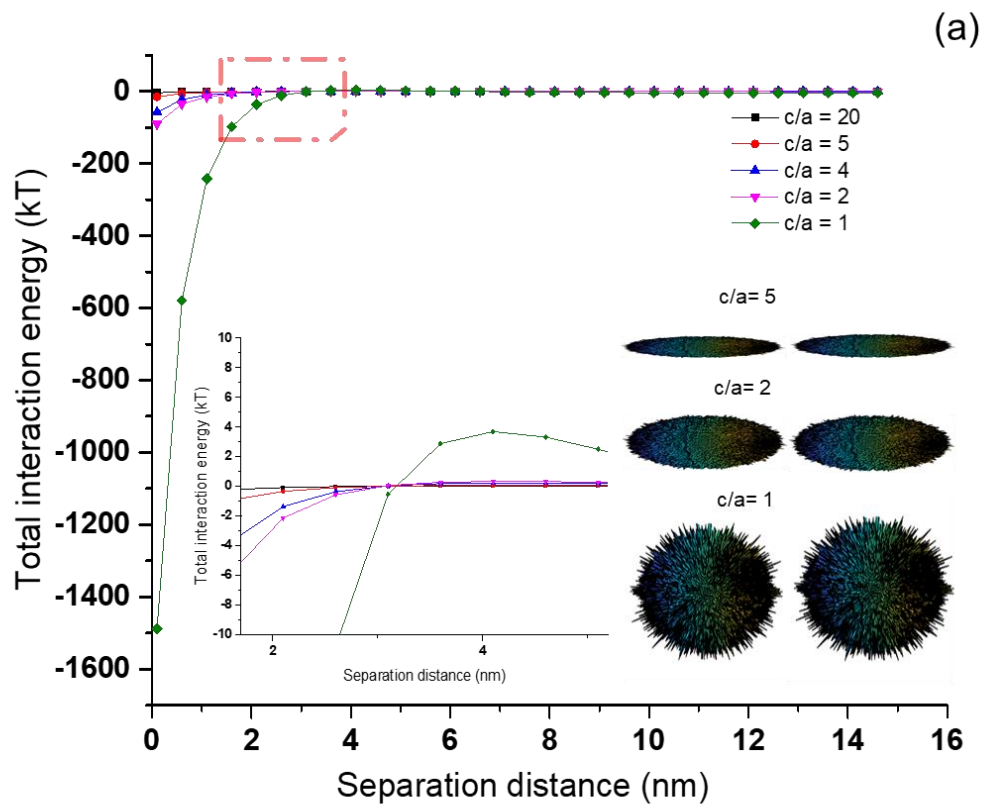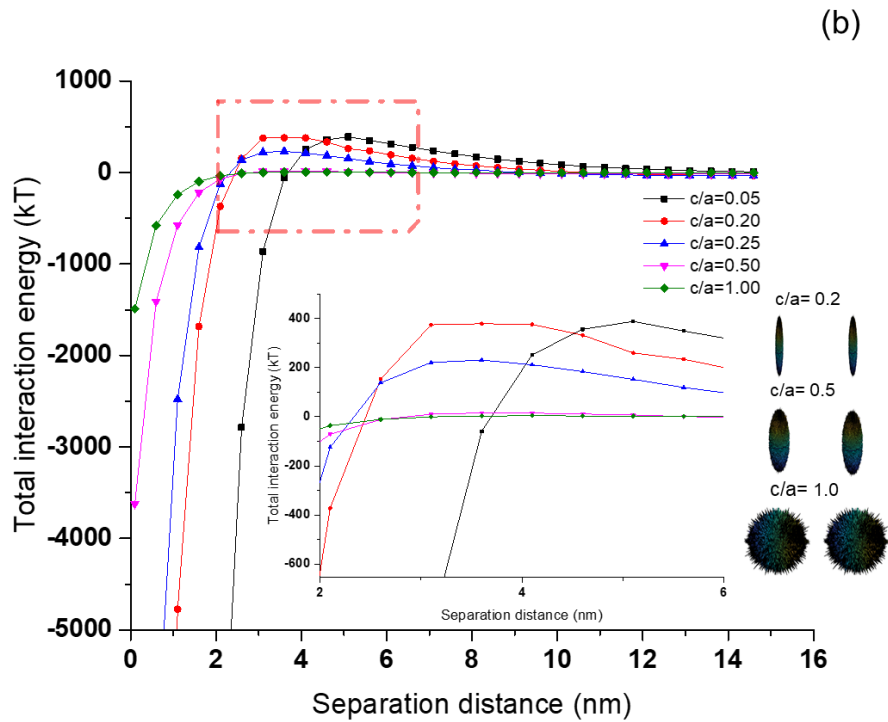
Figure 5.3 The aspect ratio effect on rough ellipsoidal particle interaction. (a) The interaction energy in an oblate-oblate scenario ($D_{f1} = D_{f2} = 2.03, o_1 = o_2 = 0.1\ nm, c = 1000\ nm$). (b) The interaction energy in a prolate-prolate scenario ($D_{f1} = D_{f2} = 2.03, o_1 = o_2 = 0.1\ nm, a = b = 1000\ nm$).

5.4.5 Particle size effect

The effect of particle size on particle interaction was shown in Figure 5.4. As Figure 5.4a shows, the interaction energy between two rough particles increased with enlarging the particles ($a = b =$10 nm, $c =$5 nm to $a = b =$1000 nm, $c = 500$ nm). The predicted results would be reasonable because the interaction area was expanded with largening the particle, and thus the interaction strength between the two particles was improved. Previous modeling works assumed the interacted particle always owned the spherical shape ($a = b = c$) and articulated that the particle size had a significant effect on the interaction of spherical shape particles [27, 55]. When the shape was changed to ellipsoid in this work, similar results were predicted.

The impact of the relative size of rough ellipsoids on their interaction is shown in Figure 5.4b. It could be illustrated that when particle 1 was enlarged, the interaction energy of particle-particle surfaces was strengthened. The main reason for this behavior is that the interaction area between two particles was

129

enlarged with increasing the size of the particle according to Equations 5.15 and 24. The energy profile could be an indicator for monitoring particle interfacial behavior, and the energy barrier larger than 5 kT would not cause aggregation [72]. Nevertheless, the repulsive energy barrier shown in Figure 5.4b is smaller than 5 kT, which suggests that the rough ellipsoidal particles would easily aggregate if two particles owned a significant size. The predicted particle size impacts may have applications, e.g., particle flotation [73], membrane fouling [4], and crystallization [74]. As the dispersion stability is in proportion to the repulsive energy barrier in the energy profile, the higher values of the repulsive energy barrier represent a more stable colloidal system. Therefore, the particle size could provide notable influences on the kinetic of particle transportation based on the magnitude of the repulsive energy barrier.
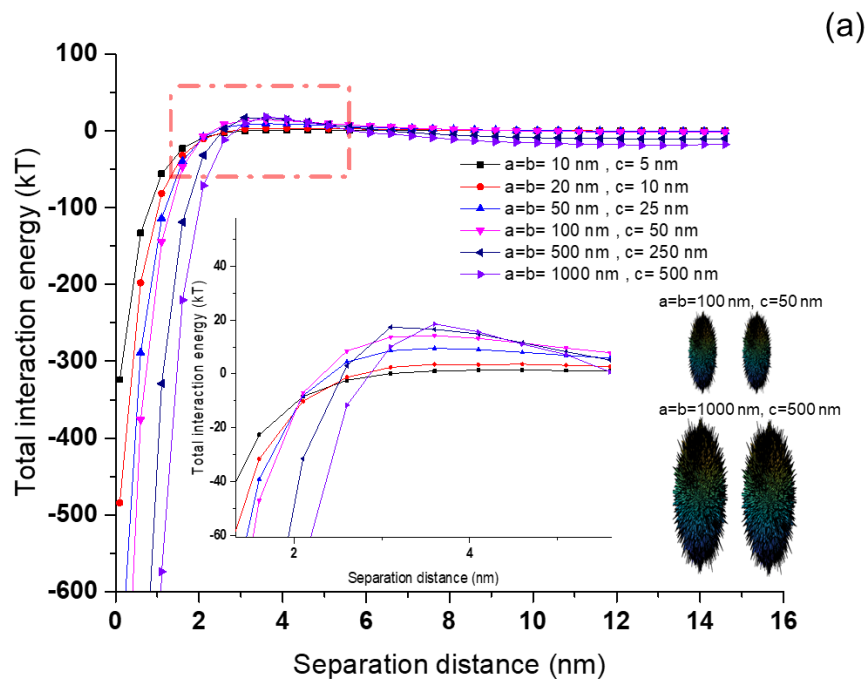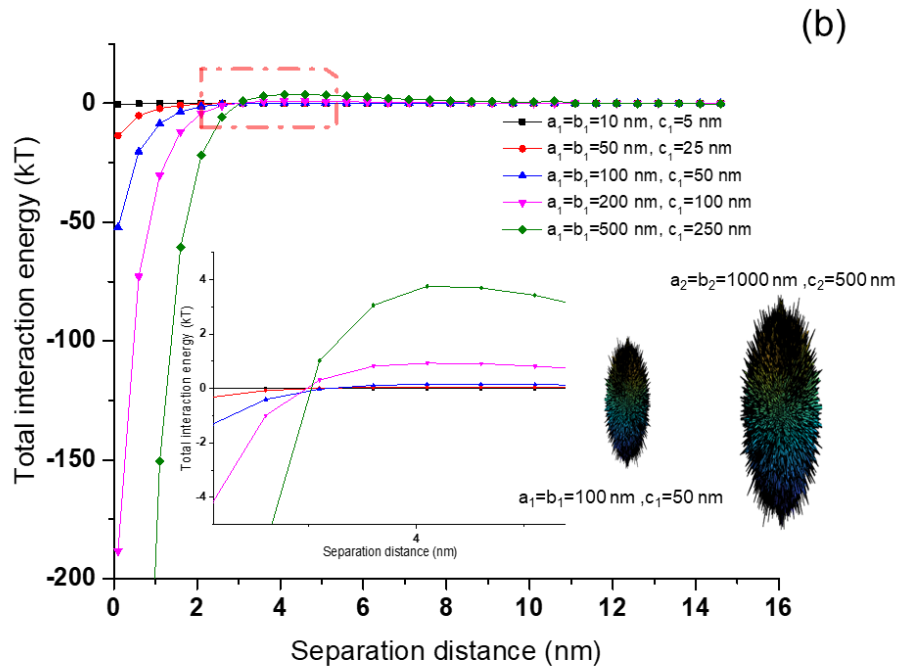
Figure 5.4 The effect of particle size on rough ellipsoidal particle interaction. (a) The effect of particle size on interaction energy ($D_{f1} = D_{f2} = 2.03, o_1 = o_2 = 0.1 \, nm$). (b) The effect of relative particle size on interaction energy ($D_{f1} = D_{f2} = 2.03, o_1 = o_2 = 0.1$ nm, $a_2 = b_2 = 1000$ nm, $c_2 = 500$ nm).

5.4.6 Orientation angle effects

The above-mentioned simulation results were made based on the assumption that the orientation angle of colloidal particles is zero for rough ellipsoidal particles. In reality, particles approach each other with random orientation angles in suspension systems. The previous literature suggested that the orientation angle had important effects on solid or hollow cylindrical particles because the particle rotation might change the separation distance between particles due to the depressions and protrusions of rough surface morphology [55, 67]. Nevertheless, the information on orientation angle effects on the interaction energy between two rough ellipsoidal particles was unavailable in the literature. Figure 5.5 shows the effects of relative orientation angle (0 and $\frac{\pi}{2}$) and averaged orientation angle (0 to $\frac{\pi}{2}$) of ellipsoidal particles on the interaction energy. The present model predicted that the total interaction energy decreased with increasing the orientation angle from 0 to $\frac{\pi}{2}$. With widening the orientation angle, the interaction area between two rough surfaces decreased, which reduced the interaction energy if the orientation angle ranged between 0 and $\frac{\pi}{2}$ [5]. A previous study reported that the total interaction energy

131

slightly decreased with increasing the rotation angle from 0 to $\frac{\pi}{2}$, which was developed between an isotropic planar surface and a single-walled carbon nanotube following DLVO theory [75]. Bhattacharjee and coworkers constructed a model to simulate a smooth ellipsoidal particle interacting with a smooth flat plate and concluded that when the particle interacted with the plate surface, the energy profile would encounter the repulsive barrier. In this case, the barrier would be larger when the orientation angle was 0 compared to when the orientation angle was $\frac{\pi}{2}$ [22]. Our results also suggested that the rough ellipsoidal particle provided a lower repulsive energy barrier when the orientation angle of the two particles was $\frac{\pi}{2}$, which would indicate that the rough ellipsoidal particle could easily overcome the energy barrier as they attach together. The orientation angle decreased the interaction area between two particles when the angle changed from 0 to $\frac{\pi}{2}$, which directly reduced the total interaction energy between particles and diminished the energy barrier. This finding may expand the particle modification methods to increase the efficiency of particle dispersion by the optimal angle for particle interaction, which could be realized by assigning the orientation angle among the particle in colloidal systems, for example, applying to low magnetic fields [76]. Bargozin and coworkers applied the rippled rough theory to construct rough spherical particles and investigated the effect of orientation angles on particle interaction [77]. Their findings suggest that the energy barrier dropped to its minimum value of 0.5 kT when the orientation angle increased from 0 to π [55]. In the case of our study, the energy barrier dropped to 5 kT, which was larger than Bargozin's work because we included the hydrophobic interaction of particles in the simulation process. As the present study considered different parameters (e.g., roughness and ellipsoidal shape) from the previous study [77], but similar results were obtained in both studies, it could be suggested that the particle orientation would significantly impact the interaction energy between particles (sphere or ellipsoid).
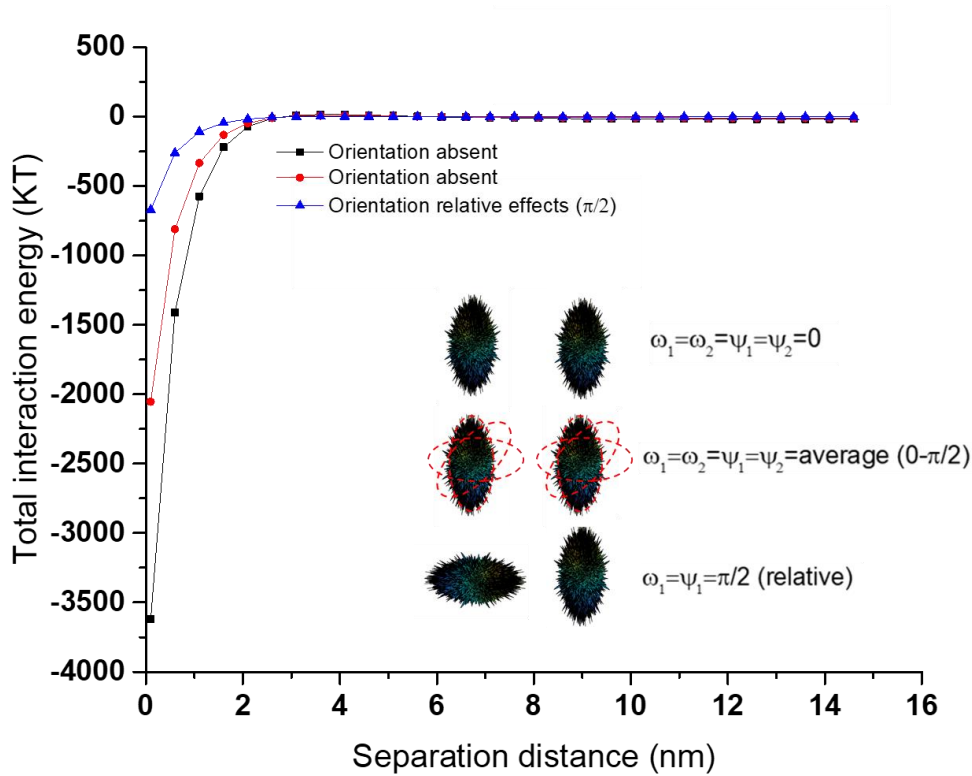
Figure 5.5 The effect of orientation angle on the interaction of randomly rough ellipsoidal particles $(a_1 = b_1 = a_2 = b_2 = 1000\ nm, c_1 = c_2 = 500\ nm,\ D_{f1} = D_{f2} = 2.03, o_1 = o_2 = 0.1)$.

5.4.7 The most effective parameter on particle interaction and model application

The constructing parameters of randomly rough ellipsoidal particles have significant effects on particle interaction. The particle shape (Figure 5.2) can play an important role in particle interaction [78]. Yekeler and coworkers also reported that the interaction force of particle surface decreased with increasing the elongation and flatness of particles [79]. However, the previous literature lacked information about the comparison between the effect of particle shape and surface roughness on particle interaction. The present study compared the effects of particle shape and surface roughness on the interaction energy of particles.

The aspect ratio was the most effective parameter in controlling interaction energy (Figure 5.3) because the aspect ratio directly controlled the interaction area (dS) between particles, which notably impacted the interaction energy (based on Equation 5.15). On the other hand, the fractal roughness provides the least effects on the particle interaction compared to other parameters shown in Figure A.3.3. Therefore, we could conclude that the shape of particles had more impact than surface morphology on particle interactions. Moreover, the predicted results of surface morphology effects on particle interaction could

provide a novel direction in material modification to acquire more efficient flocculation or dispersion. The main reason is that D_f and o significantly influences the total interaction energy between two rough ellipsoids by controlling surface roughness.

The impact of surface roughness on the interaction energy might facilitate surface coating applications. For example, to better design the coating surface and to improve the coating efficiency, the fractal dimension can guide and characterize the integrity of the coating [80]. To highlight the importance of surface roughness, the comparative effects of rough and smooth surface morphology on the ellipsoidal particle interaction were available in supplementary materials. Previous studies stated that the total interaction energy could work as an indicator for representing the stability of particles in different systems [37, 81-83]. Therefore, Modifying the surface roughness is a novel approach to increase the aggregation efficiency if the energy barrier could be reduced to be smaller than 5 kT.

To validate the present model, the predicted results were compared with the experimental and modeling results available in past literature, and the results are shown in the supplementary material (Table S4).

The predicted results from our numerical simulation could provide a quantitative assessment of natural particles involving randomly rough surfaces and ellipsoidal shapes [84, 85]. Moreover, as the XDLVO theory was the most representative theory to predict the interaction of particles [84], the model developed in the present study could have applications in coating, drug delivery, or flotation industry fields. For example, Kwok and coworkers applied the spray-drying nanosuspension to produce the controlled surface architecture, which covered the nano-matrix particles and concluded that the suspension performance of aerosol improved with increasing the surface roughness [86]. The previous modeling study constructed the rough surface with nano-pillar shape asperities, which could not fully reflect the properties of natural rough surface [87] because the realistic average of roughness fraction could not be described correctly. Generally, the most important step to accurately assess the interaction energy between particles is to characterize the properties of natural surface morphology. The present model involved the modified two-variable WM function to simulate the randomly rough surface, which simulated the texture of engineering surface or biomaterial surface more accurately. With the help of this approach, our model could reflect the properties of natural surface morphology. Therefore, the provided model could increase the accuracy of predictions of particle interaction. Additionally, the present approach can provide directions in designing the desired surface topology of ellipsoidal particles

to increase the suspension efficiency. For example, as the lignosulfonate could present an ellipsoidal conformation if the sequential fractional of lignosulfonate is conducted in ethanol/water solution [88], the present model could be used to predict the dispersibility of lignosulfonate in aqueous systems. The present work facilitates the identification of the interfacial behavior of natural colloids and the creation of effective modification strategies for designing desired products. It should be noted that the present model did not consider the chemical heterogeneity of the material in interaction energy calculations, which may limit the accuracy of predictions if the material owned surface charge heterogeneity. The previous modeling works made great efforts in simulating particle retention considering nanoscale roughness and surface charge heterogeneity and reported that the surface charge heterogeneity played a key role in controlling the particle interfacial behavior [89, 90]. Therefore, combining the impacts of surface charge heterogeneity into simulation process would be a further improvement.

5.5 Conclusions

With the help of fractal geometry theory, a mode was successfully constructed to create a randomly rough ellipsoidal morphology, which would represent the surface of natural particles very well. Our simulation approach established an accurate numerical model for predicting particle interfacial behavior based on the SEI technique and XDLVO theory. It is the first time that the numerical prediction considered the effects of ellipsoidal shape particles and natural surface morphology on particle interaction. In the present work, the total interaction energy developed between rough ellipsoidal particles with randomly located asperities was studied, considering varied fractal dimensions, fractal roughness, particle shape, aspect ratio, particle size, and orientation angle were evaluated. The modeling results showed that the increase in the fractal dimension and relative fractal dimension increased interaction energy, which was attributed to the fined texture of surface topography, which increased the asperity number but reduced the height of asperities. The elevated fractal roughness and relative fractal roughness diminished the repulsive energy barrier significantly, which was due to improving the average roughness via heightening the asperity on the particle surface. The predicted results also concluded that the ellipsoidal shape might provide more benefits for particle retention than spherical particles. The aspect ratio had the most effects on particle interactions as the interaction area changed with the value of the aspect ratio. In addition, considering the orientation angle effects on interaction

energy, the repulsive energy barrier decreased because the equivalent distance between two ellipsoidal rough particles extended.

These findings offered deep insights into the particle interface behavior in suspension systems. The numerical model presented in this study may provide guidelines for the modification of surfaces or properties of particles that are useful for designing functionalized products because the predicted results worked as indicators of the status of particle transportation and colloidal system stability. As natural-based particles are available in colloidal suspensions, more experimental work may be involved to investigate the relationship between asperity deformation and interaction force in the future

5.6 Reference

[1] S.J. Blott, K. Pye, Particle shape: a review and new methods of characterization and classification, Sedimentology, 55 (2008) 31-63.

[2] T. Knappenberger, S. Aramrak, M. Flury, Transport of barrel and spherical shaped colloids in unsaturated porous media, Journal of contaminant hydrology, 180 (2015) 69-79.

[3] L. Zhao, M. Zhang, Y. He, J. Chen, H. Hong, B.-Q. Liao, H. Lin, A new method for modeling rough membrane surface and calculation of interfacial interactions, Bioresour. Technol., 200 (2016) 451-457.

[4] T. Lin, Z. Lu, W. Chen, Interaction mechanisms and predictions on membrane fouling in an ultrafiltration system, using the XDLVO approach, J. Membr. Sci., 461 (2014) 49-58.

[5] A. Gomez-Flores, S.A. Bradford, G. Hwang, S. Choi, M. Tong, H. Kim, Shape and orientation of bare silica particles influence their deposition under intermediate ionic strength: A study with QCM–D and DLVO theory, Colloids Surf. Physicochem. Eng. Aspects, 599 (2020) 124921.

[6] S. Ohsaki, R. Mitani, S. Fujiwara, H. Nakamura, S. Watano, Effect of particle–wall interaction and particle shape on particle deposition behavior in human respiratory system, Chem. Pharm. Bull. (Tokyo), 67 (2019) 1328-1336.

[7] K. Müller, D.A. Fedosov, G. Gompper, Margination of micro-and nano-particles in blood flow and its effect on drug delivery, Sci. Rep., 4 (2014) 1-8.

[8] P. Santhoshkumar, K. Prasanna, I.N. Sivagami, Y.N. Jo, S.H. Kang, C.W. Lee, Time-efficient synthesis of MnO2 encapsulated α-Fe2O3 ellipsoids for lithium ion battery applications, Journal of Alloys and Compounds, 720 (2017) 300-308.

[9] T.W.R. Chia, V.T. Nguyen, T. McMeekin, N. Fegan, G.A. Dykes, Stochasticity of bacterial attachment and its predictability by the extended Derjaguin-Landau-Verwey-Overbeek theory, Applied and environmental microbiology, 77 (2011) 3757-3764.

[10] X. Zhang, X. Zhou, H. Xi, J. Sun, X. Liang, J. Wei, X. Xiao, Z. Liu, S. Li, Z. Liang, Interpretation of adhesion behaviors between bacteria and modified basalt fiber by surface thermodynamics and extended DLVO theory, Colloids and Surfaces B: Biointerfaces, 177 (2019) 454-461.

[11] S. Schuetz, M. Piesche, A model of the coagulation process with solid particles and flocs in a turbulent flow, Chem. Eng. Sci., 57 (2002) 4357-4368.

[12] F. Sbrizzai, P. Faraldi, A. Soldati, Appraisal of three-dimensional numerical simulation for sub-micron particle deposition in a micro-porous ceramic filter, Chem. Eng. Sci., 60 (2005) 6551-6563.

[13] J. Bergendahl, D. Grasso, Prediction of colloid detachment in a model porous media: hydrodynamics, Chem. Eng. Sci., 55 (2000) 1523-1532.

[14] S. Bhattacharjee, C.-H. Ko, M. Elimelech, DLVO interaction between rough surfaces, Langmuir, 14 (1998) 3365-3375.

[15] S. Bhattacharjee, M. Elimelech, Surface element integration: a novel technique for evaluation of DLVO interaction between a particle and a flat plate, Journal of colloid and interface science, 193 (1997) 273-285.

[16] H. Ma, C. Bolster, W.P. Johnson, K. Li, E. Pazmino, K.M. Camacho, A.C. Anselmo, S. Mitragotri, Coupled influences of particle shape, surface property and flow hydrodynamics on rod-shaped colloid transport in porous media, Journal of Colloid and Interface Science, 577 (2020) 471-480.

[17] Q. Du, P. Zhou, Y. Pan, X. Qu, L. Liu, H. Yu, J. Hou, Influence of hydrophobicity and roughness on the wetting and flow resistance of water droplets on solid surface: A many-body dissipative particle dynamics study, Chem. Eng. Sci., 249 (2022) 117327.

[18] K.Y. Wang, T.-S. Chung, M. Gryta, Hydrophobic PVDF hollow fiber membranes with narrow pore size distribution and ultra-thin skin for the fresh water production through membrane distillation, Chem. Eng. Sci., 63 (2008) 2587-2594.

[19] J. Wang, Z. Zhang, R. Shi, B.N. Chandrashekar, N. Shen, H. Song, N. Wang, J. Chen, C. Cheng, Impact of Nanoscale Roughness on Heat Transport across the Solid–Solid Interface, Advanced Materials Interfaces, 7 (2020) 1901582.

[20] J. Liu, X. Huang, K. Sulieman, F. Sun, X. He, Solution-based growth and optical properties of self-assembled monocrystalline ZnO ellipsoids, The Journal of Physical Chemistry B, 110 (2006) 10612-10618.

[21] G. Liu, X. Yang, Y. Wang, Synthesis of ellipsoidal hematite/silica/polymer hybrid materials and the corresponding hollow polymer ellipsoids, Langmuir, 24 (2008) 5485-5491.

[22] S. Bhattacharjee, J.Y. Chen, M. Elimelech, DLVO interaction energy between spheroidal particles and a flat surface, Colloids Surf. Physicochem. Eng. Aspects, 165 (2000) 143-156.

[23] R. Everaers, M. Ejtehadi, Interaction potentials for soft and hard ellipsoids, Physical Review E, 67 (2003) 041710.

[24] Y. Peng, Y. Guo, An adhesion model for elastic-plastic fractal surfaces, Journal of Applied Physics, 102 (2007) 053510.

[25] M.Y. Marusina, A.P. Mochalina, E.P. Frolova, V.I. Satikov, A.A. Barchuk, V.I. Kuznetcov, V.S. Gaidukov, S.A. Tarakanov, MRI image processing based on fractal analysis, Asian Pacific journal of cancer prevention: APJCP, 18 (2017) 51.

[26] Y. Chen, C. Zhang, M. Shi, G. Peterson, Role of surface roughness characterized by fractal geometry on laminar flow in microchannels, Physical Review E, 80 (2009) 026301.

[27] D. Lu, P. Fatehi, A modeling approach for quantitative assessment of interfacial interaction between two rough particles in colloidal systems, Journal of Colloid and Interface Science, 587 (2021) 24-38.

[28] E.M. Hoek, S. Bhattacharjee, M. Elimelech, Effect of membrane surface roughness on colloid− membrane DLVO interactions, Langmuir, 19 (2003) 4836-4847.

[29] R. Hobson, Surface roughness in topography: quantitative approach, Spatial analysis in geomorphology, Routledge2019, pp. 221-246.

[30] X. Cai, M. Zhang, L. Yang, H. Lin, X. Wu, Y. He, L. Shen, Quantification of interfacial interactions between a rough sludge floc and membrane surface in a membrane bioreactor, Journal of colloid and interface science, 490 (2017) 710-718.

[31] L. Zhao, L. Yang, H. Lin, M. Zhang, H. Yu, B.-Q. Liao, F. Wang, X. Zhou, R. Li, Modeling three-dimensional surface morphology of biocake layer in a membrane bioreactor based on fractal geometry, Bioresour. Technol.,

222 (2016) 478-484.

[32] M. Tanaka, M. Komagata, M. Tsukada, H. Kamiya, Fractal analysis of the influence of surface roughness of toner particles on their flow properties and adhesion behavior, Powder technology, 186 (2008) 1-8.

[33] P. Sahoo, S.R. Chowdhury, A fractal analysis of normal impact between rough surfaces in presence of adhesion, Wear, 261 (2006) 318-327.

[34] J. Chen, H. Lin, L. Shen, Y. He, M. Zhang, B.-Q. Liao, Realization of quantifying interfacial interactions between a randomly rough membrane surface and a foulant particle, Bioresour. Technol., 226 (2017) 220-228.

[35] D. Lu, P. Fatehi, Interfacial interactions of rough spherical surfaces with random topographies, Colloids Surf. Physicochem. Eng. Aspects, 642 (2022) 128570.

[36] C.J.C. Van Oss, S.A. Physicochemical, E. Aspects, Acid—base interfacial interactions in aqueous media, 78 (1993) 1-49.

[37] C. Van Oss, R. Giese, P.M.J.C. Costanzo, C. Minerals, DLVO and non-DLVO interactions in hectorite, 38 (1990) 151-159.

[38] T. Mahmood, A. Amirtharajah, T.W. Sturm, K.E. Dennett, A micromechanics approach for attachment and detachment of asymmetric colloidal particles, Colloids Surf. Physicochem. Eng. Aspects, 177 (2001) 99-110.

[39] C.J. Van Oss, Interfacial forces in aqueous media, CRC press2006.

[40] C. Van Oss, Acid—base interfacial interactions in aqueous media, Colloids Surf. Physicochem. Eng. Aspects, 78 (1993) 1-49.

[41] G. Hwang, C.H. Lee, I.S. Ahn, B.J. Mhin, Analysis of the adhesion of Pseudomonas putida NCIB 9816-4 to a silica gel as a model soil using extended DLVO theory, Journal of Hazardous Materials, 179 (2010) 983-988.

[42] J.J.J.o.C. Dann, I. Science, Forces involved in the adhesive process: I. Critical surface tensions of polymeric solids as determined with polar liquids, 32 (1970) 302-320.

[43] Y. Cui, J. Ravnik, P. Steinmann, M. Hriberšek, Settling characteristics of nonspherical porous sludge flocs with nonhomogeneous mass distribution, Water Res., 158 (2019) 159-170.

[44] R.J. Good, C.J. van Oss, The modern theory of contact angles and the hydrogen bond components of surface energies, Modern approaches to wettability, Springer1992, pp. 1-27.

[45] M. Zhang, H. Hong, H. Lin, G. Yu, F. Wang, B.-Q. Liao, Quantitative assessment of interfacial forces between two rough surfaces and its implications for anti-adhesion membrane fabrication, Separation and Purification Technology, 189 (2017) 238-245.

[46] H. Hong, X. Cai, L. Shen, R. Li, H.J.B.t. Lin, Membrane fouling in a submerged membrane bioreactor: new method and its applications in interfacial interaction quantification, 241 (2017) 406-414.

[47] A.M.J.C. Lenhof, S.A. Physicochemical, E. Aspects, Contributions of surface features to the electrostatic properties of rough colloidal particles, 87 (1994) 49-59.

[48] X. Qu, X. Cai, M. Zhang, H. Lin, Z. Leihong, B.-Q.J.A.S.S. Liao, A facile method for simulating randomly rough membrane surface associated with interface behaviors, 427 (2018) 915-921.

[49] W. Yan, K. Komvopoulos, Contact analysis of elastic-plastic fractal surfaces, Journal of applied physics, 84 (1998) 3617-3624.

[50] S. Feng, G. Yu, X. Cai, M. Eulade, H. Lin, J. Chen, Y. Liu, B.-Q. Liao, Effects of fractal roughness of membrane surfaces on interfacial interactions associated with membrane fouling in a membrane bioreactor, Bioresour. Technol., 244 (2017) 560-568.

[51] M. Zhang, X. Zhou, L. Shen, X. Cai, F. Wang, J. Chen, H. Lin, R. Li, X. Wu, B.-Q. Liao, Quantitative evaluation of the interfacial interactions between a randomly rough sludge floc and membrane surface in a membrane bioreactor based on fractal geometry, Bioresour. Technol., 234 (2017) 198-207.

[52] H. Hong, H. Lin, R. Mei, X. Zhou, B.-Q. Liao, L. Zhao, Membrane fouling in a membrane bioreactor: a novel

method for membrane surface morphology construction and its application in interaction energy assessment, J. Membr. Sci., 516 (2016) 135-143.

[53] S. Bhattacharjee, M. Elimelech, M.J.C.C.A. Borkovec, DLVO interaction between colloidal particles: beyond Derjaguin's approximation, 71 (1998) 883-903.

[54] H. Nielsen, The Vibration-rotation Energies of Molecules and their Spectra in the Infra-red, Atoms III—Molecules I/Atome III—Moleküle I, Springer1959, pp. 173-313.

[55] H. Bargozin, R. Hadadhania, H. Faraji, H. Yousefzadeh, Effect of rough nanoparticle orientation on DLVO energy interaction, Journal of Dispersion Science and Technology, 36 (2015) 755-764.

[56] X. Cai, L. Yang, Z. Wang, M. Zhang, L. Shen, H. Hong, H. Lin, G. Yu, Influences of fractal dimension of membrane surface on interfacial interactions related to membrane fouling in a membrane bioreactor, Journal of colloid and interface science, 500 (2017) 79-87.

[57] Q. Zhou, B. Qin, J. Wang, H. Wang, F. Wang, Experimental investigation on the changes of the wettability and surface characteristics of coal dust with different fractal dimensions, Colloids and Surfaces A: Physicochemical and Engineering Aspects, 551 (2018) 148-157.

[58] R. Pitchumani, B. Ramakrishnan, A fractal geometry model for evaluating permeabilities of porous preforms used in liquid composite molding, International Journal of Heat and Mass Transfer, 42 (1999) 2219-2232.

[59] Y. Han, A. Alsayed, M. Nobili, A.G. Yodh, Quasi-two-dimensional diffusion of single ellipsoids: Aspect ratio and confinement effects, Physical Review E, 80 (2009) 011403.

[60] A.A. Chialvo, L. Vlcek, Behaviour of rarified steam at very high temperature an orientation-averaged interaction potential approach towards its accurate description, Mol. Phys., 117 (2019) 3922-3940.

[61] Z. Adamczyk, B. Cichocki, M.L. Ekiel-Jeżewska, A. Słowicka, E. Wajnryb, M. Wasilewska, Fibrinogen conformations and charge in electrolyte solutions derived from DLS and dynamic viscosity measurements, Journal of colloid and interface science, 385 (2012) 244-257.

[62] J.H. Bae, T. Reed III, Estimation of Properties of Dilute Polar Gases from a Potential Energy Function, Industrial & Engineering Chemistry Fundamentals, 6 (1967) 67-72.

[63] C. Yigit, J. Heyda, J. Dzubiella, Charged patchy particle models in explicit salt: ion distributions, electrostatic potentials, and effective interactions, The Journal of chemical physics, 143 (2015) 08B606_601.

[64] P. Schiller, S. Kruger, M. Wahab, H.-J. Mogel, Interactions between spheroidal colloidal particles, Langmuir, 27 (2011) 10429-10437.

[65] J.W. Drelich, A simplified analysis of the effect of nano-asperities on particle-bubble interactions, Physicochemical Problems of Mineral Processing, 54 (2018).

[66] M.B. Salerno, M. Flamm, B.E. Logan, D. Velegol, Transport of rodlike colloids through packed beds, Environ. Sci. Technol., 40 (2006) 6336-6340.

[67] A. Gomez-Flores, S.A. Bradford, L. Wu, H. Kim, Interaction energies for hollow and solid cylinders: Role of aspect ratio and particle orientation, Colloids Surf. Physicochem. Eng. Aspects, 580 (2019) 123781.

[68] D.V. Sotnikov, A.N. Berlina, V.S. Ivanov, A.V. Zherdev, B.B. Dzantiev, Adsorption of proteins on gold nanoparticles: One or more layers?, Colloids Surf. B. Biointerfaces, 173 (2019) 557-563.

[69] M. Cooley, A. Sarode, M. Hoore, D.A. Fedosov, S. Mitragotri, A.S. Gupta, Influence of particle size and shape on their margination and wall-adhesion: implications in drug delivery vehicle design across nano-to-micro scale, Nanoscale, 10 (2018) 15350-15364.

[70] Q. Liu, V. Lazouskaya, Q. He, Y. Jin, Effect of particle shape on colloid retention and release in saturated porous media, J. Environ. Qual., 39 (2010) 500-508.

[71] M.B. Seymour, G. Chen, C. Su, Y. Li, Transport and retention of colloids in porous media: does shape really matter?, Environ. Sci. Technol., 47 (2013) 8391-8398.

[72] L.R. De Young, A.L. Fink, K.A. Dill, Aggregation of globular proteins, Acc. Chem. Res., 26 (1993) 614-620.

[73] B. Albijanic, O. Ozdemir, M. Hampton, P. Nguyen, A. Nguyen, D. Bradshaw, Fundamental aspects of bubble–particle attachment mechanism in flotation separation, Minerals Engineering, 65 (2014) 187-195.

[74] J.J. De Yoreo, P.U. Gilbert, N.A. Sommerdijk, R.L. Penn, S. Whitelam, D. Joester, H. Zhang, J.D. Rimer, A. Navrotsky, J.F. Banfield, Crystallization by particle attachment in synthetic, biogenic, and geologic environments, Science, 349 (2015).

[75] L. Wu, B. Gao, Y. Tian, R. Muñoz-Carpena, K.J. Zigler, DLVO interactions of carbon nanotubes with isotropic planar surfaces, Langmuir, 29 (2013) 3976-3988.

[76] D. Kokkinis, M. Schaffner, A.R. Studart, Multimaterial magnetically assisted 3D printing of composite materials, Nature communications, 6 (2015) 1-10.

[77] H. Bargozin, R. Hadadhania, H. Faraji, M. Yavari, The DLVO energy interaction of nanorough surfaces by spherical coordinates, Journal of Dispersion Science and Technology, 37 (2016) 884-893.

[78] C.P. McNew, N. Kananizadeh, Y. Li, E.J. LeBoeuf, The attachment of colloidal particles to environmentally relevant surfaces and the effect of particle shape, Chemosphere, 168 (2017) 65-79.

[79] M. Yekeler, U. Ulusoy, C. Hiçyılmaz, Effect of particle shape and roughness of talc mineral ground by different mills on the wettability and floatability, Powder Technology, 140 (2004) 68-78.

[80] L. Ren, Y. Cheng, S. Wang, X. Meng, Q. Qin, J. Yang, Oxidation behavior of the supercritical water on the ternary Ni-WP coating, Chem. Eng. J., 370 (2019) 1388-1406.

[81] R.J. Hunter, Foundations of colloid science, Oxford university press2001.

[82] J. Calero, A. Ontiveros-Ortega, V. Aranda, I. Plaza, Humic acid adsorption and its role in colloidal-scale aggregation determined with the zeta potential, surface free energy and the extended-DLVO theory, European Journal of Soil Science, 68 (2017) 491-503.

[83] M. Geiger, R. Acharya, E. Reutter, T. Ferschke, U. Zschieschang, J. Weis, J. Pflaum, H. Klauk, R.T. Weitz, Effect of the Degree of the Gate-Dielectric Surface Roughness on the Performance of Bottom-Gate Organic Thin-Film Transistors, Advanced Materials Interfaces, 7 (2020) 1902145.

[84] X. Cai, L. Shen, M. Zhang, J. Chen, H. Hong, H. Lin, Membrane fouling in a submerged membrane bioreactor: An unified approach to construct topography and to evaluate interaction energy between two randomly rough surfaces, Bioresour. Technol., 243 (2017) 1121-1132.

[85] J.-W. Liaw, M. Kuo, C. Liao, Plasmon resonances of spherical and ellipsoidal nanoparticles, Journal of Electromagnetic Waves and Applications, 19 (2005) 1787-1794.

[86] P.C.L. Kwok, A. Tunsirikongkon, W. Glover, H.-K. Chan, Formation of protein nano-matrix particles with controlled surface architecture for respiratory drug delivery, Pharm. Res., 28 (2011) 788-796.

[87] M. Bendersky, J.M. Davis, DLVO interaction of colloidal particles with topographically and chemically heterogeneous surfaces, Journal of colloid and interface science, 353 (2011) 87-97.

[88] W. Jiang, S. Liu, C. Wu, Y. Liu, G. Yang, Y. Ni, Super-stable, solvent-resistant and uniform lignin nanorods and nanospheres with a high yield in a mild and facile process, Green Chem., 22 (2020) 8734-8744.

[89] S.A. Bradford, S. Sasidharan, H. Kim, A. Gomez-Flores, T. Li, C. Shen, Colloid interaction energies for surfaces with steric effects and incompressible and/or compressible roughness, Langmuir, 37 (2021) 1501-1510.

[90] S.A. Bradford, S. Sasidharan, H. Kim, G. Hwang, Comparison of types and amounts of nanoscale heterogeneity on bacteria retention, Frontiers in Environmental Science, 6 (2018) 56.

Chapter 6: Interaction of deformable solid and hollow particles with the rough surface morphology

6.1 Abstract

6.1.1 Hypothesis and background

A majority of natural particles have deformable and rough surfaces. Past research indicated a lack of information for a numerical model to simulate the potential non-contact interaction between two deformable particles with rough surfaces. The simulation of deformable particles is critical to better understanding the interaction of deformable particles in colloidal systems. We hypothesized that the deformation process of solid and hollow particles could be simulated by numerical models and the constructed models could predict the impacts of deformation on the interaction of rough-surfaced solid or hollow deformable particles

6.1.2   Experiments

In this work, the deformable solid and hollow particles with rough surface morphologies were modeled following fractal geometry theory, and their non-contact interaction was simulated following the three-stages deformation model. Also, the impacts of surface tension, particle size, and surface roughness on the interaction of the particles were investigated.

6.1.3   Findings

It was observed that the total potential energy of deformable solid and hollow particles followed a pattern under different conditions. The difference in the energy profile between solid and hollow particle is the hollow particles generates deeper primary minima and the energy barrier disappeared, which indicated the hollow particles owned better attachment ability. The predicted results showed that the increased particle size would strengthen the deformability of deformable solid and hollow particles and their potential interaction, and particle size would be the most effective parameter to affect the deformability of particles. When the particle size increased from 10 nm to 1000 nm, the radius of the

deformation region of solid particles was enlarged from 5 nm to 90 nm. Nevertheless, increased surface tension would weaken the deformability of deformable solid and hollow particles, which would significantly elevate the attraction energy between particles and promote particle aggregation. The increased fractal dimension would reduce the deformability of solid and hollow particles but increased the potential interaction energy. The controversial results could be found by increasing fractal roughness, which would improve the deformability of particles and reduce the interaction energy. The results of this study could be applied for foreseeing the deformation and interaction of deformable particles, which has a significant application in a particle suspension system, such as microgel and biological cell suspensions.

Keywords: Deformation, surface morphology, deformable particle, non-contact, numerical model

6.2 Introduction

Colloidal suspension systems have tremendous applications in many fields, such as medical [1] and industrial fields [2]. To better understand the interaction of particles in suspension systems, the simulation of particle interaction is generally considered. While earlier studies mainly focused on evaluating the interaction of hard spherical particles, information about the interaction of deformable particles is lacking. However, deformable particles are available in natural and industrial environments remarkably, and thus understanding the interaction of particles in such systems would be essential. Different from hard particles, deformable colloids are a class of particles whose surfaces could be extended or compressed structurally when they are under forces [3]. This deformation would impact the interaction of deformable particles in colloidal systems [4, 5]. As previous studies mainly focused on particles with non-deformable shapes, the interaction energy caused by the variation in the shapes of particles is nonexistent. Therefore, applied models for studying hard spherical particles may underestimate the interfacial interaction energy created between deformable particles found in natural and industrial environments. The first objective of this work was to develop a model and study the interaction of deformable particles in colloidal systems.

The application ranges of deformable particles extend from biology to engineering, e.g., biological cells [6, 7] or latex particles [8]. The coalition of deformable solids was studied in the past [9-11]. Shanahan

described the interaction scenario of a deformable particle (i.e., vesicle) contacted with a rigid flat substrate and claimed that the contact parameters impacted the attraction energy of the two surfaces significantly [12]. Wan and Liu established a theoretical model to simulate a deformable capsule contacted with a rigid planar substrate and the relationships among contact mechanics, osmotic expansion, contact area, and angle, membrane stretch, and bond strength were quantitatively portrayed [13, 14]. Nevertheless, the previous works related to deformable particles mainly focused on surface contact deformation. Indeed, the interfacial interaction between two surfaces could generate the disjoining force to deform the deformable surface without any physical contact [15, 16]. The information on the noncontact interaction of deformable particles was not studied and thus was studied in this work. Additionally, the previous work involving deformable particles primarily assumed that particles were solid. The liquid-filled or hollow particle is commonly found in industrial or medical environments, such as hollow silica particles [17], and hollow microgels [18]. However, information on the interaction of deformable and hollow particles is lacking. Moreover, the previous numerical works articulated that the surface roughness would weaken the interfacial interaction between particles [19, 20], but these modeling studies only included nondeformable particles [9-11]. The second objective of this work was to investigate the noncontact interaction of deformable particles considering the different geometrical structures (solid and hollow particles).

As the surface of natural particles is rarely smooth, considering the impact of surface morphology on particle interaction is important. Extensive studies made great contributions to understanding the impacts of surface morphology on interfacial interaction between rough surfaces [19-24]. For example, Zhang and coworkers simulated the interaction of sludge particles with the membrane surface and postulated that the rough particle would possess weaker interaction energy with the membrane surface compared to the smooth particle [25]. However, the previous works involving the impacts of surface morphology mainly focused on the hard particles without considering the deformation characteristics of particles, such as avoiding the deformation of rough soil particles in sludge [22-25]. The third objective of this study was to investigate how the roughness of deformable particles would impact their interaction in colloidal systems.

The main purpose of the present work was to establish a non-contact model to simulate the interaction

of two rough and deformable solid and hollow particles and to investigate how the characteristics of rough and deformable particles would impact their deformation and interfacial interactions. For the first time, we have reported a comprehensive simulation study for assessing the influence of softness on the non-contact interaction of rough solid and hollow particles. The results of this work can provide a foundation for the coagulation of deformable droplets [26] and bacterial cell adhesion, for instance [27].

6.3 Material and method

6.3.1 Interaction between solid deformable particles

The coagulation of polyelectrolyte gels and silica-based hydrogels in aqueous systems can be considered as a scenario for the interaction of two deformable solid particles [28]. In these cases, a deformation region between deformable particles will be formed under interfacial forces due to the close approach of two deformable particles. According to the truncated sphere model for particle deformation constructed by Danov and coworkers [24], the van der Waals interaction between particles could be expressed with a constant Hamaker A_H based on Equation 6.1:

$$W_{vw} = -\frac{A_H}{12}\left(\frac{2a_2(l_1+h)}{l_1(l_2+h)} + \frac{2a_2(l_1-h)}{h(l_2+l_1)} + 2\ln\left(\frac{h(l_1+l_2)}{l_1(l_2+h)}\right) + \frac{r^2}{h^2} - \frac{l_1-h}{l_2}\frac{2r^2}{hl_1} - \frac{l_1-a_1-(l_1-a_2)}{2l_1-2a_1-h}\frac{2l_2^2}{hl_1} - \right.$$

$$\frac{2(l_2-a_2)-h}{2l_1-2a_1-h}\frac{d-h}{2h} + \frac{2a_2l_2^2(l_1-h)}{hl_1(l_2+l_1)(l_2+h)} - \frac{2a_2^2}{h(2l_1-2a_1-h)}\frac{l_1^2+r^2}{(l_2+l_1)(l_2+l_1-2a_2)} +$$

$$\frac{2a_2^2 d}{(2l_1-2a_1-h)[(l_2+h)(h+l_2-2a_2)-(l_1-h)(l_1-2a_1-h)]} - \left.\frac{4a^3((l_1-h)}{[(l_2+h)(l_2+h-2a_2)-(l_1-h)(l_1-2a_1-h)](l_2+l_1)(l_2+l_1-2a_2)}\right)$$

$$(6.1)$$

Where $l_1 = h + a_1 + \sqrt{a_1^2 - r^2}, l_2 = h + a_2 + \sqrt{a_2^2 - r^2}, d = \sqrt{h^2 + 4r^2}$, and the a_1 and a_2 represent the radii of deformable particles 1 and 2; r is the radius of the deformed film; h is the separation distance between two particles; and A_H is Hamaker constant ($A_H = 1.1 \times 10^{-20}$ J [29]). The interaction scenario of two solid deformable particles were shown in Figure 6.1a.

Moreover, as the total volume of particles remains constant during the deformation process, an elevated interfacial area would be generated from the deviations in the spherical shape of the particles, which would directly affect the total interaction energy between particles. Therefore, the surface extension should be taken into account for deformable spheres when their interactions are determined. The presence of the planar region between particles expanded the magnitude of the contribution of each

particle to the interfacial interaction [30]. The contribution of extended surface area in the total interaction of particles is given by [31]:

$$W_E = \int_{Sphere}^{Deformed\ sphere} \gamma(S)dS \tag{6.2}$$

Where S represents the area of the deformed region and γ represents the interfacial tension of particles. To simplify the simulation process, γ is assumed constant during the deformation, Equation 6.2 was transformed to Equation 6.3 for spheres:

$$W_E = \frac{\pi\gamma r^4}{2a^2} \tag{6.3}$$

The interaction energy caused by the alteration in the particle's interfacial curvature was also considered in the present modeling work. The corresponding contribution to the particle deformation energy would be generated because of the variations in the spherical curvature energy after and before the deformation region formed. Therefore, the interfacial bending energy would be calculated as follows:

$$W_B = -2\pi r^2 B_0 H \tag{6.4}$$

Where H represents the interfacial curvature and $H = -1/a$; the constant $B_0 = -4M_b H_0$ where M_b represents the bending moment [32]; and H_0 expresses the spontaneous curvature. The value of B_0 is selected as 1.6×10^{-12} N [33].
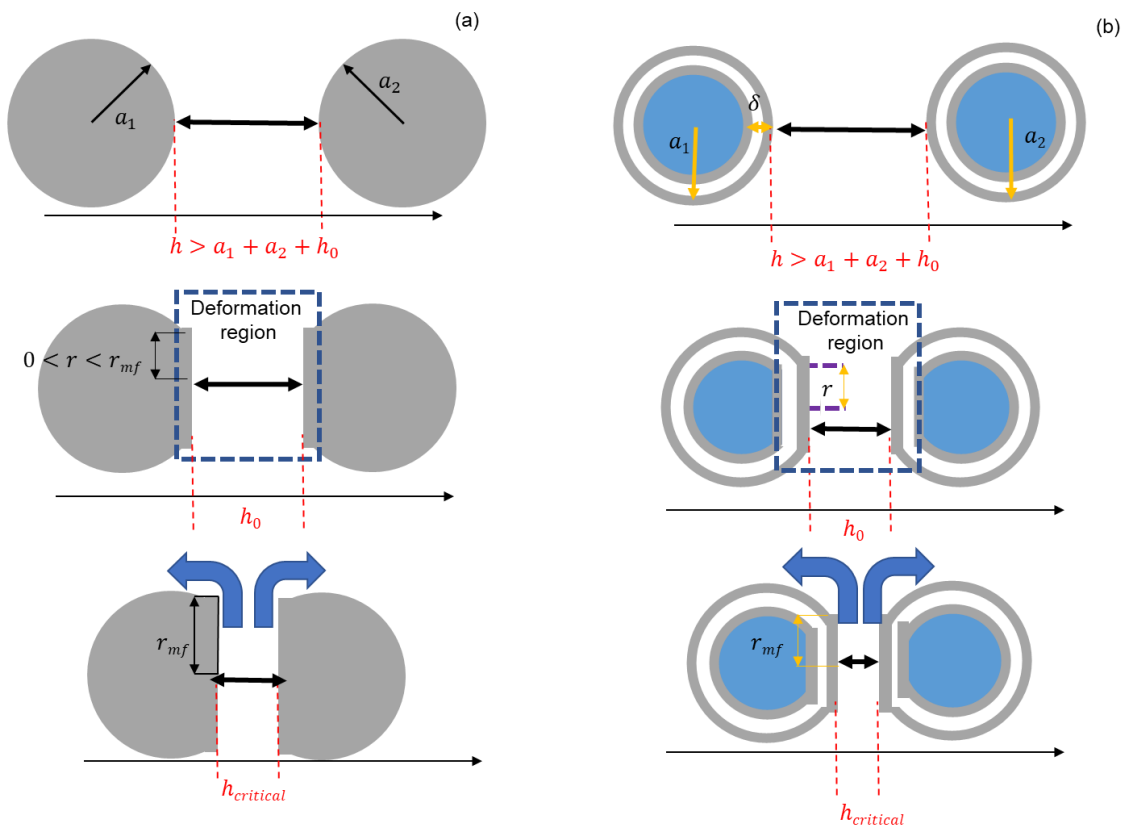
Figure 6.1 Parameters involved in the simulation of the deformable particles (a) deformable solid particles; (b) deformable hollow particles

6.3.2 Interaction between hollow deformable particles

In this work, only unilamellar particles will be considered. As the present model simulated hollow deformable particle interaction in oil emulsion, for example, the hollow particles owned the water core and were suspended in the oil phase for carboxyl-capping polystyrene emulsion systems [34]. The interaction scenario of the hollow particles was shown in Figure 1b. According to Petsev [35], the van der Waals attraction between hollow particles owning a single layer could be expressed as follows:

$$U_{vw} = -\sum_{i=1}^{M} \sum_{j=1}^{M} A(i,j) H(x_{ij}) \tag{6.5}$$

Where $A(i,j)$ represents the Hamaker constant in different phases; $H(x_{ij})$ is the geometrical function; the i, j represent different phases of solutions.

For the hollow particle, Equation 1 could be transferred to equation 6:

$$U_{VW} = -\frac{A_{so}}{12}\left[\frac{a}{h} + 2\ln\left(\frac{h}{a}\right) + \frac{3}{4} + \frac{r^2}{h^2} - \frac{2r^2}{ah}\right] - \frac{A_{sw}}{12}\left[\frac{a-\delta}{h+2\delta} + 2\ln\left(\frac{h+2\delta}{a-\delta}\right) + \frac{3}{4} + \frac{r^2}{(h+2\delta)^2} - \frac{2r^2}{(a-\delta)(h+2\delta)}\right] +$$

$$\frac{A_{sw}}{6}\left[\frac{a-\delta}{h+\delta} + 2\ln\left(\frac{h+\delta}{a-\delta}\right) + \frac{3}{4} + \frac{r^2}{(h+\delta)^2} - \frac{r^2}{(a-\delta)(h+\delta)}\left(\frac{15}{8} + \frac{h+3\delta}{8(h+\delta)}\right) + \frac{\delta}{2(h+\delta)}\right] \tag{6.6}$$

Where A_{so} and A_{sw} describe the Hamaker constants of the outer surface in oil phases and an inner surface of the water phase, respectively; the Hamaker constants $A_{so} = 5.2 \times 10^{-20} J$ and $A_{sw} = 1.1 \times 10^{-20} J$ were selected from previous work [29, 36]; and δ represented the thickness of hollow particle.

As our model aimed to simulate the deformable particle interaction, the energy of surface extension was also considered in the simulation process. The surface extension energy could be described by Equation 3. Also, one should take into account the energy related to the interfacial bending energy upon deformation that could be calculated by Equation 6.4.

6.3.3 Formation of the deformation region on solid and hollow particles

According to Equations 6.1-6.6, the interfacial interaction between deformable particles is a function of the width and radius of the deformation region. Therefore, it is necessary to establish the analytical relations between h, r and r_{ij} according to Figure 6.1. The deformation process could be divided into three steps.

146

Step I: When the separation distance between the mass centre of two particles is larger than $a_1 + a_2 + h_0$, the two particles maintained their spherical shapes without deformation. The separation distance and radius of the deformation region could be calculated according to equation 7 ($R_{ij} > a_1 + a_2 + h_0$):

$$h = R_{ij} - (a_1 + a_2), r = 0 \tag{6.7}$$

Where R_{ij} represents the separation distance between the centre points of deformable particles; the h_0 represents the distance of particles initially deformed, which could be calculated by a polynomial expression in literature [37] (equation 6.8).

$$h_0 = (1.2932 \times 10^{-8} - 8.6475 \times 10^{-9} e^{-\frac{\bar{a}}{1.8222} \times 10^{-6}}) \times \frac{3.3253 \times 10^{-9} + 5.9804 \times 10^{-9} e^{-\frac{\gamma}{0.00402}}}{3.3253 \times 10^{-9} + 5.9804 \times 10^{-9} e^{-\frac{1 \times 10^{-3}}{0.00402}}} \tag{6.8}$$

Step II: When the particles start to deform, the separation distance stays unchanged. The deformation region starts to form and the radius of deformation changes from $r = 0$ to $r = \sqrt{ah_0}$ (maximum) [38]. The separation distance and radius of the deformation region would be calculated from Equation 6.9 ($h_0 + \sqrt{a_1^2 - a_1 h_0} + \sqrt{a_2^2 - a_2 h_0} < R_{ij} < a_1 + a_2 + h_0$):

$$h = h_0, r = \sqrt{a_1^2 - \left[\left(\frac{a_1}{a_1 + a_2}\right)(q - h_0)\right]^2} \tag{6.9}$$

Step III: When the radius of the deformation region reaches its maximum of $\sqrt{ah_0}$, the particles exhibited their largest deformability, and a critical approach distance is reached. The separation distance and radius of the deformation region would be calculated following Equation 6.10 ($h_{crit} + \sqrt{a_1^2 - a_1 h_0} + \sqrt{a_2^2 - a_2 h_0} < q < h_0 + \sqrt{a_1^2 - a_1 h_0} + \sqrt{a_2^2 - a_2 h_0}$):

$$h = q - \sqrt{a_1^2 - r_m^2} - \sqrt{a_2^2 - r_m^2}, r = r_{mf} = \sqrt{ah_0}, \tag{6.10}$$

Where the h_{crit} represents the critical distance where two particles are attached. Equation 6.11 could be applied to resolve the critical distance of coalescing [33].

$$h_{crit} = \left(\frac{A_H \lambda_{crit}^2}{128\gamma}\right)^{1/4} \tag{6.11}$$

Where the $\lambda_{crit} \approx r_f / 10$. It should be noted that for hollow particles, the $A_H = \left(A_{so}^{\frac{1}{2}} - A_{sw}^{\frac{1}{2}}\right)^2$ [39].

6.3.4 Constructing randomly rough surface

As the particles owned rough surface morphology, considering the effect of roughness on the interaction of deformable particles is important. These particles could resemble polystyrene latex [40] and enveloped virus [41], whose surfaces were experimentally evaluated to have rough and deformable structures. In the present work, we applied the ripped rough particle theory to construct rough particles that can help capture the details of the peaks and valleys of the ripples on the particles. This construction method was successfully applied in modeling the interaction of rough flocs with membrane [20, 42, 43]. The average surface roughness would be calculated following Equation 6.12 [44].

$$S_a = \frac{1}{S} \iint_S^0 |F(x,y)| dx dy \tag{6.12}$$

Where the S is the definition area, S_a represents the average surface roughness, and $F(x,y)$ represents the function of a rough surface.

To simplify the numerical simulation process, it was assumed that colloidal particles could deform but the constructed asperities were not deformable (i.e., they were rigid). This scenario would resemble the surface topography of bacteria (*R. erythropolis 20S-E1-c*) [45, 46]. The process of constructing a rough surface could be satisfied by employing a modified two-variable Weierstrass-Mandelbrot (WM) function, which originated from the theory of fractal geometry [47]. The fractal geometry has been widely applied in simulating the randomly rough bio- and engineering- surfaces in the past [48, 49]. Therefore, applying the fractal geometry theory to construct a naturally rough surface could capture more characteristics of surface topographies and increase the accuracy of simulation work.

The previous works reported that the modified two-variable Weierstrass-Mandelbrot (WM) function in Cartesian coordinates (x, y, z) could be applied to simulate the features of rough planer surface [45, 50, 51]. The expression of a randomly rough planar surface would be described as Equation 6.13 [52].

$$Z(x,y) = L\left(\frac{G}{L}\right)^{D_f-2}\left(\frac{\ln\eta}{M}\right)^{1/2} \sum_{m=1}^{M} \sum_{n=0}^{n_{max}} \eta^{(D_f-3)n} \times \left(\cos\phi_{m,n} - \cos\left(\frac{2\pi\eta^n(x^2+y^2)^{\frac{1}{2}}}{L} \times\right.\right.$$

$$\left.\left.\cos\left(\tan^{-1}\left(\frac{y}{x}\right) - \frac{\pi m}{M}\right) + \phi_{m,n}\right)\right) \tag{6.13}$$

Where G is the fractal roughness representing the asperity size; D_f is the fractal dimension; η describes the density of frequency in the profile; L is the sample length; $\phi_{m,n}$ represents a random phase; M represents the number of superimposed ridges applied to generate the rough surface; and n_{max} represents the highest frequency. The values of constructing parameters in Equation 6.13 were collected

148

according to the literature study [23, 51] and shown in the supplementary material (Figure A.4.1). Based on Equations A.2.1-A.2.3, the randomly rough particle surface could be modelled following Equation 14.

$$\Delta b_i = L(\tfrac{G_i}{L})^{D_{f_i}-2}(\tfrac{ln\eta}{M})^{\tfrac{1}{2}}\sum_{m=1}^{M}\sum_{n=0}^{n_{max}}\eta^{(D_{f_i}-3)n} \times (\cos\phi_{m,nmax+1_i} - \cos(\tfrac{2\pi\eta^n r \sin\theta}{L} * \cos(\varphi -$$

$$\tfrac{\pi m}{M}) + \phi_{m,nmax+1})) \tag{6.14}$$

As the average roughness (S_a) of the randomly rough surface would be calculated based on Equations 6.12-6.14, which is denoted as $\langle\Delta b_i\rangle$ in the following investigations. Therefore, the radius of constructed randomly rough particle could be calculated as shown in Equation 6.15:

$$\Upsilon_{random\,i} = a_i + \langle\Delta b_i\rangle \tag{6.15}$$

To predict the interaction of randomly rough and deformable solid particle interaction, the van der Waals attraction energy could be expressed as follow:

$$W_{vw} = -\tfrac{A_H}{12}\left(\tfrac{2\Upsilon_{random\,2}(O_1+h)}{O_1(O_2+h)} + \tfrac{2\Upsilon_{random\,2}(O_1-h)}{h(O_2+O_1)} + 2\ln\left(\tfrac{h(O_1+O_2)}{O_1(O_2+h)} + \tfrac{r^2}{h^2} - \tfrac{O_1-h}{O_2}\tfrac{2r^2}{hO_1} - \right.\right.$$

$$\tfrac{O_1-\Upsilon_{random\,1}-(O_1-\Upsilon_{random\,2})}{2O_1-2\Upsilon_{random\,1}-h}\tfrac{2O_2{}^2}{hO_1} - \tfrac{2(O_2-\Upsilon_{random\,2})-h}{2O_1-2\Upsilon_{random\,1}-h}\tfrac{d-h}{2h} + \tfrac{2\Upsilon_{random\,2}O_2{}^2(O_1-h)}{hO_1(O_2+O_1)(O_2+h)} -$$

$$\tfrac{2\Upsilon_{random\,2}{}^2}{h(2O_1-2\Upsilon_{random\,1}-h)}\tfrac{O_1{}^2+r^2}{(O_2+O_1)(O_2+O_1-2\Upsilon_{random\,2})} +$$

$$\tfrac{2\Upsilon_{random\,2}{}^2 d}{(2O_1-2\Upsilon_{random\,1}-h)[(O_2+h)(h+O_2-2\Upsilon_{random\,2})-(O_1-h)(O_1-2\Upsilon_{random\,1}-h)]} -$$

$$\left.\tfrac{4\Upsilon_{random\,2}{}^3(O_1-h)}{[(O_2+h)(O_2+h-2\Upsilon_{random\,2})-(O_1-h)(O_1-2\Upsilon_{random\,1}-h)](O_2+O_1)(O_2+O_1-2\Upsilon_{random\,2})}\right)$$

$$\tag{6.16}$$

Where $O_1 = h + \Upsilon_{random\,1} + \sqrt{\Upsilon_{random\,1}{}^2 - r^2}, O_2 = h + \Upsilon_{random\,2} + \sqrt{\Upsilon_{random\,2}{}^2 - r^2},$

As for rough hollow particles, the van der Waals attraction energy would be rearranged as shown in equation 6.17:

$$U_{VW} = -\tfrac{A_{so}}{12}\left[\tfrac{\Upsilon_{random}}{h} + 2\ln\left(\tfrac{h}{\Upsilon_{random}}\right) + \tfrac{3}{4} + \tfrac{r^2}{h^2} - \tfrac{2r^2}{\Upsilon_{random}h}\right] - \tfrac{A_{sw}}{12}\left[\tfrac{\Upsilon_{random}-\delta}{h+2\delta} + 2\ln\left(\tfrac{h+2\delta}{\Upsilon_{random}-\delta}\right) + \right.$$

$$\tfrac{3}{4} + \tfrac{r^2}{(h+2\delta)^2} - \tfrac{2r^2}{(\Upsilon_{random}-\delta)(h+2\delta)}\Big] + \tfrac{A_{sw}}{6}\left[\tfrac{\Upsilon_{random}-\delta}{h+\delta} + 2\ln\left(\tfrac{h+\delta}{\Upsilon_{random}-\delta}\right) + \tfrac{3}{4} + \tfrac{r^2}{(h+\delta)^2} - \right.$$

$$\left.\tfrac{r^2}{(\Upsilon_{random}-\delta)(h+\delta)}\left(\tfrac{15}{8} + \tfrac{h+3\delta}{8(h+\delta)}\right) + \tfrac{\delta}{2(h+\delta)}\right] \tag{6.17}$$

Similarly, the surface extension energy and interfacial bending energy of rough solid and hollow particles could be calculated by replacing a with Υ_{random} in Equations 6.3 and 6.4 only and described as Equations 6.18 and 6.19.

$$W_E = \frac{\pi \gamma r^4}{2 \Upsilon_{random}{}^2}$$ (6.18)

$$W_B = -2\pi r^2 B_0 \frac{-1}{\Upsilon_{random}}$$ (6.19)

6.3.5 Impact of surface tension on particle interaction and deformation

The cohesive forces between liquid molecules cause surface tension, which would equilibrate inside the bulk of a liquid and result in a net force towards the bulk in interface regions [53]. Therefore, surface tension represents an important property of the colloidal particles in suspension systems [53], it would impact the deformation of deformable particles and their interfacial interactions. Therefore, it is necessary to investigate the effects of surface tension on the deformability of particles. The investigated range of surface tension γ was selected from previous work from 0.01 mN/m to 50 mN/m [29, 31], and the other parameters were kept constant ($a_i = 500$ nm, $A_H = 1.1 \times 10^{-20}$ J for solid particle, $A_H = 1.53 \times 10^{-20}$ for hollow particle [29, 36]).

6.3.6 Impact of particle size on particle deformation and interaction

A previous study discussed that the critical coagulation concentration would be decreased by reducing the particle size since the surface energy of particles was changed by particle sizes [54]. Nevertheless, previous studies primarily assumed that particles were hard and non-deformed [54, 55]. To fill the research gap, it is important to investigate the impact of particle size on the interaction of deformable particles. In this study, the particle size changes from 10 nm to 1000 nm in this section, which was selected according to previous work [52], and the other parameters were kept constant ($a_i = 500$ nm, $A_H = 1.1 \times 10^{-20}$ J for solid particle, $A_H = 1.53 \times 10^{-20}$ for hollow particles).

6.3.7 Impact of fractal dimension on particle deformation and interaction

To construct the particles with surface morphology resembling that of natural particles, the fractal geometry theory was applied in the present work. The D_f controls the surface texture of the material. Based on Figure S1, the larger value of D_f would reduce the surface roughness of the constructed particles, which would suggest that the D_f would play a key role in altering the surface morphology of particles. Previous studies stated that the range of 2 and 3 for the fractal dimension was applied to construct a three-dimensional rough surface [51, 56], Therefore, the present work analyzed the effects of D_f on the particle interaction energy and critical parameters of deformation when D_f changed from

2.01 to 2.91, and other parameters were kept constant ($\gamma = 1$ mN/m ($a_i = 500$ nm, $A_H = 1.1 \times 10^{-20}$ J for solid particles, $A_H = 1.53 \times 10^{-20}$ J for hollow particles, $G = 1$ nm).

6.3.8 Impact of fractal roughness on particle deformation and interaction

The parameter G controls the height of asperities on particles, which is also an important parameter to control the topography of the rough spherical surface. In the current work, the fractal roughness, G, between 1 nm and 50 nm was considered [25] and other parameters were kept constant ($\gamma = 1$ mN/m $a_i = 500$ nm, $A_H = 1.1 \times 10^{-20}$ J for solid particles, $A_H = 1.53 \times 10^{-20}$ J for hollow particles, D_f = 2.01).

6.4 Results and discussions

6.4.1 The effect of surface tension on the interaction of deformable particles

Figures 6.2a and 6.2b showed the impact of surface tension on the deformation of particles. As seen, the critical deformation parameters were changed by elevating the value of γ. The initial deformation distance (h_0) dropped with a larger value of γ (Figure 6.2a), which suggested that the particle with a lower γ deformed more easily by interfacial force because those particles started deforming at a farther distance. The coalesce distance ($h_{critical}$) also decreased with an increase in the value of γ, which also indicate that the particle with a higher value of γ was more difficult to coagulate (Figure 6.2a). In the case of hollow particles, the effects of surface tension of deformable particles showed a similar tendency to that of the solid particles (Figure 6.2b). In addition, the difference in deformation between the solid and hollow particle is shown in $h_{critical}$ because of the different values of the Hamaker constant in Equation 6.11. The values of $h_{critical}$ in solid particles (0.75 nm) was smaller than that of hollow particles (0.81 nm), which indicated the hollow particle was easier to coagulate compared with solid particles. The radius of the deformation region (r_{mf}) decreased with increasing γ, which is another indicator that the particle with a smaller γ could deform more greatly. Ferri and coworkers investigated the deformation of the single-Pickering-emulsion droplet and demonstrated that the surface tension contributed to the interfacial force, which would resist droplet deformation [57]. The larger γ generated stronger force to resist particle deformation. The proposed model may provide guides for the improvement in the dispersion system by altering the surface tension of the material.

The effect of surface tension (γ) on the interaction of deformable particles is shown in Figures 6.2c and

6.2d. It is observed that the energy barrier increased from 0 to 435 kT by elevating γ from 0.01 mN/m to 50 mN/m if the two solid particles had a 500 nm radius (Figure 6.2c). This phenomenon could be explained by Equation 3, where the energy of W_E is proportional to γ. According to Equation 6.6, the variation in γ would cause different values of h_0, indicating the different deformability of particles. However, the energy barrier disappeared when two hollow and deformable particles interacted as shown in Figure 6.2c. Only when γ had a larger value (50 mN/m in this study), the increase in the energy barrier was observable. The main reason for this phenomenon is that the deformation effects on attraction force between hollow particles would be stronger than that of solid particles, where the hollow particle generated the deeper primary minimum and the repulsive energy would not change significantly compared with solid particles.

It should be noticed that the generated energy barrier between deformable particles is different from the electric repulsive energy barrier, which represents the resistance of surface deformation because the surface was extended under the interfacial force and created repulsion to prevent surface deformation. This repulsion phenomenon caused by the deformable surface is called soft repulsion in past work [58]. Previous works also reported that the larger energy barrier represents the stronger soft repulsion in the deformable particle system [31], which tends to enhance the attraction force between deformable particles [59]. Therefore, the soft repulsion indeed increased the strength of attraction energy. Neumann and coworkers investigated the adhesion ability of leukocytes and platelets to solid substrates and stated that cellular adhesion ability would be elevated with increasing surface tension [60]. The previous experiment [60] verified this phenomenon in that the larger γ would represent larger soft repulsion, which increased the adhesion ability of particles.

(a)

(b)
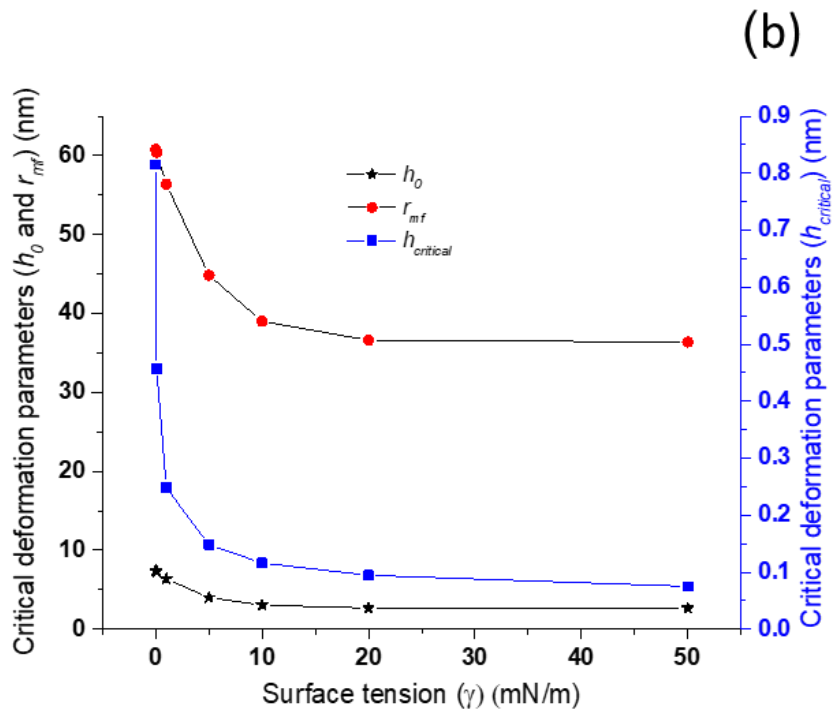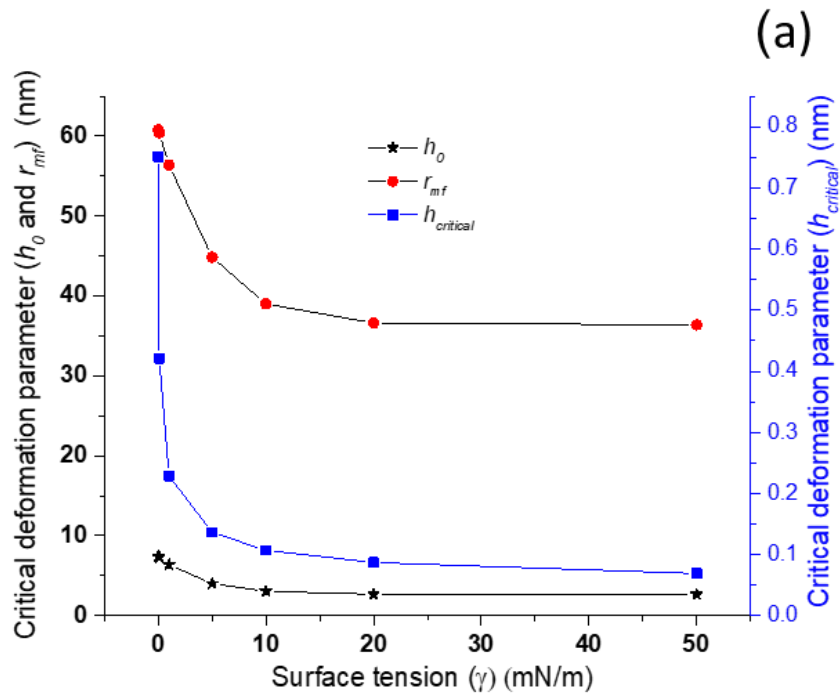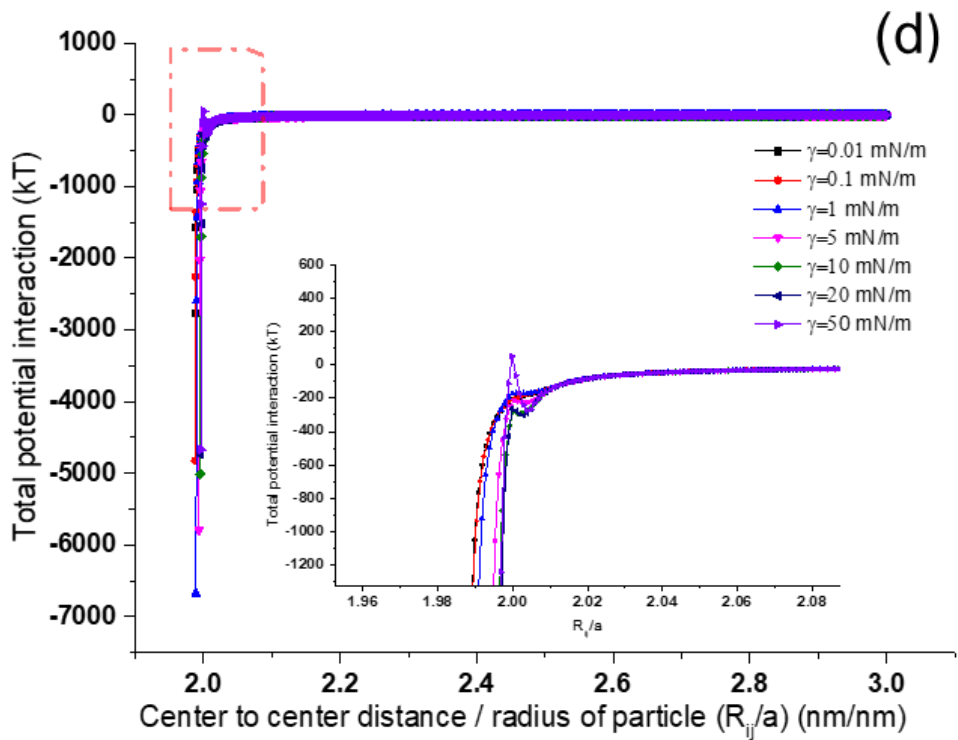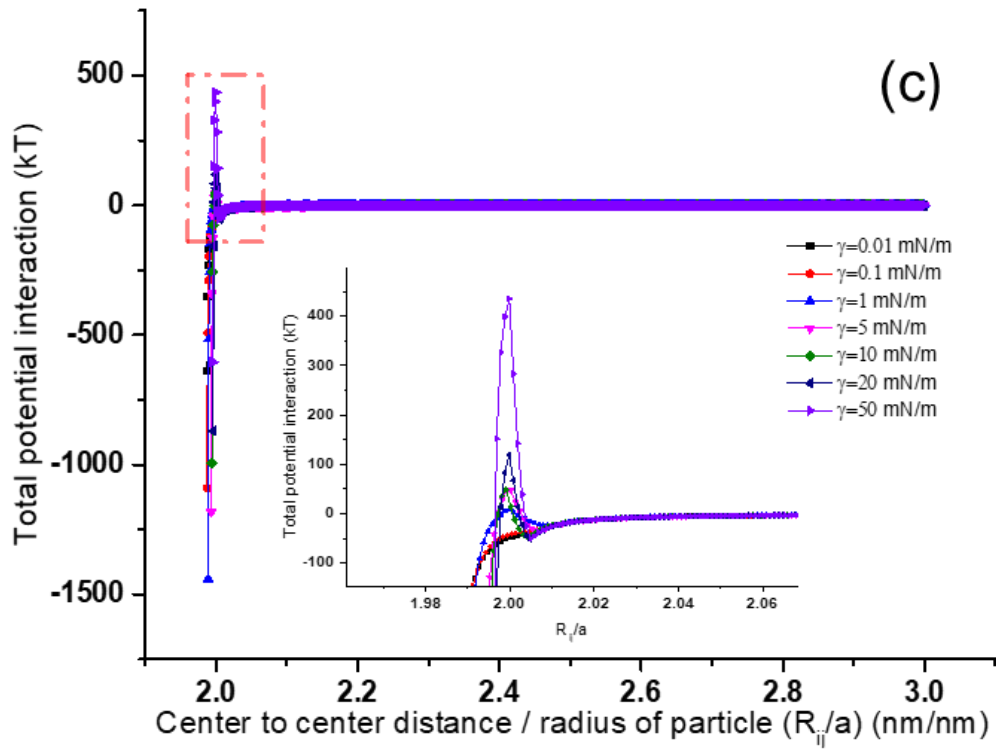
Figure 6.2 The effect of surface tension on particle deformation and particle interaction (a) deformation parameters of solid particles (b) deformation parameters of hollow particles (c) interaction energy of solid particles (d) interaction energy of hollow particles

6.4.2 The effect of particle size on particle interaction and deformation

The relationship between particle size and critical parameters of particle deformation was shown in Figures 6.3a and 6.3b. The r_{mf} increased speedily with the improved particle size for both particles, which is reasonable because the particles with larger sizes developed more interaction area and thus interfacial energy. Additionally, the increased particle size would elevate the value of r_{mf} based on Equation 8. Therefore, the particle size played a dominant role in controlling the value of r_{mf}. Yan and Geng investigated the effects of particle size on the deformation of polycrystalline α-SiC particles and reported that the stiffness of particles increased with decreasing particle size [61]. In our model, r_{mf} described the radius of deformation region, and the predicted results showed that the smaller particle exhibited more rigid particles. Ma and Gao applied Eshelby tensors to predict the effective elastic properties of multiphase composites and the modeling results showed that the decreased particle size had a large effect on the effective Young's modulus, which reduced the elasticity of the material [62]. Although our numerical study did not investigate Young's modulus of the material, it used critical parameters to express the deformation resistance and concluded that the larger particle owned stronger deformability.

Figure 6.3c shows the effect of particle size on the interaction of deformable and solid particles. The potential interaction energy increased with enlarging the particle size because the interaction area between particles intensified. When the radius of a deformable particle was 10 nm, the repulsive energy barrier was 17.8 kT, and when the radius increased to 1000 nm, the energy barrier dropped to 9.9 kT. The main reason for the dropped energy barrier is that the increased rate of van der Waals attraction forces (Equation 6.1) and bending forces (Equation 6.4) are larger than the surface extension forces (Equation 6.3) with increasing particle size. The total interfacial energy between the particles grows with increasing the particles [63]. As the energy barrier is the summation of the results in W_{vw}, W_E and W_B, the energy barrier would reduce if the increasing rate of attraction potential energies were larger than that of the repulsive energy. However, the decreased primary minimum with increased particle size suggested that the larger deformable particles provided better stability in the dispersion system. In another work, He and his coworkers analyzed the kinetic stability of hematite nanoparticles and reported

that the smaller hard particle showed larger aggregation rates because the critical coagulation concentration depended on particle size, and it dropped as particle size decreased [54]. Even though the proposed model included particle softness and deformation, the effects of particle size on deformable particles' interfacial energy showed a similar trend to the interaction of non-deformed particles [54]. However, the energy barrier disappeared in Figure 6.3d for hollow particles. The main reason for this is the significantly increased attraction energy and the increased rate of attraction force in a hollow particle system because the van der Waals interaction between hollow particles is determined not only by the interactions of a solid outer layer but also by that of the inner surface (Equation 6.17). Despite the disappeared energy barrier, the impact of particle size on interaction energy for hollow particles is similar to that of solid particles.

(b)

(c)
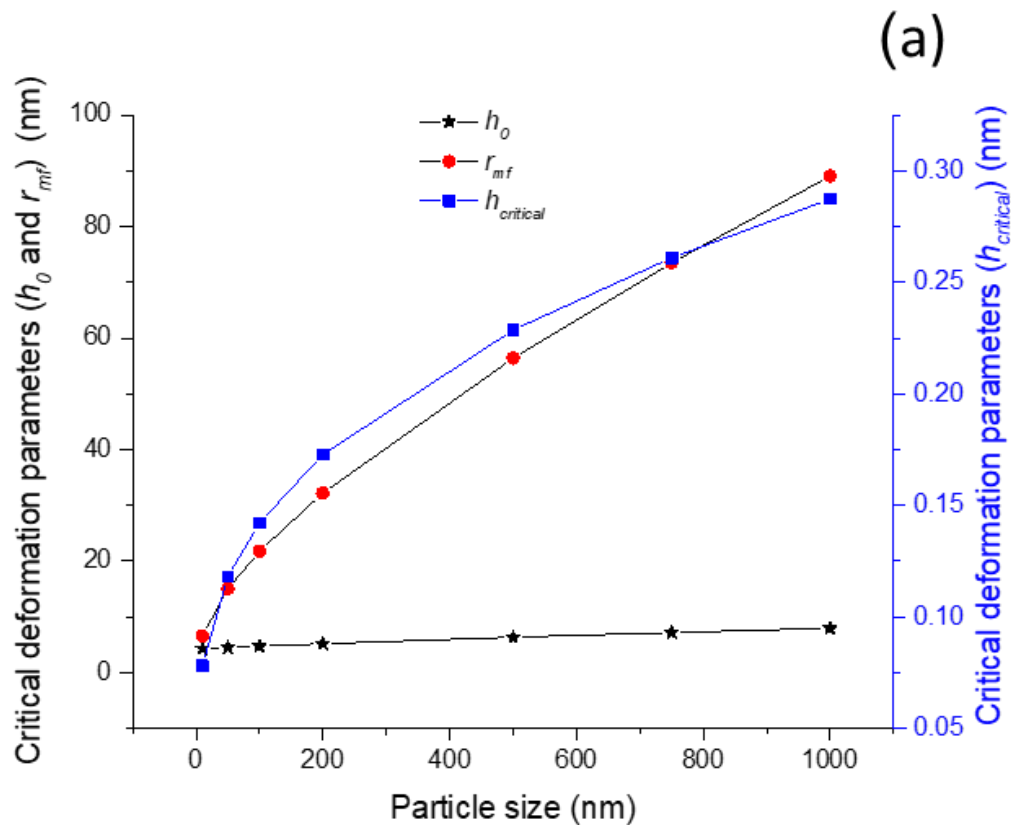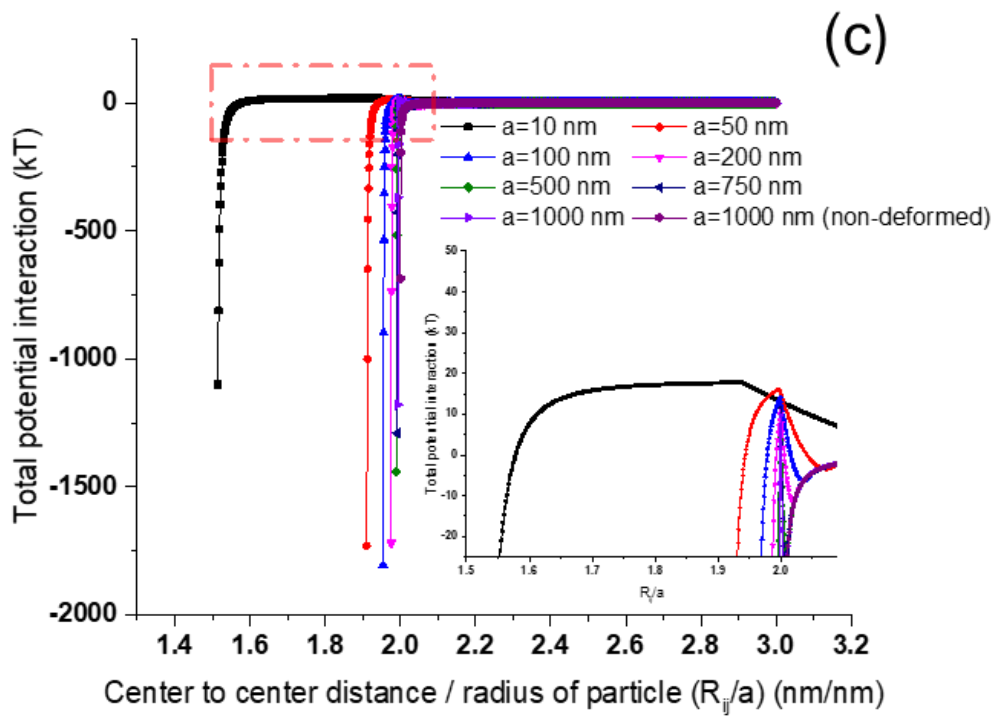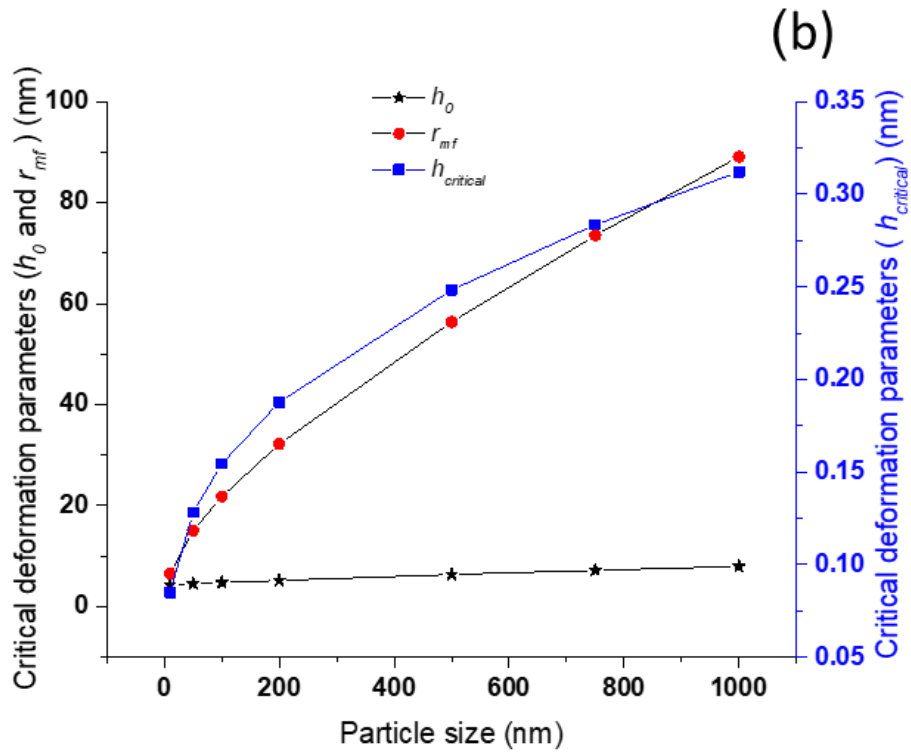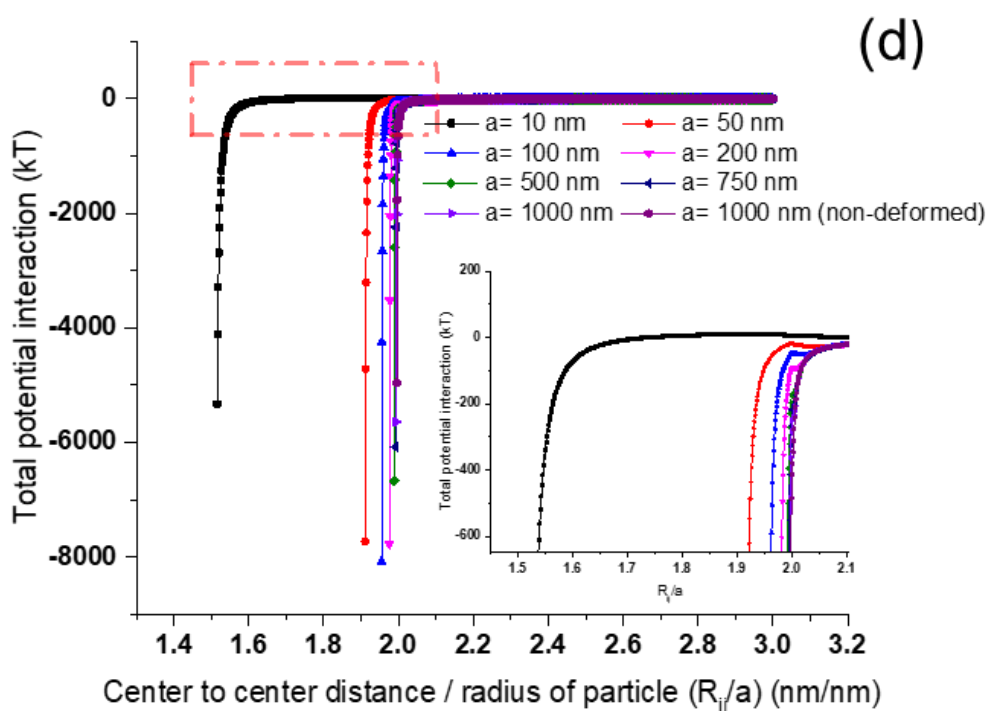
Figure 6.3 The effect of particle size on particle deformation and particle interaction (a) deformation parameters of solid particles (b) deformation parameters of hollow particles (c) interaction energy of solid particles (d) interaction energy of hollow particles

6.4.3 The effect of fractal dimension on particle interaction and deformation

The relationship between D_f and critical deformation parameters were explored in Figure 6.4a. Both critical deformation parameters decreased with increasing the value of D_f. The critical parameters showed a significant drop when D_f changed from 2.01 to 2.61, however, the decreasing rate became insignificant with further increasing the value of D_f. The reason for this behavior is that the surface topography of constructed particles becomes smooth when the value of D_f surpassed the critical value (2.6 in this work), because D_f critically impacts the surface morphology of the particles. It was postulated that the average surface roughness decreased exponentially with the enlarged value of D_f of membrane surface [49]. No significant difference could be found when D_f increased from 2.61 to 2.81. Similarly, the critical parameters of hollow particles decreased with increasing the value of D_f as shown in Figure 6.4b. Our simulation results indicated that the surface roughness significantly strengthened the deformability of particles, which implies that rougher particles are generally softer [49]. The main reason for this phenomenon is that increasing the value of D_f, the texture of the particle surface becomes denser, and the particle becomes smoother, which solidify the particle surface. In the same vein, the

158

softness was defined by the topography of the surface, particularly the asperity size and its periodicity [64]. The effects of D_f on surface softness was investigated in past [65, 66]. Yu constructed an elastic-plastic contact model to simulate the rough flat surface deformation and reported that the increased D_f created a stiffer flat surface [65]. Also, Jiang and coworkers established a contact model to simulate the deformation of rough surfaces and concluded that the increased D_f improved the stiffness of rough surface [66]. Although the previous studies mainly focused on the deformation scenario of contacted surface [65, 66], the deformation of non-contact scenario behaved very similarly.

Generally, the surface of natural particles has a rough surface with random topography [67], and the modified WM function could be applied to simulate these surfaces. As the fractal dimension controlled the texture of the rough surface, its effect on the interaction of rough deformable surfaces should be investigated. Figure 6.4c shows the effect of fractal dimension on the interaction of deformable rough particles. It is seen that the interaction energy increased when D_f became larger. In this case, the elevated value of D_f would smooth the texture of constructed surface, which will diminish the total surface roughness of particles [49]. The previous studies on hard rough particles articulated that the greater surface roughness would lessen the interfacial interaction between particles because the interaction area was reduced by the larger asperity [42, 68]. It is seen that the primary minimum was changed with the value of D_f, which directly controlled the particle deformability. As explain above, the higher value of D_f would yield harder particles, and thus the surface extend energy would be reduced with increasing D_f, which resulted the deeper primary minimum as shown in Figure 6.4c. The rougher surface would reduce the stiffness of the surface of hollow particles (Figure 6.4d), which would generate larger U_E (Equation 6.18), especially at the critical distance of coalescing. Cai and coworkers applied the fractal geometry to construct a randomly rough membrane surface and reported that the total interaction energy between rough sludge flocs and membrane improved the value of D_f, which is similar to our findings even though our model constructed the rough surface and considered the deformation energy in the simulation process [49].

(a)

(b)
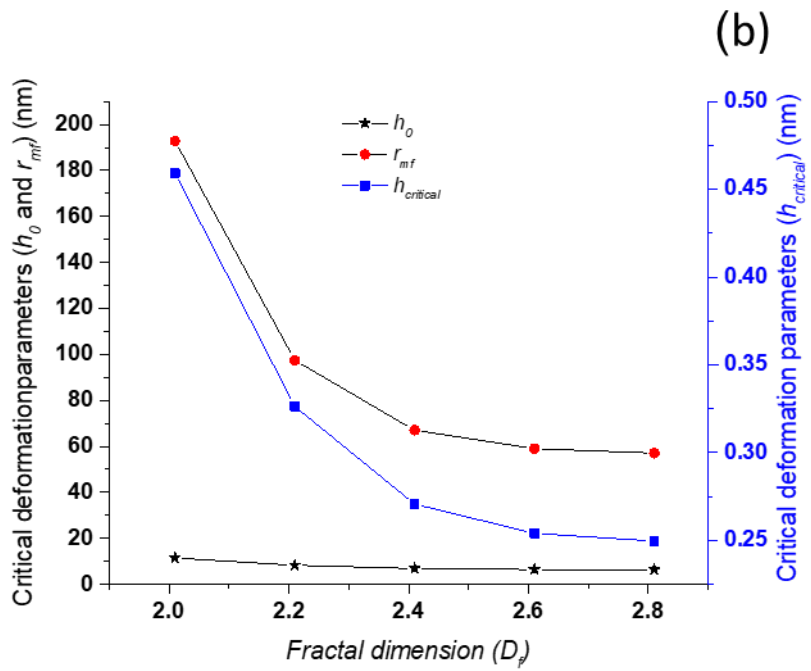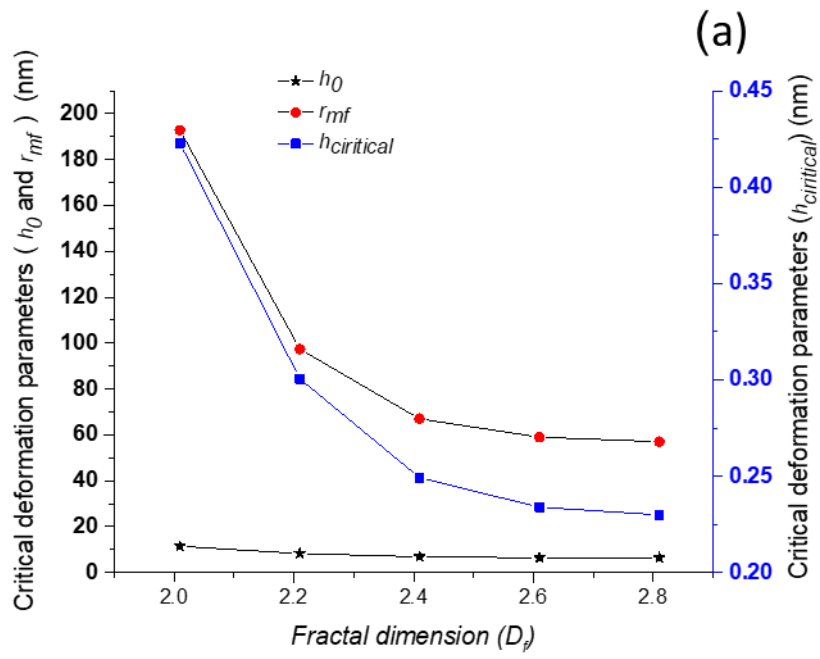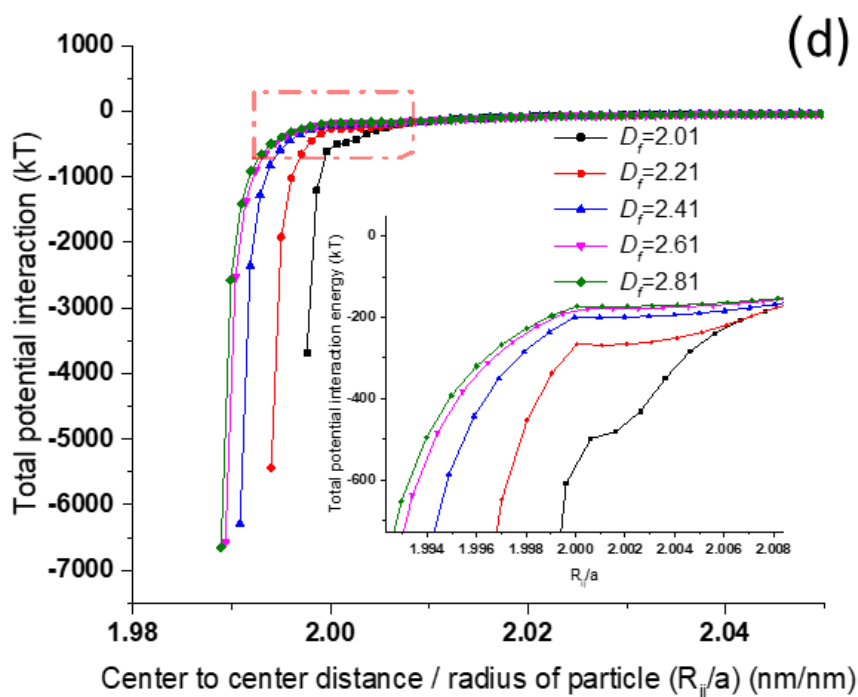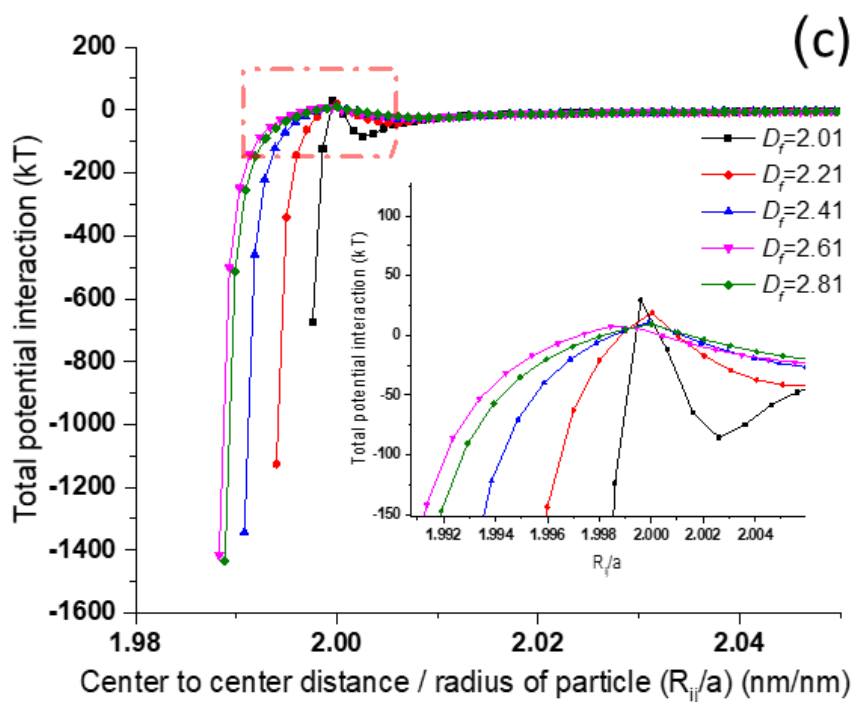
Figure 6.4 The effect of fractal dimension on particle deformation and particle interaction (a) deformation parameters of solid particles (b) deformation parameters of hollow particles (c) interaction energy of solid particles (d) interaction energy of hollow particles

6.4.4 The effect of fractal roughness on deformable particle interaction and deformation

Figure 6.5a shows the relationship between G and the deformation of solid particles. With increasing G, the critical parameters enlarged especially for a radius of the deformation region (r_{mf}), which directly characterized the degree of deformation. The increased h_0 would suggest that the rougher particle started the deformation at a larger separation distance. Similar results were found for hollow particles (Figure 6.5b). The simulated results also suggested that the increased asperity height would make the constructed surface softer, which reduced the stiffness of the particle surface. In a similar work, Miao and Huang developed a numerical contact model to simulate the deformation of a rough surface and demonstrated that the larger value of G could obtain a smaller contact stiffness [69]. Although a non-contact model was involved in this study, the simulation results showed similar predictions, where the increased r_{mf} reduced the stiffness of the material. Therefore, our results indicated that the surface roughness would negatively affect the softness of the material, regardless of the surface contact.

Figure 6.5c showed the fractal roughness effect on the interaction of deformable rough particles. As seen, the interfacial energy decreased with enlarging G from 1 nm to 50 nm. In this case, G represents the height of asperities on a randomly rough surface, and the surface roughness increased with increasing the G value [70]. As the G represents the height of asperities on a randomly rough surface, the surface roughness increased with increasing the G value [70]. The relationship between deformation and rough solid particle interaction shown in Figure 6.5c is followed our expectations. The energy barrier shown in Figure 6.5c increased with increasing the value of G, as the rough surface is softer than the smooth surface. Despite the small variation in the energy barrier, the value of G seems to influence the interaction of deformable particles. With increasing the asperity height, the particle deformation region would be increased where the r_{mf} and W_E enlarged (Equation 3). The soft repulsion energy barrier between hollow particles disappeared because of the significantly increased strength of W_{vw} and W_B force (Figure 6.5d). But the impact of G on hollow particle interaction exhibited a similar tendency to that of solid particles. As G controlled the asperity height of the material surface, our model concluded that the deformability of the material would improve if the asperity size increased, which would generate more interaction energy between particles. Interestingly, the total interaction energy would drop with roughening the surface of the particles were assumed hard [20, 71, 72]. However, previous and our models proved that the softer surface would generate more interaction energy, and increasing

the surface roughness would create a softer material surface [30]. Therefore, it could be articulated that there is an equilibrium between surface deformability, surface roughness, and interfacial interaction.

(a)

(b)

(c)
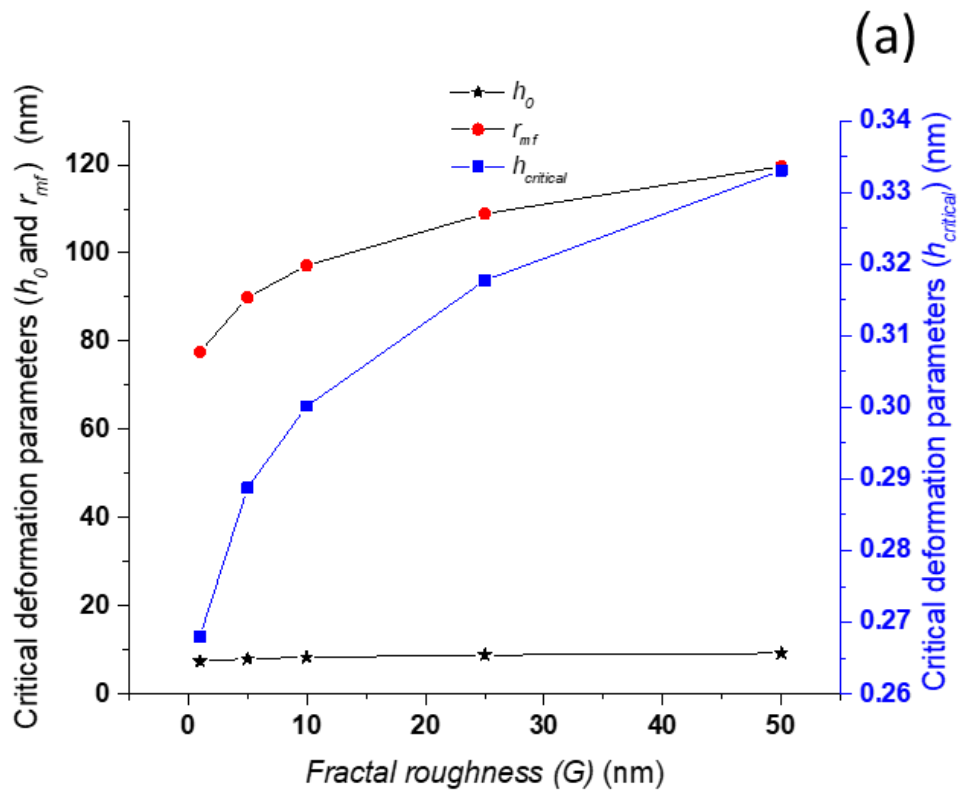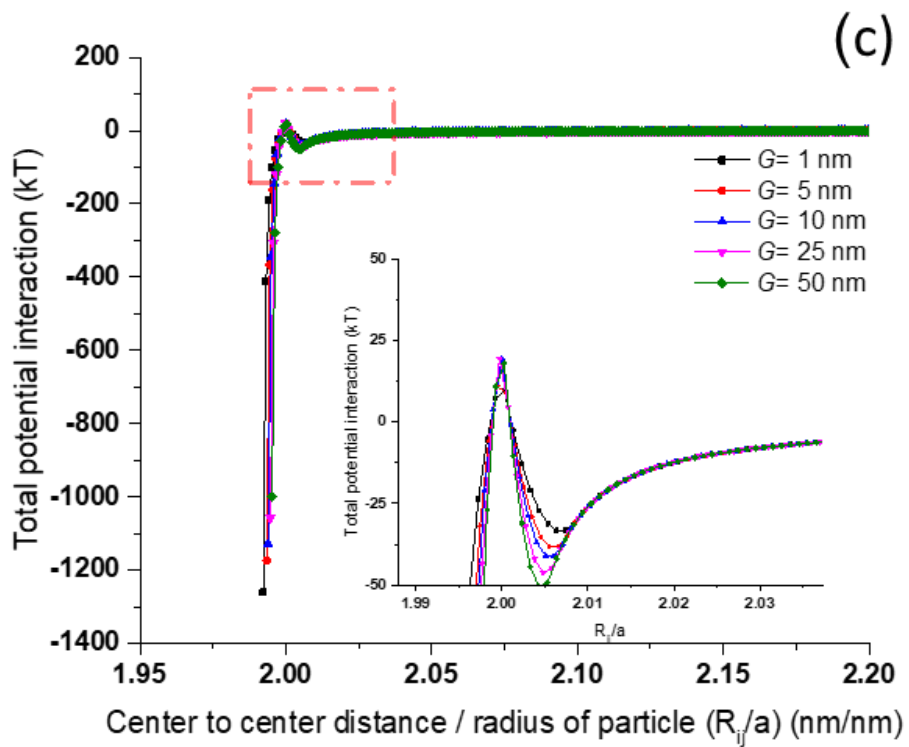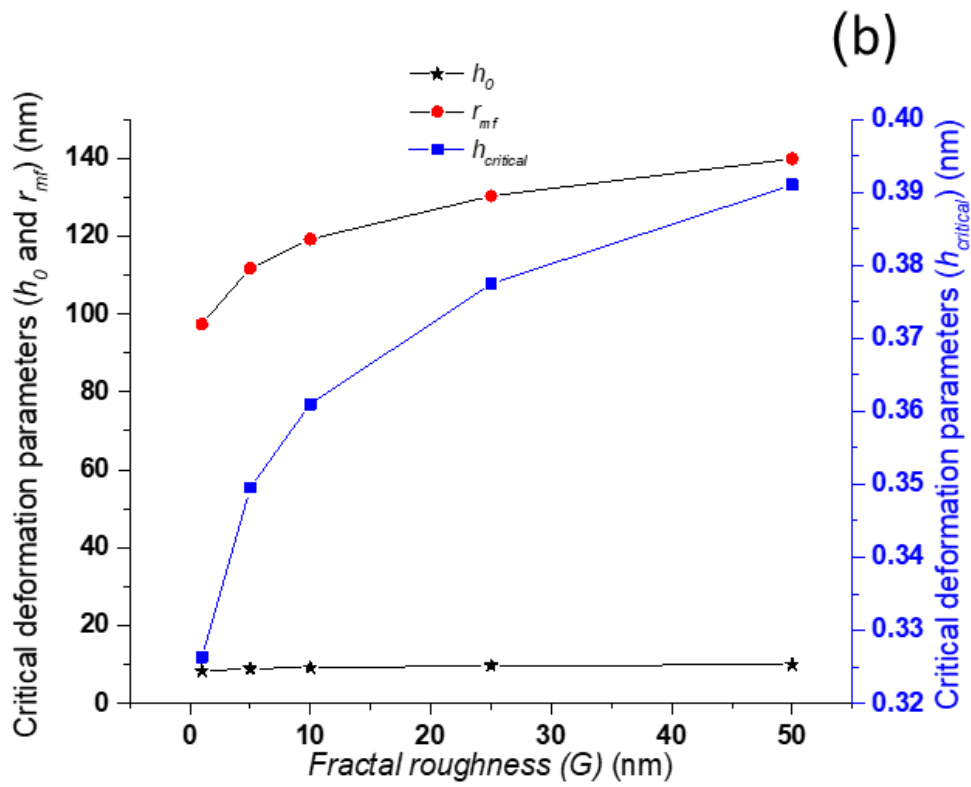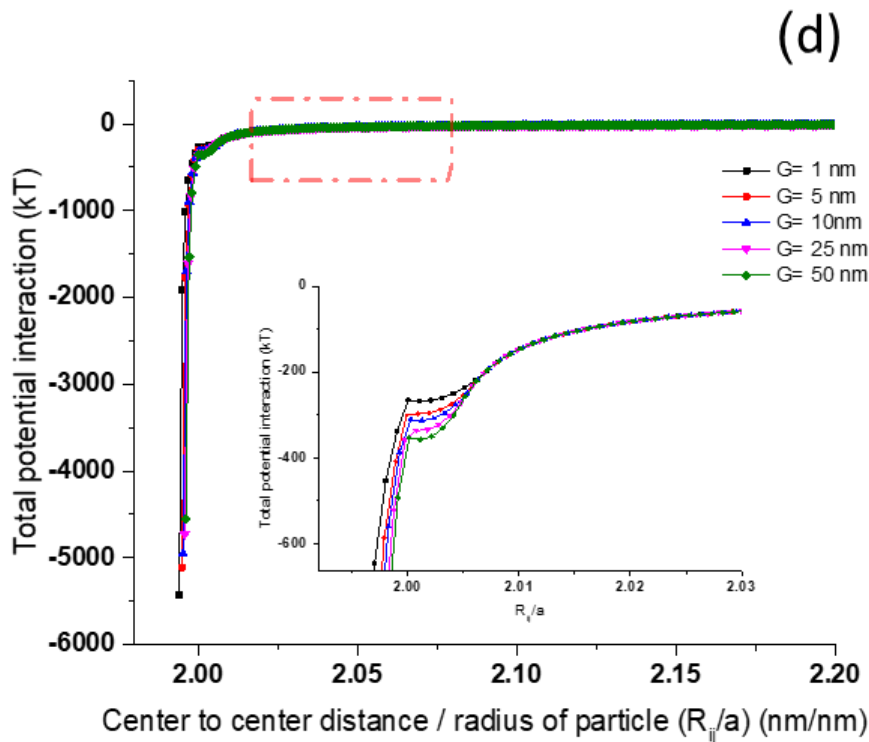
Figure 6.5 The effect of fractal roughness on particle deformation and particle interaction (a) deformation parameters of solid particles (b) deformation parameters of hollow particles (c) interaction energy of solid particles (d) interaction energy of hollow particles

6.4.5 The most effective parameter to impact deformation

A comparison between four types of particles were shown in Figure 6.6: Smooth (deformable/ non-deformable) vs rough (deformable/ non-deformable). The results confirmed that the surface roughness significantly reduced the potential interactions between deformable particles. Moreover, the primary minimum decreased and an energy barrier was created for deformable particles. This phenomenon suggested the important role of particle softness in the interfacial behaviors of particles.

The present study established a numerical model to investigate the impact of surface tension, particle size, and surface morphologies on particle deformation. The modeling results predicted that the particle size exhibited the most effective influence in controlling the deformation of particles (Figure 6.3). Moreover, it was observable that the surface morphology had a significant impact on particle deformation (Figures 6.4 and 6.5). The fractal dimension (Figure 6.4), which controlled the surface texture, showed more sensible impacts on particle deformability than fractal roughness (Figure 6.4a and 6.4b) because the fractal dimension was more influential in altering surface roughness than fractal

roughness was.
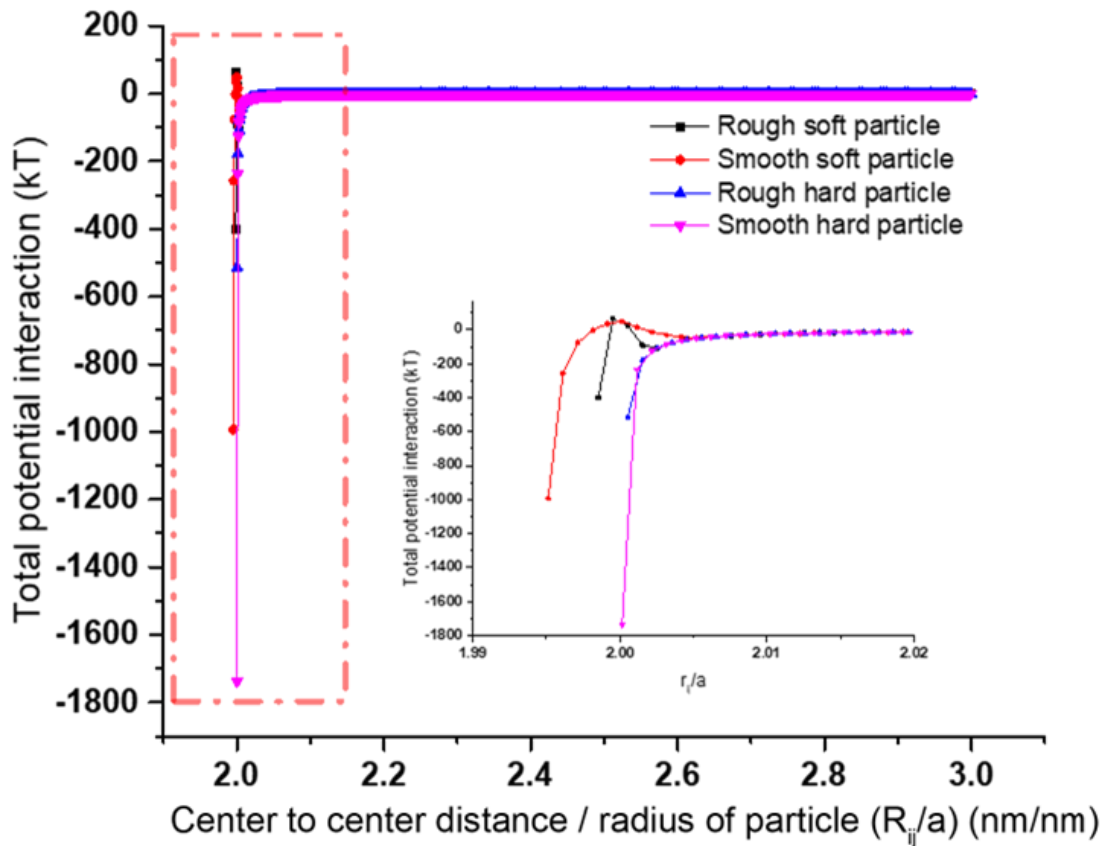
Figure 6.6 The difference in potential interaction between four types of particles

6.4.6 Comparison of results

To evaluate the accuracy of the results, the predicted results were compared with the experimental and

modeling results available in the literature, and the results are shown in Table 1.

Table 6.1 Comparison between past works and present modeling study

Type of works	Material	Interaction scenario	Key parameters	Results	Main conclusion
Experiment, [73]	Aluminum particle	Particle vs flat	Particle size	flattening parameters increased from 0.4 to 0.6	Smaller particles exhibited weak deformability
This model	-	Particle vs	a	r_{mf} enlarged from	r_{mf} increased

		particle		0.2 μm to 0.6 μm	with increasing the value of a
Experiment, [61]	polycrystalline α-SiC particles	Particle vs particle 49	Particle size	Yield stress decreased from 9.4 Mpa to 3.7 Mpa	Smaller particles exhibited weak deformability
This model	-	Particle vs particle	a	r_{mf} increased from a change of 0.5 μm to 0.8 μm	r_{mf} increased with increasing the value of a
Past modeling work, [50]	-	Asperity vs flat surface	D_f	Contact stiffness increased from 0.1 to 1.5 Kn/(N/m)	The contact stiffness increased with increasing the value of D_f
This model	-	Particle vs particle	D_f	r_{mf} dropped from 0.1 μm to 0.06 μm	r_{mf} increased with increasing the value of D_f
Past modeling work, [69]	-	Rough surface vs flat surface	G	Contact stiffness decreased from 10×10^{-12} to 1×10^{-12}K(N/mm^2)	The contact stiffness decreased with increasing the value of G
This model	-	Particle vs particle	G	r_{mf} enlarged from 0.2 μm to 0.6 μm.	r_{mf} decreased with increasing the value of G

In the experimental study carried out using aluminum particles, when the particle size increased from 5 μm to 25 μm, the flattening parameters increased from 0.4 to 0.6 [73]. For the same size particles, our

modeling results predicted the enlargement of r_{mf} from 0.2 μm to 0.6 μm. When the size of polycrystalline α-SiC particles altered from 20 μm to 55 μm, the yield stress decreased from 9.4 Mpa to 3.7 Mpa [61]. The present model predicted the increase of r_{mf} from 0.5 μm to 0.8 μm under the same conditions. Although previous experimental studies applied different parameters to describe particle deformation, the impact of particle size on particle deformation predicted in our numerical work is similar. The increased particle size elevated the flattening parameters and decreased yield stress mentioned previously [61, 73], which represented the improved deformability of particles. Our numerical results also showed that the radius of the deformation region increased with elevating the particle size. Therefore, the previous experimental results [61, 73] could verify the predictions of the present model.

In another work, the interaction of a rough surface with a flat surface was studied, and the results demonstrated that the stiffness of the material surface increased from 0.1 to 1.5 Kn/(N/m) when D_f increased from 2.4 to 2.7 [50]. Even though our model aimed at constructing a noncontact interaction scenario, the predicted results showed that r_{mf} dropped from 0.1 μm to 0.06 μm under the same conditions. In another modeling study, when two rough particles were contacted, the value of stiffness decreased from 10×10^{-12} to 1×10^{-12} K (N/mm²) when G increased from 1×10^{-16} m to 1×10^{-13} m [69]. Our current work applied a noncontact interaction scenario and predicted that r_{mf} would increase from 0.5 μm to 0.6 μm when G changed from G increased from 1×10^{-16} m to 1×10^{-13} m. The contact stiffness in the past modeling work represented the resistance to deformation upon the impact of surface morphology. Therefore, the decreased value of contact stiffness implies the reduced resistance ability of deformation, which could be expressed by the increased value of r_{mf} in the present model. Although the parameter of deformation is different in the previous and current models, the present model suggested that surface roughness would improve the deformability of particles. Even though the present model considered the surface morphology and geometrical structure (solid and hollow) in assessing the non-contact interaction energy between deformable particles, the predicted results successfully anticipated similar trends to what was reported in the literature [50, 61, 69, 73]. Therefore, the present simulation analysis displayed an accurate prediction of deformable particle interaction and deformation.

The present modeling study provides a novel method to evaluate the potential energy between two

rough and deformable particles with randomly rough surface morphology. By applying this strategy, the effect of surface morphology of deformable particles on their interactions in colloidal systems can be addressed. The proposed model demonstrated the relationship between surface morphology and surface deformation in a non-contact scenario.

6.4.7 Application

The predicted results suggested that compared with the regular hard particle, the deformable particle could exhibit some advantages in industrial applications, for example, softer vesicles required stronger adhesion energy to achieve successful internalization compared to the rigid vesicles [74]. Therefore, altering the surface softness could be considered a new direction in optimizing the properties of products.

Although previous work mainly simulated the hard particle interaction and concluded that the surface roughness had significant effects on hard particle interfacial behaviours, the present model considered softness and demonstrated that the surface morphology also had significant impacts on deformable particle interaction. The predicted results may facilitate the surface modification method for improving the efficiency of coagulation or deposition by controlling the surface roughness height or density of the deformable material.

The model may also provide a new direction to control surface morphology by a surface modification approach to achieve the optimal deformability of material [75-77]. To achieve this purpose, applying a coating technique may help, for example, coating bacterial cells with polypyrrole [78], or changing the density of the crosslinking between the polymer chains [79] to increase the softness by constructing a rougher surface. Moreover, our modeling results could provide a novel insight into improving material interfacial behaviors by modifying particle surface softness instead of only altering particle size or surface morphology [80].

6.5 Conclusion

We hypothesized that the total potential interaction developed between two deformable particles in colloidal systems would be dependent on the surface morphology of rough particles, and it could be simulated if the aspects of particle properties and surface morphology were considered. We constructed the deformation models of deformable solid and hollow particles and simulate the interaction and

deformation between randomly rough particles.

Previously, the interaction of non-deformable particles was primarily simulated [47, 48, 81-89]. When the impact of surface softness was considered, the reports were mainly focused on the smooth surface or particles and the simulated interaction scenario was the contact interaction [31, 90]. As the present numerical model included the fractal geometry theory to construct a randomly rough deformable surface to accurately capture the characteristics of the naturally rough surface, it generally predicted the non-contact interaction of the rough deformable particles more accurately than the previous experimental and theoretical studies [31, 68, 90].

The modeling results showed that the most effective parameter in affecting the deformability of particles is particle size. When the solid particle size increased from 10 nm to 1000 nm, the deformation critical parameter increased, especially r_{mf} increased from 5 nm to 90 nm. The deformation critical parameters decreased with elevating surface tension, but the attraction energy increased with increasing surface tension significantly in solid particle interactions, facilitating particle adhesion. The comparison between deformable and hard particles showed that the deformable particle exhibited a shallower primary minimum than hard particles, promoting the dissociation of deformable particles.

Our simulation process also considered the impacts of surface morphology, and the results showed that the potential energy of solid and hollow particles increased with the enlarged value of a fractal dimension, but the critical parameters of deformation decreased with an increased fractal dimension. Although the energy barrier disappeared in hollow particle interactions, the variation in the total potential energy showed a similar tendency compared to solid particle interaction when considering the rough surface morphology. The controversial prediction was observed in increasing the fractal roughness. Our simulation suggested that surface morphology played an important role in affecting the interfacial behavior and surface softness of solid and hollow particles. Compared to the interaction between smooth particles, the interaction between rough particles provided a shallower primary minimum, which suggested the easier disaggregation of rough particles.

As particles have different softness and surface morphology in natural systems, the proposed model can precisely predict the interfacial behaviors of particles by considering softness, surface morphology and geometrical structure simultaneously. To improve the accuracy of the simulation, future numerical work should account for the contributions of deformable asperities effects on the interaction of solid and

hollow particles.

6.6 Reference

[1] H. Giesche, Medical andTechnological Application of Monodispersed Colloidal Silica Particles, Medical Applications of Colloids, Springer2008, pp. 174-304.

[2] S. Hotchandani, P.V. Kamat, Charge-transfer processes in coupled semiconductor systems. Photochemistry and photoelectrochemistry of the colloidal cadmium sulfide-zinc oxide system, The Journal of Physical Chemistry, 96 (1992) 6834-6839.

[3] P.S. Mohanty, D. Paloli, J.J. Crassous, E. Zaccarelli, P. Schurtenberger, Effective interactions between soft-repulsive colloids: Experiments, theory, and simulations, The Journal of chemical physics, 140 (2014) 094901.

[4] L. Berthier, A.J. Moreno, G. Szamel, Increasing the density melts ultrasoft colloidal glasses, Physical Review E, 82 (2010) 060501.

[5] D. Heyes, A. Brańka, Interactions between microgel particles, Soft Matter, 5 (2009) 2681-2685.

[6] F. Brochard-Wyart, P.-G. de Gennes, Unbinding of adhesive vesicles, PG De Gennes' Impact on Science—Volume II: Soft Matter and Biophysics, World Scientific2009, pp. 139-145.

[7] Y.-S. Chu, S. Dufour, J.P. Thiery, E. Perez, F. Pincet, Johnson-Kendall-Roberts theory applied to living cells, Phys. Rev. Lett., 94 (2005) 028102.

[8] A. Lau, M. Portigliatti, E. Raphaël, L. Léger, Spreading of latex particles on a substrate, EPL (Europhysics Letters), 60 (2002) 717.

[9] H. Hertz, On the contact of solids—on the contact of rigid elastic solids and on hardness, Miscellaneous papers, (1896) 146-183.

[10] K. Johnson, Kendall. K, and Roberts AD Surface energy and the contact of elastic solids, Proceedings of the Royal Society of London, Series A (Mathematical and Physical Sciences), 324 (1971) 301-313.

[11] B.V. Derjaguin, V.M. Muller, Y.P. Toporov, Effect of contact deformations on the adhesion of particles, Journal of Colloid and interface science, 53 (1975) 314-326.

[12] M.E. Shanahan, Adhesion of a liquid-filled spherical membrane, The Journal of Adhesion, 79 (2003) 881-891.

[13] K.-T. Wan, K.-K. Liu, Contact mechanics of a thin-walled capsule adhered onto a rigid planar substrate, Med. Biol. Eng. Comput., 39 (2001) 605-608.

[14] K.-K. Liu, K.-T. Wan, New model to characterise cell-substrate adhesion in the presence of osmosis, Med. Biol. Eng. Comput., 38 (2000) 690-691.

[15] G. Ahmed, V.V. Kalinin, O. Arjmandi-Tash, V.M. Starov, Equilibrium of droplets on a deformable substrate: Influence of disjoining pressure, Colloids Surf. Physicochem. Eng. Aspects, 521 (2017) 3-12.

[16] L.R. White, The contact angle on an elastic substrate. 1. The role of disjoining pressure in the surface mechanics, Journal of colloid and interface science, 258 (2003) 82-96.

[17] J. Yin, M. Retsch, E.L. Thomas, M.C. Boyce, Collective mechanical behavior of multilayer colloidal arrays of hollow nanoparticles, Langmuir, 28 (2012) 5580-5588.

[18] K. Geisel, A.A. Rudov, I.I. Potemkin, W. Richtering, Hollow and core–shell microgels at oil–water interfaces: Spreading of soft particles reduces the compressibility of the monolayer, Langmuir, 31 (2015) 13145-13154.

[19] H. Bargozin, R. Hadadhania, H. Faraji, M. Yavari, The DLVO energy interaction of nanorough surfaces by spherical coordinates, Journal of Dispersion Science and Technology, 37 (2016) 884-893.

[20] S. Bhattacharjee, C.-H. Ko, M. Elimelech, DLVO interaction between rough surfaces, Langmuir, 14 (1998)

3365-3375.

[21] Z. Chen, Y. Liu, P. Zhou, A comparative study of fractal dimension calculation methods for rough surface profiles, Chaos, Solitons & Fractals, 112 (2018) 24-30.

[22] K.A. Moxon, N.M. Kalkhoran, M. Markert, M.A. Sambito, J. McKenzie, J.T. Webster, Nanostructured surface modification of ceramic-based microelectrodes to enhance biocompatibility for a direct brain-machine interface, IEEE Trans. Biomed. Eng., 51 (2004) 881-889.

[23] L. Zhao, M. Zhang, Y. He, J. Chen, H. Hong, B.-Q. Liao, H. Lin, A new method for modeling rough membrane surface and calculation of interfacial interactions, Bioresour. Technol., 200 (2016) 451-457.

[24] H. Hong, H. Lin, R. Mei, X. Zhou, B.-Q. Liao, L. Zhao, Membrane fouling in a membrane bioreactor: a novel method for membrane surface morphology construction and its application in interaction energy assessment, J. Membr. Sci., 516 (2016) 135-143.

[25] M. Zhang, X. Zhou, L. Shen, X. Cai, F. Wang, J. Chen, H. Lin, R. Li, X. Wu, B.-Q. Liao, Quantitative evaluation of the interfacial interactions between a randomly rough sludge floc and membrane surface in a membrane bioreactor based on fractal geometry, Bioresour. Technol., 234 (2017) 198-207.

[26] N.A. Mishchuk, S.V. Verbich, S.S. Dukhin, Ø. Holt, J. Sjöblom, Rapid Brownian coagulation in dilute polydisperse emulsions, Journal of dispersion science and technology, 18 (1997) 517-537.

[27] H. Hayashi, S. Tsuneda, A. Hirata, H. Sasaki, Soft particle analysis of bacterial cells and its interpretation of cell adhesion behaviors in terms of DLVO theory, Colloids Surf. B. Biointerfaces, 22 (2001) 149-157.

[28] J. Škvarla, J. Škvarla, A unified analysis of the coagulation behaviour of silica hydrosols—when the colloid and polymer science meet, Colloid and Polymer Science, 298 (2020) 123-138.

[29] J. Toro-Mendoza, A. Lozsan, M. Garcia-Sucre, G. Urbina-Villalba, Influence of droplet deformability on the coalescence rate of emulsions, Physical Review E, 81 (2010) 011405.

[30] I.U. Vakarelski, A. Toritani, M. Nakayama, K. Higashitani, Effects of particle deformability on interaction between surfaces in solutions, Langmuir, 19 (2003) 110-117.

[31] K. Danov, D. Petsev, N. Denkov, R. Borwankar, Pair interaction energy between deformable drops and bubbles, The Journal of chemical physics, 99 (1993) 7179-7189.

[32] P. Kralchevsky, K. Nagayama, Particles at fluid interfaces and membranes: attachment of colloid particles and proteins to interfaces and formation of two-dimensional arrays, Elsevier2001.

[33] P. Osorio, G. Urbina-Villalba, Influence of drop deformability on the stability of decane-in-water emulsions, Journal of Surfactants and Detergents, 14 (2011) 281-300.

[34] R.A. Ramli, Hollow polymer particles: a review, RSC Adv., 7 (2017) 52632-52650.

[35] D.N. Petsev, Interaction and adhesion of vesicles: Coupling between attractive interactions and bilayer membrane flexibility, Langmuir, 15 (1999) 1096-1100.

[36] Q. Shen, New insight on critical Hamaker constant of solid materials, Materials Research Bulletin, 133 (2021) 111082.

[37] K. Danov, N. Denkov, D. Petsev, I. Ivanov, R. Borwankar, Coalescence dynamics of deformable Brownian emulsion droplets, Langmuir, 9 (1993) 1731-1740.

[38] I. Ivanov, D. Dimitrov, P. Somasundaran, R. Jain, Thinning of films with deformable surfaces: Diffusion-controlled surfactant transfer, Chem. Eng. Sci., 40 (1985) 137-150.

[39] T. Tadros, Colloid and interface aspects of pharmaceutical science, Colloid and Interface Science in Pharmaceutical Research and Development, Elsevier2014, pp. 29-54.

[40] K. Cooper, A. Gupta, S. Beaudoin, Simulation of the adhesion of particles to surfaces, Journal of colloid and interface science, 234 (2001) 284-292.

[41] J. Tao, K. Chen, X. Su, L. Ren, J. Zhang, L. Bao, H. Dong, G. Lu, Z. Teng, L. Wang, Virus-mimicking

mesoporous organosilica nanocapsules with soft framework and rough surface for enhanced cellular uptake and tumor penetration, Biomaterials Science, 8 (2020) 2227-2233.

[42] H. Bargozin, R. Hadadhania, H. Faraji, H. Yousefzadeh, Effect of rough nanoparticle orientation on DLVO energy interaction, Journal of Dispersion Science and Technology, 36 (2015) 755-764.

[43] G. Yu, X. Cai, L. Shen, J. Chen, H. Hong, H. Lin, R. Li, A novel integrated method for quantification of interfacial interactions between two rough bioparticles, Journal of Colloid and Interface Science, 516 (2018) 295-303.

[44] S. Wei, H. Zhao, J. Jing, Investigation on three-dimensional surface roughness evaluation of engineering ceramic for rotary ultrasonic grinding machining, Applied Surface Science, 357 (2015) 139-146.

[45] Y. Peng, Y. Guo, An adhesion model for elastic-plastic fractal surfaces, Journal of Applied Physics, 102 (2007) 053510.

[46] M.Y. Marusina, A.P. Mochalina, E.P. Frolova, V.I. Satikov, A.A. Barchuk, V.I. Kuznetcov, V.S. Gaidukov, S.A. Tarakanov, MRI image processing based on fractal analysis, Asian Pacific journal of cancer prevention: APJCP, 18 (2017) 51.

[47] X. Cai, M. Zhang, L. Yang, H. Lin, X. Wu, Y. He, L. Shen, Quantification of interfacial interactions between a rough sludge floc and membrane surface in a membrane bioreactor, Journal of colloid and interface science, 490 (2017) 710-718.

[48] R. Mei, R. Li, H. Lin, Z. Shen, M. Zhang, J. Chen, Y. He, A new approach to construct three-dimensional surface morphology of sludge flocs in a membrane bioreactor, Bioresour. Technol., 219 (2016) 521-526.

[49] X. Cai, L. Yang, Z. Wang, M. Zhang, L. Shen, H. Hong, H. Lin, G. Yu, Influences of fractal dimension of membrane surface on interfacial interactions related to membrane fouling in a membrane bioreactor, Journal of colloid and interface science, 500 (2017) 79-87.

[50] P. Liu, H. Zhao, K. Huang, Q. Chen, Research on normal contact stiffness of rough surface considering friction based on fractal theory, Applied Surface Science, 349 (2015) 43-48.

[51] W. Yan, K. Komvopoulos, Contact analysis of elastic-plastic fractal surfaces, Journal of Applied Physics, 84 (1998) 3617-3624.

[52] D. Lu, P. Fatehi, Interfacial interactions of rough spherical surfaces with random topographies, Colloids Surf. Physicochem. Eng. Aspects, 642 (2022) 128570.

[53] T. Breinlinger, P. Polfer, A. Hashibon, T. Kraft, Surface tension and wetting effects with smoothed particle hydrodynamics, Journal of Computational Physics, 243 (2013) 14-27.

[54] Y.T. He, J. Wan, T. Tokunaga, Kinetic stability of hematite nanoparticles: the effect of particle sizes, Journal of nanoparticle research, 10 (2008) 321-332.

[55] X. Chu, A. Nikolov, D. Wasan, Effects of particle size and polydispersity on the depletion and structural forces in colloidal dispersions, Langmuir, 12 (1996) 5004-5010.

[56] R. Pitchumani, B. Ramakrishnan, A fractal geometry model for evaluating permeabilities of porous preforms used in liquid composite molding, International Journal of Heat and Mass Transfer, 42 (1999) 2219-2232.

[57] J.K. Ferri, P. Carl, N. Gorevski, T.P. Russell, Q. Wang, A. Böker, A. Fery, Separating membrane and surface tension contributions in Pickering droplet deformation, Soft Matter, 4 (2008) 2259-2266.

[58] O.L. Boshkova, U.K. Deiters, Soft repulsion and the behavior of equations of state at high pressures, International Journal of Thermophysics, 31 (2010) 227-252.

[59] L. Sapir, D. Harries, Is the depletion force entropic? Molecular crowding beyond steric interactions, Current opinion in colloid & interface science, 20 (2015) 3-10.

[60] A. Neumann, D. Absolom, C. Van Oss, W. Zingg, Surface thermodynamics of leukocyte and platelet adhesion to polymer surfaces, Cell Biophys., 1 (1979) 79-92.

[61] Y. Yan, L. Geng, Effects of particle size on deformation behaviour of metal matrix composites, Materials science and technology, 23 (2007) 374-378.

[62] H. Ma, X.-L. Gao, A new homogenization method based on a simplified strain gradient elasticity theory, Acta Mechanica, 225 (2014) 1075-1091.

[63] W.-z. Yin, J.-z. Wang, Effects of particle size and particle interactions on scheelite flotation, Transactions of Nonferrous Metals Society of China, 24 (2014) 3682-3687.

[64] M.Y. Ismail, M. Patanen, S. Kauppinen, H. Kosonen, M. Ristolainen, S.A. Hall, H. Liimatainen, Surface analysis of tissue paper using laser scanning confocal microscopy and micro-computed topography, Cellulose, 27 (2020) 8989-9003.

[65] R. Yu, W. Chen, Fractal modeling of elastic-plastic contact between three-dimensional rough surfaces, Industrial Lubrication and Tribology, (2018).

[66] S. Jiang, Y. Zheng, H. Zhu, A contact stiffness model of machined plane joint based on fractal theory, (2010).

[67] M. Zhang, H. Hong, H. Lin, G. Yu, F. Wang, B.-Q. Liao, Quantitative assessment of interfacial forces between two rough surfaces and its implications for anti-adhesion membrane fabrication, Separation and Purification Technology, 189 (2017) 238-245.

[68] D. Lu, P. Fatehi, A modeling approach for quantitative assessment of interfacial interaction between two rough particles in colloidal systems, Journal of Colloid and Interface Science, 587 (2020) 24-38.

[69] X. Miao, X. Huang, A complete contact model of a fractal rough surface, Wear, 309 (2014) 146-151.

[70] S. Feng, G. Yu, X. Cai, M. Eulade, H. Lin, J. Chen, Y. Liu, B.-Q. Liao, Effects of fractal roughness of membrane surfaces on interfacial interactions associated with membrane fouling in a membrane bioreactor, Bioresour. Technol., 244 (2017) 560-568.

[71] H. Bargozin, R. Hadadhania, T. Amiri, Influence of chemical heterogeneity and nanoscale roughness on the DLVO energy interaction by spherical coordinates, Journal of Dispersion Science and Technology, 37 (2016) 806-815.

[72] E.M. Hoek, S. Bhattacharjee, M. Elimelech, Effect of membrane surface roughness on colloid− membrane DLVO interactions, Langmuir, 19 (2003) 4836-4847.

[73] P.C. King, M. Jahedi, Relationship between particle size and deformation in the cold spray process, Applied Surface Science, 256 (2010) 1735-1738.

[74] X. Yi, H. Gao, Incorporation of soft particles into lipid vesicles: Effects of particle size and elasticity, Langmuir, 32 (2016) 13252-13260.

[75] A. Oliva, E. Anguiano, M. Aguilar, Fractal dimension: measure of coating quality, Surface engineering, 15 (1999) 101-104.

[76] S. Amada, H. Yamada, Introduction of fractal dimension to adhesive strength evaluation of plasma-sprayed coatings, Surf. Coat. Technol., 78 (1996) 50-55.

[77] F. Li, J. Meng, J. Ye, B. Yang, Q. Tian, C. Deng, Surface modification of PES ultrafiltration membrane by polydopamine coating and poly (ethylene glycol) grafting: Morphology, stability, and anti-fouling, Desalination, 344 (2014) 422-430.

[78] R.B. Song, Y. Wu, Z.Q. Lin, J. Xie, C.H. Tan, J.S.C. Loo, B. Cao, J.R. Zhang, J.J. Zhu, Q. Zhang, Living and conducting: coating individual bacterial cells with in situ formed polypyrrole, Angewandte Chemie, 129 (2017) 10652-10656.

[79] H. Mehrabian, J.H. Snoeijer, J. Harting, Desorption energy of soft particles from a fluid interface, Soft matter, 16 (2020) 8655-8666.

[80] H. Ohshima, Theory of electrostatics and electrokinetics of soft particles, Science and Technology of Advanced Materials, 10 (2009) 063001.

[81] C. Van Oss, R. Giese, P.M. Costanzo, DLVO and non-DLVO interactions in hectorite, Clays Clay Miner., 38 (1990) 151-159.

[82] S. Bhattacharjee, M. Elimelech, M. Borkovec, DLVO Interaction between Colloidal Particles: Beyond Derjaguin's Approximation, Croat. Chem. Acta, 71 (1998) 883-903.

[83] G. Wiese, T. Healy, Effect of particle size on colloid stability, Transactions of the Faraday Society, 66 (1970) 490-499.

[84] H. Hong, X. Cai, L. Shen, R. Li, H. Lin, Membrane fouling in a submerged membrane bioreactor: New method and its applications in interfacial interaction quantification, Bioresource Technology, 241 (2017) 406-414.

[85] H. Bargozin, J. Moghaddas, Stability of nanoporous silica aerogel dispersion as wettability alteration agent, Journal of dispersion science and technology, 34 (2013) 1454-1464.

[86] J. Argent, S. Torkzaban, S. Hubbard, H. Le, T. Amirianshoja, M. Haghighi, Visualization of micro-particle retention on a heterogeneous surface using micro-models: influence of nanoscale surface roughness, Transport in Porous Media, 109 (2015) 239-253.

[87] E. Martines, L. Csaderova, H. Morgan, A. Curtis, M. Riehle, DLVO interaction energy between a sphere and a nano-patterned plate, Colloids Surf. Physicochem. Eng. Aspects, 318 (2008) 45-52.

[88] C.Q. LaMarche, S. Leadley, P. Liu, K.M. Kellogg, C.M. Hrenya, Method of quantifying surface roughness for accurate adhesive force predictions, Chem. Eng. Sci., 158 (2017) 140-153.

[89] R. Wilson, D. Dini, B.J.P.t. Van Wachem, The influence of surface roughness and adhesion on particle rolling, 312 (2017) 321-333.

[90] D.N. Petsev, N.D. Denkov, P.A. Kralchevsky, Flocculation of deformable emulsion droplets: II. interaction energy, Journal of colloid and interface science, 176 (1995) 201-213.

Chapter 7: Conclusion and Recommendation

The present work provided evidence that the total interfacial energy generated between rough particles in colloidal systems would be dependent on the surface morphology and properties of rough particles, and it could be predicted based on numerical method if characteristics of surface topographies and particle softness could be simulated

The numerical methods for constructing 1) the different geometrical shapes of particles, 2) flat and spherical surfaces with various surface morphologies, and 3) the different interaction models based on various interaction scenarios were reviewed comprehensively. The advantages and disadvantages of the summarized numerical approaches for constructing rough surfaces with different topographies and evaluating their interactions were discussed. Compared with the summarized numerical methods, the approaches that applied fractal geometry to construct randomly rough flat surfaces and particles could be considered the most accurate models to characterize the naturally rough surface and to evaluate the interaction energy between surfaces. The usefulness of modeling results drawn from the literature reviewed in this work suggests that the numerical model will provide deep insights into predicting the interaction of colloidal particles in different colloidal systems.

In addition, it was hypothesized that the surface morphology would impact the total interaction energy between two rough particles in colloidal systems and that it could be calculated based on the XDLVO theory if the characteristics of the rough surface could be simulated. In this chapter, the uniform shape of asperities was constructed on the particle surface by MATLAB and simulated the interaction of the particles with a novel SEI approach in the XDLVO theory. The simulated results showed that the total interfacial energy dropped significantly with increasing the asperity number and asperity ratio. The most effective parameter for constructing parameters to control the primary maximum and minimum was the particle size because the varied particle size would lead to an altered interaction area between two particles. Additionally, the more effective parameter of surface morphology in monitoring the interfacial interaction energy was the asperity ratio. The constructed model could accurately predict the stabilities of the particle system and control the interfacial behaviors of the desired particle, which may facilitate metal coating, mineral suspensions, and membrane fouling.

Moreover, as previous studies did not consider the impact of the location of asperities on the rough

surface of the particles, a modified two-variable WM function based on the fractal geometry was applied to construct a randomly rough spherical surface, which could accurately capture the details of surface morphology of a naturally rough surface. The constructed interaction model under XDLVO theory explored the influence of factors affecting the construction of rough particles with randomly located asperities on particle interactions. The simulation results showed that the fractal parameters significantly affected the interaction energy between randomly rough particles. The fractal dimension altered interfacial interaction of particles more effectively than the fractal roughness did. According to the predicted value of the primary maximum of the energy profile calculated by the XDLVO theory, changing the fractal dimension of the particle surface, for example via the coating particles can be considered the most effective method to modify the surface topography of the materials to control their stability in colloidal systems.

Also, a model was created to construct a randomly rough ellipsoidal morphology, which would represent the shape and surface properties of natural particles. It was the first time that the numerical prediction considered the effects of ellipsoidal particles and natural surface morphology on particle interaction. In this work, the total interfacial energy developed between rough ellipsoidal particles with randomly located asperities was studied, considering varied fractal dimensions, fractal roughness, particle shape, aspect ratio, particle size, and orientation angle. The modelling results showed that the increase in the surface roughness could notably reduce the interfacial interaction energy. The predicted results also concluded that the ellipsoidal particles may provide more benefits for particle retention than spherical particles do. The predicted results offered deep insights into the interfacial behavior of ellipsoidal particles in suspension systems. The constructed model may obtain some guidelines for understanding the interaction of particles in colloidal systems that contain ellipsoidal particles, such as α-Fe_2O_3 ellipsoids.

Furthermore, models were constructed to generate deformable solid and hollow particles and simulate the interaction of randomly rough deformable particles for the first time. The modeling results showed that the particle size was the most effective parameter in affecting the deformability of particles because the critical deformation parameters increased with the elevated particle size. When the solid particle size increased from 10 nm to 1000 nm, the deformation critical parameter increased, especially the radius of the deformation region increased from 5 nm to 90 nm. The comparison between deformable

and hard particles showed that the deformable particle exhibited a shallower primary minimum than hard particles, promoting the dissociation of deformable particles. The predicted results suggested that surface morphology played a key role in controlling the interfacial behavior and surface softness of solid and hollow particles. Additionally, the interaction between rough deformable particles provided a shallower primary minimum than that of smooth deformable particles, which suggested the rough deformable particles would be more easily dispersed in colloidal systems.

As particles have different morphologies, shapes, and owned soft surfaces in colloidal systems, the presented modeling approaches in this thesis provide a comprehensive insight into predictions of interfacial behaviors of natural particles, which can precisely predict the behavior of colloidal systems by considering surface morphologies, geometrical structure, and softness. The provided models could be applied in many industrial or medical fields, such as metal coating, mineral suspensions, drug delivery, and membrane fouling. The predicted results also could guide the surface modification strategies to improve the properties of products that are made from colloidal suspension systems.

Future work may consider the deformation of asperities located on rough surfaces in the simulation process. As the investigation of deformable particle interaction in this thesis assumed the asperities were rigid, the present model may face limitations if the material surface roughness is deformable. Therefore, considering the deformation of asperities in the simulation process would further improve the accuracy of predictions and extend the application of the constructed models. Additionally, the effect of shapes of asperities located on particle surfaces on the interaction of rough particles may be considered to find out how the shapes of asperities would impact the interaction of particles.

The deformation of non-spherical particles in the simulation analysis may also be included in future work since particles have varied shapes and dimensions in real colloidal systems. Current numerical work mainly assumed the deformation particle owned spherical shape. Although constructing the non-spherical particle may require more complicated numerical methods, the predictions in interaction energy from such models would be desirable.

Chapter 8: Appendix

Abbreviations

A_H	Hamaker constant
D	the closest distance between the two-particle surface (nm)
dA	the differential projected area of the differential element on membrane surface (m^2)
dr	differential area radius (m)
dS	the differential projected area of differential circular arc on the particle surface (m^2)
$d\theta$	differential angle along with θ coordinates (°)
$d\varphi$	differential angle along with φ coordinates (°)
h	the separation distance between two planar surfaces (nm)
$\vec{k}_i$	unit vector along positive z-direction
$\vec{n}_i$	the unit outward normal to the surface
D_{fi}	Fractal dimension
τ_i	Fractal roughness (nm)
$\phi_{m,n}$	random phase $[0, 2\pi]$
M	number of superposed ridges
L	sample length (m)
ψ	frequency density
ν_s	cutoff frequency (m)
R_a	average roughness of hemisphere
n_{max}	highest frequency
ΔG	interaction energy per unit area (mJ/m^2)
r_i	the radius of element (smooth) particle (nm)
R_i	the radius of rough particle (nm)
U	the interaction energy between the membrane surface and particle (kT)
γ	surface tension parameter (mJ/m^2)
$\varepsilon_r \epsilon_0$	the permittivity of the suspending liquid (C/Vm)
ζ	zeta potential (mV)
κ	reciprocal Debye screening length (1/nm)
θ	angle coordinate in the spherical coordinate system
φ	angle coordinate in the spherical coordinate system
λ	decay length of AB interactions in water (0.6 nm)
h_0	minimum equilibrium cut-off distance (0.158 nm)
Superscripts	
AB	Lewis acid-base
EL	electrostatic double layer
LW	Lifshitz-van der Waals
E	Surface extented
B	Bending
Total	total
+	electron acceptor
-	electron donor
o	column with small asperities
η	column with large asperities
α	poles area

	β	equator area
Subscripts		
	l	liquid
	w	water
	i	describing particle 1 and 2 (i=1,2)

8.1 A modeling approach for quantitative assessment of interfacial interaction between two rough particles in colloidal systems
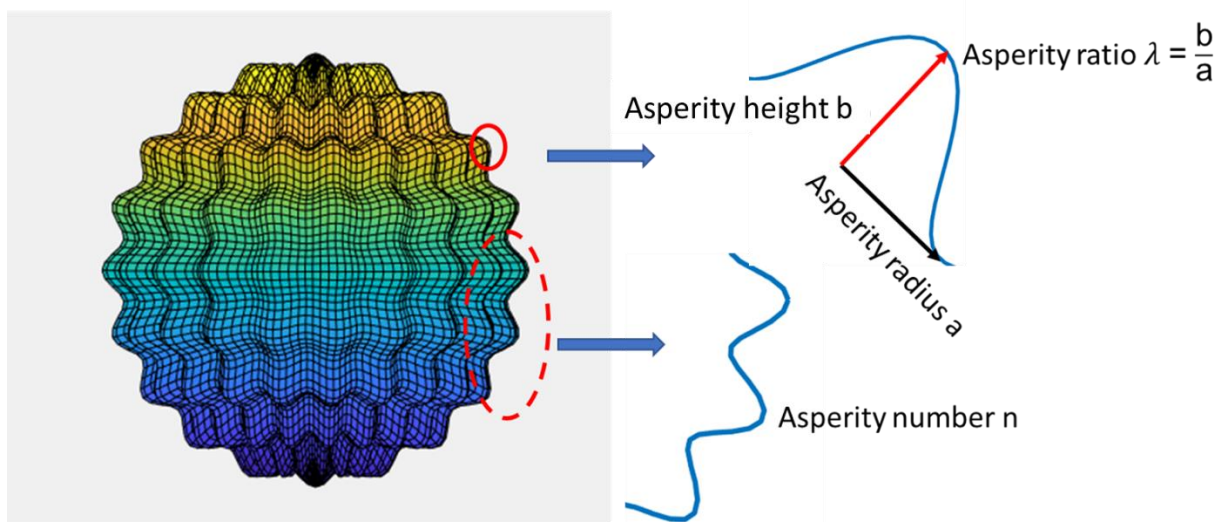


Figure A.1.1 The definition of asperity ratio and asperity number
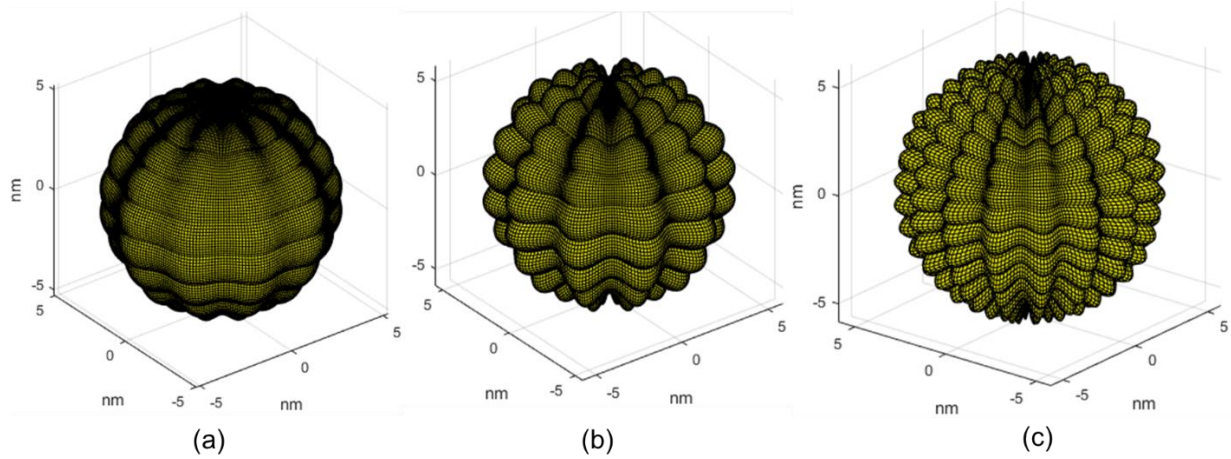
Figure A.1.2 Constructed rough particles with different parameters, (a) (r_i = 5 nm, n_i = 10, λ_i= 0.01), (b) (r_i = 5nm, n_i = 10, , λ_i= 0.1) and (c) (r_i = 5nm, n_i = 20, , λ_i= 0.1).

Table A.1.1 Surface tensions parameters (mJ/m^2) of liquid used in Young's equation [1]

Probe liquids	γ^{LW}	γ^+	γ^-	γ^{AB}	γ^{tol}
Water	21.8	25.5	25.5	51.0	72.8
Glycerol	34.0	3.9	57.4	30.0	64.0
Diiodomethane	50.8	0.0	0.0	0.0	50.8

Table A.1.2 Summary output of ANOVA data analysis of three models when the aspect ratio increases from 30 to 55

| Source of Variation	Aspect ratio from 30 to 50			Aspect ratio from 50 to 55		
	F	P-value	F crit	F	P-value	F crit
Three models	24.179	7.211E-11	3.009	6.032	0.003	3.052
Model 1 and Model 2	0.007	9.322E-01	3.862	0.001	0.972	3.929
Model 1 and Model 3	24.981	8.312E-07	3.862	6.211	0.014	3.929
Model 2 and Model 3	24.753	9.328E-07	3.862	6.166	0.015	3.929
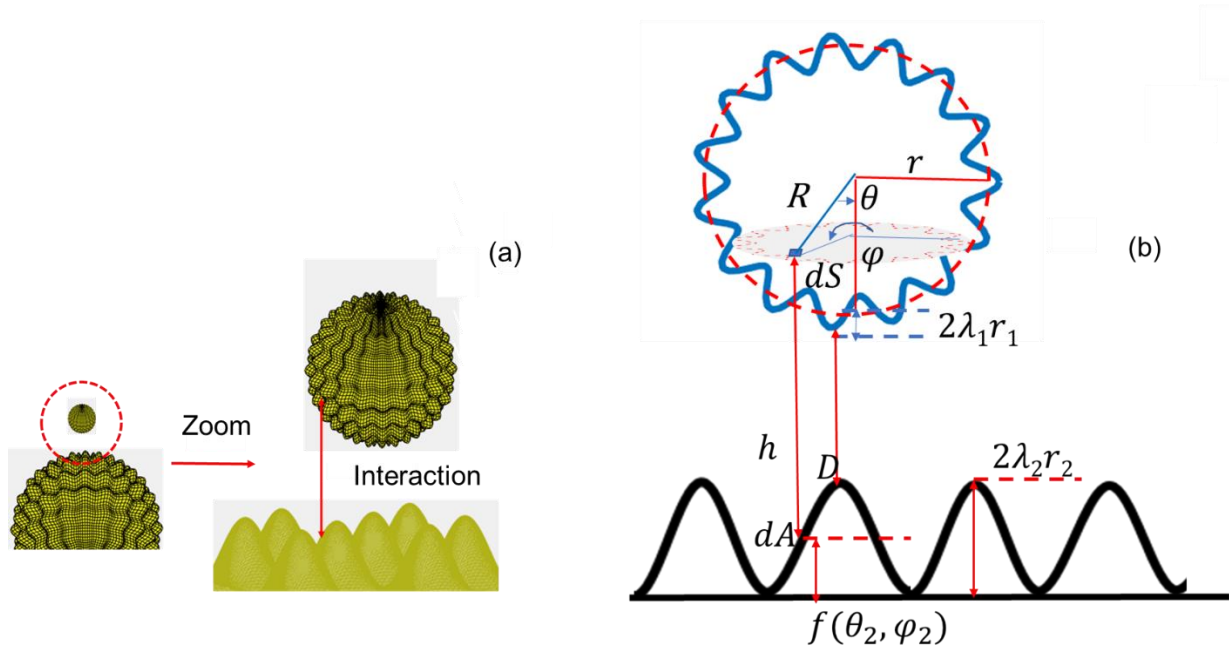
Figure A.1.3 Two rough particles interaction with the aspect ratio (r_2/r_1) between 30 and 50 (a) The 3D rough particles modeled by Matlab (b) the side view of 2D rough particle interactions
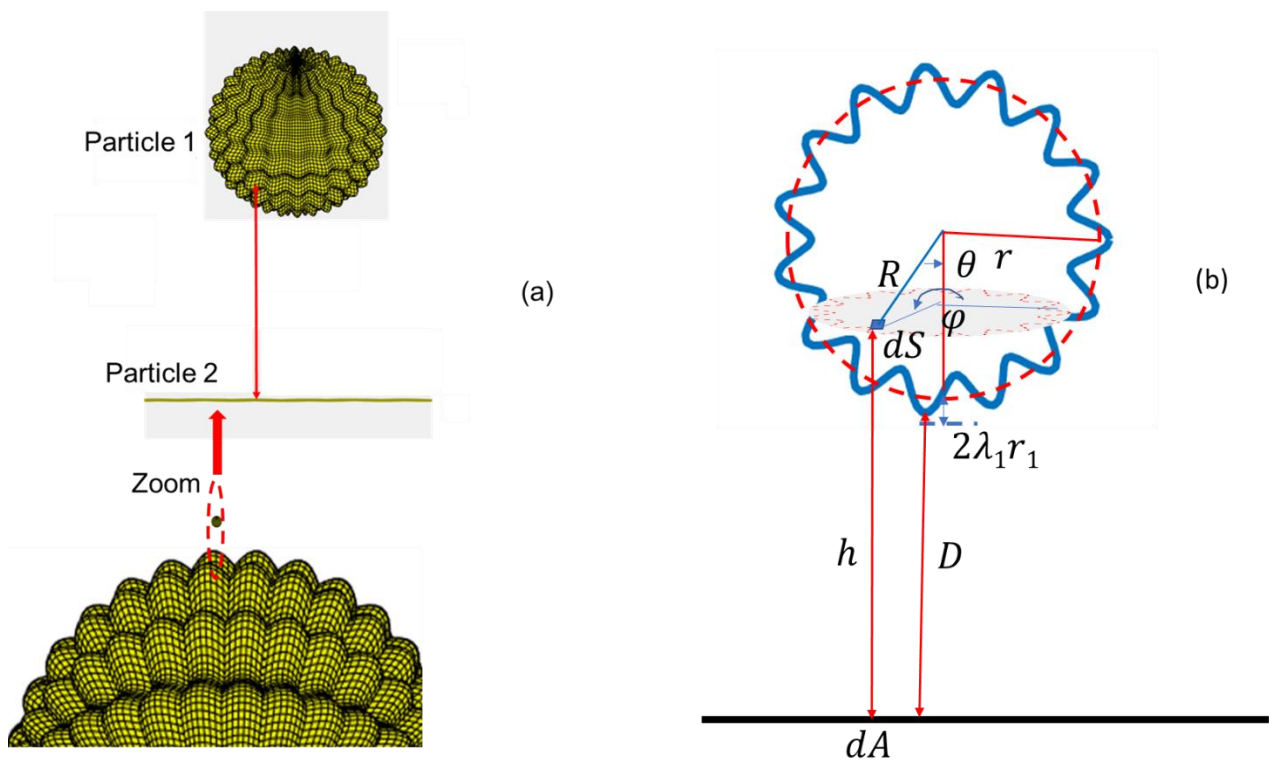

Figure A.1.4 Two rough particle interaction with the aspect ratio (r_2/r_1) of above 50) (a) The 3D rough particles modeled by Matlab (b) The side view of 2D rough particle interactions
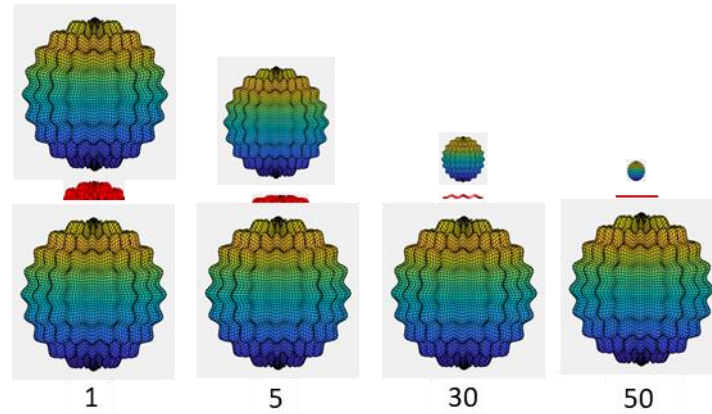
Figure A.1.5 Aspect ratio of particle 2 / particle 1 increased with the different relative shapes of particle 2 to particle 1 (The red region represents the relative shape of the large particle)

The relative shape changed from a rough sphere to a rough plate when the aspect ratio increased to 30. With further increasing the aspect ratio to 50, the relative shape of the large particle changed from a rough flat to a smooth flat.

8.1.1 Comparison of different models

The comparison of the three models when the aspect ratio was smaller than 30 is not involved in the present study because the relatively large particle can still be considered a sphere when the aspect ratio is smaller than 30 according to the literature [2]. Therefore, when the aspect ratio is smaller than 30, Model 1 is selected as the most accurate method to calculate the interaction between particles. According to Equations 24 and 26 (Figures A.1.3 and A.1.4), Model 2 and Model 3 were established to simulate rough particle interactions that had significantly different sizes. As shown in Figure A.1.5, when the aspect ratio was greater than 30, particle 2 could be regarded as a rough flat plate for particle 1 [2], and thus Model 2 was used for evaluating the interaction of particle 1 with a rough surface. Similarly, Model 3 constructed with Equation 26 was used in simulating particle 1 interaction with a smooth surface according to Figure A.1.4. To compare all models, the total interaction energy was calculated under the same conditions when the aspect ratio was changed from 30 to 55. The scale of the aspect ratio selected for this interval is based on the report by Bargonzin and coworkers [2], who viewed that a significantly large particle could be imaged as a rough flat surface for a small particle when the aspect ratio was above 30.

The comparison of results from three models via ANOVA test with replication was shown in Table A.1.2. Models 1, 2, and 3 have significant differences ($P < 0.05$, $F > F_{critical}$) when the aspect ratio was changed

from 30 to 55. This result indicated that Model 1 may not be accurate for prediction in the range of 30 to 55. When Model 1 and Model 2 were compared using the ANOVA test, the results had no significant difference ($P > 0.05$, $F < F_{critical}$). However, when Model 2 and Model 3 were compared or Model 1 and Model 3 were compared with the ANOVA test, the results showed a significant difference ($P < 0.05$, $F > F_{critical}$). Therefore, we concluded that the main reason for the significant difference between the three models was caused by the enormous gap in variances between Model 3 and the other two models. The aspect ratio of 30 was selected as an example shown in Figure A.1.6(a). The inserted graphs in the figures are used for improving the visibility of overlapped regions of the curves in the figures. Model 2 generated a deeper primary minimum than Model 1. In this case, because the aspect ratio of r_2/r_1 was increased significantly, the size of particle 1 is extremely small compared to particle 2, leading to a tiny project area of particle 1 on particle 2. Equation 24 predicted the separation distance between two different areas of particles, therefore, this equation in Model 2 did not consider the radius of particle 2. As a result, the value of h was smaller in Model 2 than in Model 1. Thus, the absolute values of U_{AB}, U_{LW}, U_{EL} would be larger based on equations 21-23 than those from equation 19. Although Model 2 predicted a deeper primary minimum, the accuracy of Model 1 is not affected when the aspect ratio was between 30 and 50 based on the ANOVA test. Therefore, Model 1 can replace Model 2 when the scale of aspect ratio is between 30 and 50.

When the aspect ratio enlarged more than 50, a significant difference ($P < 0.05$, $F > F_{critical}$) was observed between Models 1, 2, and 3 (Table S2). The results have no significant difference between Model 1 and Model 2 ($P > 0.05$, $F < F_{critical}$), which suggests that Model 1 could still be used in replacing Model 2 at this aspect ratio. However, the comparison between Model 2 and Model 3 or Model 1 and Model 3 also shows a significant difference. When the aspect ratio is above 50, Model 3 cannot be replaced by either Model 1 or Model 2 (Table A.1.2). This conclusion is still valid, although the simulation results made by Model 3 should match the results made by Model 1 or 2. In Model 3, the surface roughness and size of particle 2 were not considered in the simulation (Equation 26). The main reason for the significant difference in the simulation results is the interaction energy in the short-range between the particles (Figure A.1.6). In Figure A.1.6b, Model 3 displayed a much deeper primary minimum than Model 1 when the aspect ratio was 50 (Figure A.1.6b) because Model 3 did not count the asperity height where the projected area located on particle 2 surface. The effective separation

distance considered by Model 3 is smaller than that considered by Model 1 or Model 2, which provides a deeper primary minimum for the interaction of the rough particles. In addition, a previous study reported that the rough surface yielded a much shallower primary minimum than a smooth surface because it would significantly change the lever arms and adhesive torque [3, 4], which would also provide a reason for the deeper primary minimum predicted by Model 3. In our simulation studies, the large rough particle (particle 2) changed from a rough sphere to a smooth plate when the aspect ratio increased from 30 to 50 as shown in Figure A.1.4, which increased the primary minimum, and such a change induced a significant difference in ANOVA test for Model 3 compared with Model 1 or 2. However, considering a larger distance between the particles, the pattern generated by Model 3 is similar to that made by Model 1 or Model 2 as shown in Figure A.1.6. Thus, we considered Model 3 as a valid model in the simulation analysis. The reason for ignoring surface roughness at a large aspect ratio is that the surface asperities (Equation 11) depend on the particle radius. With enlarging particle 2 to infinite, the asperity size would be increased significantly. If particle 1 was small, the interacted area of the two particles could be located on a single large asperity of particle 2, and thus no surface roughness of particle 2 needs to be involved in the Model 3 simulation under these conditions (Figure A.1.4). In this case, we could image particle 1 interacting with a smooth flat plate instead of a spherical particle under our assumption. Thus, when the aspect ratio increases above 50, Model 3 would be more accurate than Model 1.

Therefore, only when the aspect ratio is greater than 50 (no roughness on particle 2), Model 3 can be used for improving the accuracy of the simulation results, and Model 1 can be applied to simulate the particle interactions instead of Model 2 if the aspect ratio is smaller than 50 in the present study. Based on the above evaluation results, Model 1 and Model 3 were selected to simulate the rough particle interactions in the following analysis. As we discussed above, particle 2 is regarded as a smooth plate in Model 3, and only particle 1 has variable parameters. Thus, Model 3 is mainly focused on the relative surface roughness and particle size effect analysis in the next sections.
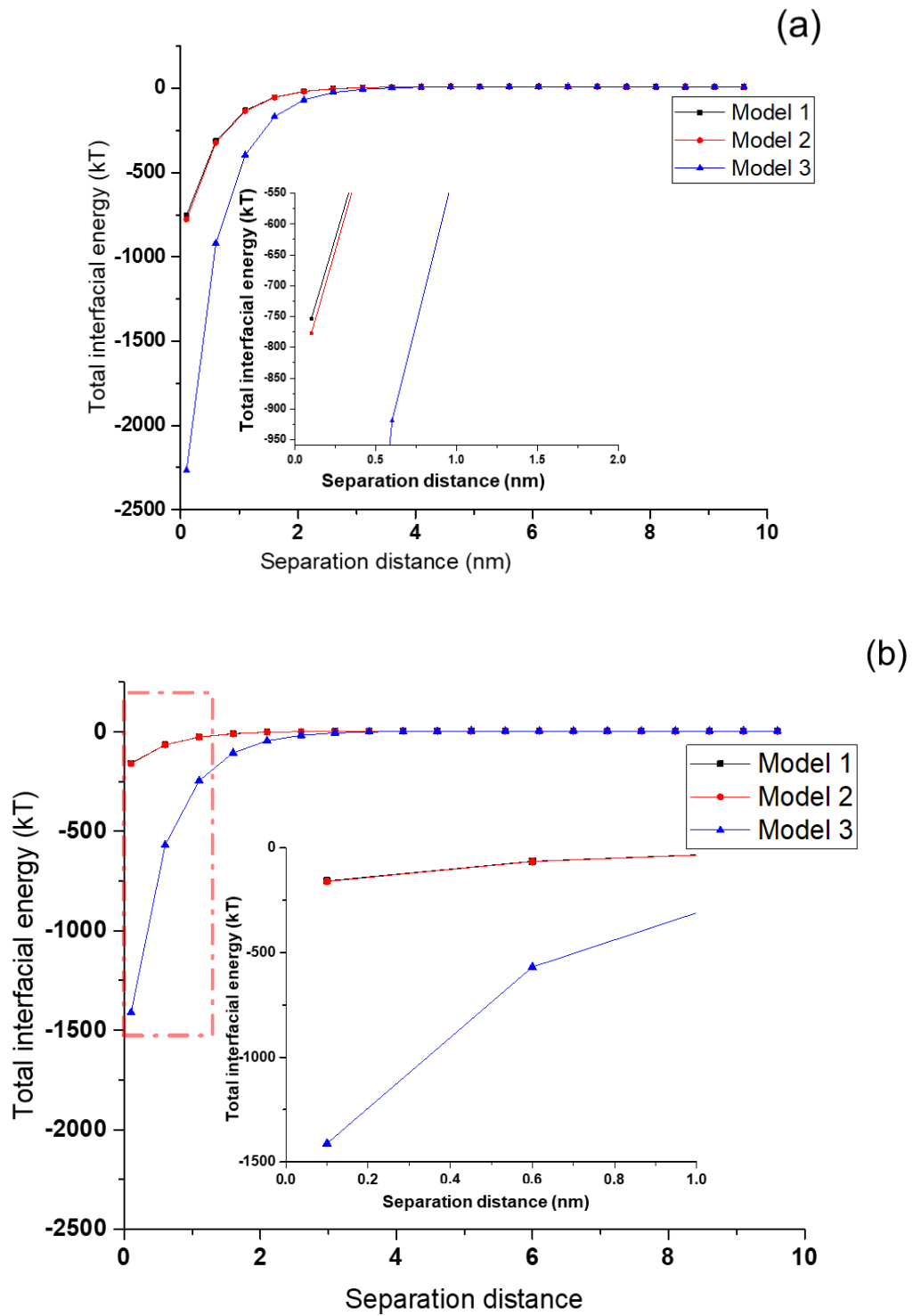
Figure A.1.6 The comparison with between Model 1, Model 2 and Model 3. (a) The aspect ratio is fixed at 30 (b) The aspect ratio is fixed at 50.
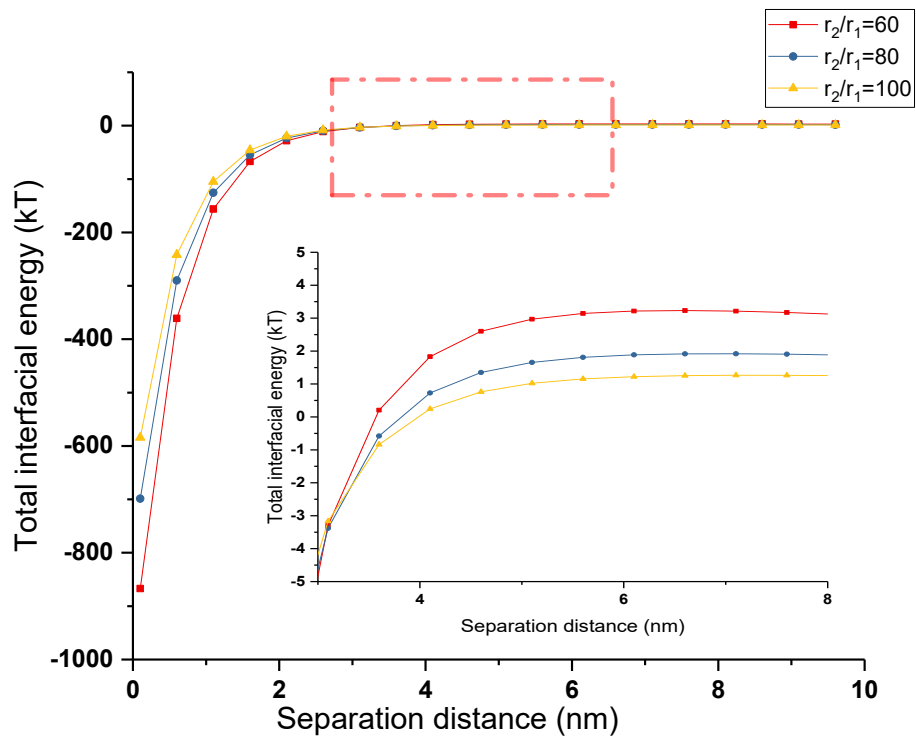
Figure A.1.7 Aspect ratio effects on total interfacial energy following Model 3 ($n_1 = 20, \lambda_1 = 0.005$)
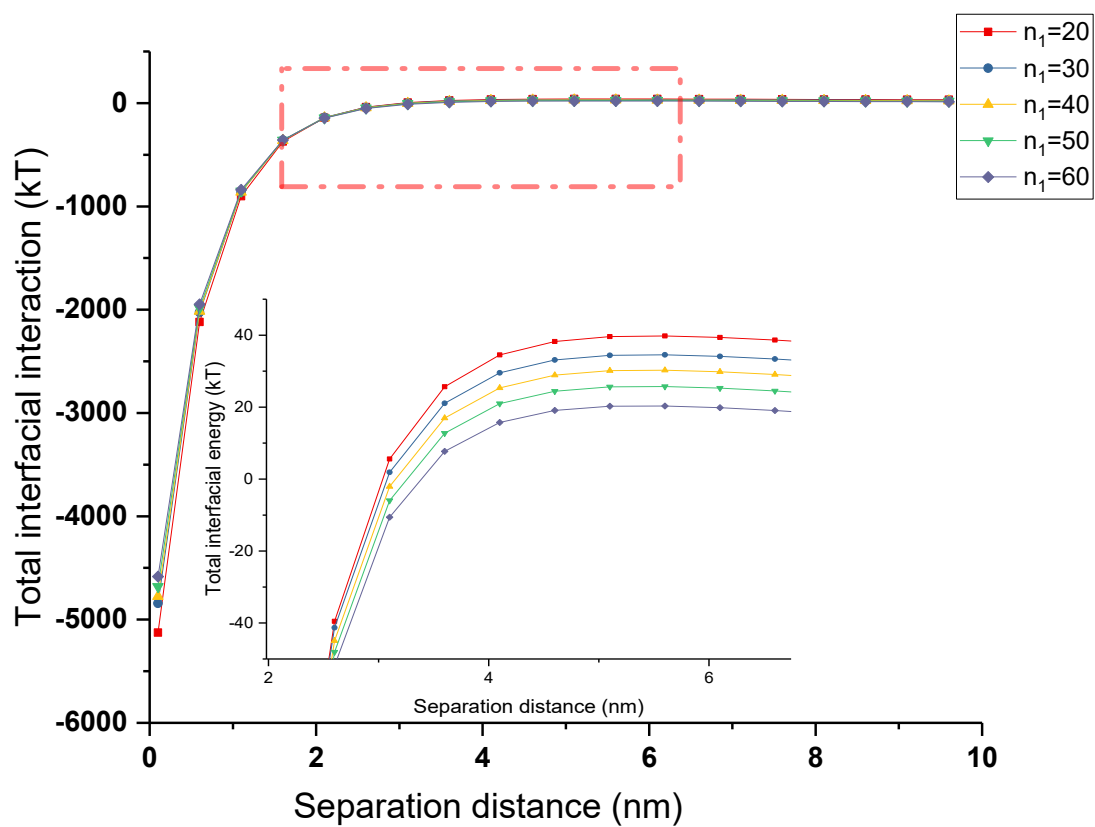
Figure A.1.8 Relative asperity number effects on total interfacial energy following Model 3 ($\lambda_1 = 0.001$, r1=100nm, r2=10000nm)
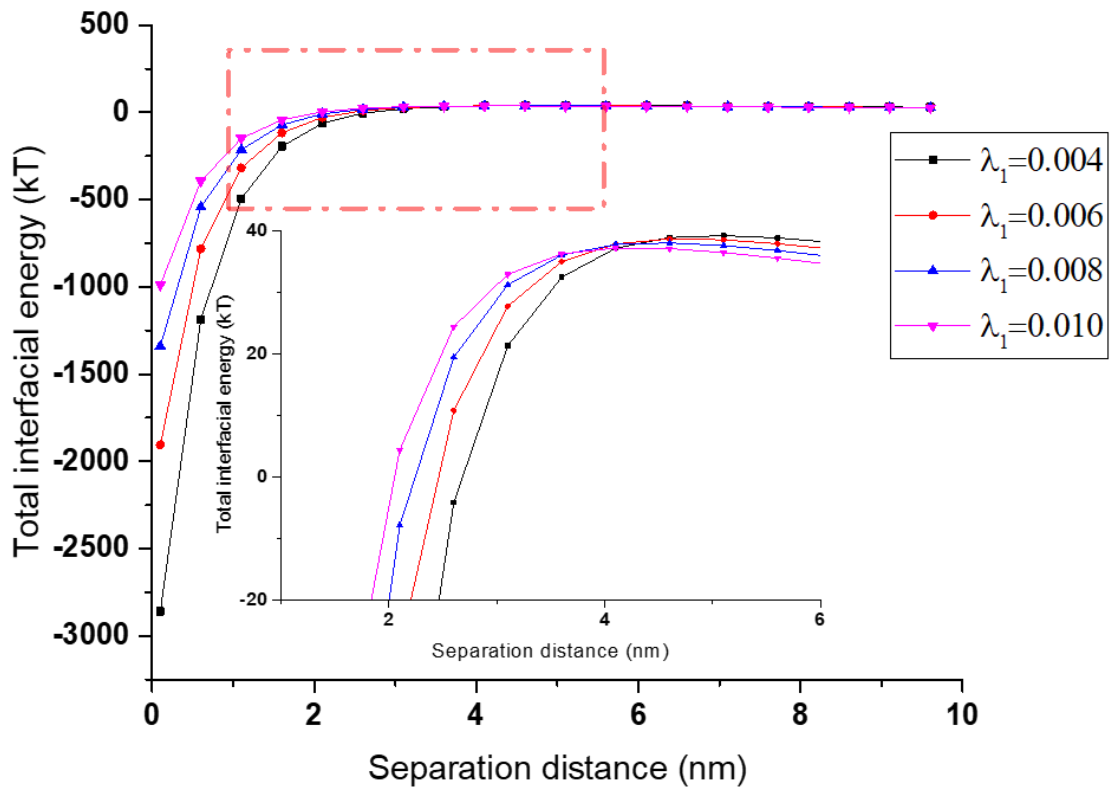
Figure A.1.9 Relative asperity ratio effects on total interfacial energy following Model 3 ($n_1 = 10$, r_1=100nm, r_2=10000nm)
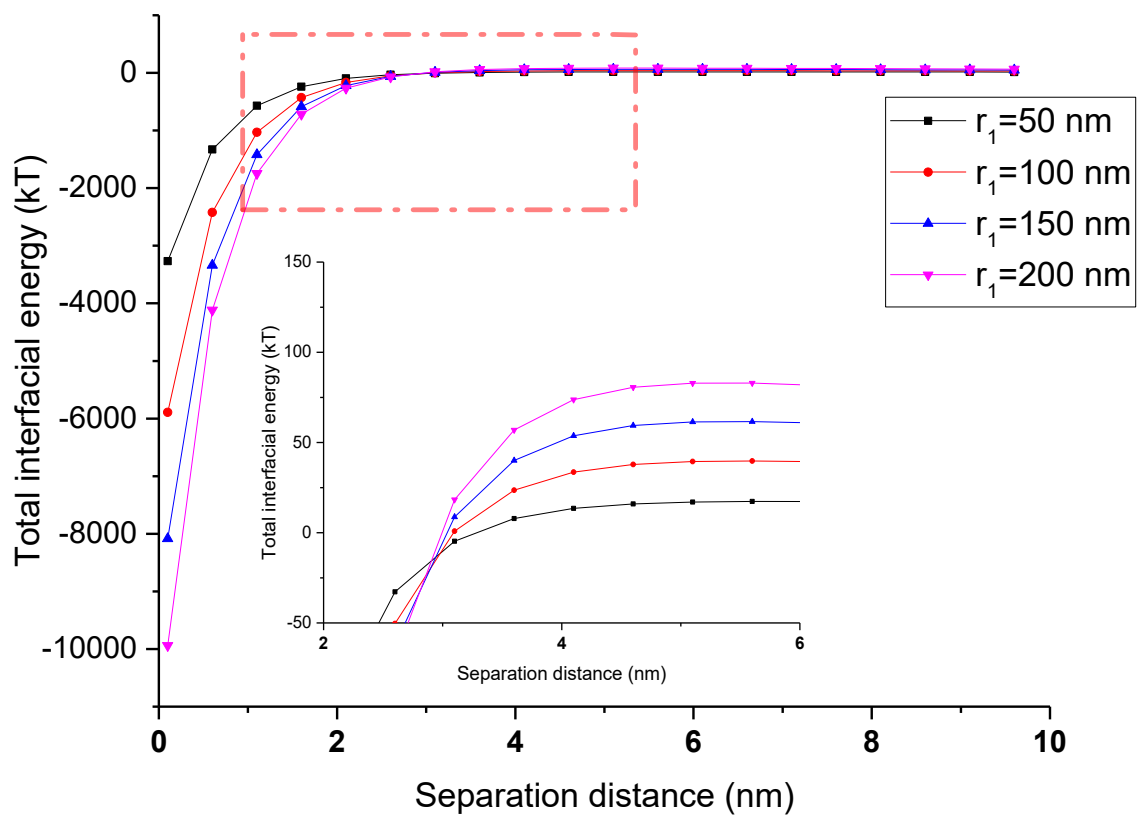
Figure A.1.10 Particle size effects on total interfacial energy following Model 3 ($n_1 = 10, \lambda_1 = 0.001$, r$_2$=10000nm)
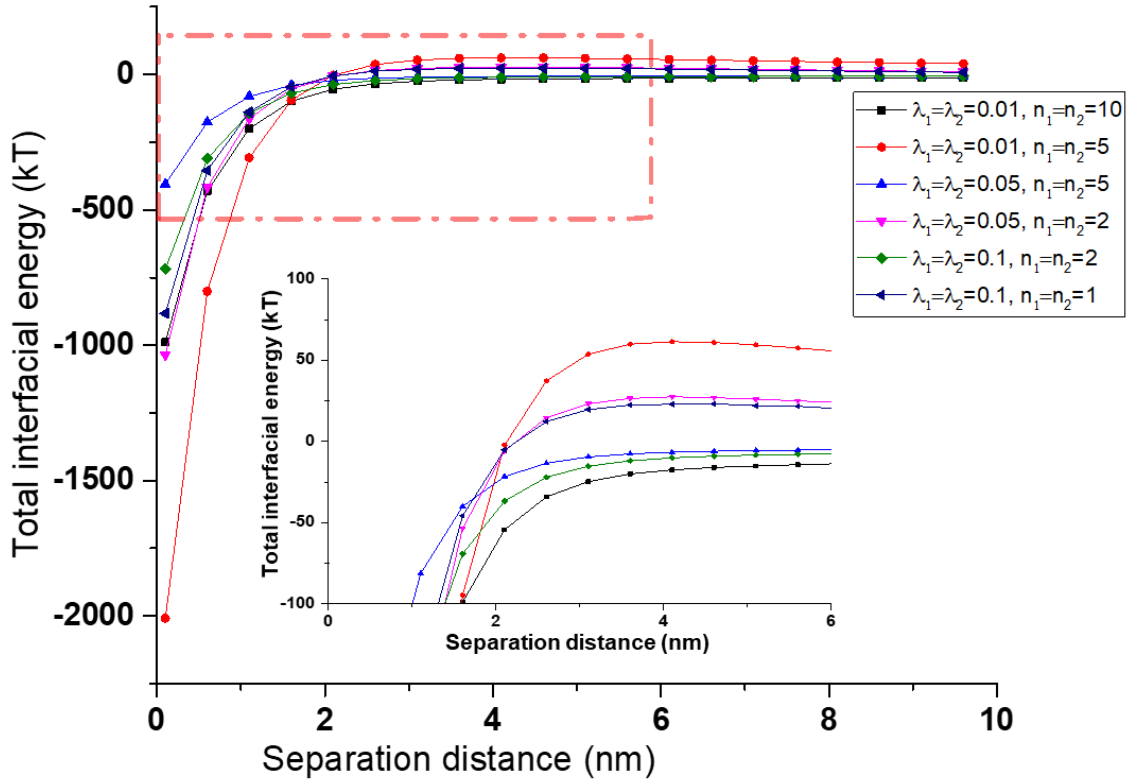
Figure A.1.11 The interfacial energy of two particles ($r_1=r_2=1000$ nm) with different asperity ratios and asperity numbers following Model 1

8.1.2 Proposed method verification

The correctness of the simulation could be verified in two strategies based on previous studies [1, 5, 6]. One is by comparing the present simulation with the classical method (DA) under predefined scenarios. The DA method has been verified as a correct methodology to simulate the interaction of two smooth spheres [7]. Once the results generated in the present work for the interaction of smooth particles agree with that of the DA method, it can be claimed that our results are accurate.

$$R_{effective} = \frac{R_1 R_2}{(R_1 + R_2)} \tag{A.1.1}$$

$$U_{LW} = 2\pi \Delta G_{h_0}^{LW} \frac{{h_0}^2 R_{effective}}{D} \tag{A.1.2}$$

$$U_{EL} = \pi \varepsilon_0 \varepsilon_r R_{effective} \left[2\xi_1 \xi_2 ln\left(\frac{1+e^{-\kappa D}}{1-e^{-\kappa D}}\right) + (\xi_1^2 + \xi_2^2) ln(1 - e^{-2\kappa D}) \right] \tag{A.1.3}$$

$$U_{AB} = 2\pi R_{effective} \nu \Delta G_{h_0}^{AB} \exp\left(\frac{h_0 - D}{\nu}\right) \tag{A.1.4}$$

The DA method to simulate two smooth particles was described in the supplementary material. The

parameters of Model 1 were set to r$_1$=r$_2$=1000 nm, n$_1$=n$_2$=0, which represents smooth particle interactions (i.e., with an asperity density of zero). As shown in Figure A.1.12, the two smooth particle interactions were simulated by the proposed method and compared with the DA method. The predicted trends of interaction energy by the present model agreed with the trend predicted by the DA method. Thus, the interaction of two smooth particles could be regarded as an exceptional scenario in the proposed method (when the asperity number equals 0). The agreement of prediction energy curves proves the correctness of our model.

Another strategy is to analyze the simulation error under different numbers of calculation segments. As the algorithm in the proposed study is a double integral, we applied the composite rule of Simpson to estimate the results. The calculation errors could be made in this approximating process. Thus, the balance of calculation error and calculation segments represent the correctness of the proposed method. In addition, the composite Simpson's rule can avoid the antiderivatives of Equations 3.21-3.23. The composite Simpson's rule is as follows (Equation A.1.5) [1, 6]:

$$\int_a^b \int_c^d f(\theta, \varphi) d\theta d\varphi = \sum_{l=1}^p \sum_{m=1}^q \int_{\varphi_{2l-2}}^{\varphi_{2l}} \int_{\theta_{2m-2}}^{\theta_{2m}} f(\theta, \varphi) d\theta d\varphi$$

$$\approx \frac{g\varrho}{9} \sum_{l=1}^p \sum_{m=1}^q (f_{2l-2,2m-2} + f_{2l,2m-2} + f_{2l,2m} + f_{2l-2,2m}) + 4(f_{2l-1,2m-2} +$$

$$f_{2l,2m-1} + f_{2l-1,2m} + f_{2l-2,2m-1}) + 16f_{2l-1,2m-1} \qquad (A.1.5)$$

Where $f_{l,m}$ is used for simplifying the function of $f(\theta, \varphi)$ in the composite Simpson's rule, the parameters p and q represent the number of the segments at the interval of $[a\,, b]$ at θ direction and the number of the segments at the interval of $[c\,, d]$ at φ direction, $\varphi_1 = a, \varphi_l = a + lg$ $(l = 1,2,\dots,2p + 1)$; $\theta_1 = c, \theta_m = c + mk$ $(m = 1,2,\dots,2q + 1)$; $g = (b - a)/2p$; $\varrho = (d - c)/2q$

The calculation error (E) of this algorithm is shown in Equation A.1.6 [6]:

$$E = \frac{(b-a)(c-d)}{180} \left[g^4 \frac{a\partial^4 f(\beta,\tau)}{\partial \varphi^4} + \varrho^4 \frac{\partial^4 f(\hat{\beta},\hat{\tau})}{\partial \theta^4} \right] \qquad (A.1.6)$$

Where $\boldsymbol{\beta}$ and $\widehat{\boldsymbol{\beta}}$, $\boldsymbol{\tau}$ and $\widehat{\boldsymbol{\tau}}$ represent the values of $[\boldsymbol{a}\,, \boldsymbol{b}]$ and $[\boldsymbol{c}\,, \boldsymbol{d}]$ intervals, respectively. The relationship between calculation error and the numbers of segments in hydrophobic interaction is shown in Figure A.12, which indicated that the larger segment number caused the lower calculation error. The pattern of Model 1, Model 2, and Model 3 suggested that the defined large segment numbers could provide validations for these three models. The results showed that the calculation error is less than 3% when the approximation segment reaches 3600 or more. Similar conclusions can be drawn for the

interaction of Van der Waals and the electric double layer. Therefore, the segment numbers are selected as 4000 for calculation. The calculation errors are negligible when the value is less than 3% in the simulation process, which also indicated the correctness of the proposed method.
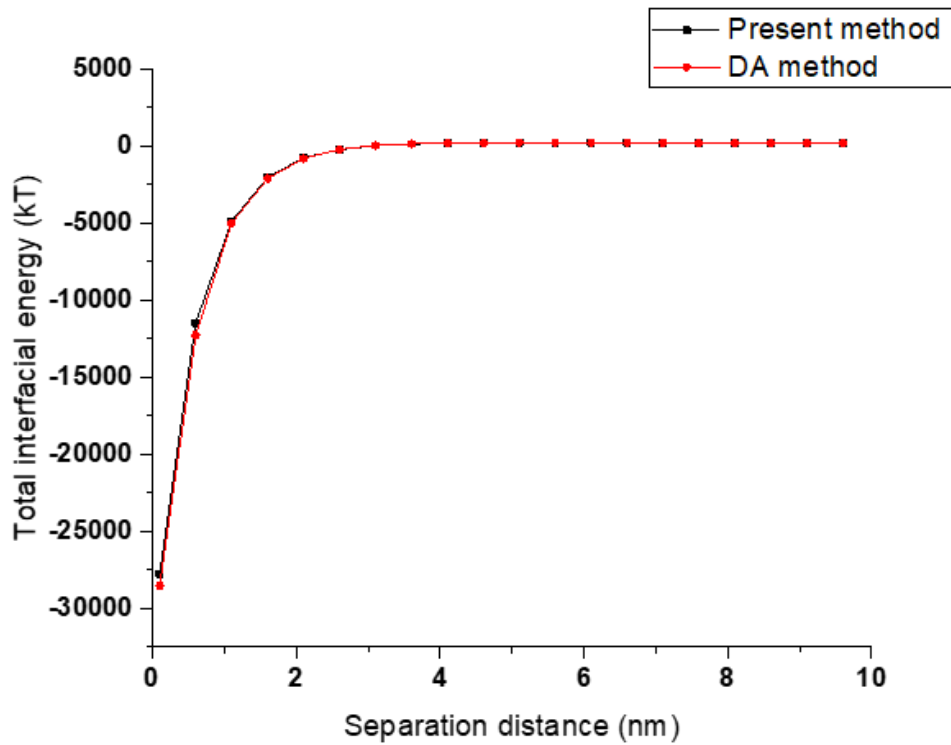

Figure A.1.12 The comparison between DA method and the present method

8.2 Interfacial interactions of rough spherical surfaces with random topographies
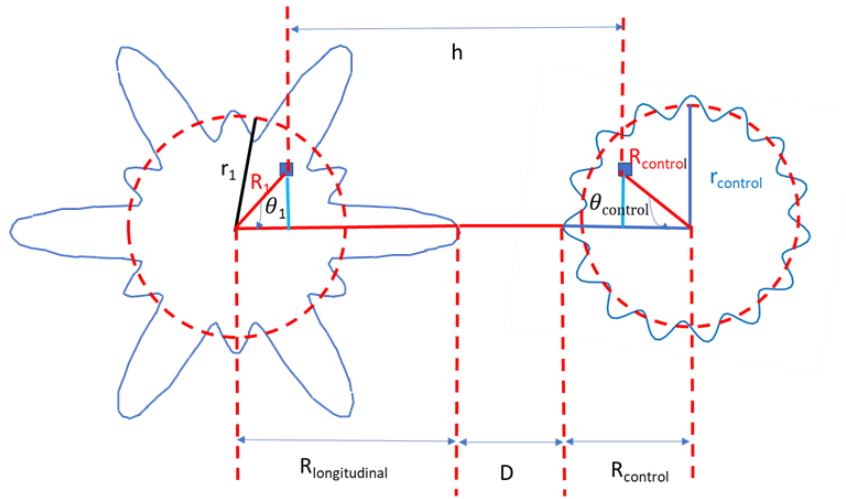
Figure A.2.1. Parameters involved in the interaction between a particle with longitudinally arranged asperities and a control particle
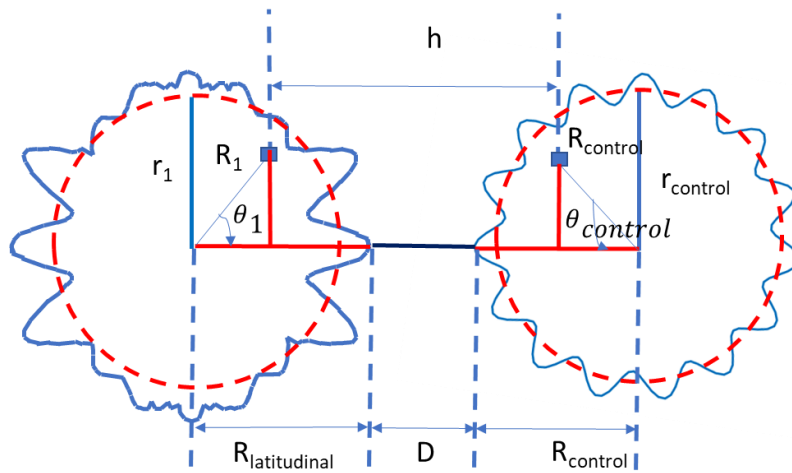
Figure A.2.2. Parameters involved in the interaction between a rough particle with latitudinally arranged asperities and a control particle

8.2.1 The transformation of coordinates

The spherical coordinates (R, θ, φ) were used to replace the cartesian coordinates (χ, y, z) for simplifying the calculation in the present study as shown in Equations A.2.1-A.2.3 [1].

$$\chi = R \sin \theta \cos \varphi \qquad (A.2.1)$$

$$y = R \sin \theta \sin\varphi \qquad (A.2.2)$$

$$z = R \cos \theta \qquad (A.2.3)$$

8.2.2 The numerical equations to define the fractal dimension and fractal roughness

In our model, a series of roughness spectrums contained in the WM function could be described by a

spectral density function.

$$S(\omega) = \frac{\tau^{2(D_f-1)}}{2ln\eta}\frac{1}{\omega^{(5-2D_f)}} \tag{A.2.4}$$

where ω and $S(\omega)$ represents the surface roughness frequency and the power of the spectrum, respectively; η represents the parameter of frequency density. The $S(\omega)$ can be calculated by following the Fast Fourier transform method [1]. For a fractal profile, plotting the logarithm of $S(\omega)$ to the logarithm of $S(\omega)$ would yield a straight line. The slope (k_p) and intercept (B) of the straight line could be obtained by regression analysis. Accordingly, solving Equations A.2.5 and A.2.6 could provide the data of D_f and τ.

$$k_p = 2D_f - 5 \tag{A.2.5}$$

$$B = 2(D_f - 1)lg\tau - lg\,(2ln\eta) \tag{A.2.6}$$

8.2.3 Young's equation and input parameter

The properties of particle surfaces can be expressed by solving them via Equation A.2.7 [2]. The surface tension values of liquid (γ_l^{LW}, γ_l^+, and γ_l^-) and contact angles (θ) also need to be measured for at least three different liquids (e.g., glycerol, diiodomethane, and water) to determine the solid surface tensions (γ_1^{LW}, γ_1^+, and γ_1^-). Table S1 lists surface tension parameters between two rough particles used in this study, which can be used to calculate Young's equation group in Equation A.2.7.

$$\frac{(1+cos\theta)}{2}\gamma_l^{Tol} = \sqrt{\gamma_l^{LW}}\sqrt{\gamma_1^{LW}} + \sqrt{\gamma_l^{-1}}\sqrt{\gamma_1^+} + \sqrt{\gamma_l^+}\sqrt{\gamma_1^{-1}} \tag{A.2.7}$$

Table A.2.1. Surface tensions parameters (mJ/m²) of liquid to set up Young's equation [3]

Probe liquids	γ^{LW}	γ^+	γ^-	γ^{AB}	γ^{tol}
Water	21.8	25.5	25.5	51.0	72.8
Glycerol	34.0	3.9	57.4	30.0	64.0

8.2.4 The unit vector calculation process

The unit vectors between two particles can be calculated as per Equation A.2.8 [1]:

$$\vec{o} = \frac{\frac{d\vec{r}}{d\theta}\times\frac{d\vec{r}}{d\varphi}}{|\frac{d\vec{r}}{d\theta}\times\frac{d\vec{r}}{d\varphi}|} \tag{A.2.8}$$

Where the $\frac{d\vec{r}}{d\theta}$ and $\frac{d\vec{r}}{d\varphi}$ represent the vectors and can be calculated following Equations A.2.9 and A.2.10:

$$\frac{d\vec{r}}{d\theta} = \vec{\imath} \times \frac{\partial(rsin\theta cos\varphi)}{\partial\theta} + \vec{\jmath} \times \frac{\partial(rsin\theta cos\varphi)}{\partial\theta} + \vec{k} \times \frac{\partial(rcos\theta)}{\partial\theta} \tag{A.2.9}$$

195

$$\frac{d\vec{r}}{d\varphi} = \vec{\imath} \times \frac{\partial(r\sin\theta\cos\varphi)}{\partial\varphi} + \vec{\jmath} \times \frac{\partial(r\sin\theta\cos\varphi)}{\partial\varphi} + \vec{k} \times \frac{\partial(r\cos\theta)}{\partial\varphi} \qquad (A.2.10)$$
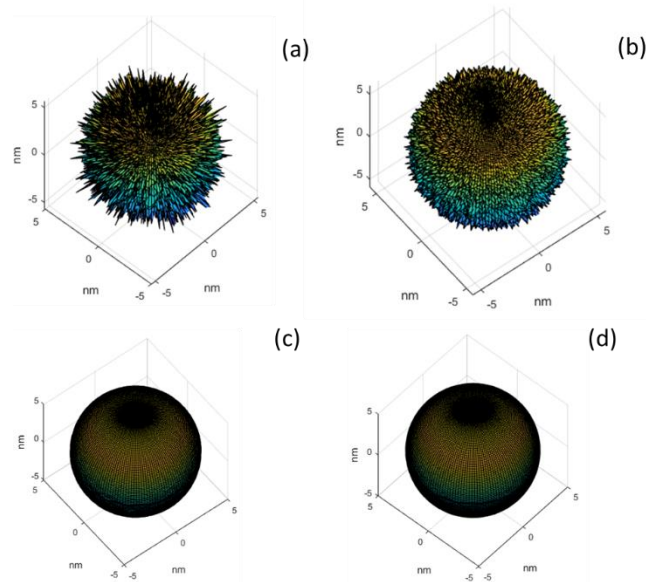

Figure A.2.3. Constructed rough spherical surfaces with different parameters, (a) $D_f = 2.2$, (b) $D_f = 2.3$, (c) $D_f = 2.4$, (d) $D_f = 2.5$

The different values of the random phase were shown in Equations A.2.11-A.2.15.

$$[\phi_1] = \begin{bmatrix} 2.2681 & 3.4148 & 5.1977 & 5.3991 & 3.9171 & 3.2029 \\ 3.7282 & 0.3488 & 3.0793 & 5.0153 & 5.0239 & 1.1093 \\ 4.0971 & 0.0225 & 0.9963 & 5.6497 & 1.8793 & 4.6751 \\ 4.4089 & 0.3153 & 1.5343 & 3.4391 & 4.3598 & 4.1709 \\ 1.2114 & 5.3985 & 4.3828 & 4.6273 & 3.9585 & 1.3544 \\ 5.1218 & 5.3310 & 0.5640 & 4.7376 & 5.1990 & 3.5070 \\ 4.9327 & 5.4101 & 0.3967 & 5.9858 & 2.4364 & 0.1511 \\ 2.8786 & 1.3616 & 0.3829 & 0.2327 & 4.0411 & 3.7663 \end{bmatrix} \qquad (A.2.11)$$

$$[\phi_{2a}] = \begin{bmatrix} 4.1191 & 2.8619 & 0.9096 & 0.4612 & 0.3180 & 3.6027 \\ 3.6189 & 4.7493 & 2.3329 & 0.7634 & 3.5270 & 0.8468 \\ 2.5344 & 5.6397 & 2.2358 & 1.9834 & 3.8325 & 3.1260 \\ 3.7808 & 2.1945 & 3.2084 & 1.5343 & 2.5146 & 5.2563 \\ 5.7687 & 1.0330 & 3.9593 & 4.7668 & 5.0661 & 0.8882 \\ 4.3296 & 3.5302 & 3.3163 & 1.6307 & 5.6540 & 6.2518 \\ 2.6011 & 4.5469 & 6.1725 & 2.3536 & 2.9490 & 4.9859 \\ 5.4271 & 2.6648 & 2.5421 & 3.0370 & 5.0575 & 5.1017 \end{bmatrix} \qquad (A.2.12)$$

$$[\phi_{2b}] = \begin{bmatrix} 0.0808 & 6.1569 & 4.1835 & 1.8631 & 3.9698 & 2.3516 \\ 4.6463 & 2.1937 & 6.0879 & 3.2715 & 4.2675 & 6.2551 \\ 2.9557 & 5.3284 & 4.6760 & 4.4495 & 1.4076 & 0.3511 \\ 3.5387 & 4.4639 & 1.3998 & 0.4655 & 5.3136 & 1.4555 \\ 0.7391 & 4.1937 & 2.9450 & 5.6548 & 3.2763 & 0.5161 \\ 5.8645 & 1.5321 & 1.6243 & 3.9077 & 5.8631 & 2.3428 \\ 4.3234 & 6.0645 & 4.9222 & 4.1252 & 2.7984 & 2.1609 \\ 1.0744 & 4.8341 & 0.7780 & 2.4890 & 3.4023 & 1.0550 \end{bmatrix} \tag{A.2.13}$$

$$[\phi_{2c}] = \begin{bmatrix} 2.2004 & 3.5182 & 1.2746 & 0.0583 & 1.8301 & 2.3935 \\ 3.6335 & 4.4653 & 3.3080 & 1.0001 & 3.9834 & 2.9716 \\ 2.4748 & 3.9381 & 5.0795 & 2.6448 & 4.8868 & 6.0861 \\ 3.9726 & 2.2546 & 4.9109 & 5.9741 & 4.7623 & 2.0438 \\ 5.0035 & 5.8720 & 1.9142 & 5.8823 & 1.3200 & 5.5729 \\ 0.7031 & 0.1575 & 5.0509 & 5.1201 & 3.0307 & 3.5421 \\ 2.7415 & 5.3811 & 1.5759 & 2.4420 & 4.4423 & 5.6568 \\ 5.2151 & 1.5263 & 4.5889 & 6.0546 & 3.9766 & 0.3021 \end{bmatrix} \tag{A.2.14}$$

$$[\phi_{2d}] = \begin{bmatrix} 6.2085 & 5.8828 & 0.5773 & 3.9317 & 1.5416 & 6.1835 \\ 3.4671 & 2.2659 & 2.1903 & 4.3228 & 5.7710 & 6.0415 \\ 5.1146 & 4.9935 & 0.4057 & 1.4898 & 1.5998 & 2.4044 \\ 5.1155 & 2.2950 & 4.8010 & 5.9191 & 3.5359 & 5.4426 \\ 5.3613 & 5.9095 & 4.1801 & 2.5438 & 3.2561 & 3.8384 \\ 4.4745 & 4.5492 & 4.7374 & 3.2625 & 1.4252 & 3.0480 \\ 4.4869 & 1.6210 & 5.1267 & 4.8220 & 2.0956 & 3.1904 \end{bmatrix} \tag{A.2.15}$$

Table A.2.2 The ANOVA test for ten different interaction scenarios for rough particles with random surface morphology

Source of Variation	F	P-value	F crit
Different random phase ϕ_{2i}	1.04E-08	> 0.05	1.509627

The reconstructed spherical surface is used to prove the hypothesis that surface roughness is the dominant factor in interfacial interaction.

$$R_{\text{reconstructed−latitudinal}} = \begin{cases} r_1 + r_1\lambda_{\alpha1}\cos(n_{\alpha1}\theta_1) + r_1\lambda_{\alpha1}\cos(n_{\alpha1}\varphi_1) & 0 \le \theta_1 \le \pi/3 \\ r_1 + r_1\lambda_{\beta1}\cos(n_{\beta1}\theta_1) + r_1\lambda_{\beta1}\cos(n_{\beta1}\varphi_1) & \pi/3 < \theta_1 < 2\pi/3 \\ r_1 + r_1\lambda_{\alpha1}\cos(n_{\alpha1}\theta_1) + r_1\lambda_{\alpha1}\cos(n_{\alpha1}\varphi_1) & 2\pi/3 \le \theta_1 \le \pi \end{cases}$$

$$\tag{A.2.16}$$
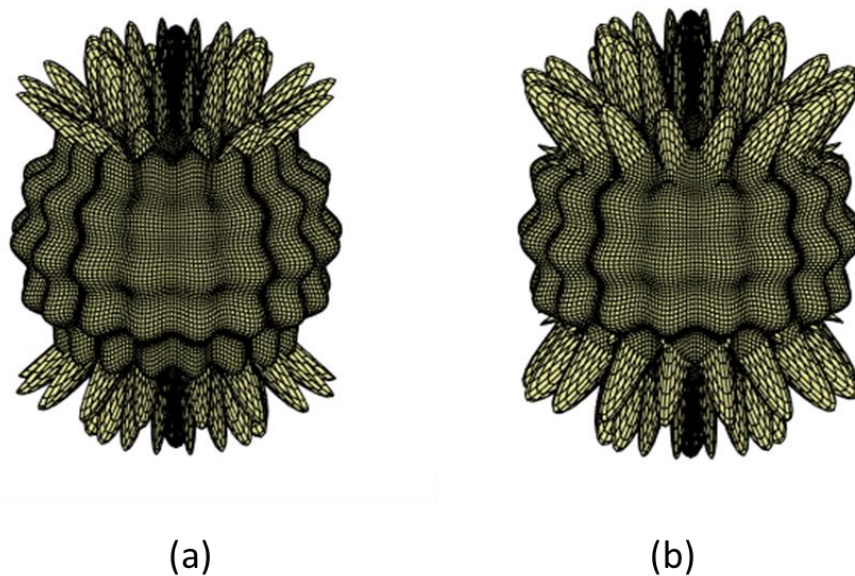
Figure A.2.4. The surface morphology comparison of the constructed spherical surfaces. To improve the visualization of the varied area, the asperity size was magnified. (a) the rough particle constructed by Equation 4.2. (b) the rough spherical surfaces constructed by Equation A.2.16, which owns a smaller area of small asperities.
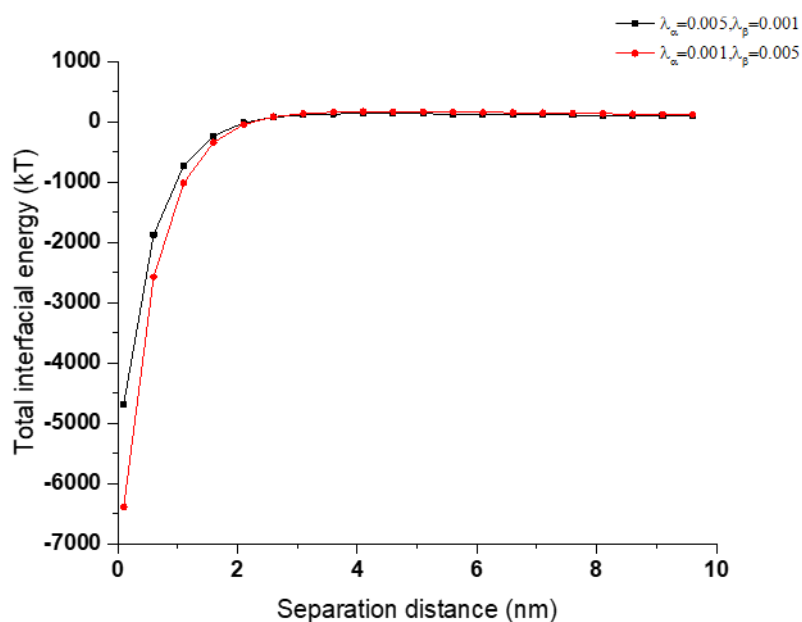
Figure A.2.5 The influences of asperity position on interfacial energy of rough spherical surfaces according to Equation A.2.16 when $r_1=r_{control}=1000$ nm, n=5, $\lambda_{control}=0.005$

8.3 Interfacial interactions of rough ellipsoidal particles with randomly located asperities

Table A.3.1. Surface tensions parameters (mJ/m^2) of liquid to set up Young's equation [2, 3]

Probe liquids	γ^{LW}	γ^+	γ^-	γ^{AB}	γ^{tol}
Water	21.8	25.5	25.5	51.0	72.8
Glycerol	34.0	3.9	57.4	30.0	64.0
Diiodomethane	50.8	0.0	0.0	0.0	50.8

Table A.3.2. Contact angle and zeta potential of modeled particle [4]

Contact angle (°)			Surface tension (Calculated based on Table S1) (mJ m^{-2})			Zeta potential (mV)
Water	Glycerol	Diiodomethane	γ^{LW}	γ^+	γ^-	
69.82±0.57	66.76±0.20	32.72±0.32	43.06	0.02	14.22	-20.74 ± 0.58

Table A.3.3 Parameters collected from literature to construct randomly rough surface [5]

Parameters	Value	Unit
L	5000	nm
η	1.5	/
M	8	/
Ls	450	nm
$\phi_{m,n}$	Randomly calculated in the interval [0, 2π]	/

8.3.1 The numerical equations to define the fractal dimension and fractal roughness

A series of roughness spectra of the surface cross-section can be expressed by spectral density function [6]

$$S(\omega) = \frac{\tau^{2(D_f - 1)}}{2ln\eta} \frac{1}{\omega^{(5-2D_f)}} \tag{A.3.1}$$

where ω and $S(\omega)$ represents the surface roughness frequency and the power of spectrum, respectively; η represents the parameter of frequency density. The $S(\omega)$ can be calculated by following the Fast Fourier transform method [6]. For a fractal profile, plotting the logarithm of $S(\omega)$ to the logarithm of $S(\omega)$ would yield a straight line. The slope (k_p) and intercept (B) of the straight line could be obtained by regression analysis. Accordingly, solving the Equations S5 and S6 could provide the data of D_f and o [1].

$$k_p = 2D_f - 5 \tag{A.3.2}$$

$$B = 2(D_f - 1)lgo - \lg(2ln\eta) \tag{A.3.3}$$

8.3.2 The numerical equations to define the vectors

Substituting Eq. (11) into Equations. (17) and (18) in the manuscript, the partial derivatives can be determined. Then, Eq. (16) of the manuscript can be expressed as:

$$\vec{n} = \frac{R sin\theta cos\varphi - A_1 sin\varphi \sum_{m=1}^{M} \sum_{n=0}^{nmax} A_2 \sin\left(\varphi - \frac{\pi m}{M}\right) - A_1 cos\theta cos\varphi \sum_{m=1}^{M} \sum_{n=0}^{nmax} A_2 \cos\left(\varphi - \frac{\pi m}{M}\right) cos\theta}{\sqrt{R^2 + A_1^2 \sum_{m=1}^{M} \sum_{n=0}^{nmax} A_2^2 \sin^2\left(\varphi - \frac{\pi m}{M}\right) + A_1^2 \sum_{m=1}^{M} \sum_{n=0}^{nmax} A_2^2 \cos^2\left(\varphi - \frac{\pi m}{M}\right) cos\theta^2}} \vec{\iota}$$

$$+ \frac{R sin\theta sin\varphi + A_1 cos\varphi \sum_{m=1}^{M} \sum_{n=0}^{nmax} A_2 \sin\left(\varphi - \frac{\pi m}{M}\right) - A_1 cos\theta sin\varphi \sum_{m=1}^{M} \sum_{n=0}^{nmax} A_2 \cos\left(\varphi - \frac{\pi m}{M}\right) cos\theta}{\sqrt{R^2 + A_1^2 \sum_{m=1}^{M} \sum_{n=0}^{nmax} A_2^2 \sin^2\left(\varphi - \frac{\pi m}{M}\right) + A_1^2 \sum_{m=1}^{M} \sum_{n=0}^{nmax} A_2^2 \cos^2\left(\varphi - \frac{\pi m}{M}\right) cos\theta^2}} \vec{J}$$

$$+ \frac{R cos\theta + A_1 sin\theta \sum_{m=1}^{M} \sum_{n=0}^{nmax} A_2 \cos\left(\varphi - \frac{\pi m}{M}\right) cos\theta}{\sqrt{R^2 + A_1^2 \sum_{m=1}^{M} \sum_{n=0}^{nmax} A_2^2 \sin^2\left(\varphi - \frac{\pi m}{M}\right) + A_1^2 \sum_{m=1}^{M} \sum_{n=0}^{nmax} A_2^2 \cos^2\left(\varphi - \frac{\pi m}{M}\right) cos\theta^2}} \vec{k}$$

$$\tag{A.3.4}$$

Where the A_1 and A_2 are coefficients, and could be described as follows:

$$A_1 = L \left(\frac{G}{L}\right)^{D_f - 2} \left(\frac{ln\eta}{M}\right)^{1/2} \tag{A.3.5}$$

$$A_2 = \eta^{(D_f - 3)n} \sin\left(\frac{2\pi\eta^n r sin\theta}{L} \times \cos\left(\varphi - \frac{\pi m}{M}\right) + \phi_{m,n}\right) \times \frac{2\pi\eta^n r}{L} \tag{A.3.6}$$

Thereafter, $\vec{n}\vec{k}$ could be expressed as follows:

$$\vec{n}\vec{k} = \frac{Rcos\theta + A_1 sin\theta \sum_{m=1}^{M} \sum_{n=0}^{nmax} A_2 \cos\left(\varphi - \frac{\pi m}{M}\right) cos\theta}{\sqrt{R^2 + A_1^2 \sum_{m=1}^{M} \sum_{n=0}^{nmax} A_2^2 \sin^2\left(\varphi - \frac{\pi m}{M}\right) + A_1^2 \sum_{m=1}^{M} \sum_{n=0}^{nmax} A_2^2 \cos^2\left(\varphi - \frac{\pi m}{M}\right) cos\theta^2}} \tag{A.3.7}$$


Prolate   Oblate
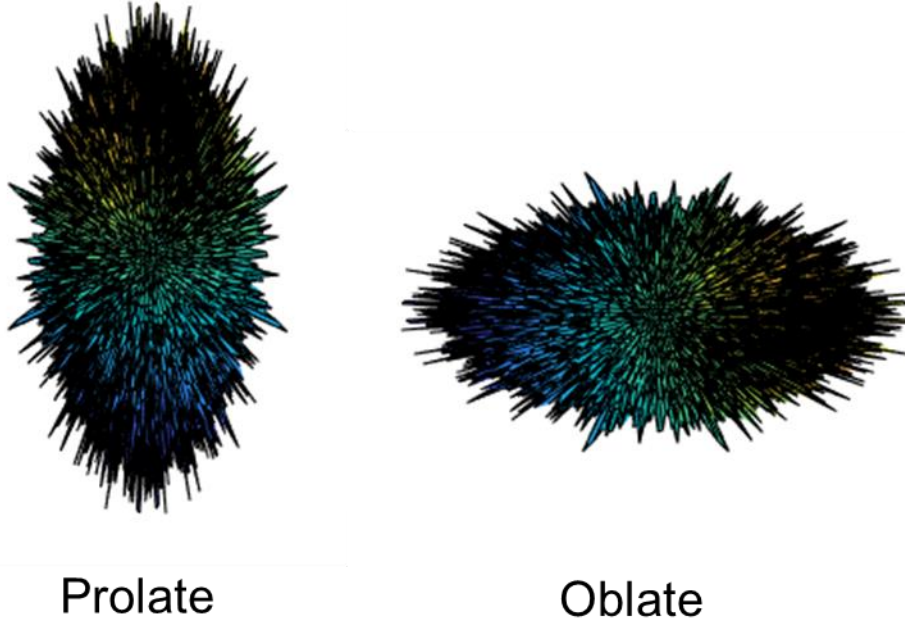
Figure A.3.1. The different shapes of randomly rough ellipsoidal particle

8.3.3 Fractal dimension effect

D_f can generate surfaces with different degrees of roughness, which may represent the topographical characteristics of surfaces. Figure A.3.2 shows the effects of fractal dimension on the interaction of rough ellipsoidal particles. As seen in Figure A.3.2a, the interfacial interaction energy was increased with growing D_f from 2.03 to 2.93 in both particles. The main reason for this phenomenon is attributed to the fact that the surface roughness of ellipsoidal particles is reduced by increasing the value of the fractal dimension. Although the increased fractal dimension generates more asperities, the total average surface roughness of particle is decreased [1] because the increased value of the fractal dimension would refine the texture of the rough surface, which would directly reduce the size of generated asperities. The previous studies generated the asperities with uniform and periodic sinusoidal functions and concluded that the greater surface roughness would lessen the interaction energy between particles because the separation distance was enlarged by inflating the asperity [7, 8]. Zhu and coworkers generated a rough uniform surface (hemisphere) with a spherical surface pattern and reported that the total interaction energy dropped with increasing the hemisphere size [9]. Our results using the modified two-variable

201

WM function to generate the randomly rough surface predicted a similar pattern (Figure A.3.2). The present model could improve the accuracy of the prediction for the interaction energy of rough surfaces with morphologies close to those of natural rough surfaces [7-9]. Moreover, the surface roughness could provide benefits in coagulation systems because the surface roughness would control the magnitude of the energy barrier developed between particles as shown in Figure A.3.2. Abdellatif and coworkers [10] investigated the relationship between the fractal dimension of gold nanoparticles and particle aggregation and noticed that the gold nanoparticles tended to aggregate when their surface fractal dimension dropped.

It should be noted that there is a critical value of a fractal dimension that would eliminate surface roughness. Cai and coworkers reported that the surface roughness decreased exponentially with increasing the value of the fractal dimension [1]. As shown in Figure A.3.2a, the interaction energy grew insignificantly with further enlarging the value of D_f >2.33, which indicated that the roughness was in fact eliminated when the D_f > 2.33 because the surface roughness expediently decreased with increasing the value of fractal dimension [1]. Therefore, the critical value of D_f in the present study is approximately 2.33.

The effect of the relative fractal dimension on the particle interaction was shown in Figure A.3.2b. The fractal dimension of particle 1 is set at D_{f1} = 2.83 to construct a relatively smooth particle, while the fractal of particle 2 (D_{f2}) is changed from 2.03 to 2.63. According to Figure A.3.2a, the total interaction energy has no remarkable difference while continually increasing the value of D_f from 2.63 to 2.93. The main reason is that the surface morphology would not change as a smooth surface is generally generated when D_f = 2.63.

As shown in Figure A.3.2b, the interaction energy between particles was intensified when the fractal dimension 2.03<D_{f2}<2.63. As the surface morphology had no change when the D_f > 2.63 in this study, the maximum D_{f2} was selected as 2.63. Once the fractal dimension of rough particle 1 was constant, the value of D_{f2} could represent the relative roughness of these two particles [11].

With growing the value of D_{f2}, the size of asperities was reduced on the surface, which would strengthen the interaction energy between particles.

As the surface roughness can be expressed by the asperity number and asperity size [12], the impact of each parameter in controlling interaction energy could be explored from the predicted results in this

study. Usually, the surface roughness would be lessened by reducing the asperity number and asperity size, which would elevate the total interaction energy [8]. However, when the D_f increased, the texture of the rough surface was refined, which strengthened the total interaction energy, where the asperity number increased but the asperity size dropped [1]. According to these results [1, 8, 12], it could be concluded that the size of asperity (surface roughness height) has more effect than the number of asperities (surface roughness fraction) on the interaction of rough ellipsoidal particles
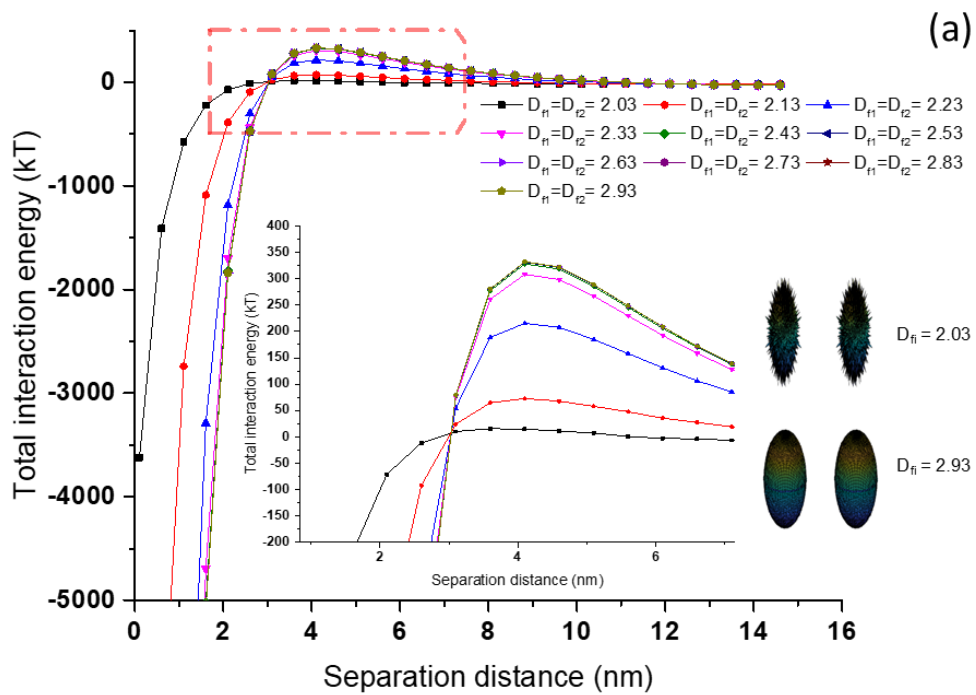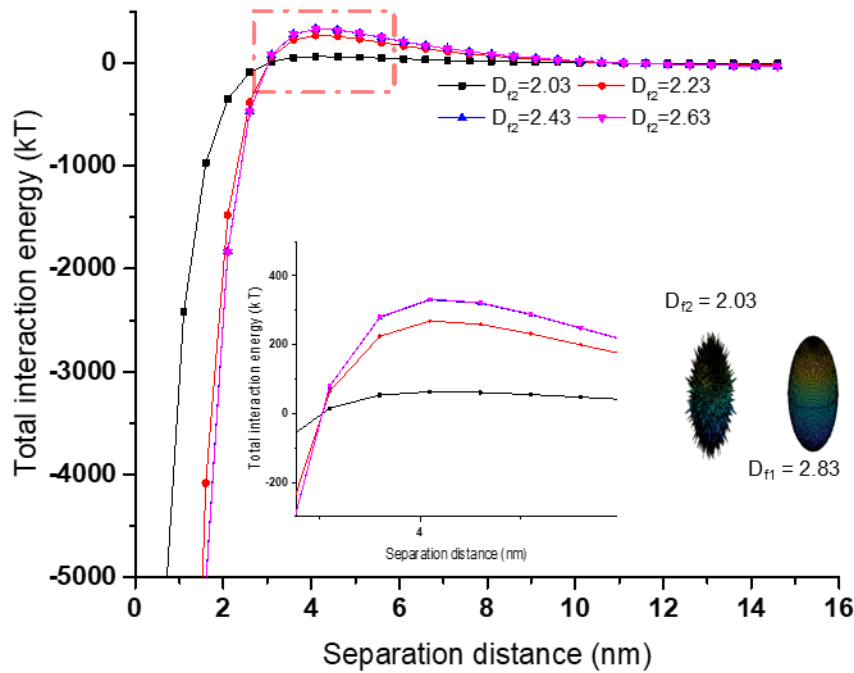
Figure A.3.2. The effect of fractal dimension on the interaction energy of the rough ellipsoidal particle with randomly located asperities (a) The effect of fractal dimension on particle interaction ($a_1 = b_1 = a_2 = b_2 = 1000\ nm, c_1 = c_2 = 500\ nm,\ o_1 = o_2 = 0.1\ nm$). (b) The effect of relative fractal dimension on particle interaction ($a_1 = b_1 = a_2 = b_2 = 1000\ nm, c_1 = c_2 = 500\ nm,\ o_1 = o_2 = 0.1\ nm, D_{f1} = 2.83$).

8.3.4 Fractal roughness effect

The effect of o on ellipsoidal particle interaction is shown in Figure A.3.3a. The total interfacial interaction energy between two rough ellipsoids decreased with varying the value of o from 0.1 nm to 50 nm in two interaction scenarios. As shown in Equation 10, one power function relationship existed between o and surface roughness, which would suggest that surface roughness was affected by o [13]. Therefore, the simulation results should be reasonable because the total interaction energy decreased with increasing surface roughness. Different from the fractal dimension, the increased value of o would change the surface morphology only via enlarging the asperity height. The role of surface roughness was to adjust the separation distance and interaction area between rough particles, which could significantly control the interfacial energy in particle interaction. The importance of surface roughness was articulated by Shen and coworkers, who studied how the roughness of quartz sand surface impacted

white carboxyl-modified polystyrene latex nanoparticle attachment [14]. The present model showed that without excluding the Born repulsion energy, the depth of the primary minimum decreased with increasing the value of o, which suggested that the surface roughness would significantly control the particle transportation (Figure A.3.3a). Shen and coworkers stated that the depth of primary minimum could be an indicator of monitoring the attachment affinity of colloidal particles, and if the depth of primary minimum decreased, disaggregation would occur in colloidal systems [15]. Therefore, the shallower depth of the primary minimum caused by the higher value of o in our model might indicate the detachment of the particles because the adhesion between particles deteriorated due to increased surface roughness [16].

The previous literature mainly focused on the effect of fractal dimension on spherical particle interactions when the fractal geometry theory was considered [17]. Nevertheless, the relative roughness has a significant effect on rough ellipsoidal particle interactions. As shown in Figure A.3.3b, the total interaction energy between particles decreased with increasing the relative fractal roughness (o_2) from 0.5 to 10 nm.

Also, this finding may facilitate the particle aggregation application because the asperities generated on the particle surface could control the repulsion energy of interfaces [18]. For example, in the system of ZnO aqueous solution, the rough ellipsoidal particle existed, which would tend to coagulate with a coarse surface. These results confirmed that by roughening the surface morphology of particles, the repulsion energy between particles deteriorated and particles tended to attach. As shown in Figure A.3.3, the energy barrier between two rough ellipsoidal particles was weakened by inflating o, which indicated that the increased asperity size reduced the obstacle of particle coagulation. In this context, Elimelech and coworkers reported that the asperities on the membrane surface diminished the interaction force between flocs and membrane, and flocs could attach to rougher surfaces more greatly than smooth surfaces [19].

(a)
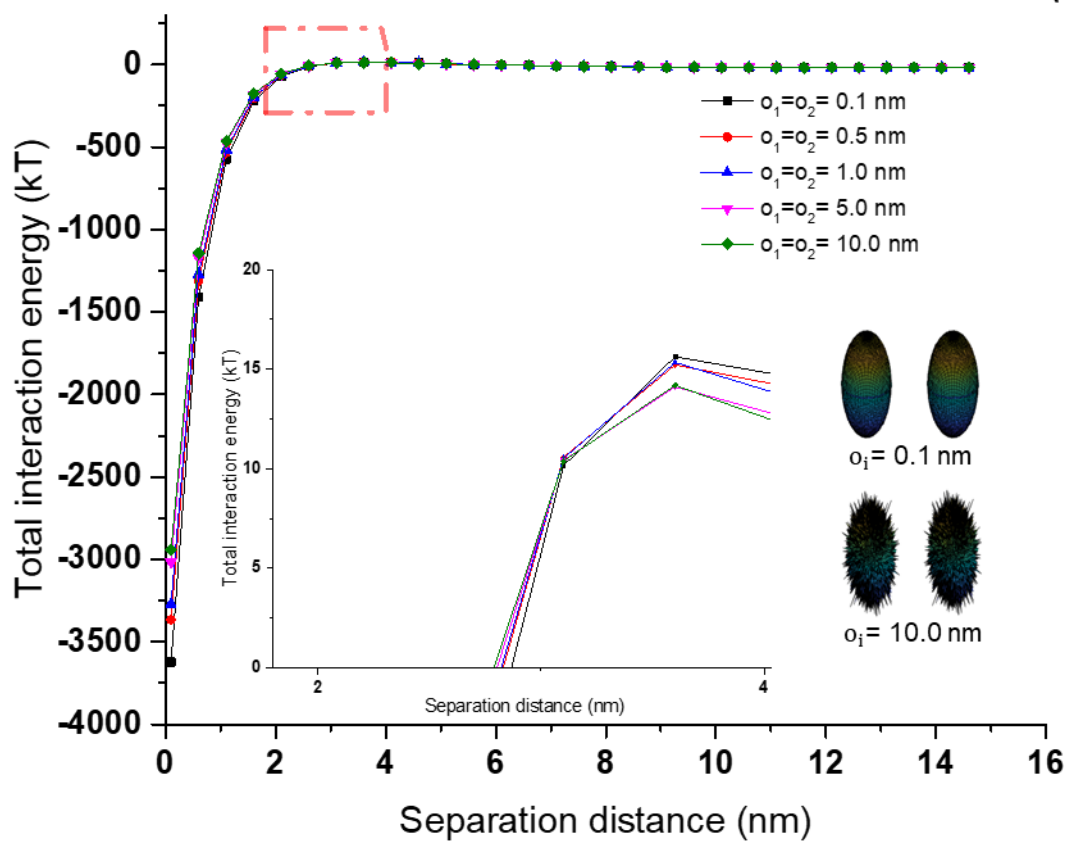
(b)
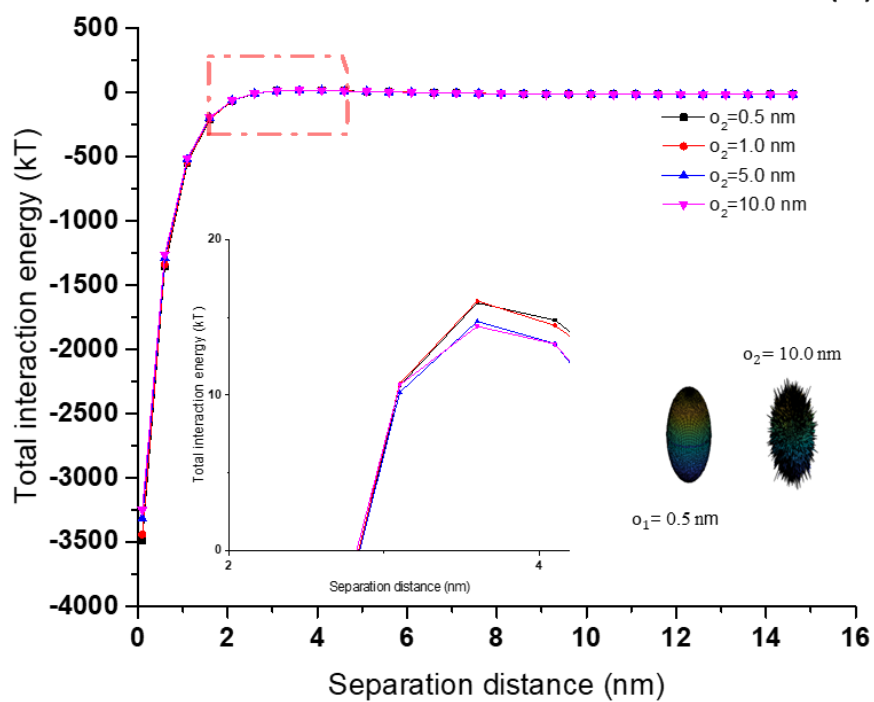
Figure A.3.3. The effect of fractal roughness on the interaction energy of rough ellipsoidal particles with randomly located asperities. (a) The effect of fractal roughness on particle interaction ($a_1 = b_1 = a_2 = b_2 = 1000\ nm, c_1 = c_2 = 500\ nm,\ D_{f1} = D_{f2} = 2.03$). (b) The effect of relative fractal roughness on particle interaction ($a_1 = b_1 = a_2 = b_2 = 1000\ nm, c_1 = c_2 = 500\ nm,\ D_{f1} = D_{f2} = 2.03, o_1 = 0.1\ nm$).

8.3.5 Comparison of the interaction energy between rough and smooth particles

The comparative effects of rough and smooth surface morphology on the ellipsoidal particle interaction were shown in Figure A.3.4. Regardless of the method of the roughness increment, it could be found that the surface roughness significantly reduced the repulsive energy barrier, which indicated that the surface roughness destroyed the dispersion stability between particles that tended to aggregate otherwise. Once the surface roughness was eliminated from the modeled particles, the largest magnitude of repulsive energy barrier could be achieved where the strongest repulsion energy existed between the two particles. Therefore, surface morphology played an important role in particle transportation. Geiger and coworkers found that the elevated surface roughness led to a significant drop in the effective charge-carrier mobility and an increase in the subthreshold swing [20]. Another phenomenon is that the rough surface generated the shallower primary minimum in energy profile as shown in Figure A.3.4, which indicated that the rough surface also weakened the initial attachment ability of particles. If the particle were assumed attached at the primary minimum, the rough particle would release more easily from the rough surface compared to the smooth surface [15]. The predicted various interaction energies in this numerical model could be an indicator for the modification of surface morphology to prepare the desired products.
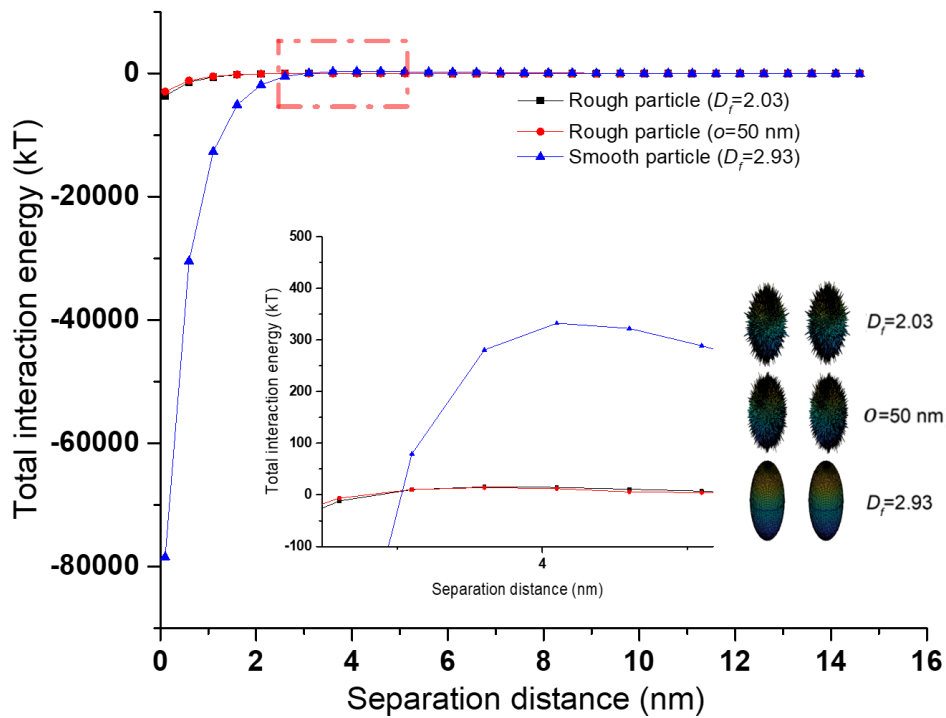
Figure A.3.4. The comparisons between the smooth and rough surface morphology effects on particle interaction ($a = b =$1000 nm, $c =$500 nm)

8.3.6 The validation of the present model

To evaluate the accuracy of the results, the predicted results were compared with the experimental and modeling results available in past literature, and the results are shown in Table S4

Table A.3.4 Comparison between past studies and present modeling study

Type of works	Material	Interaction scenario	Conditions	Theory	Main conclusion
Experiment, [21]	Bare silica particle	Particle vs flat	Orientation angle increased from 0 to $\frac{\pi}{2}$	DLVO	The repulsive energy barrier decreased from 512.1 kT to 52.7 kT

This model	-	Particle vs particle	Orientation angle increased from 0 to $\frac{\pi}{2}$	XDLVO	The repulsive energy barrier decreased from 478.4 kT to 45.2 kT
Modeling work, [22]	-	Particle vs flat surface	Orientation angle increased from 0 to $\frac{\pi}{2}$	DLVO	The repulsive energy barrier decreased from 15 kT to 5 kT
This model	-	Particle vs particle	Orientation angle increased from 0 to $\frac{\pi}{2}$	XDLVO	The repulsive energy barrier decreased from 7 to 3 kT

In the experimental study carried out using bare silica particles, when the orientation angle increased from 0 to $\frac{\pi}{2}$, the primary maximum dropped from 512.1 kT to 52.7 kT [21]. For the same size particles, our modeling results predicted the primary maximum change from 478.4 kT to 45.2 kT when D_f was 2.93 to create a smooth surface. When the orientation angle of modeled particle was altered from 0 to $\frac{\pi}{2}$ [22], the primary maximum decreased from 15 to 5 kT. Under the same conditions, our modeling results predicted the primary maximum change from 11 to 2 kT when D_f was 2.93. As the previous experimental and modeling work relied on the DLVO theory and the present work was based on the XDLVO theory, the difference between the modeling and experimental results would be related to the

inclusion of hydrophobic interaction in the present work. Another reason to cause the difference is that the present model considered ellipsoidal particle-particle interaction unlike the interaction scenario constructed in past work [22] [21]. The past experimental work considered particle-flat surface interaction, which did not involve the curvature effects of particle shape if the flat surface was replaced by the spherical particle. Therefore, the curvature effects of particle shape on interaction area were considered in this work. Generally, the experimental and modeling results successfully anticipated similar trends for the interaction of particles when the orientation angle was increased, and our model considered different interaction scenario and involved the impacts of surface morphology.

8.3.7 References

[1] X. Cai, L. Yang, Z. Wang, M. Zhang, L. Shen, H. Hong, H. Lin, G. Yu, Influences of fractal dimension of membrane surface on interfacial interactions related to membrane fouling in a membrane bioreactor, Journal of colloid and interface science, 500 (2017) 79-87.

[2] R.J. Good, C.J. van Oss, The modern theory of contact angles and the hydrogen bond components of surface energies, Modern approaches to wettability, Springer1992, pp. 1-27.

[3] C.J. Van Oss, Interfacial forces in aqueous media, CRC press2006.

[4] M. Zhang, H. Hong, H. Lin, G. Yu, F. Wang, B.-Q. Liao, Quantitative assessment of interfacial forces between two rough surfaces and its implications for anti-adhesion membrane fabrication, Separation and Purification Technology, 189 (2017) 238-245.

[5] M. Zhang, X. Zhou, L. Shen, X. Cai, F. Wang, J. Chen, H. Lin, R. Li, X. Wu, B.-Q. Liao, Quantitative evaluation of the interfacial interactions between a randomly rough sludge floc and membrane surface in a membrane bioreactor based on fractal geometry, Bioresour. Technol., 234 (2017) 198-207.

[6] C. Yuan, J. Li, X. Yan, Z. Peng, The use of the fractal description to characterize engineering surfaces and wear particles, Wear, 255 (2003) 315-326.

[7] D. Lu, P. Fatehi, A modeling approach for quantitative assessment of interfacial interaction between two rough particles in colloidal systems, Journal of Colloid and Interface Science, 587 (2021) 24-38.

[8] H. Bargozin, R. Hadadhania, H. Faraji, H. Yousefzadeh, Effect of rough nanoparticle orientation on DLVO energy interaction, Journal of Dispersion Science and Technology, 36 (2015) 755-764.

[9] Z. Zhu, D. Wang, B. Yang, W. Yin, M.S. Ardakani, J. Yao, J.W. Drelich, Effect of nano-sized roughness on the flotation of magnesite particles and particle-bubble interactions, Minerals Engineering, 151 (2020) 106340.

[10] M. Abdellatif, G. Abdelrasoul, M. Salerno, I. Liakos, A. Scarpellini, S. Marras, A. Diaspro, Fractal analysis of inter-particle interaction forces in gold nanoparticle aggregates, Colloids Surf. Physicochem. Eng. Aspects, 497 (2016) 225-232.

[11] X. Cai, M. Zhang, L. Yang, H. Lin, X. Wu, Y. He, L. Shen, Quantification of interfacial interactions between a rough sludge floc and membrane surface in a membrane bioreactor, Journal of colloid and interface science, 490 (2017) 710-718.

[12] M. Zanini, C.-P. Hsu, T. Magrini, E. Marini, L. Isa, Fabrication of rough colloids by heteroaggregation, Colloids and Surfaces A: Physicochemical and Engineering Aspects, 532 (2017) 116-124.

[13] S. Feng, G. Yu, X. Cai, M. Eulade, H. Lin, J. Chen, Y. Liu, B.-Q. Liao, Effects of fractal roughness of membrane surfaces on interfacial interactions associated with membrane fouling in a membrane bioreactor, Bioresour. Technol., 244 (2017) 560-568.

[14] C. Shen, Y. Jin, B. Li, W. Zheng, Y. Huang, Facilitated attachment of nanoparticles at primary minima by nanoscale roughness is susceptible to hydrodynamic drag under unfavorable chemical conditions, Sci. Total Environ., 466 (2014) 1094-1102.

[15] C. Shen, M. Zhang, S. Zhang, Z. Wang, H. Zhang, B. Li, Y. Huang, Influence of surface heterogeneities on reversibility of fullerene (nC60) nanoparticle attachment in saturated porous media, Journal of hazardous materials, 290 (2015) 60-68.

[16] S. Torkzaban, S.A. Bradford, Critical role of surface roughness on colloid retention and release in porous media, Water Res., 88 (2016) 274-284.

[17] L. Zhao, X. Qu, H. Lin, G. Yu, B.-Q. Liao, Simulation of foulant bioparticle topography based on Gaussian process and its implications for interface behavior research, Applied Surface Science, 434 (2018) 975-981.

[18] J.W. Drelich, A simplified analysis of the effect of nano-asperities on particle-bubble interactions, Physicochemical Problems of Mineral Processing, 54 (2018).

[19] M. Elimelech, X. Zhu, A.E. Childress, S. Hong, Role of membrane surface morphology in colloidal fouling of cellulose acetate and composite aromatic polyamide reverse osmosis membranes, J. Membr. Sci., 127 (1997) 101-109.

[20] M. Geiger, R. Acharya, E. Reutter, T. Ferschke, U. Zschieschang, J. Weis, J. Pflaum, H. Klauk, R.T. Weitz, Effect of the Degree of the Gate-Dielectric Surface Roughness on the Performance of Bottom-Gate Organic Thin-Film Transistors, Advanced Materials Interfaces, 7 (2020) 1902145.

[21] A. Gomez-Flores, S.A. Bradford, G. Hwang, S. Choi, M. Tong, H. Kim, Shape and orientation of bare silica particles influence their deposition under intermediate ionic strength: A study with QCM–D and DLVO theory, Colloids Surf. Physicochem. Eng. Aspects, 599 (2020) 124921.

[22] S. Bhattacharjee, J.Y. Chen, M. Elimelech, DLVO interaction energy between spheroidal particles and a flat surface, Colloids Surf. Physicochem. Eng. Aspects, 165 (2000) 143-156.

# 8.4 Interaction of deformable solid and hollow particles with the rough surface morphology
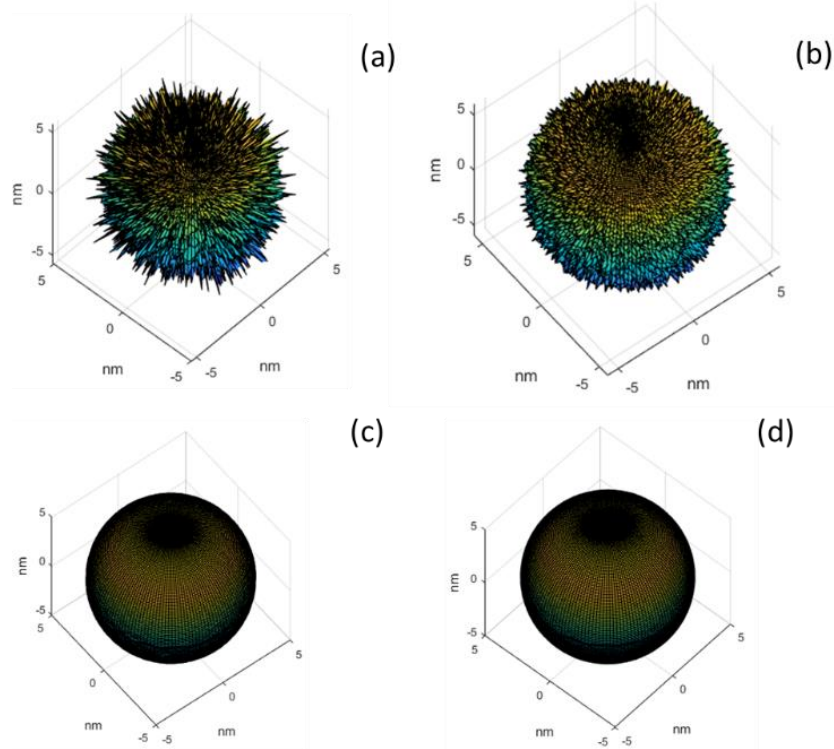
Figure A.4.1. Constructed rough spherical surfaces with different parameters, (a) $D_f = 2.2$, (b) $D_f = 2.3$, (c) $D_f = 2.4$, (d) $D_f = 2.5$

8.4.1 Reference

[1] S. Bhattacharjee, C.-H. Ko, M. Elimelech, DLVO interaction between rough surfaces, Langmuir. 14(12) (1998) 3365-3375.

[2] C. Van Oss, Acid—base interfacial interactions in aqueous media, Colloids Surf. A Physicochem. Eng. Asp. 78 (1993) 1-49.

[3] S. Feng, G. Yu, X. Cai, M. Eulade, H. Lin, J. Chen, Y. Liu, B.-Q. Liao, Effects of fractal roughness of membrane surfaces on interfacial interactions associated with membrane fouling in a membrane bioreactor, Bioresour. Technol. 244 (2017) 560-568.